Characterizing Existing Asphalt Concrete Layer Damage for Mechanistic Pavement Rehabilitation Design

U.S. Department of Transportation
Federal Highway Administration

FOREWORD

This report presents findings from an analysis of Long-Term Pavement Performance program data. This analysis was undertaken to verify and propose enhancements to the existing overlay design procedure using the *Mechanistic-Empirical Pavement Design Guide* (MEPDG) rehabilitation design methodology.[1,2]

Deflection data are used to characterize the structural condition of flexible pavements and provide a benchmark in determining the in-place damage of asphalt concrete (AC) layers for use with the MEPDG.[1,2] In-place damage is defined by the ratio of the backcalculated elastic layer modulus and laboratory-measured dynamic modulus of AC layers. This procedure, however, was not verified as part of the MEPDG approach.

The purpose of this report is to document the results from comparing the amount of fatigue cracking to the in-place damage estimated through a modulus ratio between backcalculated elastic modulus values and laboratory-measured dynamic modulus values. The audience for this report includes pavement researchers as well as practicing engineers using AASHTOWare® Pavement ME Design software for rehabilitation design.[3,4]

Cheryl Allen Richter, Ph.D., P.E.
Director, Office of Infrastructure
Research and Development

TECHNICAL REPORT DOCUMENTATION PAGE

1. Report No. FHWA-HRT-17-059	2. Government Accession No.	3. Recipient's Catalog No.		
4. Title and Subtitle Characterizing Existing Asphalt Concrete Layer Damage for Mechanistic Pavement Rehabilitation Design		5. Report Date August 2018		
		6. Performing Organization Code		
7. Author(s) Dinesh Ayyala, Hyung Lee, and Mr. Harold L. Von Quintus		8. Performing Organization Report No.		
9. Performing Organization Name and Address Applied Research Associates, Inc. 100 Trade Centre Boulevard, Suite 200 Champaign, IL 61820		10. Work Unit No. (TRAIS)		
		11. Contract or Grant No. DTFH61-14-C-00024		
12. Sponsoring Agency Name and Address U.S. Department of Transportation Federal Highway Administration 1200 New Jersey Ave., SE Washington, DC 20500		13. Type of Report and Period Covered Draft Final Report; September 2014–July 2016		
		14. Sponsoring Agency Code		
15. Supplementary Notes The Contracting Officer's Representative was Mr. Larry Wiser (HRDI-30).				

16. Abstract

Designing rehabilitation strategies for flexible pavements exhibiting various types and levels of distress is a challenge. An important factor related to the design of a rehabilitation strategy is the use of a reliable procedure to evaluate the in-place condition of pavements. A project-level pavement evaluation program should consist of multiple activities to assess structural condition, identify the types of pavement deterioration, and determine the cause of deficiencies that need to be addressed during pavement rehabilitation.

One of the critical steps for evaluating the in-place structural condition of existing pavement layers is deflection-basin testing. Deflection basins are used to backcalculate the elasticlayer modulus of existing asphalt concrete (AC) layers, which is considered input level 1 for rehabilitation designs in accordance with the *Mechanistic-Empirical Pavement Design Guide*.[1] Most agencies measure deflection basins as part of their pavement evaluation programs, but few actually use the data to determine the in-place condition of the AC layers. Deflection data are used to establish analysis sections and/or estimate the resilient modulus of the subgrade soils. However, more recently, agencies have started to use the backcalculated elastic layer modulus to determine the amount of in-place fatigue damage in the existing AC layers.

This report evaluates the use of deflection-basin data to determine the in-place structural condition of AC layers for rehabilitation design in accordance with the *Mechanistic-Empirical Pavement Design Guide—A Manual of Practice*.[2] A common use of deflection data is to backcalculate in-place layered elastic modulus values.

| 17. Key Words
Asphalt concrete, Fatigue damage, Backcalculation, Deflection data, Elastic modulus, Falling weight deflectometer, Long-Term Pavement Performance, *Mechanistic-Empirical Pavement Design Guide*, Pavement evaluation | | 18. Distribution Statement
No restrictions. This document is available to the public through the National Technical Information Service, Springfield, VA 22161
http://www.ntis.gov | | |
| 19. Security Classif. (of this report)
Unclassified | 20. Security Classif. (of this page)
Unclassified | | 21. No. of Pages
197 | 22. Price |

Form DOT F 1700.7 (8-72)   Reproduction of completed page authorized.

SI* (MODERN METRIC) CONVERSION FACTORS

APPROXIMATE CONVERSIONS TO SI UNITS

Symbol	When You Know	Multiply By	To Find	Symbol
	LENGTH			
in	inches	25.4	millimeters	mm
ft	feet	0.305	meters	m
yd	yards	0.914	meters	m
mi	miles	1.61	kilometers	km
	AREA			
in^2	square inches	645.2	square millimeters	mm^2
ft^2	square feet	0.093	square meters	m^2
yd^2	square yard	0.836	square meters	m^2
ac	acres	0.405	hectares	ha
mi^2	square miles	2.59	square kilometers	km^2
	VOLUME			
fl oz	fluid ounces	29.57	milliliters	mL
gal	gallons	3.785	liters	L
ft^3	cubic feet	0.028	cubic meters	m^3
yd^3	cubic yards	0.765	cubic meters	m^3
	NOTE: volumes greater than 1000 L shall be shown in m^3			
	MASS			
oz	ounces	28.35	grams	g
lb	pounds	0.454	kilograms	kg
T	short tons (2000 lb)	0.907	megagrams (or "metric ton")	Mg (or "t")
	TEMPERATURE (exact degrees)			
^{o}F	Fahrenheit	5 (F-32)/9 or (F-32)/1.8	Celsius	^{o}C
	ILLUMINATION			
fc	foot-candles	10.76	lux	lx
fl	foot-Lamberts	3.426	candela/m^2	cd/m^2
	FORCE and PRESSURE or STRESS			
lbf	poundforce	4.45	newtons	N
lbf/in^2	poundforce per square inch	6.89	kilopascals	kPa

APPROXIMATE CONVERSIONS FROM SI UNITS

Symbol	When You Know	Multiply By	To Find	Symbol
	LENGTH			
mm	millimeters	0.039	inches	in
m	meters	3.28	feet	ft
m	meters	1.09	yards	yd
km	kilometers	0.621	miles	mi
	AREA			
mm^2	square millimeters	0.0016	square inches	in^2
m^2	square meters	10.764	square feet	ft^2
m^2	square meters	1.195	square yards	yd^2
ha	hectares	2.47	acres	ac
km^2	square kilometers	0.386	square miles	mi^2
	VOLUME			
mL	milliliters	0.034	fluid ounces	fl oz
L	liters	0.264	gallons	gal
m^3	cubic meters	35.314	cubic feet	ft^3
m^3	cubic meters	1.307	cubic yards	yd^3
	MASS			
g	grams	0.035	ounces	oz
kg	kilograms	2.202	pounds	lb
Mg (or "t")	megagrams (or "metric ton")	1.103	short tons (2000 lb)	T
	TEMPERATURE (exact degrees)			
^{o}C	Celsius	1.8C+32	Fahrenheit	^{o}F
	ILLUMINATION			
lx	lux	0.0929	foot-candles	fc
cd/m^2	candela/m^2	0.2919	foot-Lamberts	fl
	FORCE and PRESSURE or STRESS			
N	newtons	0.225	poundforce	lbf
kPa	kilopascals	0.145	poundforce per square inch	lbf/in^2

*SI is the symbol for the International System of Units. Appropriate rounding should be made to comply with Section 4 of ASTM E380.
(Revised March 2003)

TABLE OF CONTENTS

LIST OF FIGURES

LIST OF TABLES

LIST OF ABBREVIATIONS AND SYMBOLS

Abbreviations

AASHTO	American Association of State Highway and Transportation Officials
AASHO	American Association of State Highway Officials
AC	asphalt concrete
ADOT	Arizona Department of Transportation
AI	Asphalt Institute
ANCOVA	analysis of covariance
ATB	asphalt-treated base
AUPP	area under pavement profile
BCI	base curvature index
BDI	base damage index
CDOT	Colorado Department of Transportation
CI	curvature index
COV	coefficient of variation
CPT	computed parameter table
DI	damage index
DOF	degrees of freedom
FDOT	Florida Department of Transportation
FHWA	Federal Highway Administration
FWD	falling weight deflectometer
GDOT	Georgia Department of Transportation
GPR	ground-penetrating radar
GPS	General Pavement Studies
HMA	hot mix asphalt
HS	horizontal shift
IQR	inter-quartile range
JULEA	Jacob Uzan Layered Elastic Analysis
LTPP	Long-Term Pavement Performance
MAD	median absolute deviation
MDOT	Mississippi Department of Transportation
ME	mechanistic-empirical
MEPDG	*Mechanistic-Empirical Pavement Design Guide*
NCAT	National Center for Asphalt Technology
NCHRP	National Cooperative Highway Research Program
NDT	nondestructive testing
PATB	permeable asphalt-treated base
PCC	portland cement concrete
PSD	power spectral density
RAP	recycled asphalt pavement
RMSE	root mean squared error
RWD	rolling wheel deflectometer
SCI	surface curvature index
SDR	Standard Data Release

SEE	standard error of the estimate
SMP	seasonal monitoring program
SPS	Specific Pavement Studies
UDOT	Utah Department of Transportation
VDOT	Virginia Department of Transportation
VS	vertical shift
WP	wheelpath

Symbols

a_T	temperature shift factor
A_{12}	area of the first 12 inches of the deflection basin
A_{36}	area of the first 36 inches of the deflection basin for the analysis of rigid pavements
$AREA_{12}$	area enclosed within the undeflected pavement surface and the deflection basin within 12 inches radial distance from the falling weight deflectometer loading plate
$AREA_{36}$	area enclosed within the undeflected pavement surface and the deflection basin within 3 ft radial distance from the falling weight deflectometer loading plate
c-factor	laboratory-to-field adjustment factor for resilient modulus determination
C_H	thickness correction term
C_1, C_2, and C_4	fatigue cracking transfer function regression constants
C_1* and C_2*	transfer function regression coefficients
d_0	deflection measured under the falling weight deflectometer loading plate
d_8	deflection measured at a sensor located 8 inches from the falling weight deflectometer loading plate
d_{12}	deflection measured at a sensor located 12 inches from the falling weight deflectometer loading plate
d_{24}	deflection measured at a sensor located 24 inches from the falling weight deflectometer loading plate
d_{36}	deflection measured at a sensor located 36 inches from the falling weight deflectometer loading plate
d_{AC}	fatigue damage in the existing asphalt layer
d_i	deflection measured at a sensor located i inches from the falling weight deflectometer loading plate, where i is the radial distance
d_j	deflection measured at a sensor located j inches from the falling weight deflectometer loading plate, where j is the axle load interval or distance between a sensor and the loading plate
DI_{Bottom}	cumulative damage index at the bottom of the asphalt concrete layers
$DI_{E-ratio}$	damage index based on the ratio between the damaged and undamaged modulus of the asphalt concrete layer
e	exponential
E	elastic modulus
$E*$	dynamic modulus
$|E*|$	complex modulus

$E^*_{damaged}$	field-derived damaged dynamic modulus master curve created from backaclculated elastic modulus values (E_{FWD})
E_{ac}	elastic modulus of the asphalt concrete layer
E_{FWD}	field-derived backcalculated elastic layer modulus value using static analyses
E_{HMA}	dynamic modulus of the hot mix asphalt measured in compression
E_{MED}	station average moduli
E_{NDT}	backcalculated elastic layer modulus E_{NDT} equals E_{FWD} that is used within this report
E^*_{PRED}	laboratory-derived undamaged dynamic modulus predicted from master curve parameters representing a specific temperature and load frequency
$E^*_{undamaged}$	laboratory-derived dynamic modulus master curve representing the condition without fatigue damage
E_{ST-AVG}	station average backcalculated moduli
f	frequency
FC_{Bottom}	percent total lane area of alligator cracking
F-statistic	F-value
H_{ac}	thickness of the asphalt concrete layer
H_{HMA}	total thickness of all asphalt concrete layers
i	radial distance
j	axle load interval or distance between a sensor and the loading plate
k_{f1}, k_{f2}, and k_{f3}	global field calibration parameters for fatigue cracking transfer function
l	truck type using the truck classification groups included in the *Mechanistic-Empirical Pavement Design Guide*
m	axle load type
M	mixture regression coefficient
n	actual number of axle load applications within a specific time period
N	total section count
N_{f-HMA}	allowable number of axle load repetitions
p	month
Pr	probability
t	time
t_{HS}	damage-induced horizontal shift on the reduced time scale
t_r	reduced time
T	median temperature
V_a	percent air voids in the hot mix asphalt mixture
V_{be}	effective asphalt content by volume
α	difference between maximum and minimum dynamic modulus for an asphalt mixture
α, α', β, and γ	dynamic modulus master curve coefficients
β_{f1}, β_{f2}, and β_{f3}	local or mixture-specific field calibration constants
ε_{ac}	tensile strain at the bottom of the asphalt concrete layer
ε_t	tensile strain at critical locations calculated by the structural response model
δ	logarithm of the minimum undamaged dynamic modulus
ω	angular frequency

CHAPTER 1. INTRODUCTION

BACKGROUND

During the post-war 1940s and 1950s, the United States aggressively embarked on a program to expand the Nation's interstate highway and national highway systems. This was done by constructing flexible (hot mix asphalt (HMA)), rigid (portland cement concrete (PCC)), and composite (HMA over PCC) pavements. Although this construction effort continues today, the focus has changed from new construction to rehabilitation (including overlays) regarding the aging of the Nation's highway pavement infrastructure. A key aspect of pavement rehabilitation design is the characterization of existing pavements' structural conditions. If done properly, pavement engineers can determine with reasonable accuracy the baseline pavement's structure traffic-carrying capacity and develop enhancements to the existing capacity mostly by placing overlays to carry future traffic loads. This leads to more reliable pavement overlay designs, resulting in significant reductions in premature failures and maintenance costs.

With the development of the new *Mechanistic-Empirical Pavement Design Guide* (MEPDG) in the mid-2000s, significant improvements were made to new and rehabilitated pavement design technology.[1] The local calibration and implementation of the MEPDG by several State agencies, however, revealed the need for some improvements and/or proofs of concepts to some aspects of the MEPDG. Examples of improvements initiated by the National Cooperative Highway Research Program (NCHRP) include Project 01-41, *Models for Predicting Reflection Cracking of Hot-Mix Asphalt Overlays*, and Project 09-30A, *Calibration of Rutting Models for HMA Structural and Mixture Design*, both of which have already been integrated into the pavement mechanistic-empirical (ME) design software AASHTOWare Pavement ME Design®; Project 01-51, *A Model for Incorporating Slab/Underlying Layer Interaction into the MEPDG Concrete Pavement Analysis Procedures*, which was completed in 2016; and Project 01-52, *A Mechanistic-Empirical Model for Top-Down Cracking of Asphalt Pavement Layers*, which is ongoing.[3–8]

With increasing use of flexible pavement rehabilitation, some State transportation departments have questioned the appropriateness of the MEPDG HMA overlay design methodology, specifically in determining the in-place damage of the existing HMA layers.[1] Although ME-based methodology is a great improvement to the 1993 American Association of State Highway and Transportation Officials (AASHTO) purely empirical HMA overlay design procedure, some concerns that have been identified related to its use include the following:[9]

- The rehabilitation input-level-1 procedure for characterizing existing HMA pavement structural capacity/condition was never verified but was recommended for the rehabilitation design of higher-volume roadways.[1] The procedure is based on falling weight deflectometer (FWD) deflection testing, backcalculated elastic layer moduli, coring, and laboratory testing of the HMA cores (mixtures and binder properties) to determine the in-place damage of the HMA. The in-place damage has a significant effect on the fatigue cracking predictions and requires overlay thickness to satisfy the design criteria.

- Rehabilitation input levels 2 and 3 were used during the calibration process under NCHRP project 1-37A and are based on the amount of load-related fatigue cracking and condition rating, respectively.[1] Input level 2 was used during the initial calibration process, but many State transportation departments are using input-level-3 surface-condition ratings. Use of input level 3 is, at best, highly subjective and includes both load and non-load-related distresses.

As such, there is a need to confirm use of the in-place fatigue damage index (DI) in selecting a rehabilitation strategy for a specific project and determining the overlay thickness.

PROJECT OBJECTIVE

The objective of this research was to evaluate the existing overlay design procedure using the MEPDG input-level-1 rehabilitation methodology and provide enhancements to the procedure if required.[1] In other words, the objective was to provide proof of concept for estimating the in-place damage of HMA layers for use in rehabilitation design. If enhancements were found to be needed, researchers sought to develop and calibrate those enhancements for characterizing existing flexible pavement damage for HMA and PCC overlay design that can be integrated into the current MEPDG software, AASHTOWare Pavement ME Design®.[3,4]

SCOPE OF WORK

The technical approach, or scope of work, for this research was completed in a series of task activities, which are summarized as follows:

- **Task 1**: Collect and review literature.

- **Task 2**: Develop an experimental plan and extract Long-Term Pavement Performance (LTPP) data. Task 2 subtasks include the following:

  - **Task 2.1**: Select sites.

  - **Task 2.2**: Extract LTPP data.

- **Task 3**: Assemble data and perform a preliminary data analysis. Task 3 subtasks include the following:

  - **Task 3.1**: Review deflection data and determine backcalculated moduli.

  - **Task 3.2**: Determine FWD load frequency.

  - **Task 3.3**: Review LTPP HMA dynamic modulus (E^*) data and adjust for aging.

  - **Task 3.4**: Establish time–series history of the ratio of field-derived backcalculated elastic layer modulus using static analyses (E_{FWD}) to the laboratory-derived undamaged dynamic modulus predicted from master curve parameters representing a specific temperature and load frequency (E^*_{PRED}) (i.e., the ratio is expressed as E_{FWD}/E^*_{PRED}).

- o **Task 3.5**: Develop an enhancement plan to MEPDG models.

- **Task 4**: Verify and enhance current MEPDG approach.[1] Task 4 subtasks include the following:

  - o **Task 4.1**: Verify and enhance HMA damaged modulus master curve.

  - o **Task 4.2**: Verify and enhance HMA fatigue damage model.

  - o **Task 4.3**: Apply deflection indices and dissipated energy in levels 2 and 3 of the rehabilitation design.[1]

  - o **Task 4.4**: Verify fatigue endurance limit with FWD backcalculated layer moduli.

- **Task 5**: Develop recommendations for enhancements to the MEPDG software, AASHTOWare Pavement ME Design®.[2–4]

ORGANIZATION OF REPORT

This report is organized by chapters that describe the work completed and findings from each task listed in the scope of work. The following list details the chapters and information included within each chapter:

- Chapter 2 provides an overview and summary of the methods used to estimate damage in terms of the in-place structural condition of HMA layers for use in rehabilitation design (i.e., selecting an appropriate repair strategy and determining overlay thickness). This chapter also identifies some of the confounding factors and/or issues that present a challenge in confirming the appropriateness of determining the in-place structural condition of flexible pavements for rehabilitation design.

- Chapter 3 presents the experimental plan and identifies the candidate LTPP test sections that were used in the preliminary analyses for providing proof of concept regarding the different MEPDG rehabilitation input levels. This chapter also provides a discussion on how the sites were selected relative to the experimental sampling matrix or factorial and identifies the data extracted from the LTPP database for use in the analyses.[10]

- Chapter 4 discusses the process used to determine the backcalculated elastic moduli for the HMA layers and the analysis of those values to determine the in-place elastic modulus (E) of the HMA layers. The backcalculated elastic moduli were used to establish the most representative damaged modulus master curve for each test date. It also reviews the variability of the in-place E and the procedure used to reduce that variability for this project.

- Chapter 5 applies the process for calculating the in-place damage in accordance with the MEPDG rehabilitation input level 1 and presents the results for providing proof of concept relative to the ME approach embedded in the MEPDG for flexible pavements.

- Chapter 6 uses dynamic backcalculation to confirm some of the observations made from the preliminary analyses presented in chapter 5. Specifically, this chapter compares HMA laboratory-derived dynamic modulus master curves representing the condition without fatigue damage ($E^*_{undamaged}$) to field-derived damaged dynamic modulus master curves created from E_{FWD} values ($E^*_{damaged}$) and compares the FWD backcalculated frequencies using static analyses to those from dynamic analyses.

- Chapter 7 explains and summarizes the bottom–up fatigue cracking–strength relationship and transfer function calibration coefficients for the individual sections included in the preliminary analysis. These project-specific calibration coefficients were used to evaluate and compare the predicted and measured bottom–up fatigue cracking of flexible pavements to verify the relationship between damage as estimated through the backcalculated elastic layer moduli and the amount of cracking.

- Chapter 8 lists and discusses the major findings and conclusions from this study.

CHAPTER 2. DAMAGE CHARACTERIZATION

The accurate structural condition of existing asphalt concrete (AC) pavements is a key input for the design of AC or PCC overlays.[1] Various pavement design procedures provide guidance on how to determine the structural condition of existing AC pavement.[1,9] The design procedures range from using pavement surface distresses (cracking, rutting, smoothness, etc.) to nondestructive testing (NDT) methods. NDT involves the use of FWD deflection basins to measure pavement responses, ground-penetrating radar (GPR) to evaluate layer thickness and volumetric properties, and/or seismic testing (through the use of a portable seismic pavement analyzer) to determine mixture integrity.

The use of deflection basins for pavement evaluation varies from identifying design segments and location of destruction samples to estimating the in-place damage of the AC layers. The MEPDG is one of the latest rehabilitation design procedures that recommends the use of FWD deflection basins to estimate the structural condition of all pavement layers, including the AC layers.[1] Deflection-based overlay design methods, however, do not explicitly account for all distresses individually. The overall AC-layer damage is reflected in terms of increased pavement deflection that is used as input in the calculation of overlay thickness.

A review of various overlay design methods, including the MEPDG methodology, was conducted to (1) identify any shortcomings with the current MEPDG procedure, (2) summarize the state of practice, and (3) recommend how the current MEPDG procedure can be improved with the state of practice.[1] This chapter presents the outcome of the review of various techniques and methodologies used to characterize existing AC pavement structural condition.[2]

AC DAMAGE DEFINITION

Damage in AC layers results in a loss of stiffness that is commonly referred to as "softening" by the authors. This loss of stiffness is initially caused by microcracks in the AC layer, which eventually formulate into macrocracks that are observed and measured at the pavement's surface. These microcracks can be caused by repeated loads from truck traffic and/or moisture-related damage. The microcracks and macroacks result in increased deflections around the loaded area. Fatigue cracking and moisture damage are the two most important distresses that reduce the stiffness of the AC layer.

The causes of structural distresses in pavements can be attributed to a combination of traffic loading, materials, subgrade, environment, and construction with one or more being the predominant cause for a given situation. The overall condition of the existing pavement, regardless of the causes of deterioration, has a major effect on existing AC pavement structural condition and, thus, the outcome of AC or PCC overlay design. Quantifying the existing AC pavement structural condition (i.e., extent of damage/deterioration) is important to a successful

---

[1]The terms HMA and AC are used interchangeably within this report and have the same meaning. HMA is used more in the existing literature, while AC is used within the MEPDG AASHTOWare Pavement ME Design® software input screens and other MEPDG-related documents.[3,4,1]

[2]A more comprehensive review of the literature was provided in the unpublished 2015 interim report, *Task 1— Interim Report, Literature Review*. This report provided information and discussion on establishing directions of future tasks.

rehabilitation project. Traditional overlay design methods mostly consider only fatigue cracking, which is a load-related distress, as the primary cause of damage in the AC layer.

AC DAMAGE CHARACTERIZATION METHODS

State transportation departments use various methods to characterize structural conditions of existing flexible pavement for AC and PCC overlay designs. The approaches can be broadly categorized as follows:

- **NDT approach**: Measuring deflection basins and relating those to structural condition.

- **Destructive testing approach**: Conducting destructive testing (coring and lab examination and testing of cores) to assess pavement layer condition/damage and relating that to structural condition.

- **Distress survey approach**: Performing a survey of pavement surface condition and relating that to structural condition.

The NDT and distress survey approaches are suggested for use in the MEPDG.[2] The destruction testing approach is integrated into these two approaches and used to confirm the condition and physical features and/or properties derived from the other two approaches. NDT involves examining the pavement by means that do not induce damage or change the pavement structure. In accordance with the MEPDG, NDT involves performing FWD testing to determine pavement deflections, GPR testing to determine pavement thickness, and profile and friction testing to determine surface characteristics of the pavement.

Profile and friction testing define the functional adequacy or condition of the existing AC pavement. Functional condition was not a focus of this study, so it was excluded from the literature review. The NDT approach and distress survey approach are discussed in the following sections.

Deflection-Based Methods—NDT Approach

Deflection-basin testing is a quick method used to assess the structural capacity and condition of pavement sections as well as the characterization of base and subgrade stiffness properties. Pavement evaluation procedures using deflection basins for rehabilitation design can be grouped into two broad categories: (1) deflection-basin parameters or indices and (2) backcalculation of E from deflection-basin data.

Two recent studies sponsored by the Federal Highway Administration (FHWA) focused on the use of FWD deflection data to establish the in-place condition of the pavement structure.[11,12] Smith et al. conducted an earlier study that focused on using FWD deflection data for project-level pavement evaluation and rehabilitation design in accordance with the MEPDG.[11] The latter study was conducted by Carvalho et al., which focused on using simplified techniques to interpret FWD deflection data for network-level pavement analysis.[12] Both studies reviewed analysis techniques and deflection-derived parameters to estimate the condition of existing pavements. Smith et al. targeted the backcalculation process of computing elastic layer moduli

from deflection basins for the project-level analysis, while Carvalho et al. targeted using deflection-derived indices for the network-level analysis.[11,12]

Deflection-Basin Indices

Deflections measured near the load plate are primarily influenced by the behavior of the surface and near-surface layers, while deflections measured further from the load plate indicate the subgrade and embankment responses. Both the magnitude and shape of the deflection basin highly depend on the stiffness and thickness of each pavement layer. As a result, different deflection-basin parameters have been used to infer the relative stiffness or condition of individual pavement layers. The deflection-based indices that have been used to evaluate the condition of the bound or surface layers, unbound aggregate base layers, and subgrade are defined as shown in the equations in figure 1 through figure 6.

The curvature index (CI) is defined as the difference in deflections measured at two distinct locations, as shown by the equation in figure 1. This is a general equation that relates to multiple deflection indices. A special case of CI is obtained when the deflection measured at radial distance (i) from the FWD loading plate (d_i) equals the deflection measured under the FWD loading plate (d_0). Also, deflection measured at a sensor located j inches from the falling weight deflectometer loading plate (d_j), where j is the axle load interval or distance between a sensor and the loading plate, equals the deflection measured at a sensor located 12 inches from the FWD loading plate (d_{12}) and has been referred to as the surface curvature index (SCI), as shown by the equation in figure 2. The subscript number following the deflection variable d (e.g., d_{12}) represents the radial distance in inches of deflection measurement from the loading plate.

$$CI = d_i - d_j$$

Figure 1. Equation. CI.

$$SCI = d_0 - d_{12}$$

Figure 2. Equation. SCI.

Similarly, other CIs that are frequently used include the base damage index (BDI) and the base curvature index (BCI), as defined in figure 3 and figure 4, respectively.

$$BDI = d_{12} - d_{24}$$

Figure 3. Equation. BDI.

Where d_{24} is the deflection measured at a sensor located 24 inches from the FWD loading plate.

$$BCI = d_{12} - d_{36}$$

Figure 4. Equation. BCI.

Where d_{36} is the deflection measured at a sensor located 24 inches from the FWD loading plate.

In addition, the area under pavement profile (AUPP) has also been used for characterizing the condition of AC layers. AUPP is defined as the area below the deflection basin (see figure 5).

$$AUPP = \frac{5d_0 - 2d_{12} - 2d_{24} - d_{36}}{2}$$

Figure 5. Equation. AUPP.

The 1993 *AASHTO Guide for Design of Pavement Structure*s introduced an area parameter, A_{36}, defined as the area of the first 36 inches of the deflection basin for the analysis of rigid pavements.[9] However, Stubstad et al. indicated that A_{36} was inappropriate for use with flexible pavements due to the smaller radius of curvature (i.e., steeper deflection basin).[13] Consequently, the researchers derived a new area parameter, A_{12}, which is defined as the area of the first 12 inches of the deflection basin. This parameter was subsequently used in their forward-calculation model for flexible pavements. The new area parameter (A_{12}) is expressed in figure 6.[13]

$$A_{12} = \frac{2(2d_0 + 3d_8 + d_{12})}{d_0}$$

Figure 6. Equation. A_{12}.

Where d_8 is the deflection measured at a sensor located 8 inches from the FWD loading plate.

The most common indices used to characterize the AC layers are SCI, BCI, and AUPP. State transportation departments that have used these indices for evaluating the condition of the pavement include the Florida Department of Transportation (FDOT), the Texas Department of Transportation, the Utah Department of Transportation (UDOT), and the Virginia Department of Transportation (VDOT), to name a few. FDOT initially used a Dynaflect trailer to measure deflection basins as part of its pavement management program. Through years of measuring deflections and monitoring the surface condition, FDOT observed cracks shortly after the deflection started to increase.[3] Thus, a rehabilitation project was planned when FDOT observed an increase in the normalized deflection basins. As such, there are data to show trends or relationships between the deflection basin indices and forms of cracking. The accuracy of these relationships, however, has not been clearly defined.

Forward-Calculated Layer Response Properties

Several of the previously mentioned deflection-basin indices or parameters were used to calculate the modulus and critical strain in the AC layer. The most common forward-calculation procedure for estimating the modulus of the pavement and subgrade is the 1993 *AASHTO Guide for Design of Pavement Structure*s.[9] The subgrade's resilient modulus is calculated from the measured load and resulting deflection at a distance from the center of the load. The pavement

---

[3]This finding is based on an in-person discussion between an FDOT pavement management engineer and Harold Von Quintus in the early 1980s; the month and year of the interview and discussions were not documented for historical records.

composite E is calculated using different factors. Individual layer E values are not determined, so estimating the in-place damage from these values becomes problematic.

Multiple correlations or regression equations have been developed between the deflection-basin indices and the AC modulus and tensile strain. Some of these are shown in figure 7 through figure 12. Unless otherwise noted, the units used in the equations presented in the following figures are English units (i.e., mil for deflection, inches for thickness, microstrain for strains, and kilopounds or pounds per square inch for modulus).

The equations shown in figure 7 and figure 8 were developed by Xu et al. for prediction of the elastic modulus of the AC layer (E_{ac}) and the tensile strain at the bottom of the AC layer (ε_{ac}), respectively.[14,15]

$$\log(E_{ac}) = -1.7718 \cdot \log(SCI) + 0.8395 \cdot \log(BDI)$$
$$- 2.5124 \cdot \log(H_{ac}) - 0.0762 \cdot H_{ac} + 5.09186$$

Figure 7. Equation. Prediction of HMA modulus from SCI and BDI.

Where H_{ac} is the thickness of the AC layer.

$$\log(\varepsilon_{ac}) = 0.5492 \cdot \log(SCI) + 0.3850 \cdot \log(BDI)$$
$$+ 0.7812 \cdot \log(H_{ac}) - 0.04318 \cdot H_{ac} + 4.14515$$

Figure 8. Equation. Prediction of HMA critical strain from SCI and BDI.

Similar to figure 7 and figure 8, Kim and Park developed the equations in figure 9 and figure 10 for calculating E_{ac} and ε_{ac}.[16]

$$\log(E_{ac}) = -1.103 \cdot \log(SCI) - 1.183 \cdot \log(H_{ac}) + 4.356$$

Figure 9. Equation. Prediction of HMA modulus from SCI.

$$\log(\varepsilon_{ac}) = \begin{cases} 1.082 \cdot \log(BDI) + 0.259 \cdot \log(H_{ac}) + 1.409 \\ 1.034 \cdot \log(AUPP) + 0.932 \end{cases}$$

Figure 10. Equation. Prediction of HMA critical strain from BDI and AUPP.

Garg and Thompson developed and proposed a correlation between AUPP and ε_{ac}, as shown in figure 11.[17]

$$\log(\varepsilon_{ac}) = 0.821 \cdot \log(AUPP) + 1.2105$$

Figure 11. Equation. Prediction of HMA strain from AUPP.

Thompson developed an equation to calculate E_{ac} from the *AREA* parameter, AC thickness, and deflection measured under the loading plate.[18] The *AREA* parameter used in figure 12 is the area enclosed within the undeflected pavement surface and the deflection basin within 3 ft radial distance from the FWD loading plate ($AREA_{36}$) rather than the area enclosed within the

undeflected pavement surface and the deflection basin within 12 inches radial distance from the FWD loading plate ($AREA_{12}$), as $AREA_{12}$ is believed to be more suitable for flexible pavements due to the smaller radius of curvature (i.e., steeper deflection basin).[9,18]

$$\log(E_{ac}) = 1.76 \cdot \log(AREA / d_0) + 0.26 \cdot (AREA / H_{ac}) + 1.48$$

Figure 12. Equation. Prediction of HMA modulus from *AREA* parameter.

A deflection–strain relationship was developed by Thyagarajan et al. for loading conditions corresponding to both the FWD and rolling wheel deflectometer (RWD).[19] The layered linear elastic analysis program, Jacob Uzan Layered Elastic Analysis (JULEA), was used to develop the deflection–strain relationship from the calculated deflection and strains from randomly generated pavement structures.[1] JULEA is a layered elastic program embedded in the AASHTOWare Pavement ME Design® software for calculating pavement responses from wheel loads.[3,4] Curvature indices computed from two surface deflections of high-speed deflection data were found to be good measures to capture variation in structural capacity on a network level. The study showed that tensile strains estimated from deflections from high-speed continuous deflection equipment were effective indicators of structural capacity, and this was validated using advanced modeling and FWD testing.[19]

Similarly, VDOT compared the deflection results obtained from the RWD and FWD on three routes to compare pavement deterioration in the form of cracking to changes in pavement response.[20] Results of this study indicated that the range of FWD and RWD deflection values were similar. The RWD and FWD deflection values, however, did not correlate well. A confounding factor within the study was the potential influence from seasonal variability of RWD and FWD deflection readings. Mostafa et al. conducted a similar study in Louisiana on 16 sites with various pavement types to assess the repeatability and characteristics of RWD measurements, the effect of truck speeds, and the relationship between RWD and FWD deflection measurements and pavement conditions.[21] Results indicated that RWD deflection results were repeatable and in general agreement with FWD deflection measurements. The mean center deflections from the RWD and FWD, however, were statistically different for 15 of the 16 sites.

In summary, different regression equations have been developed to predict E_{AC} and critical tensile strain from different deflection-basin indices and other parameters. Most of these regression equations, however, are in the form of a multivariate linear model when the logarithmic transformation is taken on the variables. Such a finding suggests that a similar model could possibly be established based on the most recent LTPP data.[10] If the deflection-basin indices can be successfully correlated to the MEPDG-computed DI and in-place moduli, then it may provide a more objective means for characterizing the HMA damage for rehabilitation input levels 2 and/or 3.

E_{FWD} *Values*

Some agencies backcalculate E for each pavement structural layer to determine the in-place condition similar to the MEPDG procedure for rehabilitation input level 1. The following list briefly discusses some of the procedures to characterize the in-place structural condition of the AC pavement layers:

- The relationship between surface cracking and structural capacity of pavement structures was investigated using field data from FHWA testing facilities.[22] Results indicated that the backcalculated moduli of the HMA layers were reduced by 50 percent before any cracking appeared on the surface. This demonstrated the loss of structural capacity of HMA pavements before surface cracking and the fact that using surface cracking by itself (rehabilitation input level 2) to assess damage might underestimate cumulative damage.

- Yin presented a mechanistic approach to simulate full-depth flexible pavement responses when subjected to FWD loads assuming that all materials were linearly elastic.[23] Results indicated that the average adjusted moduli from laboratory testing for surface layers were about 70 percent of the backcalculated values.

- A methodology to backcalculate the E^* master curve of the AC layer using a time history of FWD surface deflections was developed by Kutay et al.[24] The method utilized a layered-viscoelastic forward-algorithm in an iterative backcalculation procedure for linear viscoelastic characteristics of asphalt pavements. By using deflection–time histories from a typical FWD test, it is possible to backcalculate the relaxation modulus curve up to about a time (t) of ~10^{-1} s and the complex modulus ($|E^*|$) curve for frequency values of 10^{-3} Hz and greater. This study noted that the relaxation modulus–determination procedure is highly dependent on deflection data, as readings from individual drops are often truncated and result in insufficient information for calculation of relaxation modulus.[24]

- Deflection basins were and are being measured along the National Center for Asphalt Technology (NCAT) test track to evaluate the change in structural response with time and traffic.[25] Instrumentation has also been installed in selected test sections at the NCAT test track to measure tensile strain and deflection and how these change with pavement deterioration. Instrumentation was also placed at Minnesota's cold-weather-pavement-testing facility, MnROAD; the WesTrack test facility in Nevada; and other test facilities. An FWD was used to measure deflections over time. One of the authors backcalculated elastic layer moduli and concluded that the results from these facilities supported the hypothesis that an increase in deflections was related to layer deterioration or fatigue cracking. The backcalculated elastic layer moduli of the AC also supported the reduction in elastic layer moduli with increasing amounts of load-related cracking.

Pavement Distress–Based Methods—Distress Survey Approach

Pavement distress and/or performance indicators are also used to characterize the structural condition of the existing AC layer. Fatigue cracking of AC has been widely used as the primary distress measure for determining the condition factor in most overlay design methods. Other forms of cracking (e.g., longitudinal, transverse, and edge), rutting, and material-related distresses (raveling) have also been used to characterize damage in flexible pavements. Longitudinal cracking is either reported separately as wheelpath (WP) and non-WP cracks or combined into total crack length. Factors such as patching, roughness, and ride-quality indicators, which are used to calculate the overall distress index, do not quantify the structural condition of the pavement and were therefore excluded from this study.

Individual surface distresses measured for flexible pavements are converted to an overall performance indicator for characterizing damage. The distress indicators to quantify the structural condition of the pavement, however, vary from agency to agency. A Delaware Department of Transportation study reviewed indicators used by several States and classified them into the following two categories:[26]

- **Estimated condition indicators**: Ratings are derived from visual examination of pavement distress conditions and are reported qualitatively from very poor (lowest) to excellent (highest).

- **Measured condition indicators**: Ratings or indices are calculated from field-measured distresses (both magnitude and severity) using mathematical models. Some State transportation departments use agency-specific indicators, which are different from those included in the LTPP Infopave[TM] website. For example, the Georgia Department of Transportation (GDOT) related its total load-cracking number to the percent of total lane area with fatigue cracking, which was used to estimate the in-place damage of the AC layers for using the MEPDG for rehabilitation design.[27]

Overall, distress ratings or condition indicators are used to monitor pavement condition with respect to structural health and ride quality. Several State transportation departments use condition rating indices to estimate the structural condition of AC from various measured pavement distresses.[28] The indices are calculated by defining the types of distresses to be measured and the severity levels and magnitude of each distress, which are then weighted to compute a final index representing the structural condition of the pavement.[28,29] From the literature review completed under this project, the authors found no relationship between individual distresses or indices and the damage accumulated in the existing AC layer for the purpose of overlay design.

The Asphalt Institute (AI) and AASHTO empirical overlay design methods are known as component analysis methods, which translate pavement performance data into equivalency factors or indices for existing AC layer characterization.[30,9] The conversion factors compare the structural condition of the pavement at the time of distress measurement to that of a new pavement.[31]

AI Method

Condition assessment of various pavement layers is used to calculate remaining life of the pavement in the AI method.[30] The constituent layers of a pavement are converted to an equivalent AC thickness using a conversion factor for each layer. The conversion factors are based on performance measures for different pavement layers such as the following:

- **AC surface**: Cracking, rutting, bleeding, raveling, and aggregate degradation.

- **Cement-treated bases**: Pumping and instability.

- **Granular subbase or base courses and natural subgrade**: Gradation, Atterberg limits, and strength (typically defined by the California bearing ratio).

The conversion factors are multiplied with the corresponding layer thicknesses to calculate the effective pavement thickness, which represents damage induced by the previously mentioned factors. Overlay design thickness is then calculated as the difference between the thickness required for a new pavement designed for estimated future traffic and the computed effective thickness of existing pavement.

1993 AASHTO Guide for Design of Pavement Structures[9]

For flexible pavements, condition of the existing pavement is determined by varying the structural layer coefficient values in the standard structural number.[9] The layer coefficient values vary based on the amount of deterioration present in the existing layers, and the values assigned to the existing layers will be less than those assigned to materials with new construction. Limited guidance is provided in the guide for selection of the appropriate layer coefficient for existing layers. The 1993 AASHTO method determines the layer coefficient of the existing layers based on the amount of alligator and transverse cracking, as shown in table 1.[9]

Table 1. Suggested layer coefficients for existing pavement layer materials.

Material	Surface Condition	Coefficient
AC surface	Little or no alligator cracking and/or low-severity transverse cracking	0.35–0.40
AC surface	<10 percent low-severity alligator cracking and/or <5 percent medium- and high-severity transverse cracking	0.25–0.35
AC surface	>10 percent low-severity alligator cracking and/or <10 percent medium-severity alligator cracking and/or >5–10 percent medium- and high-severity transverse cracking	0.20–0.30
AC surface	>10 percent medium-severity alligator cracking and/or <10 percent high-severity alligator cracking and/or >10 percent medium- and high-severity transverse cracking	0.14–0.20
AC surface	>10 percent high-severity alligator cracking and/or >10 percent high-severity transverse cracking	0.08–0.15
Stabilized base	Little or no alligator cracking and/or low-severity transverse cracking	0.20–0.35
Stabilized base	<10 percent low-severity alligator cracking and/or <5 percent medium- and high-severity transverse cracking	0.15–0.25
Stabilized base	>10 percent low-severity alligator cracking and/or <10 percent medium-severity alligator cracking and/or >5–10 percent medium- and high-severity transverse cracking	0.15–0.20
Stabilized base	>10 percent medium-severity alligator cracking and/or <10 percent high-severity alligator cracking and/or >10 percent medium- and high-severity transverse cracking	0.10–0.20
Stabilized base	>10 percent high-severity alligator cracking and/or >10 percent high-severity transverse cracking	0.08–0.15
Granular base or subbase	No evidence of pumping, degradation, or contamination by fines	0.10–0.14
Granular base or subbase	Some evidence of pumping, degradation, or contamination by fines	0.00–0.10

MEPDG PROCEDURE FOR ESTIMATING DAMAGE IN ASPHALT PAVEMENTS[1]

An overview of the MEPDG methodology for estimating in-place damage of new and existing asphalt pavements is described in the following sections.[1]

New AC Layer

For newly placed HMA layers, the MEPDG calculates the incremental damage for performance simulation based on the cumulative damage concept given by Miner's hypothesis. Cumulative DI is defined as the accumulation of the incremental DI, which is determined as a function of the allowable and actual number of axle load repetitions. The equation for the cumulative DI is shown in figure 13.

$$DI = \sum (\Delta DI)_{j,m,l,p,T} = \sum \left(\frac{n}{N_{f-HMA}} \right)_{j,m,l,p,T}$$

Figure 13. Equation. Cumulative DI.

Where:

j = axle load interval.
m = axle load type (single, tandem, tridem, quad, or special axle configuration).
l = truck type using the truck classification groups included in the MEPDG.[1]
p = month.
T = median temperature for the five temperature intervals or quintiles used to subdivide each month (°F).
n = actual number of axle load applications within a specific time period.
N_{f-HMA} = allowable number of axle load repetitions, which is a function of AC E^*, tensile strain at critical locations, asphalt thickness, asphalt content, and air voids. It is calculated by the equation in figure 14.

$$N_{f-HMA} = k_{f1} \left(10^M \right) \left(C_H \right) \beta_{f1} \left(\varepsilon_t \right)^{k_{f2} \beta_{f2}} \left(E_{HMA} \right)^{k_{f3} \beta_{f3}}$$

Figure 14. Equation. Allowable number of load applications.

Where:

k_{f1}, k_{f2}, and k_{f3} = global field calibration parameters for fatigue cracking transfer function (from the NCHRP 1-40D recalibration), where $k_{f1} = 0.007566$, $k_{f2} = -3.9492$, and $k_{f3} = -1.281$.[32]
M = mixture regression coefficient, which is defined by volumentric properties (see figure 15).
C_H = thickness correction term, which is dependent on the type of cracking, as shown in figure 16 for bottom–up cracking and figure 17 for top–down cracking.
β_{f1}, β_{f2}, β_{f3} = local or mixture-specific field calibration constants. For the global calibration effort, these constants were set to 1.0.
ε_t = tensile strain at critical locations calculated by the structural response model (inch/inch).
$E_{HMA} = E^*$ of the HMA measured in compression (psi).

$$M = 4.84\left(\frac{V_{be}}{V_a + V_{be}} - 0.69\right)$$

Figure 15. Equation. *M*-value from volumetric properties.

Where:

V_{be} = effective asphalt content by volume (percent).
V_a = percent air voids in the HMA mixture.

$$C_H = \frac{1}{0.000398 + \dfrac{0.003602}{1 + e^{(11.02 - 3.49 H_{HMA})}}}$$

Figure 16. Equation. Thickness correction term for bottom–up area fatigue cracking.

Where H_{HMA} is the total thickness of all AC layers (inches) and e represents exponential.

$$C_H = \frac{1}{0.01 + \dfrac{12.00}{1 + e^{(15.676 - 2.8186 H_{HMA})}}}$$

Figure 17. Equation. Thickness correction term for top–down longitudinal fatigue cracking.

The percent total lane area of alligator cracking is calculated from the total DI (see figure 13) over time using a sigmoidal transfer function. The relationship used to predict the percent total lane area of alligator cracking (FC_{Bottom}) is shown in figure 18.

$$FC_{Bottom} = \left(\frac{1}{60}\right)\left(\frac{C_4}{1 + e^{\left(C_1 C_1^* + C_2 C_2^* Log(DI_{Bottom} * 100)\right)}}\right)$$

Figure 18. Equation. Transfer function for alligator cracking.

Where:

C_1, C_2, and C_4 = fatigue cracking transfer function regression constants where C_1 and C_2 = 1.00 and C_4 = 6,000.
C_1^* and C_2^* = transfer function regression coefficients, which are further defined in figure 19 and figure 20, respectively.
DI_{Bottom} = cumulative DI at the bottom of the AC layers.

$$C_1^* = -2C_2^*$$

Figure 19. Equation. Definition of C_1^*.

$$C_2^* = -2.40874 - 39.748(1 + H_{HMA})^{-2.856}$$

Figure 20. Equation. Definition of C_2^*.

Existing AC Layer

For existing AC layers, the MEPDG calculates the incremental DI using the same equation shown in figure 13.[1] The difference between new and existing AC layers is that a damaged master curve is defined and used for the existing AC layers based on their in-place condition. The damaged master curve becomes the basis for calculating future AC responses and fatigue damage in the existing AC layers after the placement of a new overlay. The MEPDG methodology does not continue to reduce the AC modulus with continued increases in the cumulative fatigue DI. In other words, the damaged master curve remains constant with continued truck loadings and additional fatigue damage.

As previously shown in figure 13, future damage of a new or existing AC layer is obtained as a function of the actual and allowable numbers of axle-load repetitions for simulation of cracking performance. The in-place damage of the existing pavement for rehabilitation design, however, is not related to the amount of traffic but to a reduction in modulus. To determine the modulus of an existing damaged AC layer, the MEPDG computes the undamaged AC modulus, which is then adjusted for existing damage, as shown by the equation in figure 21.[1] Note that E_{HMA} in figure 14 equals E^*_{PRED} in figure 21.

$$E^*_{damaged} = 10^\delta + \frac{E^*_{PRED} - 10^\delta}{1 + e^{-0.3 + 5log(d_{AC})}}$$

Figure 21. Equation. Asphalt E^* adjusted for d_{AC}.

Where:

δ = logarithm of the minimum undamaged E^*.
d_{AC} = fatigue damage in the existing asphalt layer, as calculated by the equation in figure 22.

$$Log(d_{AC}) = 0.2 \left[\ln \left(\frac{E^*_{PRED} - E_{FWD}}{E_{FWD} - 10^\delta} \right) + 0.3 \right]$$

Figure 22. Equation. Asphalt layer damage in terms of E_{FWD} and E^*_{PRED}.

The method for determining d_{AC} varies with the hierarchical input levels of the MEPDG. For input level 1, damage is determined through a combination of deflection testing and field investigation involving coring, inspection, laboratory testing, and evaluation to determine the existing mix volumetric parameters. More specifically, d_{AC} is estimated using a modulus reduction factor defined from E_{FWD} values from deflection basins. For input levels 2 and 3, the existing AC damage is determined from distress surveys and visual inspections. Input level 2 uses the amount of alligator cracking on the pavement surface, while input level 3 uses an overall condition-based pavement rating for assessment of existing damage.[1,3]

The following sections summarize how in-place damage is defined for each rehabilitation input level.

Rehabilitation Input Level 1: Backcalculated Elastic Layer Moduli

The damaged AC modulus is obtained through FWD testing in the WP at locations along the project. The FWD deflection data are used to backcalculate E_{FWD}, which represents $E^*_{damaged}$ at the FWD test temperature and frequency or reduced time (t_r). The damaged AC master curve is derived by adjusting the coefficients of undamaged master curve with E_{FWD}. The shift is defined as a vertical adjustment of the undamaged E^* master curve to match the results from the E_{FWD} values. The process is schematically shown in figure 23 and involves the following steps:

1. Determine E_{FWD} from deflection data where E_{FWD} represents or is equal to $E^*_{damaged}$.

2. Estimate an equivalent E^*_{PRED} from the undamaged modulus master curve at a reduced frequency that represents FWD test temperature and frequency. E^*_{PRED} is E^* measured in the laboratory.

3. Calculate AC damage from the equation shown in figure 22, which is the same equation in figure 21 but reorganized to yield the damage as a function of E_{FWD} and E^*_{PRED}.

4. Calculate the damaged modulus at other frequencies using the equation presented in figure 21 by substituting the damage calculated in step 3 and E^*_{PRED} at the corresponding frequencies.
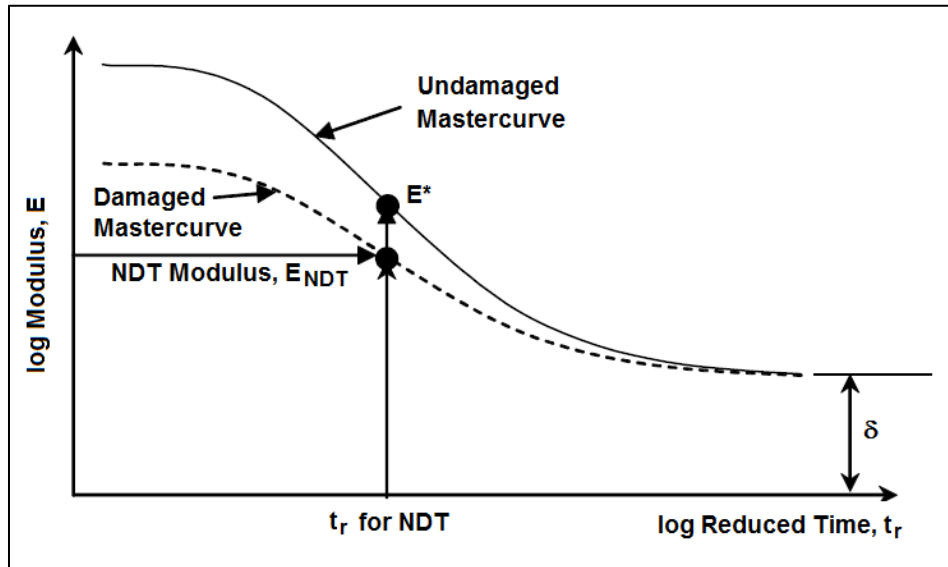
©Applied Research Associates, Inc.

E_{NDT} = backcalculated elasticlayer modulus. E_{NDT} equals E_{FWD} used in this report.

Figure 23. Graph. HMA layer–damage computation for level 1.[1]

The MEPDG rehabilitation input level 1 also assumes E_{FWD} and E^*_{PRED} for AC layers are the same with no fatigue damage. In other words, E_{FWD} is not adjusted by a factor to equal the results from laboratory-measured moduli unlike for unbound layers. E_{FWD} for aggregate base course layers and the subgrade are adjusted by the laboratory-to-field adjustment factor (*c*-factor) as an input to the MEPDG.[8] This assumption for the AC layer is debatable. For example, Yin found the AC moduli from laboratory tests for AC layers were about 70 percent of the

backcalculated moduli.[23] Similarly, Von Quintus and Killingsworth reported the difference or ratio between the laboratory-measured moduli using the indirect tensile test and backcalculated elastic moduli for AC layers was temperature dependent.[33] At cold temperatures (e.g., 40 °F), E^*_{PRED}/E_{FWD} was 1.0, while the ratio decreased to 0.36 at an intermediate temperature of 77 °F and to 0.25 at a high temperature of 104 ºF.

Rehabilitation Input Level 2: Total Area of Load-Related Alligator Cracking

The following steps are required to characterize damage in existing AC layers for hierarchical level 2:

1. Calculate the amount or percent of total lane area of alligator cracking measured on the pavement surface from the field condition survey.

2. Estimate d_{AC} from the amount of alligator cracking. This is done by substituting d_{AC} in the equation in figure 18 and then inverting the equation. The derived relationship is shown in the equation in figure 24.

3. Calculate the undamaged master curve and the damage calculated by the equation in figure 24. From this, the damaged master curve is obtained in a similar method as described for rehabilitation input level 1.

$$\log(d_{AC}) = \frac{\ln\left(\frac{C_4}{60 \cdot FC_{Bottom}} - 1\right) - C_1 C_1^*}{C_2 C_2^*} - 2$$

Figure 24. Equation. HMA layer damage computation for rehabilitation input level 1.

Rehabilitation Input Level 3: Pavement Condition Rating

For input level 3, d_{AC} is estimated based on general condition rating of the pavement, as shown in table 2. The general condition rating is typically determined using information derived from windshield distress surveys. The AASHTO *Mechanistic-Empirical Pavement Design Guide—A Manual of Practice* provides guidance on assigning a rating based on the existing pavement surface condition.[2] With the undamaged master curve and current damage, the damaged master curve is obtained in a similar method as described for rehabilitation input levels 1 and 2.

Table 2. In-place AC pavement damage based on pavement condition rating.

Condition Rating Category	DI
Excellent	0.00–0.20
Good	0.20–0.40
Fair	0.40–0.80
Poor	0.80–1.20
Very poor	>1.20

DISSIPATED WORK

Von Quintus and Killingsworth indicated that load and deflection–time histories measured by an FWD can be used to gain insight into whether pavement response is elastic or viscoelastic.[33] The study concluded that pavements showing significant viscoelastic behavior compared to elastic behavior exhibited increased magnitude of dissipated work, which is defined as the area under the load-deflection curve (i.e., hysteresis loop). Figure 25 and figure 26 show the load–deflection curves of two LTPP General Pavement Studies (GPS) sections from the study—the former showing elastic behavior of the pavement and the latter showing viscoelastic behavior.[33]
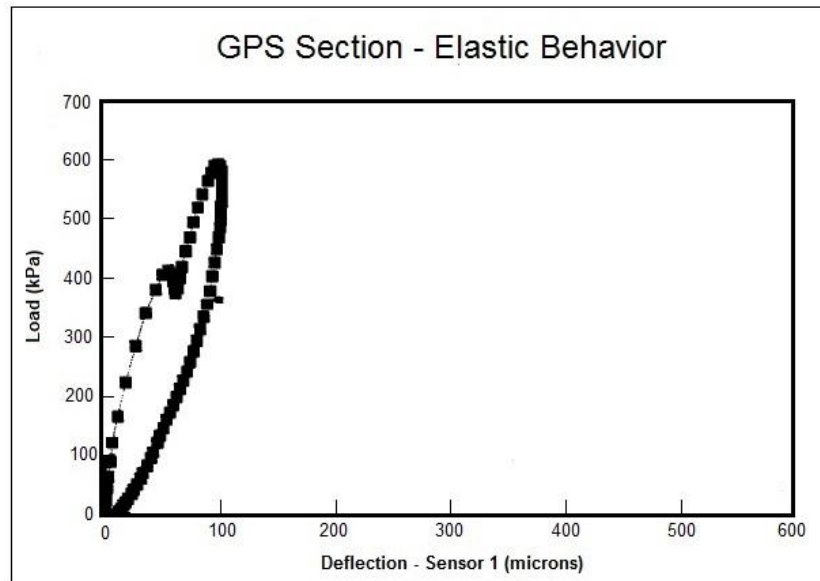
Source: FHWA.
1 kPa = 0.145 psi.

Figure 25. Graph. Hysteresis loop from a pavement showing elastic behavior.[33]

19
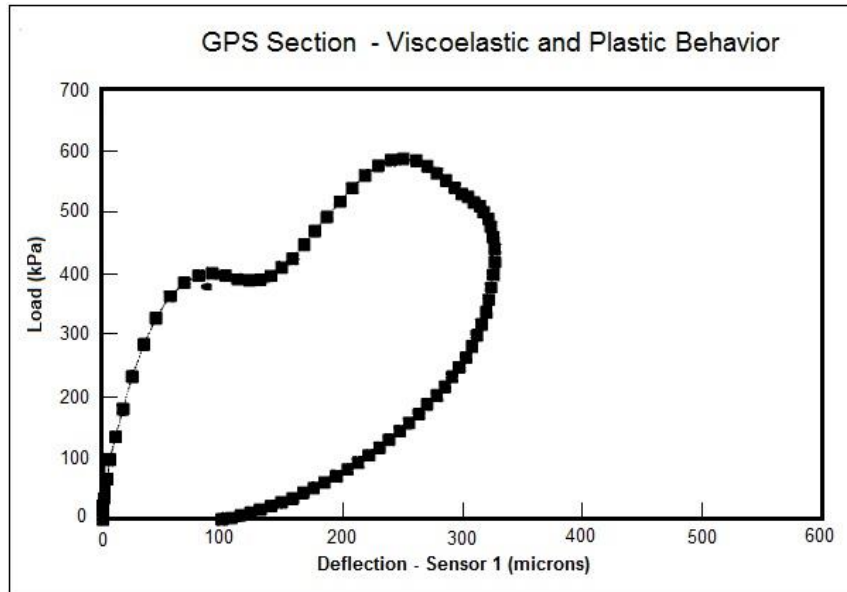
Source: FHWA.

1 kPa = 0.145 psi.

Figure 26. Graph. Hysteresis loops from a pavement showing viscoelastic behavior.[33]

Based on their cursory review of the LTPP data with various International Roughness Index values, distress magnitudes, and traffic levels, Von Quintus and Killingsworth hypothesized that dissipated work calculated from the FWD load–deflection curve was related to pavement deterioration and/or damage, similar to the dissipated energy defined as the area under the stress–strain curve and used in AC fatigue analysis.[33] In other words, pavements with greater dissipated work exhibited an increased amount and severity of different types of distresses, as shown in figure 27.[4] The question not addressed by Von Quintus and Killingsworth was whether the dissipated work from the FWD deflection–time series data was an indication of the quality of the mixture, or was the dissipated work a result of higher levels of distress.

As pointed out by Von Quintus and Killingsworth and verified by some field data shown by Deblois et al., Salour and Erlingsson, and Maruyama and Kumagai, the dissipated work varied significantly over the year due to the seasonal temperature fluctuations.[33–36] In addition, the dissipated work was also found to vary significantly for different pavement types and structures as well as number of applied traffic loadings. These findings suggest there is evidence showing dissipated work measured by an FWD is related to pavement distresses and/or damage. The dissipated work magnitude, however, is also associated with the viscoelastic nature of the asphalt material (e.g., effect of temperature), which is not related to damage.

---

[4]The one data point in figure 27 for "no distress" and a dissipated work value near 97 lbf-inch was believed to be an outlier. The potential cause or explanation for the outlier was not investigated.
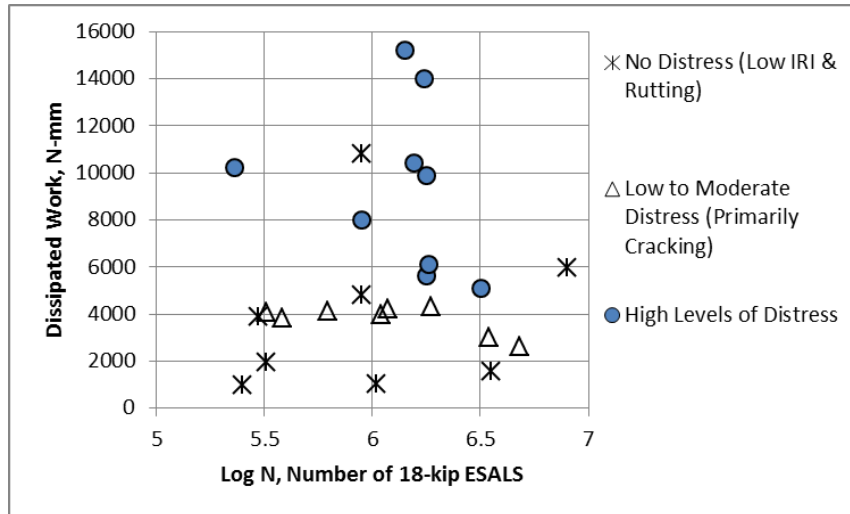
Source: FHWA.
1 N-mm = 0.00885 lbf-inch.
ESAL = equivalent single axle load.
IRI = International Roughness Index.

Figure 27. Graph. Comparison of dissipated work to pavement condition for different traffic levels for LTPP sites located in the southern region.[33]

Thus, the increase in dissipated work due to temperature and other viscoelastic effects should be isolated and separated from the actual damage or distress causing an increase in dissipated work. Broadly speaking, there are two potential approaches for achieving this as follows:

- **Empirical approach**: Adjust the magnitude of dissipated work to a standard temperature. This approach is similar to the temperature correction applied to the FWD deflections presented in the 1993 AASHTO and AI rehabilitation design procedures.[9,30]

- **Mechanistic approach**: Use a theoretical model capable of simulating the FWD deflection–time histories to obtain the dissipated work at various temperatures and moduli. In concept, this approach is similar to simulating the seasonal fluctuation of peak FWD deflections using a layered elastic program by increasing/decreasing the E_{ac} or increasing/decreasing the deflections being reflected through the decrease/increase in E_{FWD}.

CONFOUNDING FACTORS: LOADING FREQUENCY, PULSE DURATION, AND TEMPERATURE

As is true for any other rehabilitation design methodologies, E_{ac} is an important input for MEPDG overlay design methods. The major difference between MEPDG rehabilitation input level 1 when compared to levels 2 and 3 is that it uses E_{FWD} to assess the damage in the existing AC layer. However, the undamaged modulus at the temperature and frequency corresponding to FWD tests are needed to calculate the in-place damage (see figure 21 and figure 22). The FWD test temperature and loading frequency are directly used in reduced time computations for the undamaged modulus and have a significant impact on calculating fatigue damage. Thus, the

FWD test temperature and frequency are as important as the backcalculated modulus in rehabilitation designs using input level 1.

FWD loading pulse was recorded as a function of time rather than frequency. Von Quintus and Killingsworth investigated typical deflection–time history data collected during FWD testing and found that deflection–time data can be used as an indicator of the elastic and viscoelastic responses of HMA pavements.[33] For pavements with more elastic response, most of the deflection was recovered immediately after the load pulse reached zero (see figure 25) In the case of more viscoelastic responses, the deflection was recovered with a delay, and a certain time lag (or phase shift) existed between the load and deflection response (see figure 26.). The typical time range of the load pulse produced during FWD testing was 15–35 ms, and the time to recover all of the peak deflection varied between 25 and 60 ms. The variation in the FWD load duration as well as the inconsistent shape of the FWD load pulse contributed to the challenge in the conversion between time and frequency.

Dongre et al. summarized some of the simplified methodologies frequently used for time–frequency conversion, including the one currently used in the MEPDG as shown in table 3.[37] Among the list of studies shown in the table, Leiva-Villacorta and Timm and Hall used two different methodologies and studied the duration of the FWD load.[38,39] Despite the difference in the time–frequency conversion method, both studies suggest the loading duration (and hence frequency) induced by an FWD is equivalent to a vehicle traveling at a speed in excess of 120 mi/h. Based on this observation, these studies emphasized that time-frequency conversion of FWD loading pulses is a crucial component in reducing discrepancies between the pavement response under an FWD load and truck loading at highway speeds.

Table 3. Summary of different approaches for frequency and time conversion.

Source	Frequency/ Time Conversion
Guide for Mechanistic-Empirical Design of New and Rehabilitated Pavement Structures[1]	$t = 1/f$
Viscoelastic Properties of Polymers[40]	$t = 1/\omega$
Prediction of Deflection Response of Flexible Pavements under Dynamic Loads[33]	$t = 1/2f$
Falling Weight Deflectometer Loading Pulse Duration and its Effect on Predicted Pavement Responses[32]	$t = 1/f$

ω = angular frequency.
t = time.
f = frequency.

Furthermore, Chatti and Lee and Al-Qadi et al. stated that loading pulse induced by vehicular loading is not composed of a single frequency but a range of frequencies from 1.5 to 15 Hz.[41,42] This range of frequencies is a result of the vehicular loading pulse having different shapes and duration (e.g., single, tandem, tridem, and quad axles), which is also observed in the FWD loading pulse. Al-Qadi et al. stated the simplified methodologies shown in table 3 can be used for time–frequency conversion of the harmonic (sinusoidal) loading pulse encountered in laboratory tests, but they do not provide an accurate estimate of the loading frequency for vehicular loads.[42] To provide a methodology for estimating the frequency of a loading pulse with

arbitrary shape and varying duration, Al-Qadi et al. proposed the dominant frequency concept. Under this concept, the loading frequency is obtained by first transforming the loading pulse from the time domain to the frequency domain through the Fast Fourier Transform and then calculating the weight center of the frequency spectrum.[42] Al-Qadi et al. also concluded that the simplified methodologies shown in table 3 may underestimate or overestimate the dominant frequency of the load pulse, with the error in frequency estimation ranging from 40 to 140 percent with the MEPDG approach.

These findings indicate that there is no consensus on what FWD load frequency should be used and which method should be used for time–frequency conversion in rehabilitation designs. Although the suggested FWD loading frequency values found in the literature vary generally from 15 to 35 Hz, there is no clear understanding on how loading frequency (and duration) changes with AC-layer thickness and pavement temperature (i.e., an indicator of viscoelastic response), as well as the sensitivity of FWD load frequency to pavement response, fatigue damage, and overlay thickness.

SUMMARY OF ISSUES CONSIDERED IMPORTANT TO ACCURATE ESTIMATES OF IN-PLACE DAMAGE

Various distress rating methods and deflection testing-based indices that are used to characterize pavement structural condition for rehabilitation design were reviewed within this chapter. This section identifies and summarizes two important issues that need to be addressed to ensure an accurate assessment of the in-place damage for rehabilitation design in accordance with the *Mechanistic-Empirical Pavement Design Guide—A Manual of Practice*.[2]

Damage Assessment Differences Between Deflection- and Distress-Based Methods

Traditional distress-based overlay design methods, including MEPDG rehabilitation input levels 2 and 3, mostly consider load-related fatigue cracking as the primary result of damage in AC layers. Other types of cracking, however, do impact a pavement's resistance to movement under loads or deflection. Deflection-based overlay design methods do not explicitly account for all distresses individually but indirectly account for distresses that affect the deflection basin.

The disparity between the distress-based method (MEPDG rehabilitation input levels 2 and 3) and deflection-based method (MEPDG rehabilitation input level 1) can cause differences in selecting a rehabilitation strategy as well as in the required overlay thickness when using both methods for the same project. The authors of this report have seen significant differences in AC overlay thickness between using rehabilitation input levels 1 and 2 with everything else being equal for the same project. The following list briefly describes two unpublished non-LTPP projects for which large differences in overlay thickness were the outcome between using rehabilitation input levels 1 and 2:

- **Michigan project**: The MEPDG was used to check the rehabilitation strategy for an interstate highway that exhibited extensive premature alligator and longitudinal cracks in the WP. Distress surveys, FWD deflection tests, and borings were performed along the project to be rehabilitated. An AC overlay thickness in excess of 4 inches was required when using rehabilitation input level 2 because 20 percent fatigue cracks were recorded

at the surface, while no structural overlay was required when using rehabilitation input level 1. The FWD backcalculated elastic moduli were almost equal to the AC dynamic moduli derived from the laboratory undamaged modulus master curve. The cores recovered along the roadway showed the fatigue cracks were confined to just below the middepth of the wearing surface, which explained the difference in outcomes between using rehabilitation input levels 1 and 2.

- **Arizona project**: The MEPDG was used to check a rehabilitation design for a lower-volume secondary collector roadway that was in need of repair because of surface raveling but was also being upgraded to carry more truck traffic. Distress surveys, FWD deflection tests, and borings were performed along the project to be rehabilitated. No structural overlay was required when using rehabilitation input level 2 because only minimal fatigue cracks were observed or recorded during the distress survey. On the other hand, reconstruction or full-depth reclamation was the preferred rehabilitation strategy when using rehabilitation input level 1. The FWD backcalculated elastic moduli were significantly less than the AC dynamic moduli derived from the laboratory undamaged modulus master curve. Cores of the AC lower layers showed extensive moisture damage and stripping, which explained the difference in outcomes between using rehabilitation input levels 1 and 2.

In both of these examples, cores were available to explain the differences in overlay thickness. In other cases, however, the layer thicknesses were found to be inaccurate along the project, resulting in invalid backcalculated elastic moduli. Although cores should always be completed, when few or no cores are available, other parameters are needed to confirm or ensure the distress- and deflection-based methods provide similar values for in-place damage. AC-layer damage is reflected in terms of increased pavement deflection that is used as input in the calculation of overlay thickness. As such, other cracks and the type of crack may need to be considered in characterizing damage for overlay design.

Difference Between FWD and Laboratory Temperatures and Frequencies

Two AC moduli were needed to estimate the in-place damage of AC layers: E_{FWD} from FWD deflection basins and an E^*_{PRED} measured at the same temperature and frequency. To determine damage in accordance with the MEPDG, the undamaged E^*_{PRED} must have been determined at the same temperature and frequency from the FWD test. However, temperatures in the laboratory specimen were controlled and were equal throughout the test specimen, but in the pavement, temperatures varied with time and depth. A small load was applied to the test specimen in the laboratory at specified frequencies, but on the pavement, an impact load was applied by the FWD, and the load–time response varied. That time was dependent on temperature and thickness. More importantly, cracks and other defects in the AC layer probably affected the deflection–time response.

The *Mechanistic-Empirical Pavement Design Guide—A Manual of Practice* suggests that the middepth temperature of the AC layer be used and the frequency be within the range of 15 to 25 Hz.[2] Application of this guidance, however, can result in large differences between the laboratory-derived $E^*_{undamaged}$ and the field-derived, backcalculated $E^*_{damaged}$, even for AC layers that have been recently placed. Thus, the conversion from load pulse time to frequency and the

temperature effect need to be evaluated to provide better guidance in minimizing any difference between the damaged and undamaged moduli on mixtures recently placed, a condition for which no fatigue damage can be assumed. In other words, deflection–time histories conducted at selected LTPP sites were evaluated to calculate the representative load pulse frequency, which is an important factor for comparison of AC modulus backcalculated from FWD testing data with the corresponding modulus from undamaged master curve to estimate the amount of damage.

CHAPTER 3. EXPERIMENTAL PLAN AND DATA

As summarized in chapter 2, fatigue damage in the existing AC layer is characterized by a reduction of its modulus over time in comparison to the layer's modulus in its undamaged state under identical conditions of temperature and loading. The accumulation of fatigue damage is affected by several factors, including traffic, climate, moisture, materials, layer stiffness (thickness and modulus), and construction quality. Load-induced damage was observed on the pavement surface primarily as bottom–up fatigue (alligator) cracking and longitudinal cracking. As such, cracking measured on the pavement surface was used for fatigue damage assessment along with the in-place modulus.

This chapter presents the experimental plan and contains information about the sources and details of data extracted for this study. Databases were developed in Microsoft® Access™ and Microsoft® Excel™. Data extraction, calculations, and analysis were either performed directly within the databases or through programs written in C++/Microsoft® Visual Basic™. The following data were used in this study and are described in this chapter:

- Pavement performance indicators including various forms of cracking.

- E_{FWD} of the AC layers or the in-place pavement layer moduli backcalculated from FWD data. E_{FWD} represents a composite value where multiple layers were combined in the backcalculation process.

- $E*$ calculated from the Witczak regression equation embedded in the MEPDG AASHTOWare Pavement ME Design® software.[3,4]

- Properties of the AC layers within the pavement structure.

- Deflection-basin data including FWD deflection–time histories.

- General design information relative to the site features for each test section included in the analyses (e.g., climate and traffic).

EXPERIMENTAL ASSUMPTIONS AND HYPOTHESES

This section presents the assumptions and hypotheses used in evaluating the rehabilitation design methodology for flexible pavements. The assumptions set the stage for providing proof of concept for determining the in-place fatigue damage of AC layers.

Assumptions included the following:

1. Two types of load-related cracking occur in flexible pavements: (1) bottom–up area fatigue cracks that are identified as alligator cracks and (2) top–down linear cracks that are identified as longitudinal cracks within or adjacent to the WPs. The mechanism causing both types of cracks is the same (i.e., repeated tensile strains from truck axle loadings) as the hypothesis used in the MEPDG methodology.[1] The mechanism of repeated tensile strains at or near the top of the wearing surface for top–down longitudinal cracks, however, is debatable. The *Mechanistic-Empirical Pavement Design*

Guide—A Manual of Practice recommends
that top–down cracking be excluded as a design criterion for both new pavement and rehabilitation designs.[2] In addition, NCHRP project 01-52 was authorized to confirm the mechanism for top–down cracking or develop a new methodology.[8] As such, top–down cracking was excluded from this study in terms of damage accumulation, but longitudinal cracks in the WP were included and added to the total amount of cracking observed at the pavement surface. It was assumed that cracks within or adjacent to the WP (alligator or longitudinal) will impact the deflection basin and result in a loss of stiffness of the AC layer if the cracks propagate through the AC layer.

2. Few forensic investigations have been performed on newly constructed flexible pavements within the LTPP program. Thus, it was assumed that (1) all cracks within or adjacent to the WPs were bottom–up fatigue cracks and were combined for the analyses, (2) all AC layers and lifts were fully bonded, and (3) none of the AC mixtures for the selected test sections exhibited moisture damage or stripping. The amount of cracking observed over time at each LTPP test section was evaluated to identify anomalous cracking data that could be the result of other factors, such as debonding between AC layers, stripping or moisture damage in the AC mixture, and cracking that is restricted to the wearing surface or upper AC layers.

3. E_{FWD} is equal to E^*_{PRED} at the same temperature and load frequency without any fatigue damage. In other words, it was assumed no adjustment was needed for translating field-derived (E_{FWD}) to laboratory-derived (E^*_{PRED}) moduli.

Hypotheses included the following:

1. The mechanism causing top–down and bottom–up cracks is the same—repeated tensile strains from truck axle loadings. Top–down cracking is defined by the tensile strain adjacent to the wheel at or near the surface of the pavement, while bottom–up cracking is defined by the tensile strain at the bottom of the AC layer.

2. The amount of cracking is directly related to or caused by damage accumulation in the form of the DI, as defined by figure 13. With accumulated damage, there is a threshold DI value for which cracks will propagate through the AC layers and will be observed at the pavement surface. These cracks result in a softening of the AC layer or lower dynamic moduli.

3. Damage in the AC layer can be solely simulated as a softening effect or loss of modulus from its original condition at the time of placement. No in-place fatigue damage should exist in the AC layers shortly after placement. As such, the ratio of E_{FWD} and E_{PRED} should be unity. As cracking increases, the modulus ratio should decrease.

4. The AC E^* master curve, air voids, and effective asphalt content by volume can be used to accurately predict the occurrence of bottom–up fatigue cracks. In other words, one set of fatigue strength coefficients is applicable to and can explain differences in fatigue cracking between projects for all AC mixtures placed within the LTPP program (see figure 14).

5. Crack propagation is independent of AC mixture type and asphalt grade and only affected by the magnitude of the fatigue DI. Finn et al. applied this hypothesis to the American Association of State Highway Officials (AASHO) road test cracking data and derived the intercept of the fatigue relationship (K_{f1} in figure 14) for different amounts of fatigue cracking.[43]

EXPERIMENTAL SAMPLING MATRIX/FACTORIAL

An experimental sampling matrix or factorial was prepared to select candidate LTPP test sections for providing proof of concept for determining the in-place damage of AC layers in accordance with the MEPDG methodology. Factors that affected the structural condition or in-place damage of the existing AC layer can be grouped into the following four basic categories:

- **AC-mixture-property-related factors**: Include AC volumetric properties such as air voids and asphalt content. These also include asphalt stiffness or performance grade.

- **Pavement- or structure-related factors**: Include layer thickness, layer stiffness properties (i.e., aggregate base layers and subgrade), and interlayer bonding.

- **Site features or related factors**: Include traffic loadings and volume as well as climate or temperature.

- **Outcome- or performance-indicator factors**: Include amount and/or rate of cracking to evaluate the transfer function or the relationship between the cumulative DI and cracking.

An experimental matrix was designed to include sites that have a range of these factors. However, there is an interrelationship between some of the factors, so only the primary factors were used in identifying sites to be included in the sampling matrix. Primary factors included the following:

- AC thickness and traffic were interrelated for the GPS sites because these projects represent individual projects where the AC-layer thickness was determined for various site features including traffic. As traffic increased, AC thickness increased, while all other factors remained constant. For the Specific Pavement Studies (SPS)-1 projects, however, test sections with different AC-layer thicknesses were constructed along the same project. In either case, AC-layer thickness was identified as the primary factor, while traffic was a secondary factor.

- Interlayer bonding had a significant impact on fatigue cracking and performance, and bond (full transfer of shear) between all AC layers was assumed for the LTPP test sections. Cores were only taken at one point in time for many of the LTPP sites, so it was difficult to confirm that any cracking observed at the surface was a result of debonding or some other mechanism. As such, it was excluded as a primary factor in the sampling matrix, and it was assumed that all layers were bonded together. There were LTPP sections, however, which were believed to exhibit debonding. Some of these sections were identified and included in the sampling matrix in terms of cracking progression or the increase in cracking over time. As an example, the fatigue cracking reported for many

of the Iowa SPS-1 test sections increased from nearly 0 to over 50 percent within 1 yr.[10] This increase in cracking would not be solely caused by traditional repeated truck loadings.

- Asphalt stiffness is another factor that is related to other material properties and mixture components in addition to climate, which can have a significant impact on the increase in cracking over time. For cold climates, softer asphalts are specified, while in warmer climates, harder or stiffer asphalts are specified. In some of the earlier LTPP data analysis projects (e.g., the Rauhut et al. study described as the "good and poor" investigation), it was reported that asphalt grade had no impact on cracking and rutting.[44] This was a confounding outcome because of the interrelationship between climate and asphalt grade. For this sampling matrix, climate was the primary factor identified, while asphalt grade was a secondary factor.

- Air voids and asphalt content had a significant effect on the resistance of the mixture to cracking. Low air-void and high asphalt-content mixtures generally had much more resistance to bottom–up fatigue cracking. In addition, the rate of increase in cracking was heavily influenced by the volumetric properties of the AC mixture, especially the lower AC layers. Air voids and asphalt contents can and do vary between the different AC layers of a pavement structure. Thus, it was difficult to select projects with the same or similar volumetric properties (i.e., air void and asphalt content) for all AC layers within the same project. Differences in volumetric properties between the lower AC layers represent a confounding factor associated with the volumetric properties. Thus, the primary factor of sampling matrix was the rate of increase in bottom–up fatigue cracks. It was hypothesized that the different rates of cracking can explain these factors because asphalt content and air void level determine M of the fatigue strength relationship shown in figure 14. The volumetric properties are the secondary factors.

The sampling matrix for the site selection process for this project is shown in table 4.

Table 4. Experimental sampling matrix.

AC Thickness (Inches)	Rate of Cracking	Climate by U.S. Region			
		Hot Desert (Southern and Southwestern)	Warm (Southern)	Cool (Upper Southern and Lower Northern)	Cold (Northern)
Thin (>2 and <6 inches)	Low	Arizona SPS-1, Texas SPS-1, and New Mexico SPS-1	Alabama SPS-1	Ohio SPS-9	Montana SPS-1
Thin (>2 and <6 inches)	Moderate	Nevada SPS-1	Georgia SPS-1 and Mississippi SPS-1	Utah SPS-8	Wisconsin SPS-1
Thin (>2 and <6 inches)	High	—	Oklahoma SPS-1	North Carolina SPS-8, Virginia SPS-1, and Iowa SPS-1	New York SPS-8
Moderate (6–12 inches)	Low	Arizona SPS-1, Texas SPS-1, and New Mexico SPS-1	Alabama SPS-1	North Carolina SPS-9 and Utah SPS-8	Wisconsin SPS-1 and Montana SPS-1
Moderate (6–12 inches)	Moderate	Arizona SPS-9 and Nevada SPS-1	Georgia SPS-1 and Mississippi SPS-1	—	New York SPS-8
Moderate (6–12 inches)	High	—	Oklahoma SPS-1	North Carolina SPS-8 and Virginia SPS-1	—
Thick (>12 inches)	Low	Arizona SPS-1, Texas SPS-1, and New Mexico SPS-1	Alabama SPS-1	—	Wisconsin SPS-1 and Montana SPS-1
Thick (>12 inches)	Moderate	Nevada V SPS-1	Georgia SPS-1 and Maine SPS-1	—	—
Thick (>12 inches)	High	—	Oklahoma SPS-1	Virginia SPS-1 and Iowa SPS-1	—

—There were no LTPP sections in the climatic region having AC layers within the thickness range.

SELECTION OF CANDIDATE LTPP TEST SITES

This section summarizes some of the other factors considered in selecting the LTPP sites used in the preliminary analyses (see table 4).

Type of Test Section

Flexible pavement test sites for which the LTPP database contained all necessary data were identified. The selection process was restricted to LTPP projects and test dates without rehabilitation because the data collected for these pavements contained the history of damage (and distress) accumulation from the undamaged state. The types of LTPP projects considered for this study included SPS-1, -8, and -9N (project-level designation is SPS-9A) as well as the seasonal monitoring program (SMP) project sites. Figure 28 presents a map showing the general locations of the LTPP SPS and SMP sites. Figure 29 shows the number of 500-ft test sections for different LTPP experiment types. As shown, the SPS-1 sites had a higher number of test sections compared to SPS-8 and -9N.
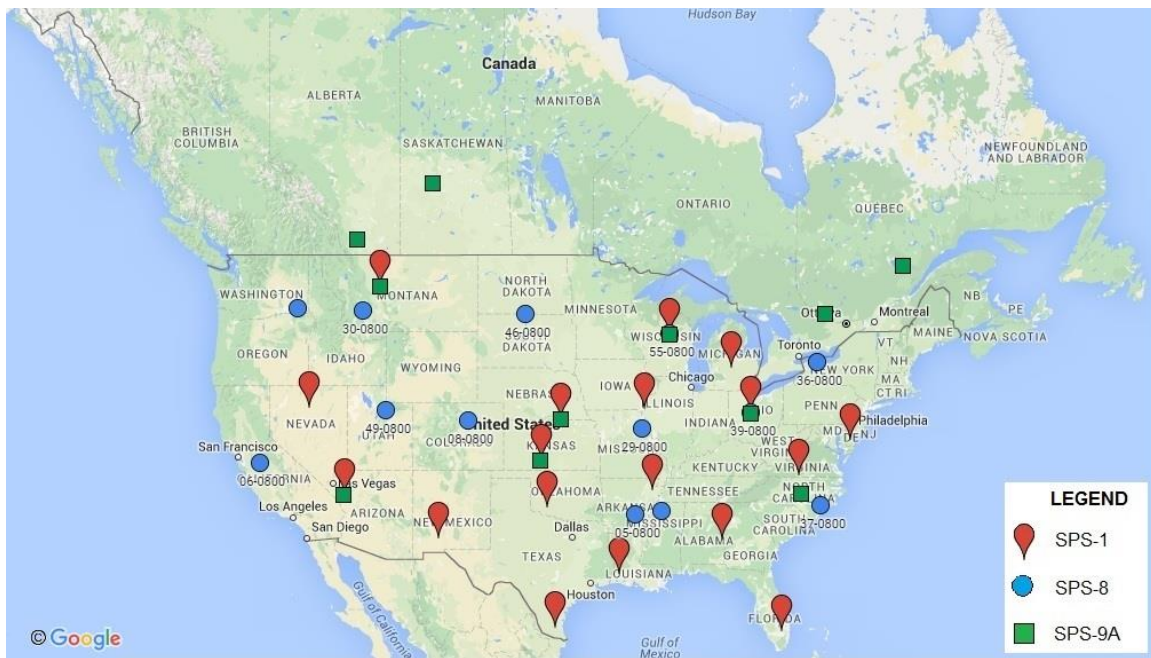
©Google® 2016. See Acknowledgements section for additional information on map overlay.

Figure 28. Map. General locations of SPS sites.[(45)]

Count of SPS Sections by Project Type
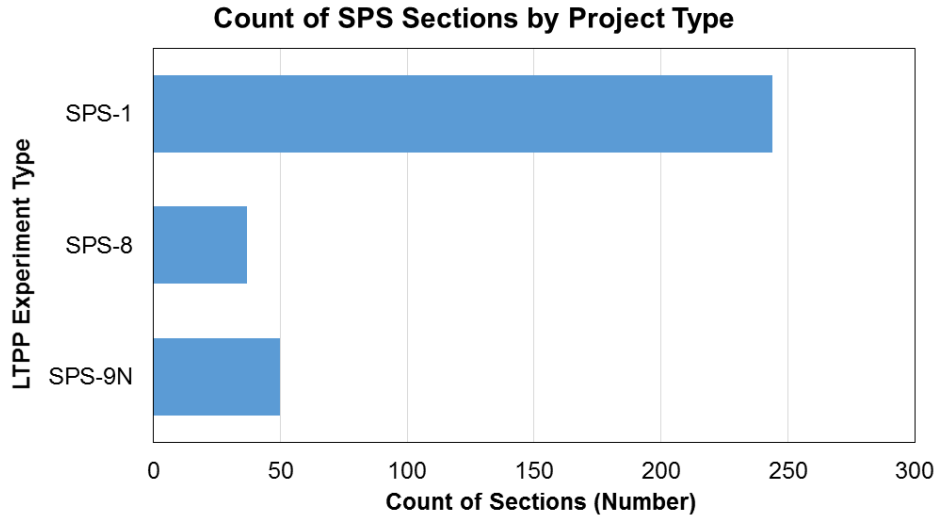
Source: FHWA.

Figure 29. Graph. Distribution of candidate LTPP sections.

The following list summarizes how the data from different LTPP section types were used:

- Data from the SPS-1 and -9 projects were used to investigate layer softening or damage due to the occurrence of cracking. (Note that the occurrence of cracking implies in-place damage.) The deflection-basin data (backcalculation of elastic layer moduli) measured shortly after construction were used to determine the loading frequency to match E_{FWD} to E_{PRED}. It was assumed that no in-place damage was present in the AC layers shortly after construction.

- The SPS-8 projects were used to supplement the SPS-1 and -9 as well as SMP projects with time–series data of layer modulus and distresses except that the data collected for SPS-8 sites corresponded to damage due to environmental effects in the absence of heavy traffic loading. A detailed analysis of SPS-8 projects was recently completed to investigate and define environmental damage.[46] One finding from this study was that transverse or thermal cracks were related to the number of truck loadings. This finding represents a potential confounding factor on sites with extensive transverse cracks.

- The SMP sites were used to investigate the seasonal variations in E_{FWD} values as related to fatigue cracking to determine whether the adjustments made to the master curve are seasonal dependent or independent.

- The SPS-1 and SMP sites were both used to evaluate aging or time effects on the undamaged moduli. In other words, they were used to determine if a shift factor was required to increase $E^*_{undamaged}$ over time to account for aging after construction. Aging is the hardening or stiffening of asphalt over time. The MEPDG does take hardening into account by calculating an increase in asphalt viscosity with age.[1] The increase in asphalt viscosity is used to increase $E^*_{undamaged}$ over time. Asphalt hardening simulated in the MEPDG is dependent on depth and age.

33

- The SPS-5 projects include AC overlays over existing flexible pavements. It was determined that sites with AC overlays potentially contained too many confounding factors to include them in the preliminary evaluation. Thus, the SPS-5 projects and others with AC overlays in the other experiments were used to validate any new or improved concepts.

Type of Base Layer

Another factor considered in eliminating sites as candidates was the type of base material. None of the candidate test sections included semi-rigid pavements, which are defined as AC surfaced pavements having any cement-stabilized layer directly beneath the AC layers. The reason for excluding the semi-rigid pavements was the occurrence or reflection of shrinkage cracks through the AC layer. This potential cracking was envisioned as a confounding factor in estimating the in-place damage. More importantly, it was difficult to estimate the in-place damage of the existing cement stabilized layer.

Data Completeness and Structures Without Special Features and Extreme Values

The candidate sites selected were evaluated based on the availability and completeness of construction records and materials test data. The sites were also screened for the presence of confounding factors that could impact the cracking time–series data, such as maintenance treatments, seal coats or chip seals, geotextiles, special thin lift AC layers, and materials or construction-related distresses. A decision was made at the beginning of the study to exclude sites with extensive materials- and construction-related issues. Excessive raveling and bleeding represent material-related distresses, while potholes were an indication of debonding of the wearing surface. Test sections with extensive patches were also excluded from the analysis because it was not always clear why the patch was placed. Figure 30 includes the distribution of AC-layer thicknesses for the candidate flexible-pavement sites. The thickness ranged from 3 to almost 25 inches. Similar distributions of other primary and secondary factors were used to exclude LTPP sites with values more than two standard deviations from the mean or median. The authors decided not to use test sections with extreme values in the preliminary analyses because extreme values can potentially skew the initial results or findings.
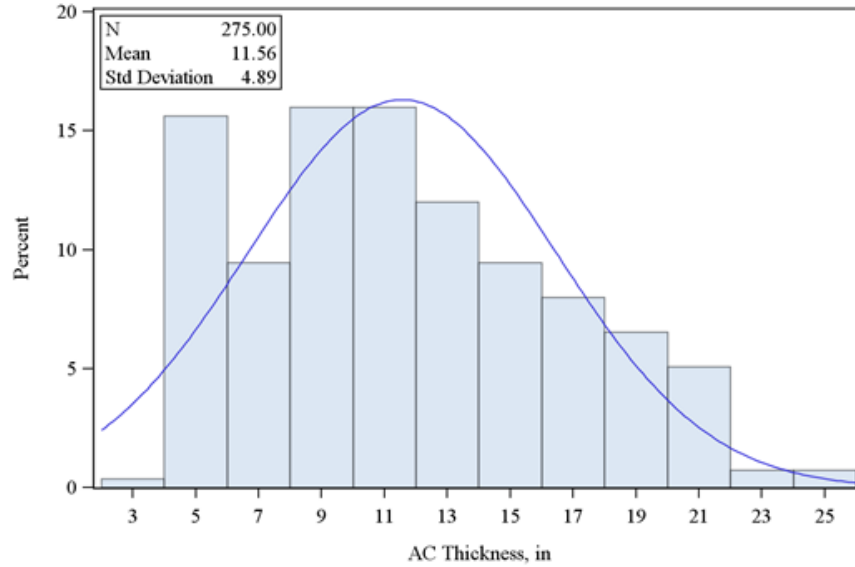
N = total section count.

Figure 30. Graph. Frequency distribution of AC-layer thickness for the candidate LTPP flexible pavement sections.

Time–Series Data

Another factor considered in selecting potential LTPP sites for the preliminary analyses was the availability of multiple years of data, including FWD deflection–time histories, backcalculated elastic layer moduli that met the requirements used in the FHWA backcalculation study, and cracking data.[47–49]

Cracking Rate

The final factor considered in selecting specific sites for this study was the cracking amount and rate (see table 4). This parameter was considered the most important factor in identifying and selecting individual test sections because fatigue cracking was assumed to be correlated to the in-place fatigue damage. Projects or test sections were selected to include a minimal amount of fatigue or alligator cracking to extensive alligator cracking over the monitoring period of at least 10 yr.

Cracking rate was also used to select test sections. Sections were selected with typical (low and high) and nontypical rates of cracking. Figure 31 and figure 32 show two of the test sections included in the study for which fatigue cracking went from 0 to over 50 percent total lane area of cracking within 1 or 2 yr. These figures are examples of high rates of fatigue cracking.
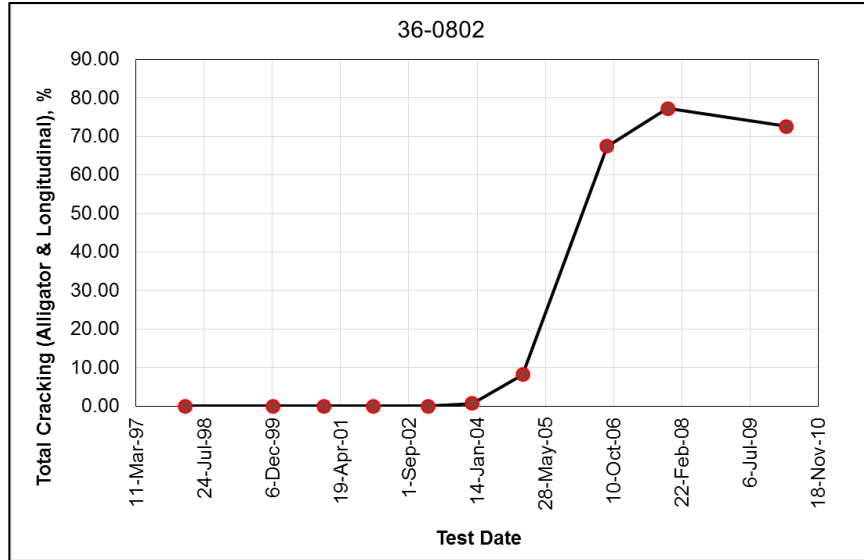
Source: FHWA.

Figure 31. Graph. LTPP test section 36-0802 exhibiting a high rate of fatigue cracking within a short time period.
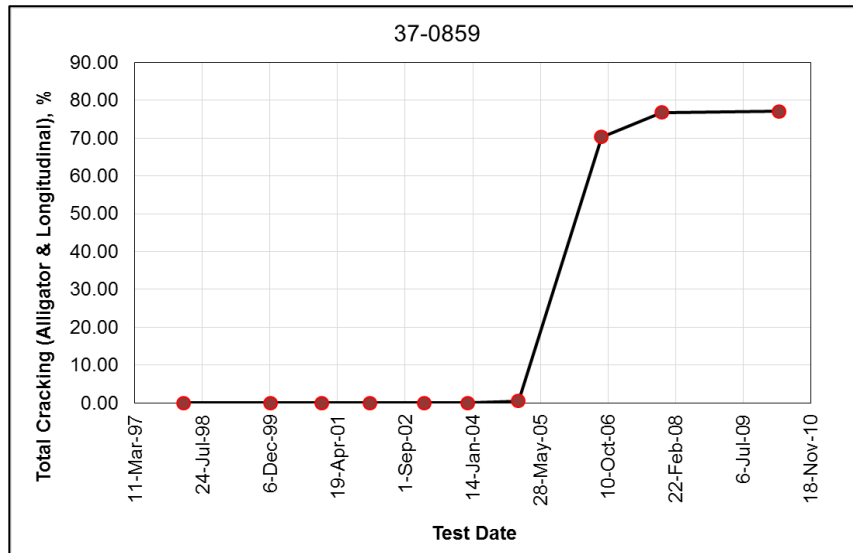
Source: FHWA.

Figure 32. Graph. LTPP test section 37-0859 exhibiting a high rate of fatigue cracking within a short time period.

Figure 33 and figure 34 show test sections where the increase in fatigue cracking was more gradual. These sites were typical in that the percent cracking increased at an increasing rate. Other sites were selected that exhibited a different or nontypical cracking trend that occurs when cracking increases but at a decreasing rate. This trend is illustrated in figure 35 and figure 36.

36
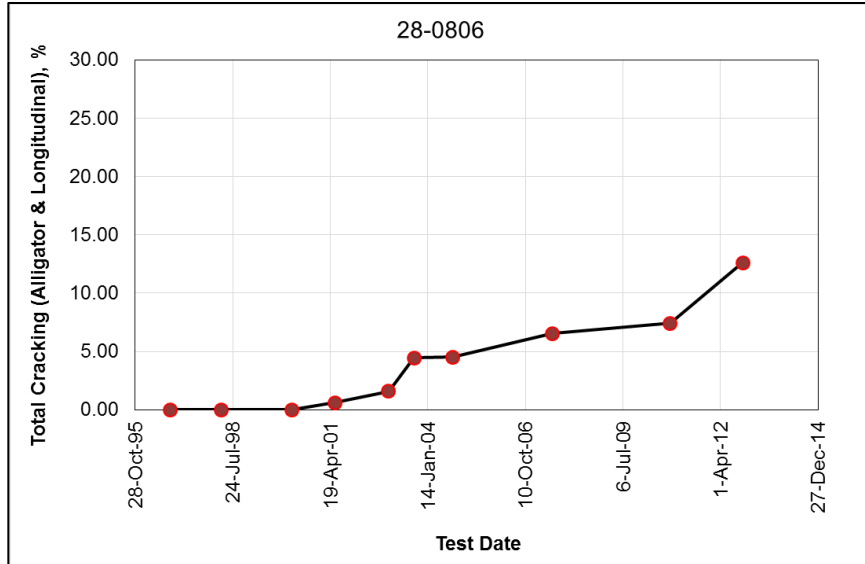
Source: FHWA.

Figure 33. Graph. LTPP test section 28-0806 exhibiting a typical low rate of fatigue cracking.
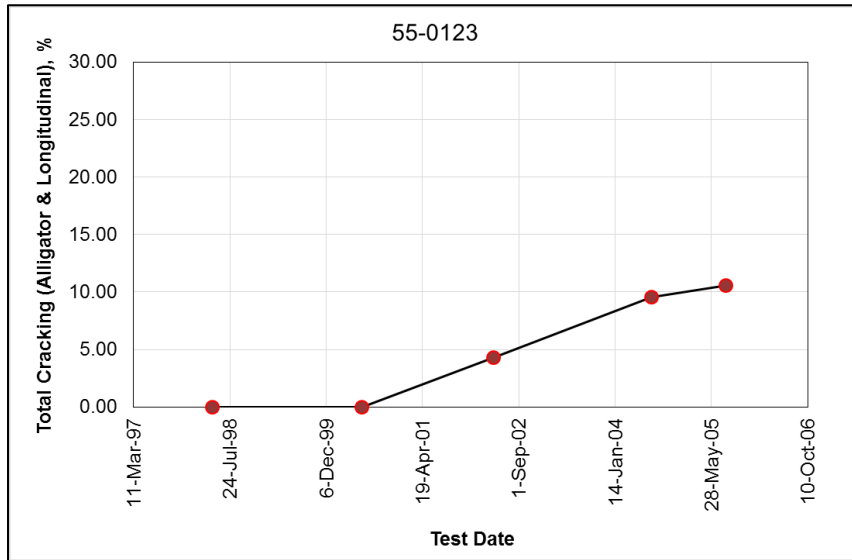
Source: FHWA.

Figure 34. Graph. LTPP test section 55-0123 exhibiting a typical low rate of fatigue cracking.
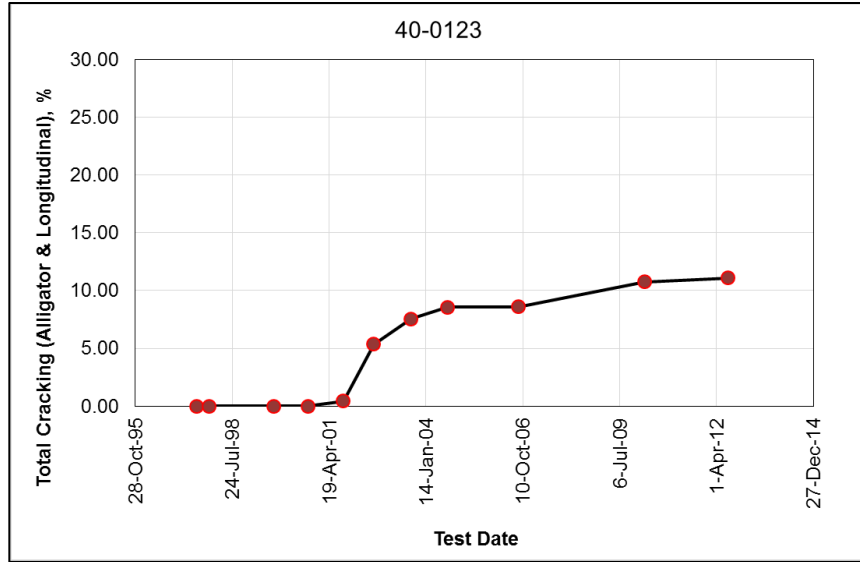
Source: FHWA.

Figure 35. Graph. LTPP test section 40-0123 exhibiting a nontypical rate of fatigue cracking.
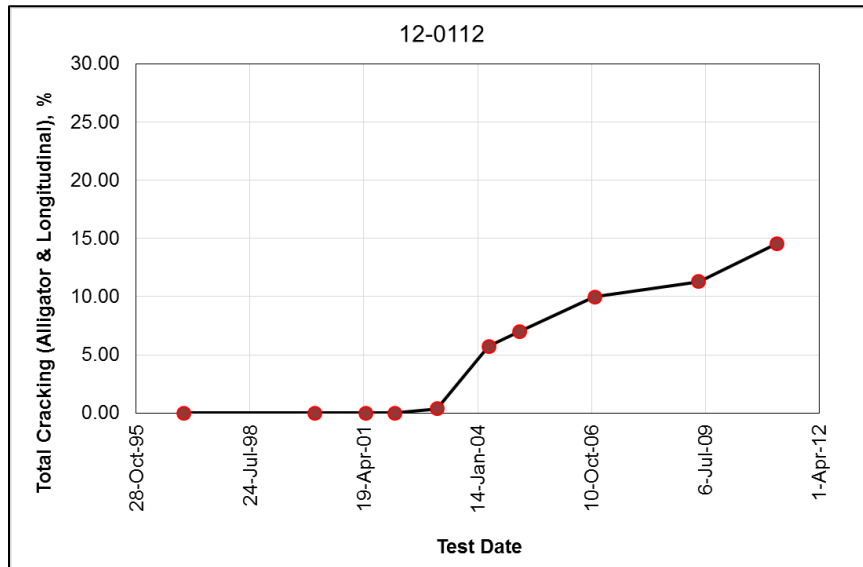
Source: FHWA.

Figure 36. Graph. LTPP test section 12-0112 exhibiting a nontypical rate of fatigue cracking.

Sections with the different amounts and rates were important to confirm the determination of damage from the E_{FWD} values. It was hypothesized that an increase in cracking for these sections was associated with a reduced E_{FWD} value and thus an increase in damage of that layer. Table 5 lists the candidate LTPP projects selected for this study. For the most part, the projects were conventional flexible and full-depth AC pavements, as defined by the *Mechanistic-Empirical Pavement Design Guide—A Manual of Practice*.[2]

38

Table 5. LTPP projects selected for this study.

State/Province	LTPP State Code[3]	LTPP Project Identification Code
Alabama	1	0100
Arizona	4	0100
Arizona	4	0900
Arizona	4	A900
Arkansas	5	0100
Arkansas	5	0800
Arkansas	5	0801
California	6	A800
Delaware	10	0100
Florida	12	0100
Iowa	19	0100
Kansas	20	0100
Kansas	20	0900
Louisiana	22	0100
Michigan	26	0100
Mississippi	28	0800
Missouri	29	0800
Missouri	29	A800
Montana	30	0100
Montana	30	0800
Montana	30	0900
Nebraska	31	0100
Nebraska	31	0900
Nevada	32	0100
New Jersey	34	0800
New Mexico	35	0100
New Mexico	35	0800
New York	36	0800
North Carolina	37	0800
North Carolina	37	0900
Ohio	39	0100
Ohio	39	0900
Ohio	39	A800
Oklahoma	40	0100
South Dakota	46	0800
Texas	48	0100
Texas	48	0800
Texas	48	0900
Utah	49	0800
Virginia	51	0100

State/ Province	LTPP State Code[3]	LTPP Project Identification Code
Washington	53	0800
Wisconsin	55	0100
Wisconsin	55	0800
Wisconsin	55	C900
Alberta	81	A900
Ontario	87	0900
Quebec	89	0900
Quebec	89	A900
Saskatchewan	90	0900

DATA EXTRACTION FROM LTPP DATABASE

The primary source of data used in this study was the LTPP database. LTPP Standard Data Release (SDR) 28 was used to obtain LTPP site and design information, material properties, and distress data.[10] The backcalculated in-place moduli from FWD drop data was obtained from the results of a study by Von Quintus and Rao.[47] These data are currently available in SDR 29.[10] The load deflection–time histories for individual FWD drops were extracted from the LTPP database in SDR 28.[10]

All data except backcalculated pavement layer modulus data were extracted from SDR 28 of the LTPP database. The individual tables within the Microsoft® Access™ files of the LTPP database were reduced to contain records corresponding to the selected sections, as shown in table 5.[10]

General Design Information

Information related to design and construction of the flexible pavement sections was extracted from the EXPERIMENT_SECTION table of the LTPP database.[10] The data included experiment type (SPS-1, -8, or -9); pavement construction and deassign dates; and the number, date, and type of construction event (e.g., new construction, maintenance (i.e., nonstructural changes), and rehabilitation (i.e., structural changes)).

Pavement data collected after major rehabilitation events were not used for analysis because the in-place modulus of the reconstructed surface was different from the expected value resulting from incremental damage. Surface maintenance treatments such as crack sealing, shoulder repairs, and seal coats were considered nonstructural changes. Overlays with or without milling and full-depth patch repairs were treated as structural changes that result in a change in the damaged modulus of existing AC layers.

Pavement Structure and Layer Thicknesses

Layer structures of the selected flexible pavements were obtained from the SECTION_LAYER_ STRUCTURE table of the LTPP database.[10] Thickness of the individual asphalt layers and other layers were extracted from the TST_L05B table of the LTPP database.[10] The type of base

course (i.e., granular and asphalt base layer) was also identified. As noted previously, cement- and asphalt-treated permeable base layers were excluded from the proof-of-concept study.

Cracking Data

Pavement cracking data were obtained from the LTPP database table MON_DIS_AC_REV for all dates on which distress surveys were conducted for each test section.[10] The distress data included load-induced cracking of the pavement (i.e., alligator cracking, longitudinal cracking (sum of WP and non-WP cracking), and transverse (thermal) cracking). Transverse cracks were included because these cracks do result in increased deflections in localized areas. All cracking data were converted to percentage cracking per total lane area.

Alligator cracking data for different distress survey dates were obtained for the LTPP sections from the following fields from the MON_DIS_AC_REV table within the LTPP database:[10]

- GATOR_CRACK_A_L.
- GATOR_CRACK_A_M.
- GATOR_CRACK_A_H.

Within these fields, "A" represents the total area that exhibits alligator cracking, while "L," "M," and "H" represent low-, medium-, and high-severity cracking, respectively. The definition of severity of distress is provided in *Distress Identification Manual for the Long-Term Pavement Performance Program*.[50] The length of section used for calculation was 500 ft, and surveyed lane width was obtained from the SURVEY_WIDTH field of MON_DIS_AC_REV table.[10] Alligator cracking data were converted to square feet of cracked area for the combined area along the 500-ft section and divided by the total lane area to calculate percentage area cracked. The calculation of total alligator cracking as percentage of lane area is shown in the equation in figure 37.

$$\% \text{ Alligator Cracking} = \frac{(\text{GATOR\_CRACK\_A\_L} + \_M + \_H)}{\text{Section Length} \times \text{Lane Width}}$$

Figure 37. Equation. Percent fatigue (alligator) cracking.

Total length of longitudinal cracks measured both in the WP and non-WP in sealed and nonsealed condition was obtained for each section from the following fields:

- LONG_CRACK_WP_L_L.
- LONG_CRACK_WP_L_M.
- LONG_CRACK_WP_L_H.
- LONG_CRACK_WP_SEAL_L_L.
- LONG_CRACK_WP_SEAL_L_M.
- LONG_CRACK_WP_SEAL_L_H.
- LONG_CRACK_NWP_L_L.
- LONG_CRACK_NWP_L_M.
- LONG_CRACK_NWP_L_H.

41

- LONG_CRACK_NWP_SEAL_L_L.
- LONG_CRACK_NWP_SEAL_L_M.
- LONG_CRACK_NWP_SEAL_L_H.

Within these fields, WP and NWP represent WP and non-WP cracking measured in terms of crack length.[50] The letter "L" represents total length of longitudinal crack, while "L," "M," and "H" represent the severity cracking defined previously. Areal extent of longitudinal cracking was calculated by assuming a 1-ft width for the cracks and converted to percentage lane area using the equation shown in figure 38.

$$\% \text{ Longitudinal Cracking} = \frac{\sum (\text{LONG\_CRACK\_WP\_} + \text{\_NWP\_})}{\text{Section Length} \times \text{Lane Width}}$$

Figure 38. Equation. Longitudinal cracking.

Transverse cracks were typically excluded from the in-place damage analysis because they are climate related. However, a study of the SPS-8 experiment reported transverse cracks were correlated to the number of truck loadings.[46] As a result, transverse cracks were considered in the total amount of cracking of a section but as a separate value that could be added to the total load-related cracks. Transverse cracking was calculated similar to the longitudinal cracking. The total cracking with and without transverse cracks was calculated for all selected LTPP sections and reported as a percentage by total lane area. Table 6 through table 8 lists the LTPP sections that were used in the study and the total percent lane area cracked, which are grouped into low-, moderate-, and high-severity levels of cracking over the monitoring period.

Table 6. Low-severity cracking LTPP sections included in the preliminary analysis by area of total cracking.

LTPP Section	Low-Severity Cracking (Percentage of Total Lane Area)
01-0103	13.0
10-0104	14.1
12-0112	14.6
19-0111	15.0
28-0806	12.6
40-0123	11.1
55-0123	10.6

Table 7. Moderate-severity cracking LTPP sections included in the preliminary analysis by area of total cracking.

LTPP Section	Moderate-Severity Cracking (Percentage of Total Lane Area)
04-A902	53.6
20-0111	53.4
20-0903	53.4
26-0121	55.2
29-A801	56.3
29-A802	58.7
36-0801	50.8
39-0104	66.1
39-0111	63.4
39-0160	58.3
51-0114	58.4
51-0120	53.3
55-C960	66.5
87-0960	67.6
90-0902	54.4

Table 8. High-severity cracking LTPP sections included in the preliminary analysis by area of total cracking.

LTPP Section	High-Severity Cracking (Percentage of Total Lane Area)
04-0903	73.2
26-0118	95.2
26-0123	73.5
26-0124	73.7
37-0802	77.2
37-0859	77.1
39-0903	78.8
87-0961	72.1

Asphalt Material Properties

The volumetric properties extracted from the LTPP database for each structural layer or mixture included asphalt content, bulk specific gravity, and maximum specific gravity. The bulk specific gravity and maximum specific gravity were used to calculate the in-place air voids at construction or time of sampling. The asphalt content and air void levels were used along with the asphalt viscosity to calculate the AC E^*_{PRED} at a specific temperature and load frequency.

Undamaged AC Dynamic Modulus Master Curve

Parameters required for constructing the $E^*_{undamaged}$ master curve for individual asphalt layers (E^* sigmoidal function coefficients and temperature shift factors) were obtained from the

ESTAR tables in the LTPP database.[10] The master curve quality, as defined in the LTPP tables, was checked to ensure that the master curve parameter and shift factor values were reasonable for calculating the laboratory-derived $E^*_{undamaged}$ of asphalt layers.

The two parameters needed for the $E^*_{undamaged}$ master curve are temperature and frequency. They are used for calculating E^*_{PRED} for an individual test section and test date. The temperature initially used in the calculation represents the middepth temperature included in the LTPP database on backcalculation. The frequency range initially used (10 to 25 Hz) was recommended in the *Mechanistic-Empirical Pavement Design Guide—A Manual of Practice*.[2] A constant value of 20 Hz was initially used in comparing $E^*_{undamaged}$ and $E^*_{damaged}$ values.

E^* included in the LTPP tables were for a specific mixture and project. In other words, they were not for individual sections; rather, the moduli were assumed to be the same for all sections within an SPS project. Two moduli values were calculated for sections having more than one asphalt layer: E_ST_PRED as a direct average of all AC layer E^* and E_WT_PRED as an average weighted by the thickness of each AC layer.[10]

Load frequencies of 15 and 30 Hz and the middepth pavement temperature were used to calculate $E^*_{undamaged}$. The middepth pavement temperature is the temperature at the middepth of all combined AC layers. In addition, the frequency at which E^*_{PRED}, was predicted for the first FWD test date, was equal to the E_{FWD} (i.e., damage ratio equal to 1) was also determined. The calculated load frequency is discussed in further detail in chapter 5.

When multiple AC structural layers were placed at a test section, an equivalent E^*_{PRED} was calculated using the equivalent stiffness concept. The $E^*_{undamaged}$ AC master curve was derived for each AC layer included in the simulated structure used within the backcalculation process, as listed and defined in the LTPP database.

Backcalculated AC Elastic Layer Modulus

As stated previously, E_{FWD} and other FWD parameters were extracted from the LTPP database. The root mean squared error (RMSE) from the backcalculation process was considered in the process to determine the best representative modulus value for a specific test date, as recommended by Von Quintus et al.[47] As an example, if the backcalculation process yielded results for which the RMSE exceeded 3 percent, those results or E_{FWD} were excluded from the computation for damage in this project. In addition to the E_{FWD}, the data also contained information for each drop regarding the following variables:

- FWD test location information including LTPP section ID and station number (within the 500-ft section).

- Test configuration including drop load (drop height) and drop number.

- Pavement surface.

- Middepth temperature.

- Layer number.

- Types and thicknesses used in the backcalculation program.

- Presence of and depth to rigid layer.

The analysis and selection of E_{FWD} for a test date is discussed in more detail in chapter 4.

FWD Deflection–Time Histories

The FWD deflection–time histories for each individual drop were extracted from the LTPP database for all selected sections. The deflection–time histories were saved as separate comma-separated value files with the file names containing several identifiers such as the LTPP section ID, test date, lane number, timestamp, and station and drop numbers. The deflection–time histories were used to calculate the duration of the FWD load pulse and dissipated work for each drop.

CHAPTER 4. ANALYSIS OF BACKCALCULATED ELASTIC AC MODULI

One of the issues with backcalculation or deflection-derived E_{FWD} is that no unique solution or set of elastic layer moduli is determined for a specific set of measured deflection basins. The quality of the results is heavily dependent on the knowledge and expertise of the user in setting up the problem. In other words, different users can obtain different results for the same set of deflection basins. This nonuniqueness of solutions has been a deterrent for some agencies to take full advantage of backcalculation methods for routine rehabilitation design. More importantly and related to this project, nonunique solutions can add variability to the deflection-derived damaged moduli for estimating fatigue damage.

The deflection-derived moduli for selected LTPP flexible pavement sections were extracted from the results of the study by Von Quintus, Rao, and Irwin.[47] This chapter provides a general overview of the backcalculation process/procedure and data and describes the results from the analysis of backcalculation data to reduce the variability in the values to estimate fatigue damage.

BACKCALCULATION PROCESS OF LAYERED ELASTIC MODULUS

The deflection-derived E values used to populate the LTPP database were determined from the process or procedure established by Von Quintus, Rao, and Irwin.[47] A user guide was prepared for the automated backcalculation process as well as executing the utility and software tools for organizing the results included in the LTPP computed parameter tables (CPTs).[47] The purpose of the automated process was to reduce the difference in results between users.

The CPTs included a series of data tables with the results for all stations and drop heights regardless of the outcome. For this project, however, only the deflection-based moduli that were defined as "acceptable" were extracted and used in the proof-of-concept work. The Von Quintus et al. report provides an explanation for how the solutions were characterized or grouped into acceptable and unacceptable results.[47] Specifically, three criteria were used to define acceptable results: (1) the RMSE, (2) the typical range of material specific values, and (3) a normality test for a day's test results.

The solutions defined as unacceptable could be valid but exceeded one of the threshold criteria used to evaluate the results, so they were not used in the proof of concept. For some of the stations along a project, if the backcalculated modulus for an aggregate base or subgrade layer exceeded the allowable range of typical values established for that material or soil, the solutions for all layers were identified as unacceptable because of potential compensating layer effects.

Two backcalculation programs were used, but only one set of solutions was included in the LTPP CPTs: the solution with the lower RMSE, which met all evaluation criteria. The two programs included the following:

- EVERCALC© was the primary program used for the analyses and was used for all data and all pavement types in LTPP.[51] The pre- and postprocessing utility tools for the EVERCALC© analyses were fully automated. The automation process included generating input files based on pavement simulation rules, executing EVERCALC©, and postprocessing the results.

- Version 6.0 of MODCOMP© was used as the auxiliary program to backcalculate results for those LTPP sections that did not yield acceptable results with EVERCALC©, even after multiple iterations.[52] The MODCOMP© analyses were semi-automated as an iterative approach, and the simulated backcalculation structure was selected on a case-by-case basis until the results converged within the selected criteria. A few test sections or portions of test sections did not converge to produce acceptable results even after multiple efforts using EVERCALC© and MODCOMP©, so these results were flagged as unacceptable.

SPATIAL VARIABILITY OF BACKCALCULATED AC MODULUS WITHIN LTPP SECTIONS

FWD testing was performed at different locations (or stations) along the length of an LTPP section, typically at four levels of loading or drop heights and four drops at each level. The original database assembled for this project contained backcalculated E values of flexible pavement layers for each individual FWD drop. Average E values were first calculated for each station along a section and later for the entire section for a particular test date. The averages calculated are referred to as "station average" and "section average moduli" and are explained graphically in figure 39.
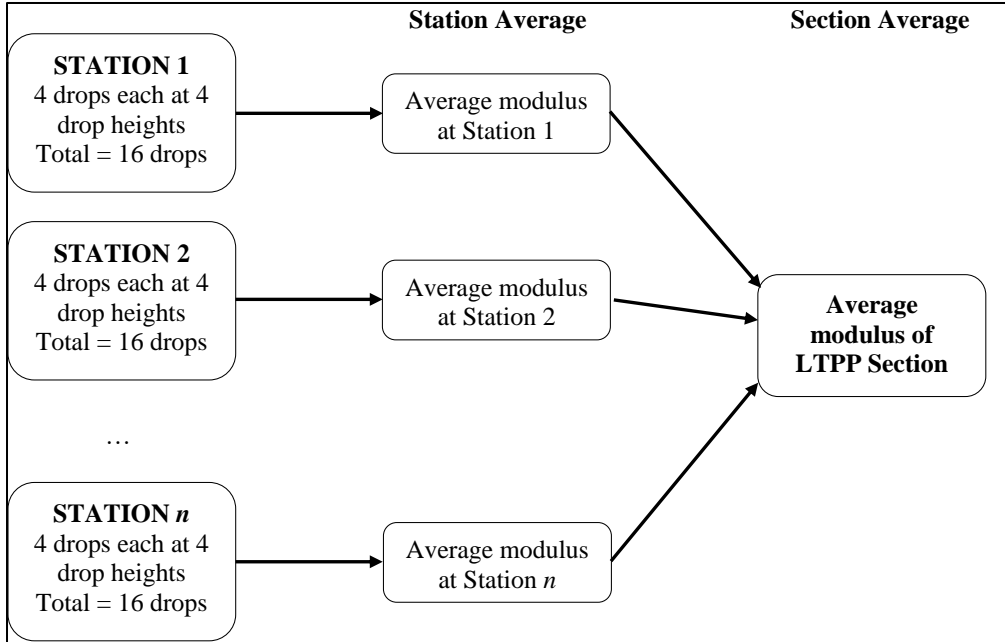
Source: FHWA.
Note: *n* represents a specific station within the number of stations in an LTPP section where FWD testing was conducted.

Figure 39. Flowchart. Station and section average backcalculated *E*.

The station average and section average *E* showed variability to different extents, which could be attributed to several factors. Variability within individual drop moduli backcalculated at a station can arise from random error associated with testing, different drop heights, errors from backcalculation process including deflection basins, and others. Variability among section average moduli can be related to variation in pavement layer thicknesses, different magnitudes of damage in pavement layers, variability during construction, materials along the section, random error from testing, etc.

Figure 40 shows an example of the station average backcalculated AC layer *E* values in non-WP for section 19-0109, which was tested on September 11, 1995. This section has relatively low spatial variability. Statistics such as the average *E* for the section, standard deviation, and coefficient of variation (COV) were calculated for each test date and lane position (WP and non-WP) for all selected LTPP sections.
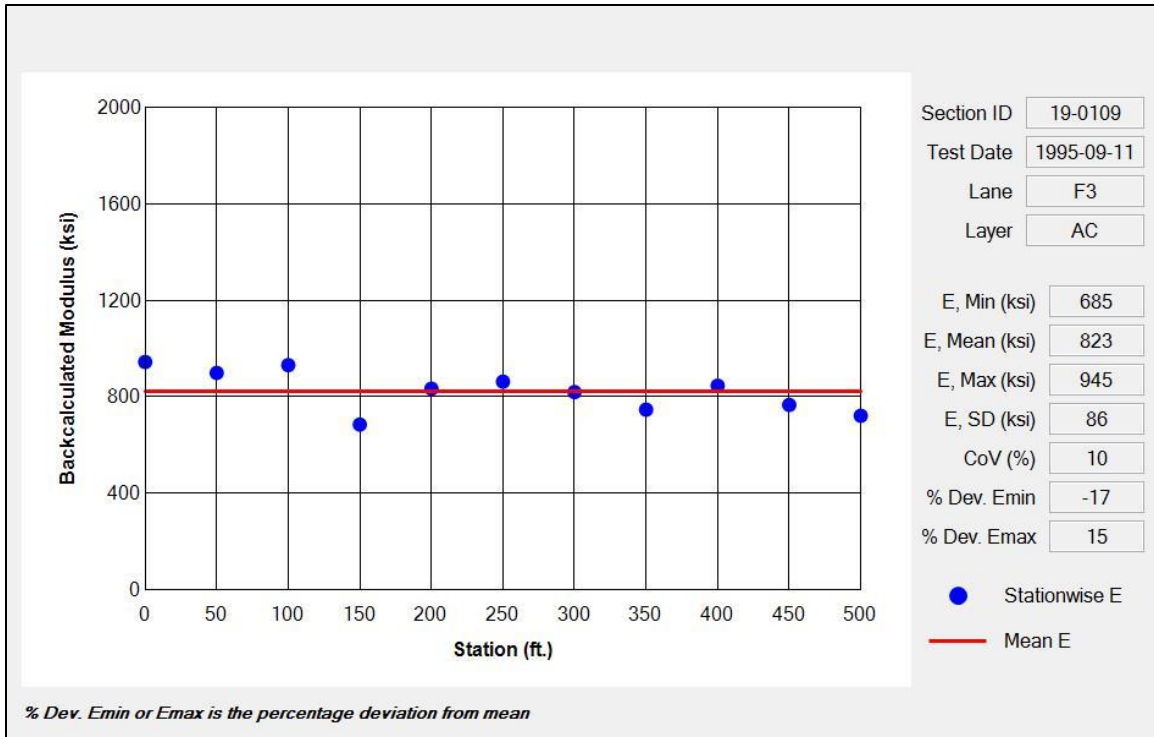
Source: FHWA.

Figure 40. Graph. Example of spatial variability of backcalculated AC *E*.

AVERAGE BACKCALCULATED AC MODULUS

The backcalculated AC *E* values for individual FWD drops were reduced using statistical methods to obtain average values for each test date. Average *E* values were calculated separately for the WP (i.e., outer WP, which was designated as lane F3 for LTPP flexible pavements) and non-WP (i.e., midlane, which was designated as lane F1) locations.

Statistical checks were performed on backcalculation data to determine average AC *E* value for each combination of LTPP section ID, test date, and lane position (WP or non-WP). Median-based statistical techniques were used instead of average or mean-based techniques, as the latter did not yield satisfactory results in reducing variability, especially in cases with low mean and high standard deviation. In order to study the spatial variability in relation to the mean or section average *E* value, the relative standard deviation or COV was used as the filtering criterion. COV is the ratio of the standard deviation to the mean of the station average moduli.

The COV of section average AC layer moduli was found to be highly variable, with about 47 percent of all values having a COV lower than 20 percent, as shown in figure 41. Hence, a 20 percent COV was selected as the cutoff value for inclusion of stations in calculating the section averages. To reduce the spatial variability (i.e., variability in station average *E* values), stations were filtered using two statistical methods—median absolute deviation (MAD) method and inter-quartile range (IQR) method—which are discussed in greater detail in the following subsections.

50
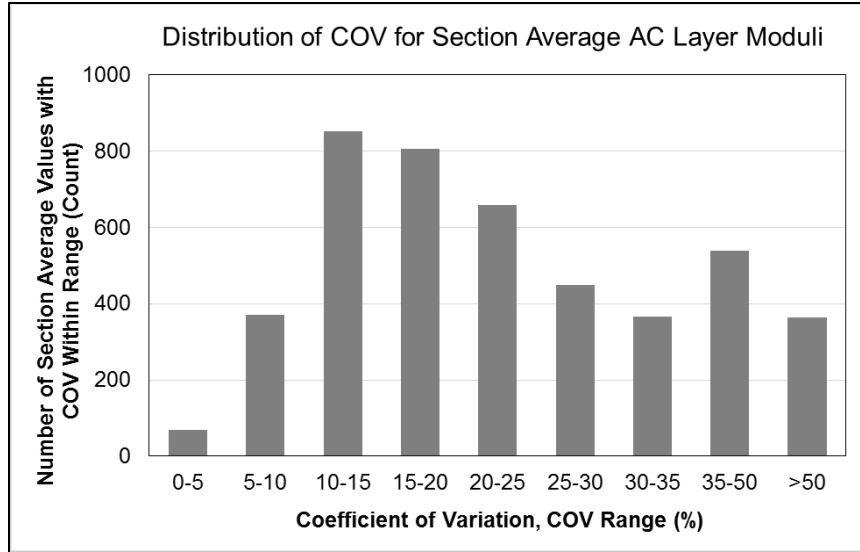
Source: FHWA.

Figure 41. Graph. Distribution of COV for section average AC *E* values.

Removal of Outliers Using the MAD Method

The station average backcalculated moduli ($E_{ST\text{-}AVG}$) was calculated using individual drop modulus values for a station. $E_{ST\text{-}AVG}$ for each section was plotted separately for all test dates. The first statistical check applied was to remove outliers using the MAD method. Individual station averages whose values were significantly higher or lower than the median were eliminated as outliers in this step. MAD was calculated as follows:

1. Calculate $E_{ST\text{-}AVG}$.

2. Calculate the median of the station average moduli (E_{MED}).

3. Subtract E_{MED} from $E_{ST\text{-}AVG}$ and calculate the absolute value of the differences (i.e., $|E_{ST\text{-}AVG} - E_{MED}|$).

4. Calculate MAD as the median of the absolute deviations calculated in step 3 ($|E_{ST\text{-}AVG} - E_{MED}|$).

The MAD method is a robust statistical measure to identify outliers and data points (stations) that were more than three MADs from E_{MED}. All outliers were removed. Figure 42 shows an example of spatial variation in AC layer *E* for LTPP test section 39-0101, where the COV prior to removal of outliers was 26 percent. Figure 43 shows the stations that were removed as outliers according to the MAD procedure, which reduced the COV for section average *E* to 8 percent. After the removal of outliers, the COV was recalculated for the assembled dataset for further analysis.
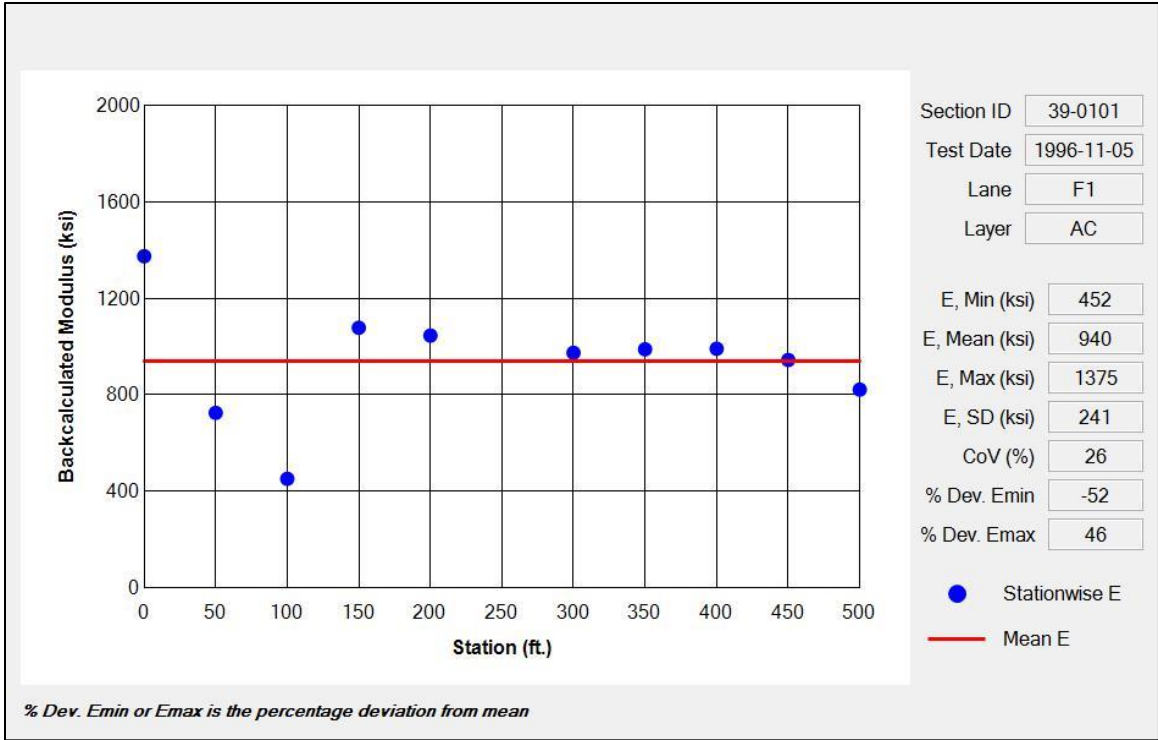
Source: FHWA.

Figure 42. Graph. Stationwise AC *E* plot for test section 39-0101 including outliers.
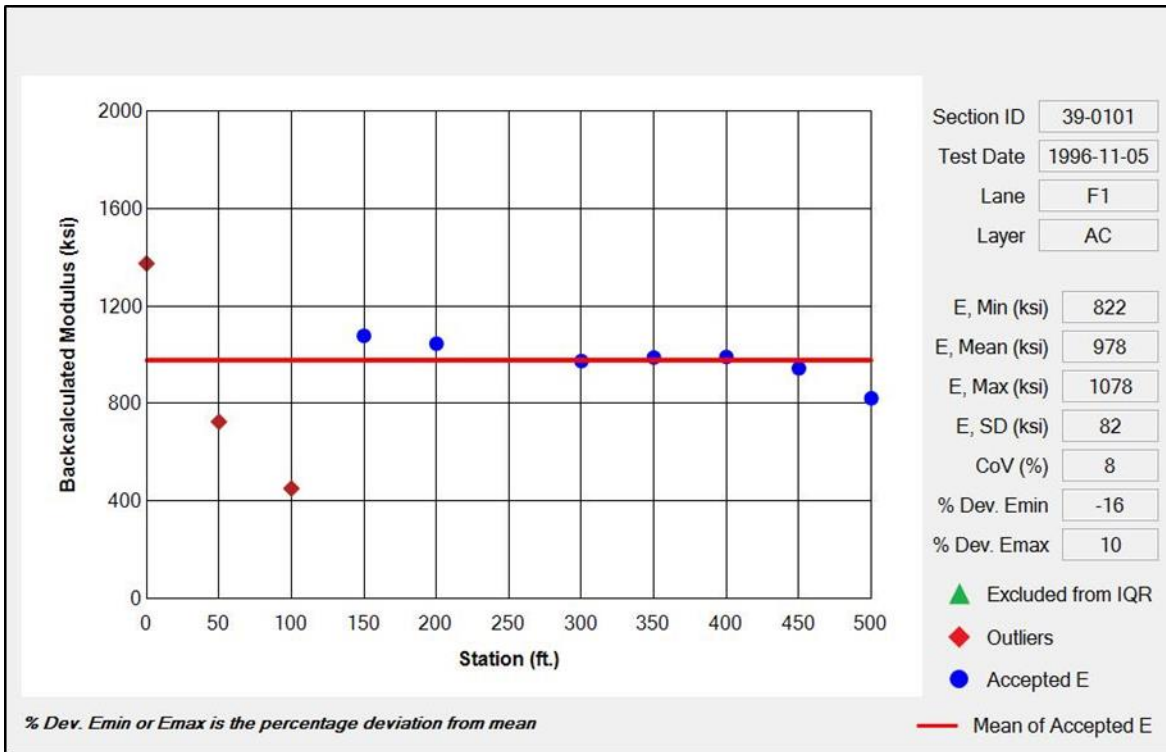
Source: FHWA.

Figure 43. Graph. Stationwise AC *E* plot for test section 39-0101 excluding outliers.

Reducing COV Using the IQR Method

After eliminating the outliers identified by the MAD method, COV was calculated for the remaining $E_{ST\text{-}AVG}$. A 20 percent COV criterion was used based on the variability observed in charts generated for all LTPP sections used in this study. $E_{ST\text{-}AVG}$ with a COV greater than 20 percent were further refined by removing stations outside the IQR. The IQR for any dataset was calculated as the interval between the first quintile (25th percentile data value) and the third quintile (75th percentile data value). Stations for which the average HMA backcalculated E was outside the IQR were removed, and COV was recalculated for the remaining stations. The IQR procedure was applied only to those datasets for which the COV after step 1 of the MAD method was greater than 20 percent. No further filtering was performed if the section average still did not satisfy the 20 percent COV criterion. Figure 44 shows an example of spatial variation in AC layer E for LTPP test section 31-0116, where the COV prior to removal of outliers was 56 percent. Figure 45 shows the outliers as well as stations whose average E was outside the IQR, whose removal reduced the COV to 17 percent.
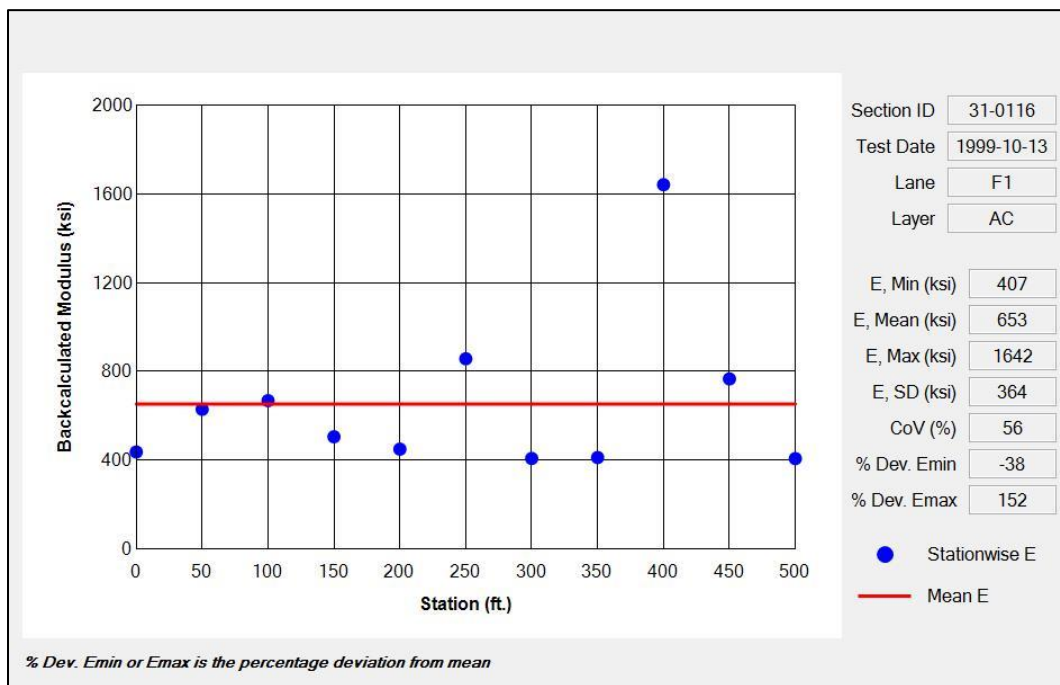
Source: FHWA.

Figure 44. Graph. Stationwise AC *E* plot for test section 31-0116 for all stations.
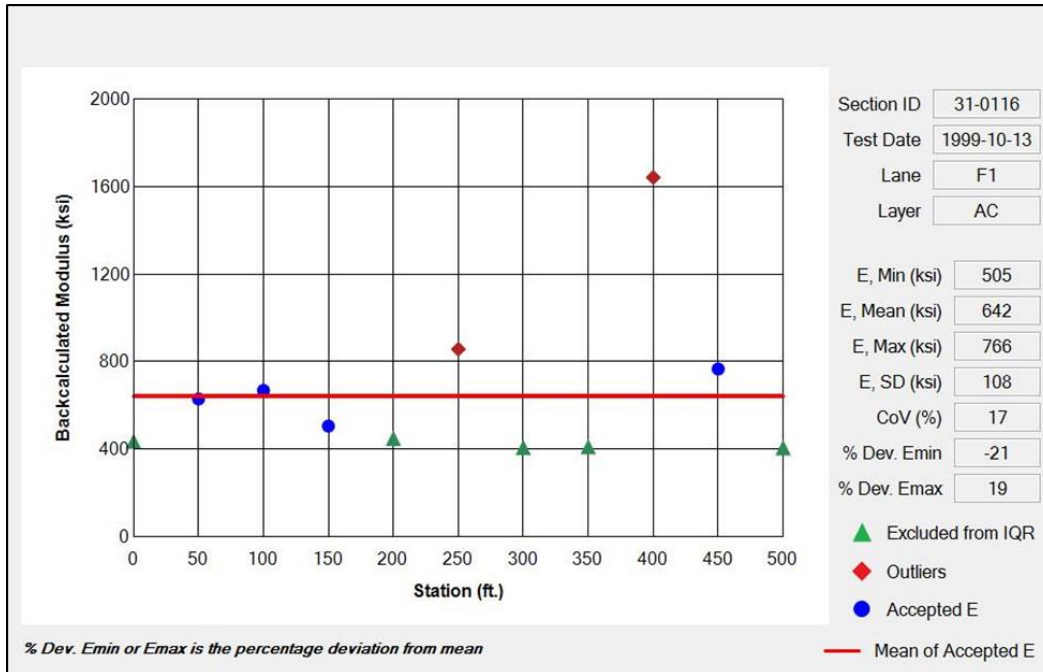
Figure 45. Graph. Stationwise AC *E* plot for test section 31-0116 excluding outliers and stations outside the IQR.

SENSITIVITY OF DEFLECTION-DERIVED AC ELASTIC MODULI ON SELECTED PARAMETERS

The following subsections provide a brief evaluation and discussion on the sensitivity of the deflection-derived elastic AC moduli to a couple of parameters related to the pavement structure and testing procedure.

AC Thickness

AC thickness was a variable within the SPS-1 experiment as well as for the type of base layer. Thin and thick pavement structures were placed with the AC thickness varying from around 4 to over 12 inches, including the asphalt-treated base (ATB) layer. However, the same AC mixture was placed along the same SPS-1 project. As such, E_{FWD} should be the same for the deflection basins measured shortly after construction, accounting for temperature differences between thin and thick layers.

Figure 46 shows the results for the Arizona SPS-1 project from deflection basins measured right after construction (April 1994), while figure 47 shows the same comparisons but for the deflection basins measured at the end of the monitoring period (February 2005).[10] As shown, the AC deflection–derived E_{FWD} values were different between thin and thick AC layers that was not explained by middepth temperature differences. The thinner AC layer consistently exhibited higher E_{FWD} in comparison to the thicker AC layer. Both temperature and load frequency during FWD testing, however, can vary between thin and thick AC layers. Both factors are evaluated in further detail in chapter 5.
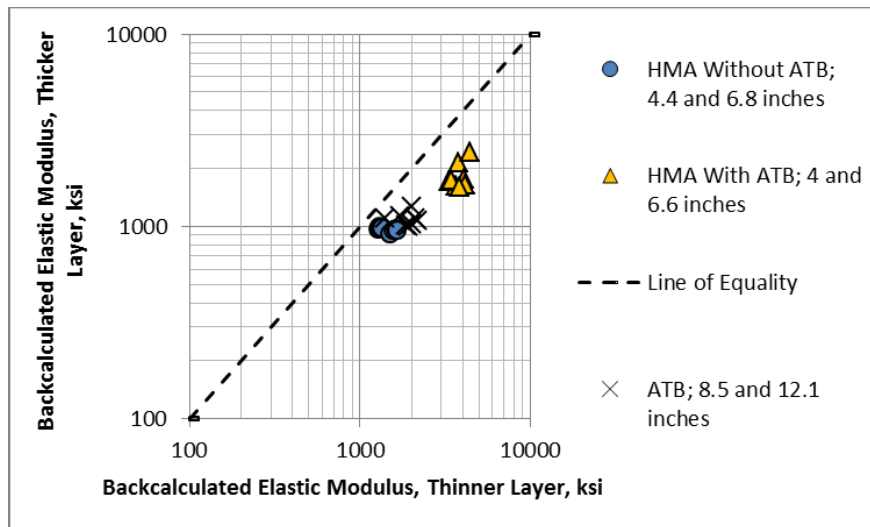
Source: FHWA.

Figure 46. Graph. Arizona SPS-1 project with thickness effect on AC E_{FWD} and deflection basins measured in February 1994.
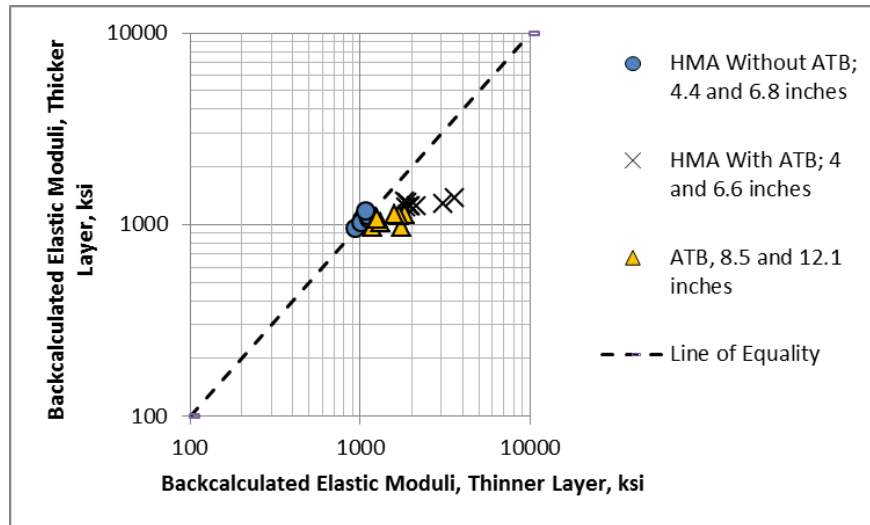
Source: FHWA.

Figure 47. Graph. Arizona SPS-1 project with thickness effect on AC E_{FWD} and deflection basins measured in April 2005.

Drop Height

It is well known that the resilient modulus of unbound aggregate layers and subgrade soils is dependent on the stress state. Coarse-grained soils typically exhibit a stress-hardening response where the resilient or elastic modulus increases with increasing stress state, while fine-grained soils typically exhibit a stress-softening response where the resilient modulus decreases with increasing stress state. AC layers are considered visco-elastic where E_{FWD} is dependent on temperature and loading frequency but independent of stress level.

Many of the solutions, however, do suggest a dependency on stress level or drop height. Figure 48 shows results from the Arizona SPS-1 project where the E_{FWD} increased with higher drop heights during the FWD testing program for the HMA wearing surface. Conversely, the ATB E_{FWD} decreased with increasing drop height.
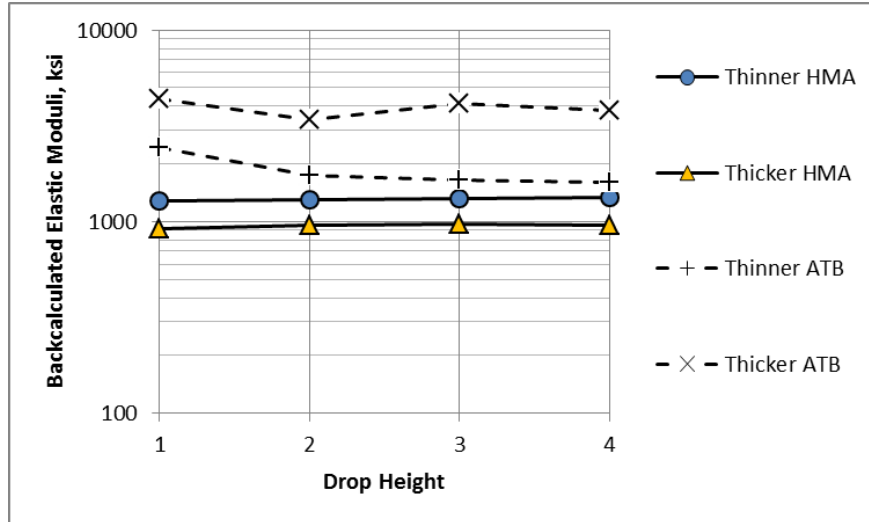
Source: FHWA.

Figure 48. Graph. Arizona SPS-1 project with stress-softening effect for ATB and stress-hardening effects on E_{FWD} of the AC wearing surface.

Figure 49 shows a comparison of the E_{FWD} from drop heights 1 and 4 for the Arizona SPS-1 project. As shown, the ATB or deeper layers were less affected by drop height, while the upper HMA layers consistently exhibited high E_{FWD} for drop height 1 in comparison to the values for drop height 4. Similar results were observed for other SPS-1 projects. Although the stress sensitivity was considered low, this issue was investigated in an effort to reduce the variability and explain as much of the variance as possible. This evaluation is included in chapter 5.
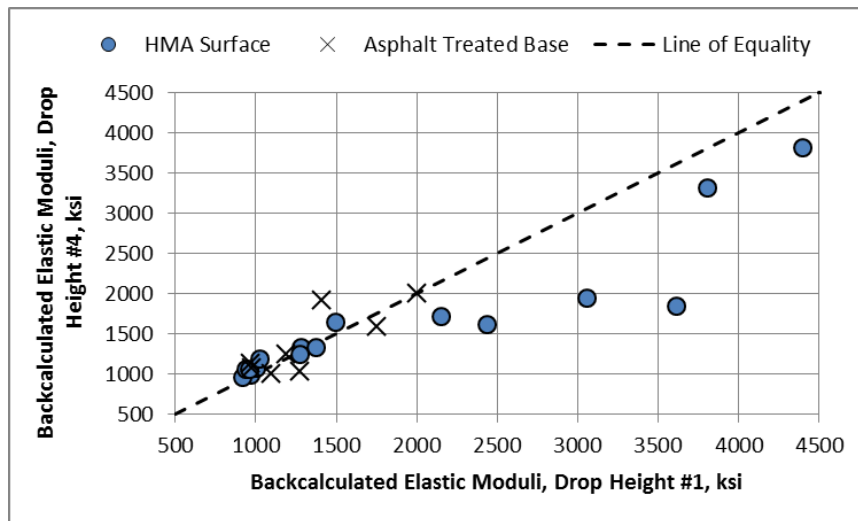
Source: FHWA.

Figure 49. Graph. Arizona SPS-1 project with drop height effect on E_{FWD} of the AC layer.

MEPDG AC DAMAGE CONCEPT: PRELIMINARY PROOF OF CONCEPT

One of the unique components of the MEPDG methodology for rehabilitation design is the characterization of the in-place asphalt layers in terms of damage.[1] The MEPDG method uses

E_{FWD} of the HMA or bituminous layer to determine the amount of damage in the existing asphalt layers by comparing the in-place E_{FWD} to E^*_{PRED} measured in the laboratory. The damage is defined as the ratio of the E_{FWD} to the laboratory-measured E^*_{PRED}. The greater the damage or the lower the ratio, the greater the structural thickness required for an overlay. If this concept is correct, E_{FWD} should decrease over time as damage starts to accumulate (hypothesis 3 in chapter 3).

Time-Dependent Damage Values

Figure 51 illustrate the change in modulus within a narrow temperature range of 60–66 °F for Minnesota GPS test sections 27-1016 and 27-6251, respectively. As shown, there was a continuous decrease in E_{FWD} from the deflection-basin tests conducted between these temperatures. Many other LTPP test sections exhibited this same characteristic for similar FWD middepth test temperatures. Thus, the LTPP E_{FWD} and the area of cracking exhibited over time could be used to confirm or reject this damage concept determination for pavement evaluation and rehabilitation design.
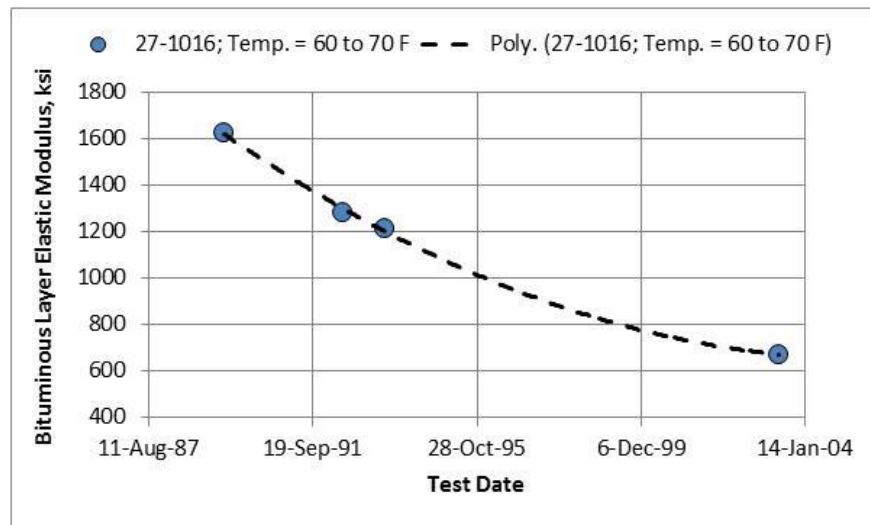
Source: FHWA.

Figure 50. Graph. Decreasing E_{FWD} of the AC layer between 60 and 66 °F over time for use in rehabilitation design for Minnesota GPS test section 27-1016.[47]
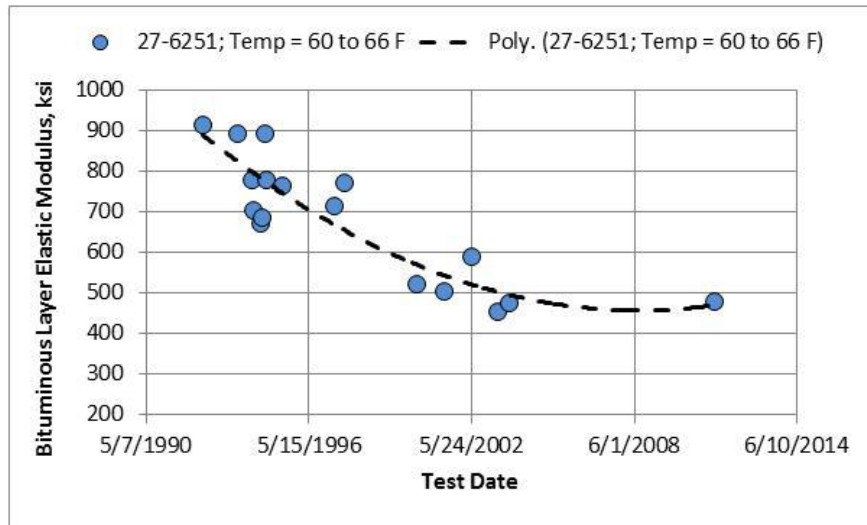
Source: FHWA.

Figure 51. Graph. Decreasing E_{FWD} of the AC layer between 60 and 66 °F over time for use in rehabilitation design for Minnesota GPS test section 27-6251.[47]

Figure 52 illustrates the change in modulus over time and temperature for Minnesota GPS test section 27-6251. As shown, the E_{FWD} values were about the same between 1990 and 1993, while there was a significant decrease in E_{FWD} in 2003 when the pavement was about 10 yr older. This decrease or softening in the moduli is considered to be damage by the MEPDG.[1] Conversely, figure 53 illustrates no change in moduli and no damage or softening between 1990 and 1997 for Minnesota GPS test section 27-1018. In other words, this section did not exhibit any damage between 1990 and 1997.

Source: FHWA.

Figure 52. Graph. Decreasing E_{FWD} of the AC layer over time for use in rehabilitation design for Minnesota GPS test section 27-6251.[47]

59
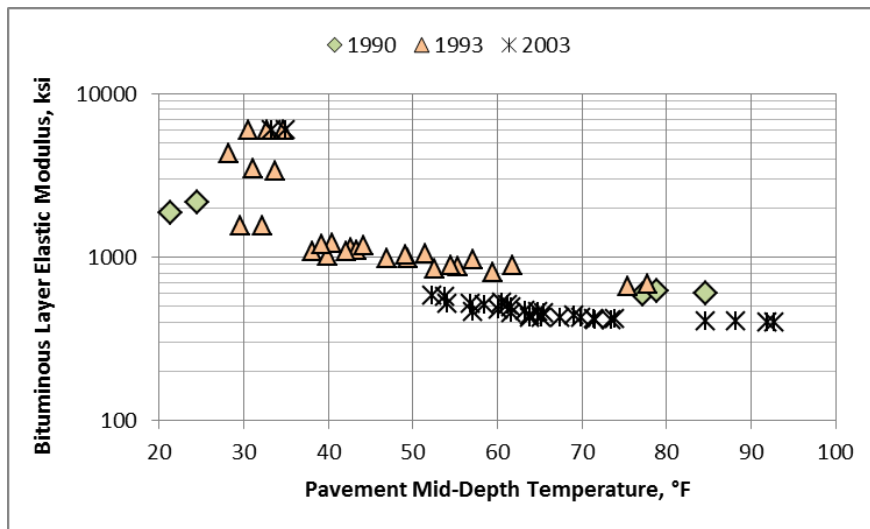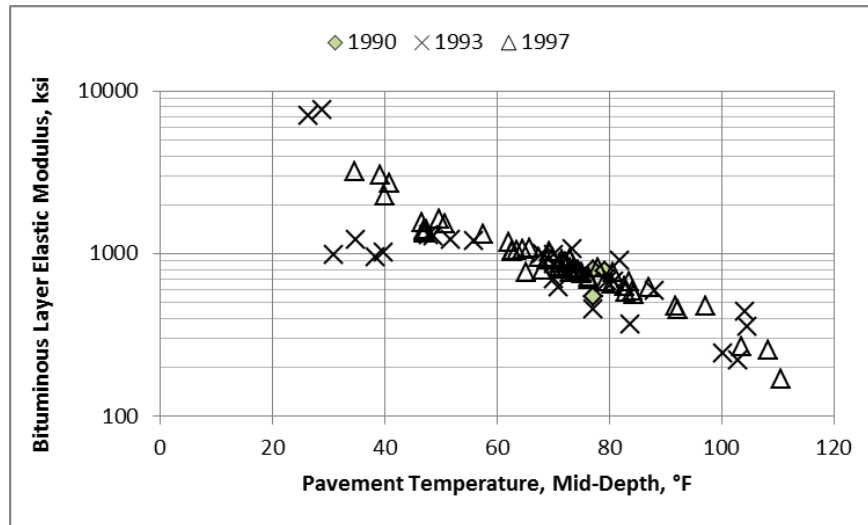
Source: FHWA.

Figure 53. Graph. Decreasing E_{FWD} of the AC layer over time for use in rehabilitation design for Minnesota GPS test section 27-1018.[47]

Another observation that was made relates to the temperature effect or dependence on damage that was based on an analysis of the seasonal monitoring sites where deflections were measured each month over multiple years.[39] As shown in figure 52, the E_{FWD} values were about the same at colder temperatures during the winter months and approached each other at the higher temperatures during the summer months. The greater difference in moduli over time was exhibited within the intermediate temperature range.

Other LTPP sites exhibited this same temperature-dependent damage or softening effect. Thus, the time of year for measuring the amount of in-place damage is probably important. More importantly, the mathematical relationship used in the MEPDG for calculating damage may need to be revised to be temperature dependent.[1] The temperature dependency effect is discussed in more detail in chapter 5.

Modulus Differences Between WPs and Non-WPs

Deflection basins in LTPP were measured in the WPs (lane F3) as well as out of the WPs (lane F1) to determine if the load-response properties were different between the two areas. If the damage concept is correct, then the measurements within the WP should be statistically different than the non-WP measurements for the test section exhibiting damage, and there should be no difference between the two lines for the section not exhibiting damage. Figure 54 and figure 55 include a comparison of the backcalculated elastic layer moduli for the WP and non-WP areas for these two LTPP sections in Minnesota. As shown, a significant difference was observed for GPS test section 27-6251, and no difference was observed for GPS test section 27-1018. This observation provides support for the damage concept incorporated within the MEPDG and makes it easier for agencies to determine whether there is a difference in the loaded and nonloaded areas of the pavement.[1] Simply testing along two lanes can reduce the number of cores that are now required to determine the in-place damage for rehabilitation design and to manage an agency's roadway network for planning future rehabilitation projects.
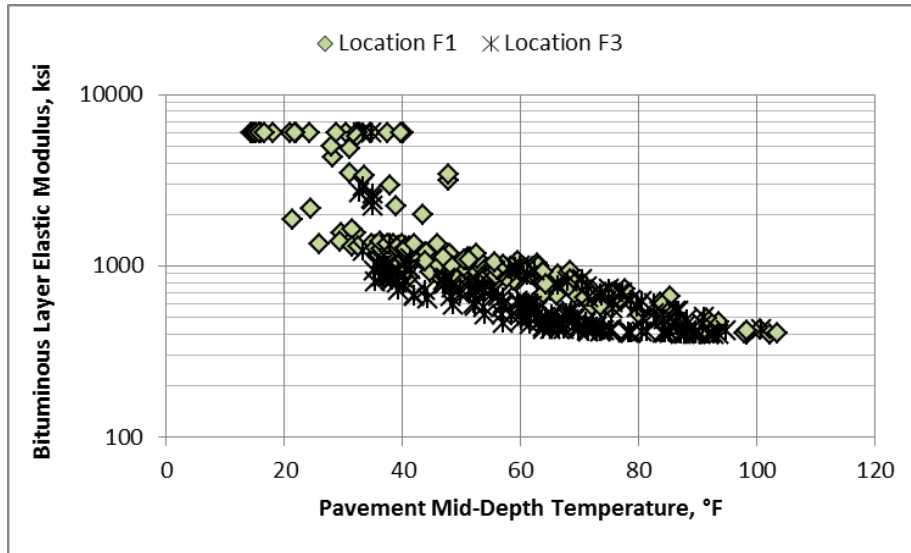
Source: FHWA.

Figure 54. Graph. E_{FWD} of the AC layer between the WP and non-WP for Minnesota GPS test section 27-6251.[47]
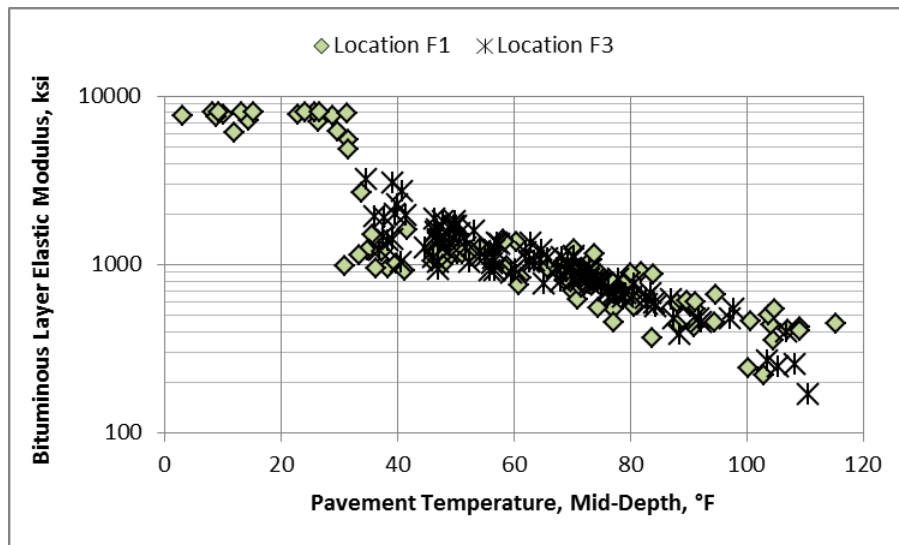
Source: FHWA.

Figure 55. Graph. E_{FWD} of the AC layer between the WP and non-WP for Minnesota GPS test section 27-1018.[47]

This observation by itself should be of significant value to agencies for improving their management prediction and planning capabilities. Simply measuring the deflection basins in the WP versus outside the WP provides a comparison of elastic moduli and whether damage is starting to occur. As extensive surface cracking starts to occur and spread beyond the WPs, however, any difference between measurements made within and outside the WPs is expected to decrease.

CHAPTER 5. PROOF-OF-CONCEPT PRELIMINARY ANALYSES

Some State transportation departments have investigated the correspondence between the damaged/undamaged modulus ratios and fatigue cracking as part of their local calibration of the MEPDG fatigue cracking transfer function.[27,53,1] In fact, some agencies initially defined the coefficients of the transfer function using deflection-based moduli.[27] The purpose of this chapter is to use the process for calculating the in-place damage in accordance with the MEPDG and complete initial analyses for providing proof of concept relative to the rehabilitation approach embedded in the MEPDG for flexible pavements.[1]

CORRESPONDENCE BETWEEN FATIGUE CRACKING AND DEFLECTION-BASED FACTORS

The Arizona Department of Transportation (ADOT), Colorado Department of Transportation (CDOT), GDOT, and Mississippi Department of Transportation (MDOT) are four agencies that revised their fatigue cracking calibration coefficients to fit their data.[27,53–55] Figure 56 and figure 57 are from the GDOT and MDOT studies in relating the modulus ratio used to define the in-place DI to the amount of cracking.[27,53] In both of these studies, DI was calculated using the equation in figure 58. The DI based on the ratio between the field-derived or damaged and laboratory-deriveid or undamaged modulus of the AC layer ($DI_{E\text{-}ratio}$) was correlated to the total amount of fatigue cracking. Some interesting observations from both studies include the following:

- Fatigue cracking was observed at the AC surface at a $DI_{E\text{-}ratio}$ of about 0.15.

- A $DI_{E\text{-}ratio}$ of 0.50 or a 50 percent reduction in modulus corresponds to about 15 percent (GDOT study) to 25 percent (MDOT study) total fatigue cracks.[27,53]

- A total of 50 percent fatigue cracking occurred at a $DI_{E\text{-}ratio}$ of about 0.80 (an E_{FWD}/E^*_{PRED} ratio of 0.20) based on FWD testing within the intermediate temperature range.
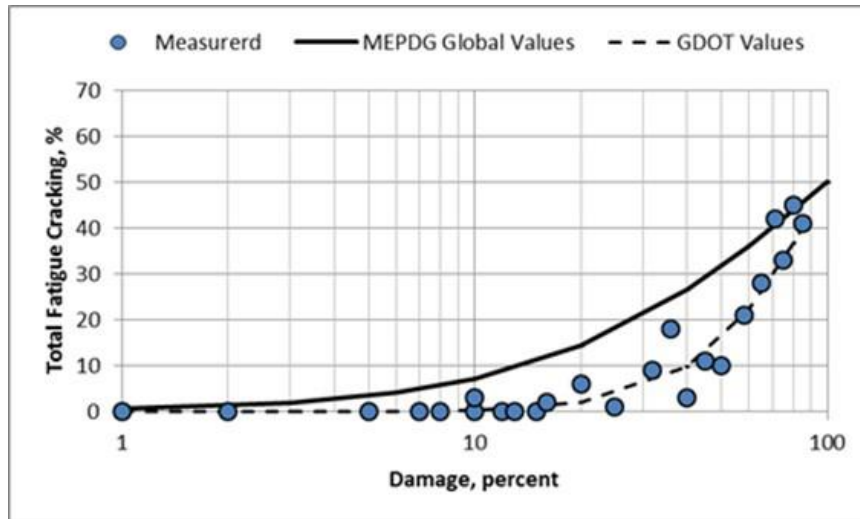
Source: FHWA.
Note: Fatigue cracking transfer function coefficients C_1 and C_2 from the FWD deflection tests and E_{FWD} for the amount of cracking measured on the pavement surface were determined as $C_1 = 2.2$ and $C_2 = 2.2$.

Figure 56. Graph. Comparison of predicted and measured fatigue cracking after local calibration per GDOT study.[27]
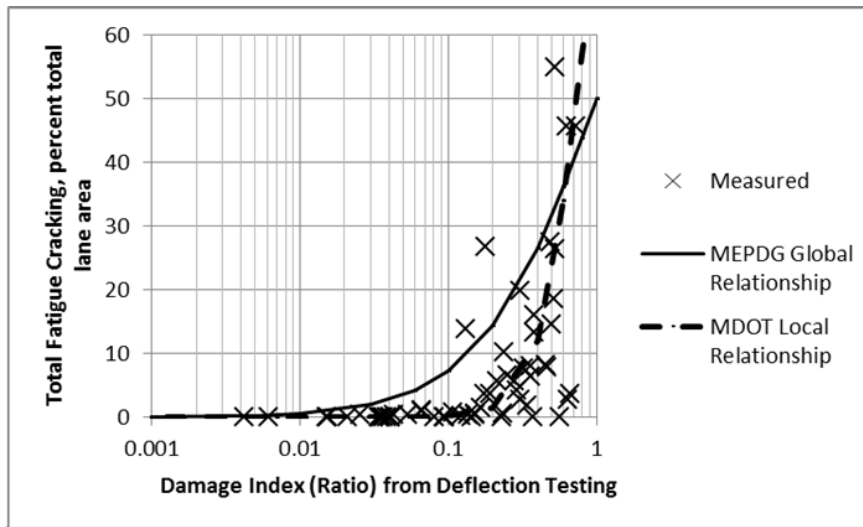
Source: FHWA.
Note: Fatigue cracking transfer function coefficients from the FWD deflection tests and E_{FWD} for the amount of cracking measured on the pavement surface were $C_1 = 3.0$ and $C_2 = 2.8$.

Figure 57. Graph. Comparison of measured total fatigue cracking and the fatigue DI after local calibration per MDOT study.[53]

$$DI_{E\text{-}ratio} = 1 - \frac{E_{FWD}}{E_{PRED}^*}$$

Figure 58. Equation. Calculation of DI using a simplified equation.

Table 9 summarizes the fatigue cracking transfer function coefficients (C_1, C_2, and C_4) for bottom–up cracking derived by different agencies from the local calibration process. As shown, the values varied significantly between different agencies. Later in this chapter, some of the reasons for the variation in the fatigue cracking damage estimates used to derive the transfer function coefficients are identified, and the preliminary analyses used for evaluating the MEPDG input-level-1 rehabilitation design procedure are discussed.[1]

Table 9. Local calibration factors for predicting fatigue cracks.

Agency	Fatigue Strength Relationship			Cracking Transfer Function		
	β_{f1}	β_{f2}	β_{f3}	C_1	C_2	C_4
Global value	1.0	1.00	1.0	1.00	1.00	6,000
ADOT[54]	249.01	1.00	1.23	1.00	4.50	6,000
CDOT[55]	130.37	1.00	1.22	0.07	2.35	6,000
GDOT[27]	0.20	1.00	1.00	2.20	2.20	6,000
MDOT[53]	2.01	1.00	1.00	3.00	2.80	6,000
Missouri Department of Transportation	1.00	1.00	1.00	1.00	1.00	6,000
North Carolina Department of Transportation[56]	3.50	0.72	0.60	0.24	0.24	6,000
Ohio Department of Transportation	1.00	1.00	1.00	1.00	1.00	6,000
Oregon Department of Transportation	1.00	1.00	1.00	0.56	0.23	6,000
UDOT	1.00	1.00	1.00	1.00	1.00	6,000
Washington Department of Transportation	0.96	0.97	1.03	1.07	1.00	6,000
Wisconsin Department of Transportation	1.00	1.00	1.00	1.00	1.00	6,000
Wyoming Department of Transportation[57]	1.00	1.00	1.00	0.50	1.47	6,000

Note: The local calibration coefficients were extracted from the agency design manuals and/or software; most of these documents are not formally published.

A complete database of pavement response parameters was prepared for this study that included five primary data elements: (1) deflection data (i.e., peak deflection data for individual drops from the MON_DEFL_DROP_DATA table), (2) E_{FWD} for individual drops, (3) FWD deflection–time history files, (4) AC master curve coefficients calculated in accordance with the MEPDG procedure, and (5) cracking data measured over time.[10,1] For the preliminary data analysis, the focus was on the E_{FWD} data from the peak deflection data and the deflection–time history data. The preliminary analyses included several steps or calculations using two deflection-based factors that were discussed in chapter 2: (1) E_{FWD} and (2) dissipated work. The steps and calculations included the following:

1. Segregate the deflection data into two groups: (1) test dates shortly after construction when no fatigue cracks were recorded and (2) test dates for which fatigue cracks were observed.

2. Use a constant frequency of 15 Hz and the middepth temperature to calculate E^*_{PRED} for each FWD test date.

3. Calculate the E_{FWD}/E^*_{PRED} ratios between (test lane F1) and within (test lane F3) the WPs. These ratios should be different when cracks start to occur within the WP, as illustrated in figure 54 in chapter 4.

4. Normalize the E_{FWD}/E^*_{PRED} ratios calculated over time to the ratio for the first FWD test data after construction.

5. Estimate the frequency for which E^*_{PRED} modulus equals E_{FWD} for the first FWD test date without any fatigue cracks.

6. Compare the total amount of cracking measured over time to the E_{FWD}/E^*_{PRED} time–series data using the two frequencies. A significant difference should exist along test lane F3 (within WP) between the test dates before and after cracks start to occur.

7. Calculate the dissipated work from the deflection–time series data and compare the same trends as noted in the calculations above.

LTPP SECTIONS USED TO DEMONSTRATE THE PRELIMINARY ANALYSES

Five LTPP test sections were selected to demonstrate the preliminary analyses used for all sections included in table 4 and table 5 in chapter 3. These LTPP test sections were from the Alabama SPS-1 and Kansas SPS-9 experiments and represent new construction. The five test sections include the following:

- **Test section 1—Alabama SPS-1 test section 01-0103**: Full-depth section.

- **Test section 2—Alabama SPS-1 test section 01-010**2: Thin-strength section.

- **Test section 3—Alabama SPS-1 test section 01-0110**: Thick section with a drainage layer.

- **Test section 4—Kansas SPS-9 test section 20-0901**: Superpave® designed HMA mixture.

- **Test section 5—Kansas SPS-9 test section 20-0903**: Conventionally designed HMA mixture.

The Alabama and Kansas test sections were selected because both exhibited higher amounts of cracking within the monitoring period, had multiple days of testing before any cracks were recorded in the LTPP database, had similar subgrade soil classifications, and did not represent extreme climate conditions. Details on the construction, AC mixtures, E_{FWD} values, dissipated work, and distress measurements for these sections are discussed in the following subsections.

Pavement Construction Details

This section describes the pavement structure, measured fatigue cracking performance, FWD loading frequency, and damage calculations for the Alabama SPS-1 and Kansas SPS-9 sections.

Alabama SPS-1 Test Sections

The Alabama SPS-1 project was opened to traffic on April 30, 1991, and the first day of FWD testing was on March 11, 1993, less than 2 yr after the date of construction.[10] The subgrade was a fine-grained, low-plasticity clay soil. The three test sections from this project included the following:

- **Test section 1—01-0103**: The pavement structure consisted of 4.2 inches of AC and 7.4 inches of an asphalt-stabilized base layer (defined as a full-depth AC pavement). The AC consisted of two layers: a 2.8-inch AC base and 1.4-inch wearing surface. After construction, no major construction or maintenance event occurred within the monitoring period.

- **Test section 2—01-0102**: The pavement structure consisted of 4.2 inches of AC and a 12-inch crushed aggregate base layer. The AC consisted of two layers, which were identical to section 01-0103. Full-depth patching was used to repair areas along this section, which was done on April, 17, 2003.

- **Test section 3—01-0110**: This section was a full-depth AC pavement with a permeable ATB (PATB) layer. The PATB layer was placed for drainage to investigate the effect of drainage layers on pavement performance. The pavement structure consisted of 7.4 inches of AC, 3.7 inches of an ATB layer, and 4 inches of a PATB layer. The AC consisted of two layers: a 6-inch AC base and 1.4-inch wearing surface. The section also included a nonstructural engineering fabric placed under the PATB layer. After construction, no major construction or maintenance event occurred within the monitoring period.

Kansas SPS-9 Test Sections

The Kansas SPS-9 project was opened to traffic on November 1, 1993, and the first day of FWD testing was on March 11, 1993, less than 1 yr after construction.[10] The subgrade soil for this project was a fine-grained, low-plasticity clay soil—the same classification as the soil along the Alabama SPS-1 project. The two test sections from this project included the following:

- **Test section 4—20-0903**: The pavement structure consisted of 11 inches of AC and a 6-inch ATB layer. The AC consisted of two layers: a 9.5-inch AC base and 1.5-inch wearing surface. After construction, no major construction or maintenance event occurred within the monitoring period.

- **Test section 5—20-0901**: The structure for this section was the same as for test section 20-0903. The differences between test section 20-0901 and test section 20-0903 include the asphalt binder used in the AC mixtures and how those mixtures were designed. Test section 20-0903 represents the conventional asphalt binder and mixture designed

by the Kansas Department of Transportation, while test section 20-0901 represents the Superpave® binder and mixture design procedure. All other materials and structure details are the same. The other difference between test sections 20-0903 and 20-0901 was that crack sealing was performed on June 1, 1999, for test section 20-0901, while no maintenance was performed on section 20-0903.

Load-Related Cracking

The total amount of cracking was extracted from LTPP database table MON_DIS_AC_REV for all distress survey dates.[10] Figure 59 through figure 63 show the total amount of load-related fatigue cracking observed for each of the five LTPP test sections. As shown, all test sections exhibited an appreciable amount of cracking. Test section 01-0102 exhibited the highest amount of cracking over time, as expected, because it was the thinnest section with the same traffic and on-site conditions of the Alabama SPS-1 sections. Kansas test section 20-0903 exhibited a high level of cracking, while Kansas test section 20-0901 exhibited significantly less cracking even though both had similar pavement cross sections. The major difference between these two sections was the asphalt binder grade. Different binder grades were selected for the different test sections, one that was commonly used by the agency for the local climate conditions and the other in accordance with the Superpave® binder specification for the local climate conditions.
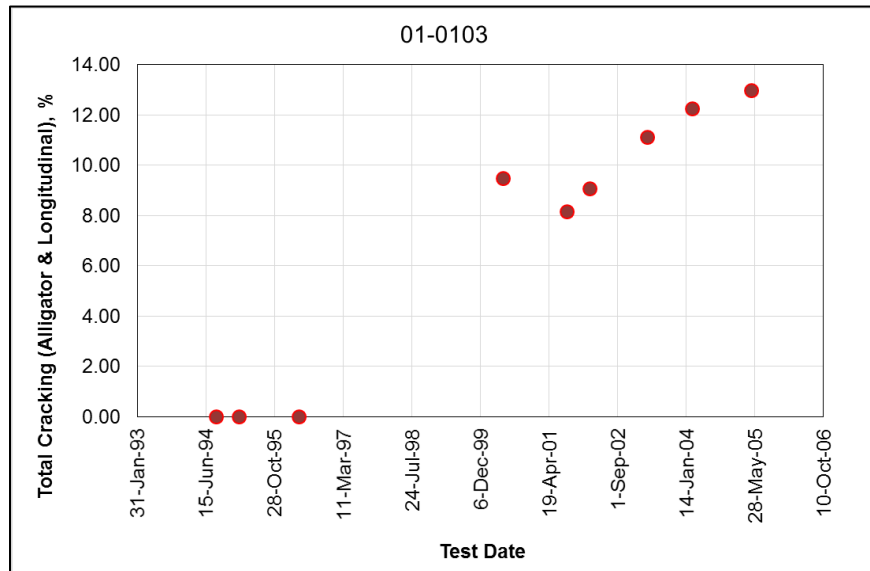
Source: FHWA.

Figure 59. Graph. Total cracking measured over time for Alabama test section 01-0103.
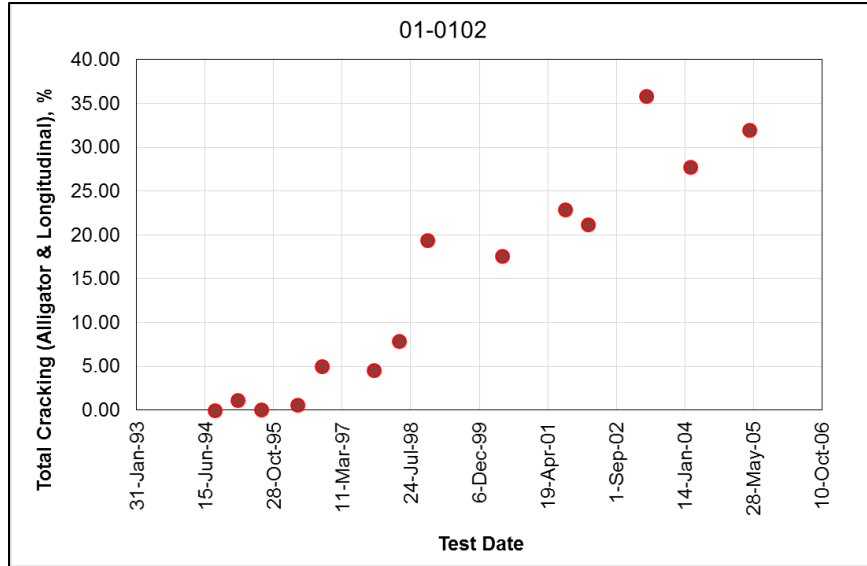
Figure 60. Graph. Total cracking measured over time for Alabama test section 01-0102.
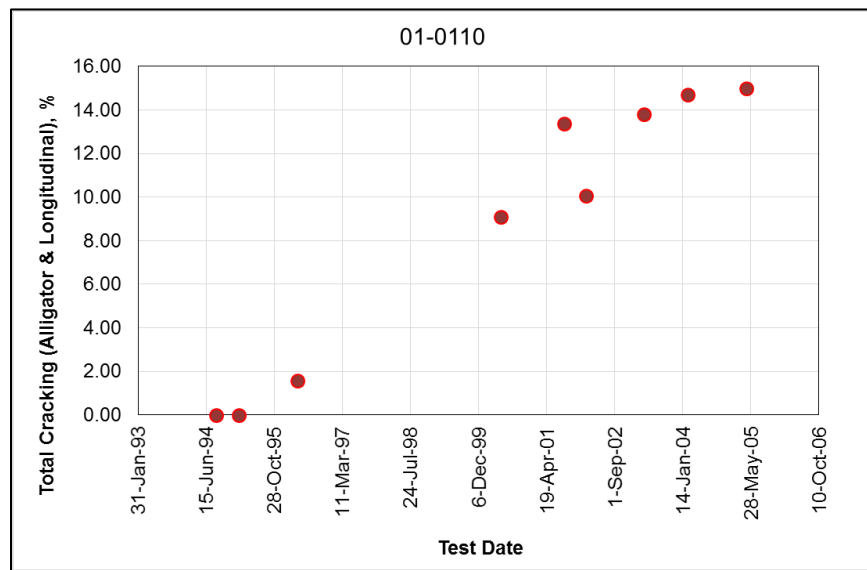
Figure 61. Graph. Total cracking measured over time for Alabama test section 01-0110.

69
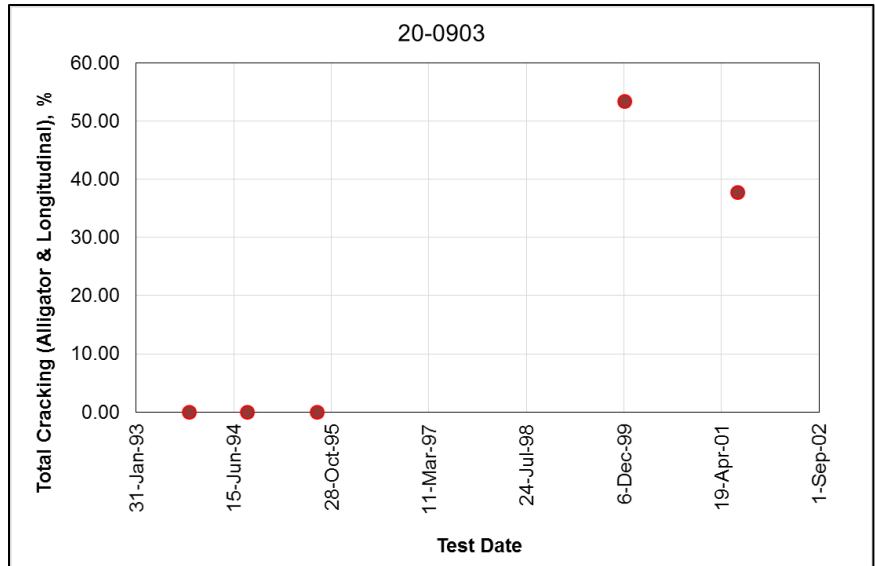
Source: FHWA.

Figure 62. Graph. Total cracking measured over time for Kansas test section 20-0903.
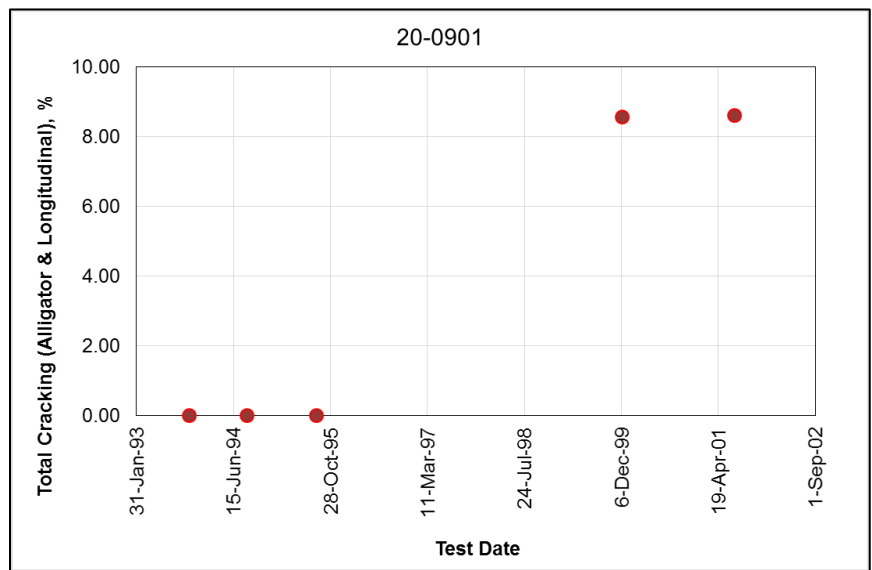
Source: FHWA.

Figure 63. Graph. Total cracking measured over time for Kansas test section 20-0901.

AC Dynamic Moduli Master Curve Coefficients

E^* master curve parameters were extracted from the LTPP table TST_ESTAR_ MODULUS_COEFF and are summarized in table 10.[10] E^*_{PRED} was significantly different between the two LTPP projects with different AC mixtures. However, a loading frequency was needed to calculate E^*_{PRED} for the FWD middepth temperature during deflection testing.

Table 10. *E** master curve parameters.

E* Master Curve Parameter	Coefficient	Test Section				
		Alabama			Kansas	
		01-0102	01-0103	01-0110	20-0901	20-0903
Surface Layer Mixture						
Modulus	1	3.6570	3.6570	3.6570	3.6100	3.6100
Modulus	2	2.9960	2.9960	2.9960	3.0570	3.0570
Modulus	3	−0.9780	−0.9780	−0.9780	−1.0840	−1.0840
Modulus	4	0.4760	0.4760	0.4760	0.4530	0.4530
Shift factor	1	0.0010	0.0010	0.0001	0.0010	0.0010
Shift factor	2	−0.1650	−0.1650	−0.1650	−0.1930	−0.1930
Shift factor	3	3.1610	3.1610	3.1610	3.6070	3.6070
Lower Layer Mixture						
Modulus	1	3.8440	3.8440	3.8440	N/A	N/A
Modulus	2	2.7530	2.7530	2.7530	N/A	N/A
Modulus	3	−0.5750	−0.5750	−0.5750	N/A	N/A
Modulus	4	0.4910	0.4910	0.4910	N/A	N/A
Shift factor	1	0.0010	0.0010	0.0010	N/A	N/A
Shift factor	2	−0.1650	−0.1650	−0.1650	N/A	N/A
Shift factor	3	3.1610	3.1610	3.1610	N/A	N/A

N/A = not available.

One of the questions identified in chapter 2 was what frequency should be used to estimate the $E*_{PRED}$. Most of the previous studies have used a constant frequency but recognized that frequency was probably dependent on temperature and/or structure.[27] The following section discusses the different approaches for determining the FWD loading frequency.

LOAD FREQUENCY FOR UNDAMAGED DYNAMIC MODULUS CALCULATION

As noted previously, a constant frequency has been the common method used to determine the laboratory equivalent $E*_{PRED}$ to represent the undamaged condition of AC layers. The *Mechanistic-Empirical Pavement Design Guide—A Manual of Practice* suggests the use of a frequency varying from 10 to 25 Hz.[2] This range of frequency was used to derive $E*_{PRED}$ in estimating DI. However, the FWD load frequency has been found to be dependent on temperature and structure. As such, two other approaches besides using a constant value were used for estimating the FWD load frequency: (1) frequency calculated from the E_{FWD} and (2) frequency calculated from the load duration. These two approaches are described in more detail in the following subsections.

Frequency Derived from E_{FWD}

In this approach, FWD frequency was estimated as the reduced frequency at which $E*_{PRED}$ was equal to E_{FWD}. A flowchart illustrating the frequency backcalculation procedure is shown in figure 64. In the figure, δ is the logarithm of minimum $E*$, and α is the difference between maximum and minimum $E*$ for an asphalt mixture.
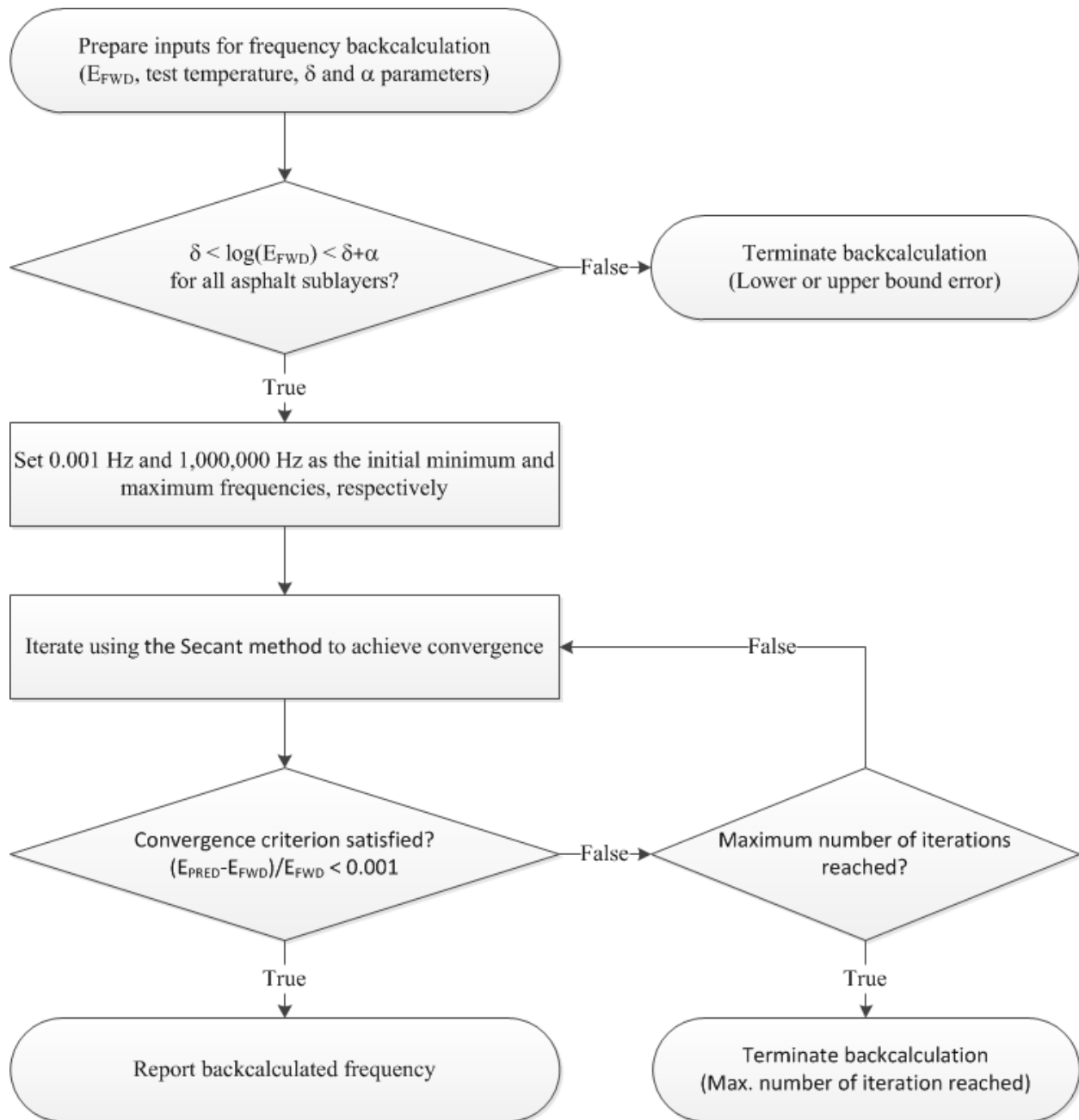
Source: FHWA.

Figure 64. Flowchart. Steps to backcalculate the FWD loading frequency.

Almost about all of the new flexible pavement test sections within the LTPP Program have multiple AC layers. The backcalculation process discussed in chapter 4 combined like layers where appropriate because of the limit on number of layers and thin layers. For a test section having two or more AC sublayers with different master curve coefficients, $E*$ was calculated for each sublayer, and the thickness-weighted average of these individual values was taken as the representative $E_{undamaged}$ of the entire AC layer that was used in the backcalculation process.

To ensure that the FWD moduli were within the range defined by sigmoidal function (i.e., to avoid frequency backcalculation when the FWD modulus is above or below the entire range of the master curve), the FWD modulus was checked against the minimum and maximum values of the individual sublayer. The frequency was backcalculated using the secant method (also known as the bisection method) and compared to the minimum and maximum frequency limits of 0.001 and 10^6 Hz, respectively. The frequency backcalculation iterative process was terminated if any of the following limits were encountered, as shown in figure 64:

- **Upper bound error encountered**: The FWD modulus was greater than the maximum dynamic modulus defined by the sigmoidal function.

- **Lower bound error encountered**: The FWD modulus was less than the minimum dynamic modulus defined by the sigmoidal function.

- **Maximum iterations reached**: The secant method reached the maximum number of iterations (i.e., 100) without achieving the convergence criterion.

Table 11 summarizes the number of observed errors during the frequency backcalculation. Although the lower limit was completely removed after removing sections from Ontario, the other errors were still evident in the data. The reason for the low frequencies for the Ontario test section was unknown but is probably related to the pavement structure simulation or a construction anomaly. These FWD drops that did not converge were subsequently removed from further analysis.

Table 11. Number of errors encountered in the frequency backcalculation process.

LTPP Test Section	Number of Maximum Iterations Reached	Number of Upper Bound Exceed Error	Number of Tolerance Criterion Fulfilled	Grand Total
01-0102	0	0	23,698	23,698
01-0103	13	99	1,660	1,772
01-0110	6	18	2,369	2,393
04-0903	10	0	911	921
04-A902	25	0	894	919
10-0104	0	0	1,409	1,409
12-0112	0	0	17	17
19-0111	106	364	638	1,108
20-0111	0	3	1,364	1,367
20-0901	0	0	1,396	1,396
20-0903	0	0	1,300	1,300
26-0118	20	218	1,009	1,247
26-0121	11	15	854	880
26-0123	139	621	1,243	2,003
26-0124	198	229	1,507	1,934
28-0806	0	0	1,729	1,729

LTPP Test Section	Number of Maximum Iterations Reached	Number of Upper Bound Exceed Error	Number of Tolerance Criterion Fulfilled	Grand Total
29-A801	60	0	685	745
29-A802	15	0	884	899
30-0113	0	0	1,626	1,626
32-0109	26	0	2,075	2,101
36-0801	9	5	40,732	40,746
37-0802	0	0	2,015	2,015
37-0859	223	186	1,070	1,479
39-0104	0	0	1,645	1,645
39-0111	36	116	380	532
39-0160	3	0	964	967
39-0903	0	2	1,222	1,224
40-0123	40	21	1,265	1,326
51-0114	0	0	30,866	30,866
51-0120	0	0	1,699	1,699
55-0123	2	0	898	900
55-C960	0	0	867	867
90-0962	0	0	960	960
Grand Total	**942**	**1,897**	**131,851**	**134,690**

Figure 65 shows an example of the process used to backcalculate load frequencies for drop heights 1 and 4 from Alabama test section 01-0103. As shown, drop height 4 (target load of 16 kip) yielded a reasonable loading frequency of 35 Hz, but the loading frequency from drop height 1 (target load of 6 kip) was an order of magnitude greater. This suggests that the backcalculated frequency was highly variable and/or outside the typical range reported in the literature. It is also important to note that many of the backcalculated frequencies for drop height 1 were significantly greater than for drop heights 2, 3, and 4, which is consistent with the observation from figure 49 in chapter 4.
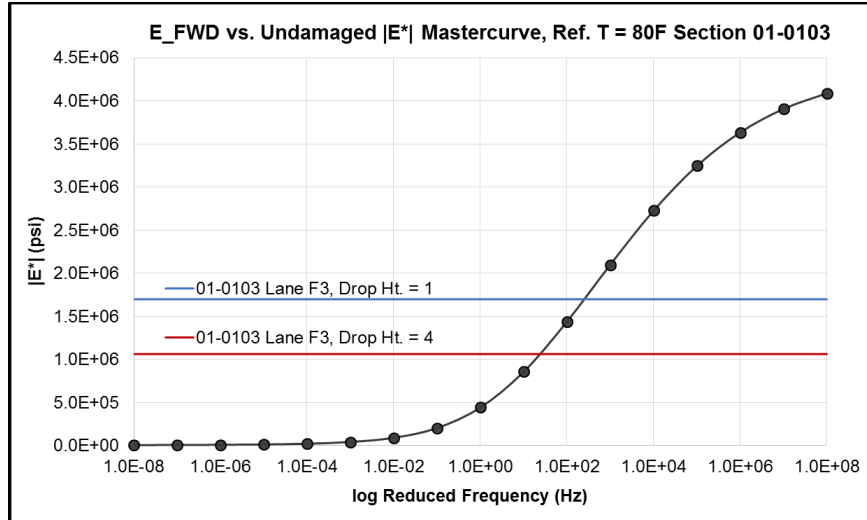
Source: FHWA.

Figure 65. Graph. Backcalculated FWD load frequency for drop heights 1 and 4 for Alabama test section 01-0103.

To assess the variability of the backcalculated frequencies, basic statistics (i.e., the average, standard deviation, and COV) were determined from the first FWD test date right after construction when no damage was assumed and should be appropriate. The results are summarized in table 12 for the test sections included in the preliminary analysis. As shown, the variability of the backcalculated frequency was extremely high, with COVs ranging from 36.6 to 625.0 percent. In addition, most of the average backcalculated frequencies were outside the typical FWD frequency range used for measuring the dynamic modulus in the laboratory, ranging from as low as 0.04 Hz to as high as 500,094.82 Hz. Obviously, these values should not be used to estimate the dynamic modulus from the undamaged AC master curve. One reason for this wide range of values is a result of the stress-sensitivity from the backcalculated FWD moduli, while no stress-sensitivity is considered or included in the laboratory-derived $E*_{undamaged}$ master curve.

75

Table 12. Summary of backcalculated frequencies from first FWD test date.

LTPP Test Section	Average Frequency (Hz)	Standard Deviation (Hz)	COV (Percent)
01-0102	2.59	1.93	74.5
01-0103	835.78	1,966.68	235.3
01-0110	1.62	1.21	74.7
04-0903	0.17	0.14	81.9
04-A902	0.43	0.49	112.3
10-0104	0.20	0.25	123.8
12-0112	40.53	NA	N/A
19-0111	22.43	11.16	49.7
20-0111	41.96	134.52	320.6
20-0901	5.17	2.87	55.4
20-0903	3.18	1.42	44.6
26-0118	83,398.51	77,779.92	93.3
26-0121	0.16	0.17	108.0
26-0123	500,094.82	467,588.91	93.5
26-0124	3,724.98	7,628.72	204.8
28-0806	1.40	0.68	48.7
29-A801	0.04	0.04	84.0
29-A802	0.05	0.04	81.8
30-0113	1.53	1.29	84.6
36-0801	2.94	2.00	68.2
37-0802	0.28	0.15	52.8
37-0859	1,639.37	2,082.25	127.0
39-0903	8.87	9.10	102.6
40-0123	18,967.74	118,551.08	625.0
51-0114	0.17	0.15	86.9
51-0120	512.22	187.55	36.6
55-0123	5.54	4.87	87.9
55-C960	2.89	1.71	59.1

N/A = not available or an insufficient number of backcalculated frequencies converged.

Frequency Calculated from FWD Load Duration

The other approach to determine the FWD load frequency was to estimate it as a function of the load duration recorded during FWD testing. Figure 66 shows an example for determining the FWD load duration from the load–time history plot. To facilitate this methodology, the duration of the FWD load was calculated based on the following steps:

1. Determine the magnitude of the peak load and the time at which the peak load is observed for each FWD drop.

2. Identify the points corresponding to 1 percent of the peak load magnitude from both sides of the peak load. These points were regarded as the starting and ending points of the FWD load.

3. Calculate the FWD load duration as the time difference between the starting and ending points.
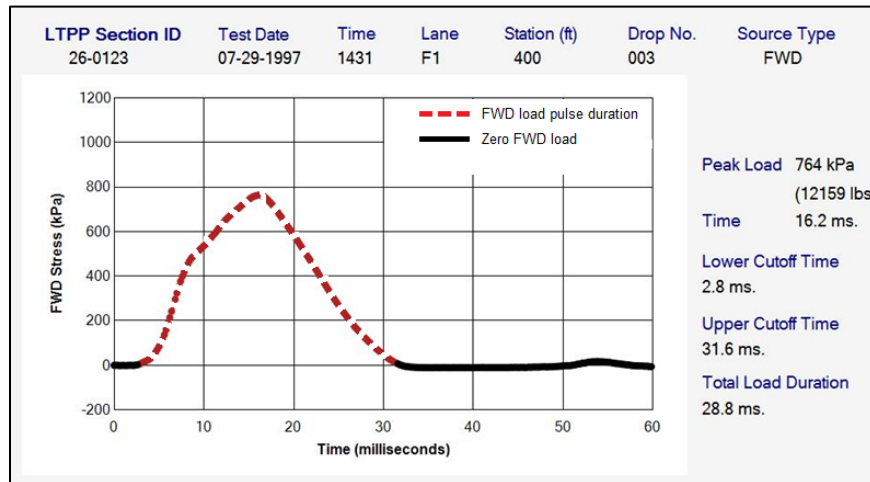
Source: FHWA.
1 kPa = 0.145 psi.

Figure 66. Graph. FWD load duration from the load–time history data.

Figure 67 shows a plot of the FWD load duration versus the peak load measured during FWD testing. As shown, the FWD load duration generally decreased with increasing peak load, even though the comparison has a lot of variability. For example, the load duration for drop height 2 (target load of 9 kip) ranged from approximately 21 to 35 ms. Load frequency is inversely proportional to load duration, which was documented previously in table 3. Thus, a decrease in load duration with increasing drop height or impact load infers the load frequency increased with drop height. This observation is just the opposite for many sites where the backcalculated frequency from E_{FWD} for drop height 1 was greater than the frequency from E_{FWD} for drop height 4.
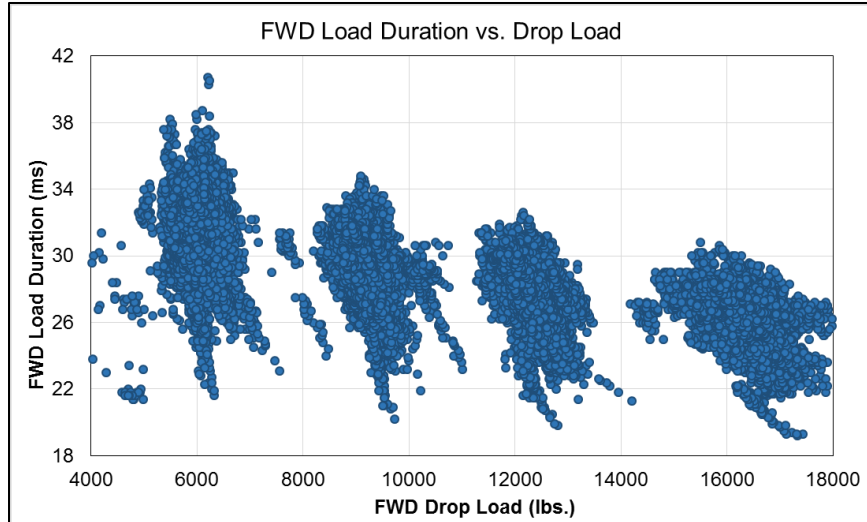
Source: FHWA.

Figure 67. Graph. FWD load duration measured for the peak load of the four drop heights.

Figure 68 shows the mean and the standard deviation of the load durations calculated for each site for drop height 2 (target load of 9 kip). The mean of the FWD load duration varied between the sites, with the lowest mean value of 27.0 ms observed from test section 26-0121 and the highest value of 31.4 ms observed from test section 20-0903. As such, the FWD load duration was probably dependent on other site or structural factors, such as temperature gradient, moisture content of the underlying base and soils, total thickness of the AC layers, E of the supporting layers, etc.
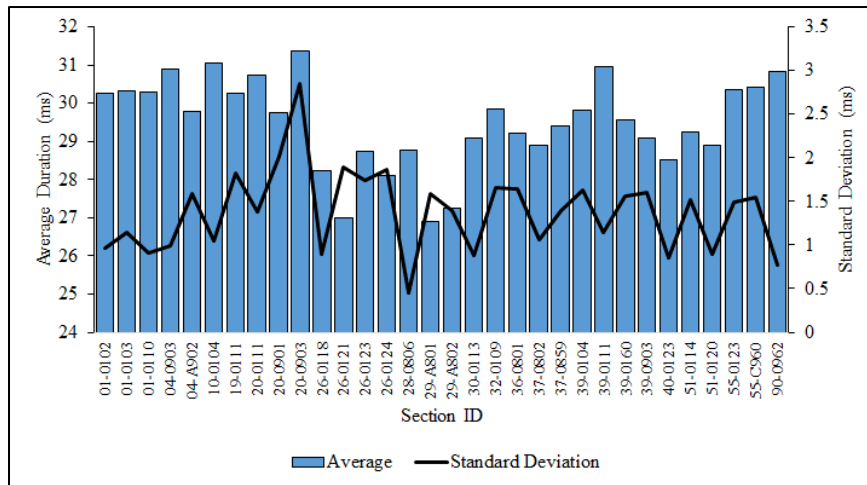
Source: FHWA.

Figure 68. Graph. Average and standard deviation of FWD load duration for each LTPP test section used in the preliminary analyses.

An analysis of covariance (ANCOVA) was performed to determine the site-dependent factors that were affecting the FWD load duration. The variables included in the ANCOVA were peak load magnitude, climate zone, pavement age, lane, asphalt thickness, base type, backcalculated modulus, asphalt temperature, total cracking, and presence of a rigid layer. Table 13 summarizes

the results from the ANCOVA, which found all variables significantly affected the FWD load duration, with the exception of total cracking. The ANCOVA results in table 13 show the degrees of freedom (DOF), sum of square (SS), mean square, F-statistic (F-value), and probability (Pr) of the F-value ($Pr > F$-value). This finding potentially eliminates any simplistic method for determining the FWD load frequency. Chapter 6 includes a more detailed analysis of the FWD load–time history data to confirm this observation.

Table 13. ANCOVA results for FWD load duration.

Variable	DOF	SS	MS	*F*-value	*Pr* > *F*-value
Peak load	1	46,130	46,130	39,223.150	<2.2E-16
Climate zone	3	253	84	71.687	<2.2E-16
Pavement age	1	763	763	648.677	<2.2E-16
Lane number	1	1,109	1,109	942.667	<2.2E-16
HMA thickness	1	179	179	152.308	<2.2E-16
Base type	6	2,174	362	308.077	<2.2E-16
Backcalculated HMA modulus	1	6,581	6,581	5,595.757	<2.2E-16
HMA temperature	1	9,878	9,878	8,398.551	<2.2E-16
Total cracking	1	2	2	2.107	0.1466
Presence of rigid layer	1	42	42	35.835	2.21E-09
Residuals	12,039	14,159	1	—	—

—Residuals were not calculated for the F-value.
SS = sum of square.
MS = mean square.

Table 3 in chapter 2 summarizes the different methodologies proposed and used by different researchers for converting the FWD load duration to frequency. Two of the most frequently used methodologies are (1) frequency is inversely proportional to (t) and (2) frequency is inversely proportional to $2 \times t$. Figure 69 and figure 70 show E_{FWD} plotted against E^*_{PRED} calculated using a load frequency of $1/t$ and $1/2t$, respectively.
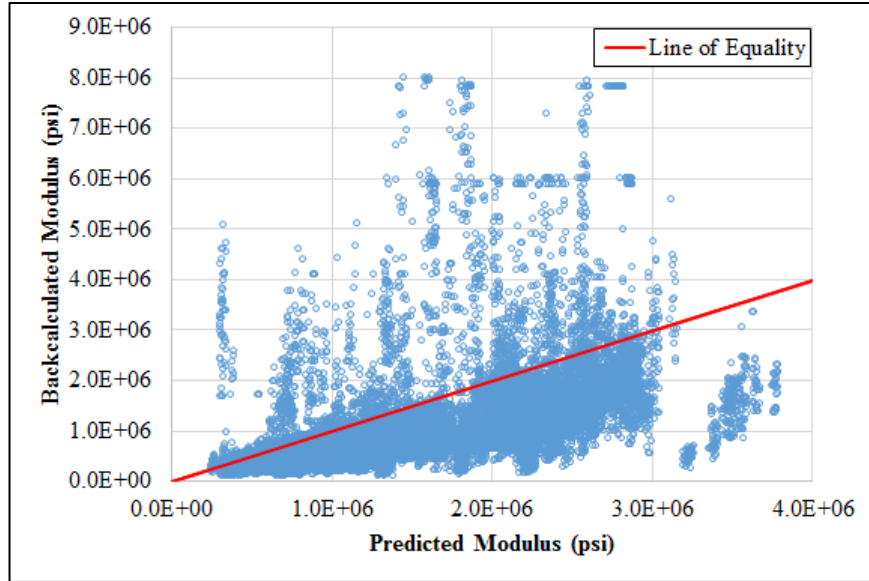
Source: FHWA.

Figure 69. Graph. E^*_{PRED} calculated using frequency computed as the inverse of loading duration ($1/t$) compared to E_{FWD}.
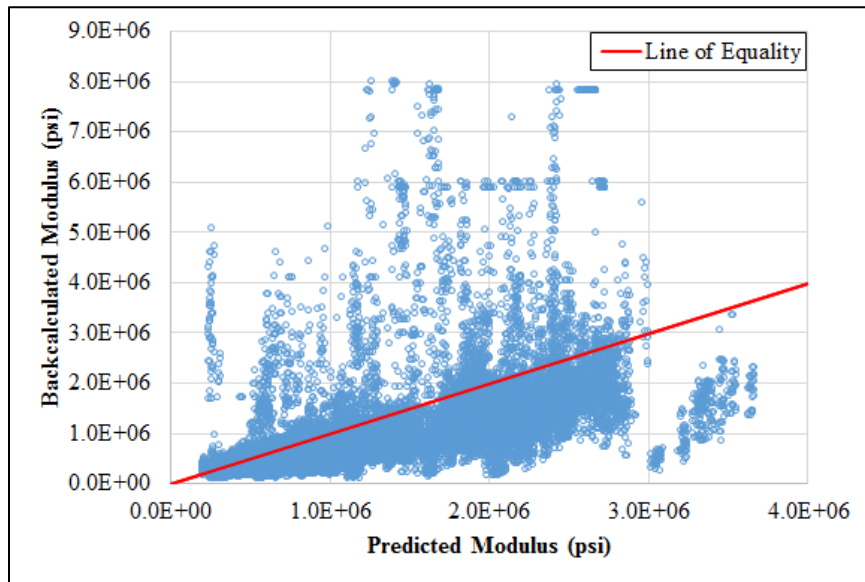
Source: FHWA.

Figure 70. Graph. E^*_{PRED} calculated using frequency computed as the inverse of twice the loading duration ($1/2t$) compared to E_{FWD}.

Constant Frequency

Two frequencies (15 and 30 Hz) were used to compute E^*_{PRED} using the master curve coefficients extracted from the LTPP database.[10] Figure 71 and figure 72 show E_{FWD} compared to E^*_{PRED} calculated for 15 and 30 Hz, respectively.
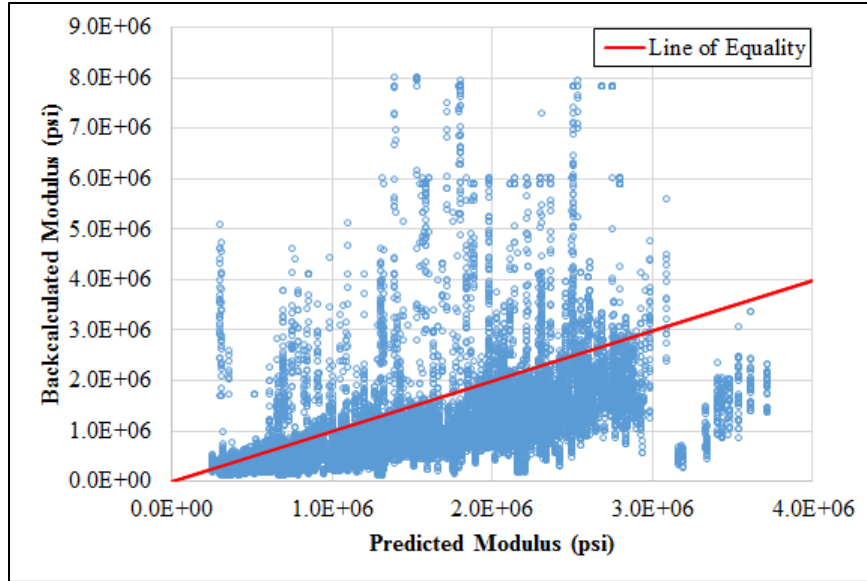
Source: FHWA.

Figure 71. Graph. E^*_{PRED} calculated using a constant frequency of 15 Hz compared to E_{FWD}.
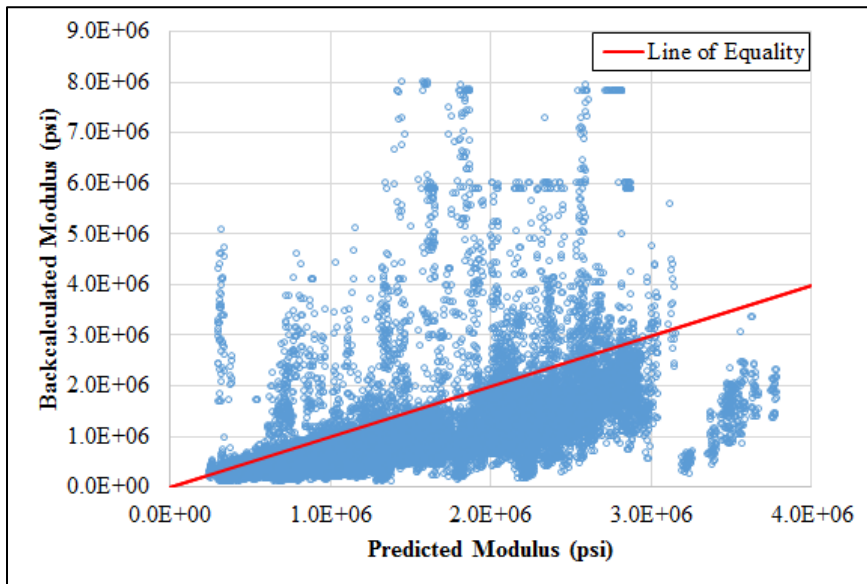
Source: FHWA.

Figure 72. Graph. E^*_{PRED} calculated using a constant frequency of 30 Hz compared to E_{FWD}.

Summary of FWD Load Frequency to Estimate the Undamaged E^*

Ideally, E_{FWD} should not exceed E^*_{PRED}. In other words, no data points should exist above the line of equality in figure 69 through figure 72. However, figure 69 through figure 72 all show a significant number of data points above the line of equality. Table 14 summarizes the number of data points above the line of equality for all four frequency estimations or assumptions. In

summary, the inverse of load duration, t, and simply assuming 30 Hz exhibited about the same percentage of points (10 percent) above the line of equality because they are similar. Use of a frequency of 15 Hz (which is much lower than 30 Hz) and the inverse of two times the load duration (which is much higher than 30 Hz) resulted in a higher percentage of field-derived E_{FWD} values being greater than the laboratory-derived E^*_{PRED} values. The resulting frequency from the inverse of the load duration varied from 24 to 54 Hz, with an overall average of about 39 Hz.

Table 14. Number and percentage of observations for which E_{FWD} is greater than E^*_{PRED}.

FWD Load Frequency (Hz)	Number of Observations	Percentage of Observations
$1/t$	2,495	9.6
$1/2t$	3,838	14.7
15	4,220	16.2
30	2,719	10.4

Note: The count number is out of 26,072 data points that have FWD time histories available in the LTPP database.

Although the inverse of load duration and a fixed frequency of 30 Hz resulted in fewer E_{FWD} from the FWD deflection basins greater than E^*_{PRED}, it does not mean the resulting $E^*_{damaged}$ master curve was more representative of the in-place damage. The following section provides examples for individual sections to illustrate the process in determining the load frequency for estimating the $E^*_{undamaged}$ master curve for calculating the in-place DI.

E_{FWD}/E^*_{PRED} RATIO FOR ALABAMA AND KANSAS LTPP SECTIONS

As discussed previously, there should be no fatigue damage estimated along the test sections shortly after construction. As a result, the deflection basins and E_{FWD} were grouped into two datasets: without and with fatigue cracks. Analyses were performed on each group, and the results from each set compared relative to the methodology used for rehabilitation input level 1.

The first step in the preliminary analyses was to compare the in-place or E_{FWD} to E^*_{PRED} extracted from the LTPP database for the first FWD test data after construction. The E_{FWD}/E^*_{PRED} ratio should be near unity because no cracking was recorded at the time during the first FWD test date. In addition, the modulus ratio for between and within the WP should be similar. It was hypothesized that the E_{FWD}/E^*_{PRED} ratio should slightly increase over time without cracking because of aging, and as cracking occurs, the ratio should decrease with increases in the amount of cracking, as illustrated in figure 56 and figure 57.

Five LTPP test sections were used to demonstrate the analysis performed on all of the preliminary test sections. Table 15 summarizes E_{FWD} and E^*_{PRED} as well as the modulus ratio E_{FWD}/E^*_{PRED} for the five test sections used in the preliminary analyses. As shown in the table, the ratios determined for the Kansas sections were near unity, as expected, but the ratios from the Alabama sections were significantly above and below unity. The ratios between the WP and non-WP test lanes were similar for all sections, as expected. Analyses of the E_{FWD}/E^*_{PRED} ratios related to cracking are discussed in this section. It should be noted that the same average load

frequency without any cracking was determined for the same AC mixture with each LTPP project.

Table 15. E_{FWD}/E^*_{PRED} ratios shortly after construction.

State	LTPP Test Section	AC Layer Structure Type	E_{FWD} (ksi)		E^*_{PRED} (ksi)		E_{FWD}/E^*_{PRED} Ratio	
			WP	Non-WP	WP	Non-WP	WP	Non-WP
Alabama	01-0103	Full-depth AC	1,816	1,313	869	802	2.206	1.732
Alabama	01-0102	Thin AC	697	725	1,049	1,130	0.697	0.670
Alabama	01-0110	Thick AC with PATB	454	508	838	809	0.573	0.664
Kansas	20-0901	Full-depth AC	1,713	1,775	1,680	1,694	1.07	1.11
Kansas	20-0903	Full-depth AC	1,545	1,522	1,504	1,504	1.082	1.067

Test Section 1: 01-0103—Full-Depth AC Pavement Structure

Figure 73 and figure 74 illustrate the E_{FWD} data evaluation for the first FWD test data after construction for between and within the WP, respectively. E_{FWD}/E^*_{PRED} ratios were calculated for each test date between and within the WP test lanes using the procedure and computational tool outlined in chapter 4. Graphs throughout this report that show the E_{FWD} values were generated automatically for all section-test-date-lane combinations using an automated process. As such, the entire datasets were created using the automated graph generation, so the E_{FWD} values for some sections may be missing outliers or values outside the IQR.
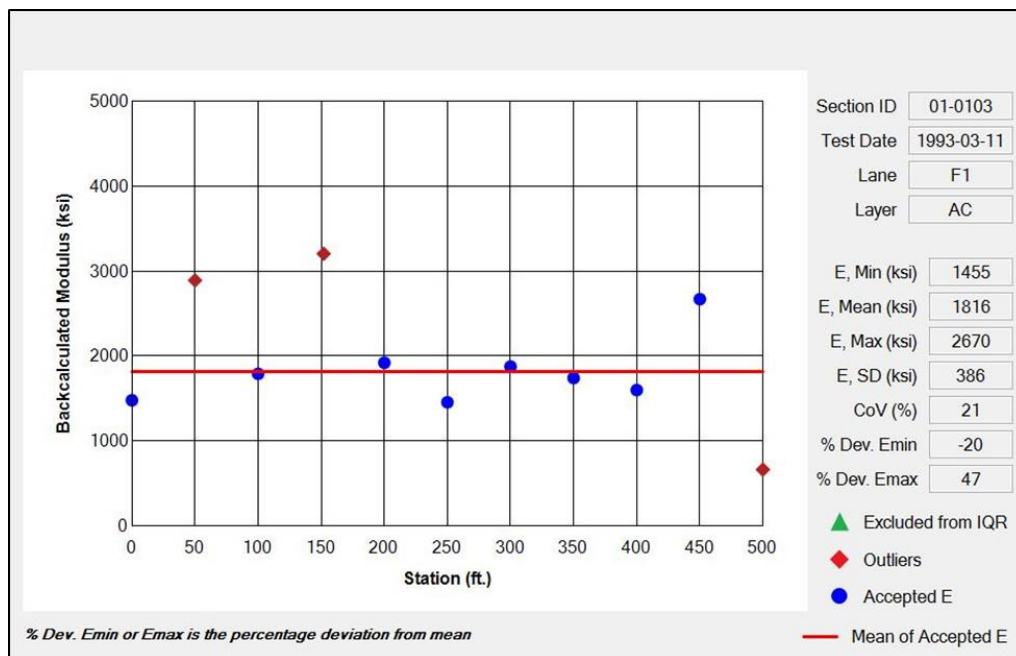
Source: FHWA.

Figure 73. Graph. Station backcalculated E for test lane F1 for Alabama test section 01-0103.
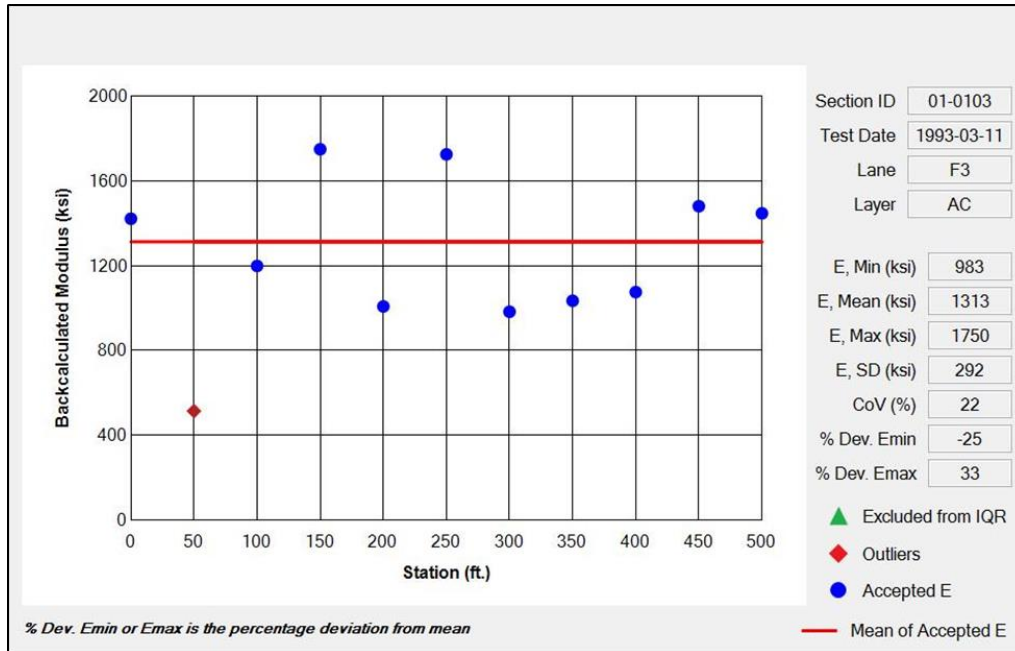
Source: FHWA.

Figure 74. Graph. Station backcalculated *E* for test lane F3 for Alabama test section 01-0103.

A final table with the list of accepted stations for each LTPP section was developed, and backcalculation data for sections in this list were used in subsequent stages of the preliminary analysis. As an example, table 16 shows the list of accepted stations, average backcalculated HMA *E*, standard deviation, and COV for LTPP test section 01-0103. Tables for all other test sections were generated but are not included in the report.

Table 16. List of accepted stations for LTPP test section 01-0103.

Test Date	Lane	Accepted Stations	Mean E (ksi)	Standard Deviation (ksi)	COV (Percent)
3/11/1993	F1	0, 100, 200, 250, 300, 350, 400, and 450	1,816	385.7	21.2
3/11/1993	F3	0, 100, 150, 200, 250, 300, 350, 400, 450, and 500	1,313	292.2	22.3
6/21/1995	F1	100, 150, 200, 250, 300, 350, and 450	460	86.4	18.8
6/21/1995	F3	0, 50, 100, 150, 200, 250, 300, 350, 400, and 450	359	58.4	16.3
4/19/1996	F1	0, 150, 200, 250, 300, 350, 400, 450, and 500	1,443	345.3	23.9
4/19/1996	F3	100, 150, 250, 300, 350, and 400	2,075	807.5	38.9
7/22/1998	F1	50, 100, 152, 200, 250, 300, 350, and 450	118	8.5	7.2
7/22/1998	F3	0, 100, 150, 200, 250, 300, 350, 400, 450, and 500	157	35.0	22.2
5/18/2000	F1	100, 150, 200, 250, 300, and 350	323	58.3	18.1
5/18/2000	F3	100, 150, 200, 250, 350, and 400	378	68.5	18.1
5/24/2002	F1	100, 150, 200, 350, 400, and 450	—	—	—
5/24/2002	F3	100, 150, 200, 250, 300, and 450	793	139.2	17.6
2/23/2004	F1	0, 100, 200, 250, 300, 350, 450, and 500	4,889	937.9	19.2
2/23/2004	F3	0, 50, 150, 200, 350, and 500	5,006	1,555.1	31.1
4/28/2005	F1	200, 250, 300, 350, 450, and 500	1,487	746.0	50.2
4/28/2005	F3	0, 150, 250, 350, 400, and 450	—	—	—

—All accepted stations were excluded from IQR for the test date and lane.

The next step was to normalize the modulus ratio assuming no damage for the first FWD test date. In other words, the E_{FWD}/E^*_{PRED} ratios were normalized using the ratio calculated for the first test date, which was equivalent to setting the damage ratio to 1 (no damage). Since the E_{FWD}/E^*_{PRED} ratio was calculated as backcalculated modulus divided by the predicted undamaged modulus, the normalization procedure had the same effect as applying a field correction factor.

Figure 75 compares the E_{FWD}/E^*_{PRED} AC moduli ratio measured between and within the WP (WP as designated in figure 75 and all other similar figures) test lane for test section 01-0103. E^*_{PRED} was calculated using the middepth AC temperature and a loading frequency of 15 Hz. The plot of total pavement cracking versus time for this section is shown in figure 59. No cracks were recorded within the first 3 yr of construction. Comparing the cracking data to the E_{FWD}/E^*_{PRED} ratio, no trend or relationship was found between the two parameters (cracking and E_{FWD}/E^*_{PRED}). In fact, the E_{FWD}/E^*_{PRED} ratio for a moderate level of cracking was consistently higher than for the FWD test dates without cracking.
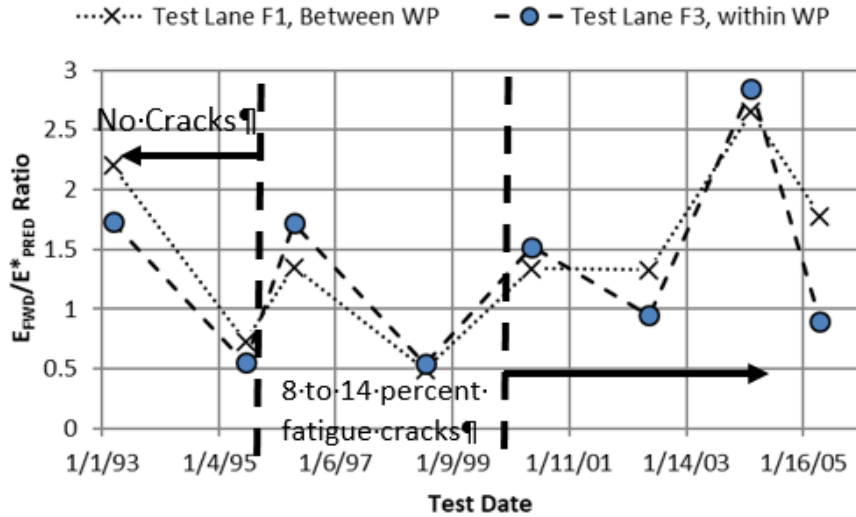
Source: FHWA.

Figure 75. Graph. $E_{FWD}/E*_{PRED}$ ratios for test lanes F1 and F3 for average of all AC layers for Alabama test section 01-0103.

The third step was to determine the frequency so that $E*_{PRED}$ equaled E_{FWD} as previously explained. The average backcalculated frequency for each FWD test date compared to the middepth temperature is provided in figure 76. As shown, the backcalculated load frequency was highly variable. An equivalent frequency of 500 Hz was calculated for each FWD test date for which $E*_{PRED}$ was approximately equal to E_{FWD} for test section 01-0103. The average adjusted modulus ratio (laboratory equivalent frequency to match the E_{FWD} value) for the first FWD test date was calculated as 1.056. The plot of normalized modulus ratios versus time for test section 01-0103 is shown in figure 77 for between and within WP test lanes. Comparing the cracking data to the frequency adjusted $E_{FWD}/E*_{PRED}$ modulus ratio, no trend was found between the two parameters.
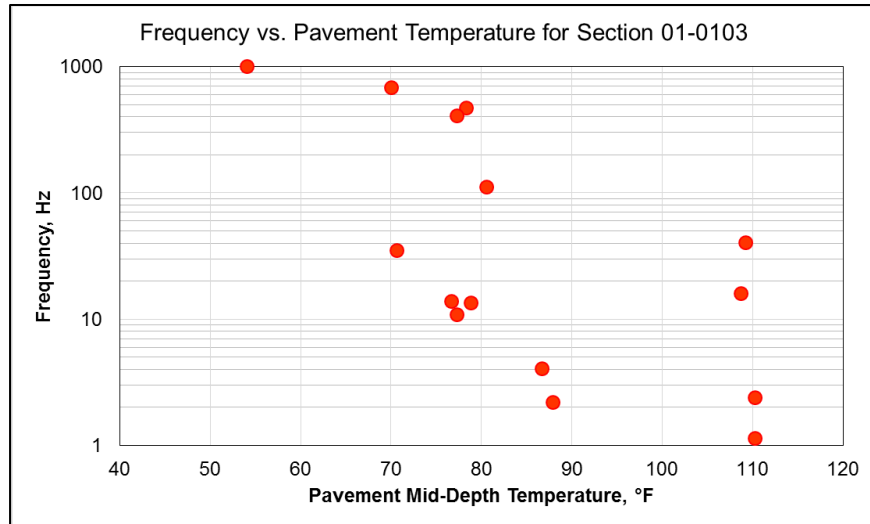
Source: FHWA.

Figure 76. Graph. Backcalculated FWD loading frequency for an E_{FWD}/E^*_{PRED} ratio of unity versus temperature for Alabama test section 01-0103.
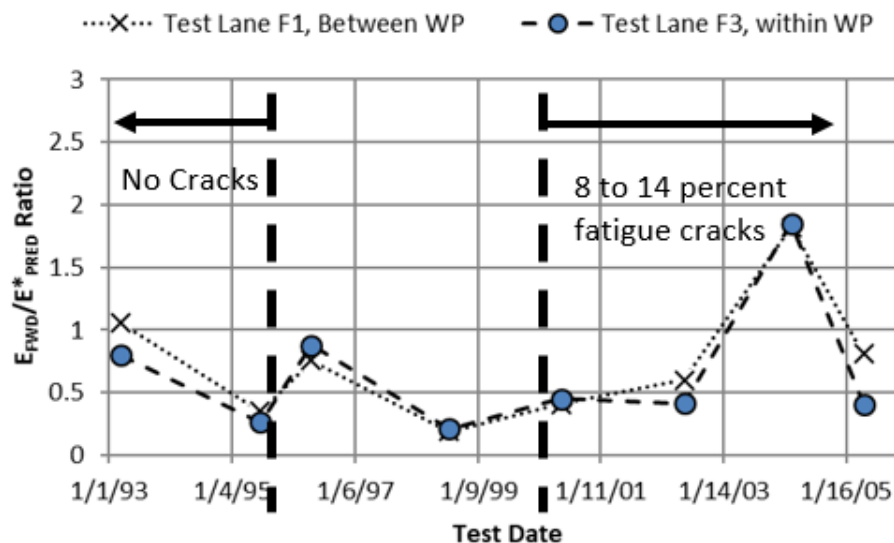
Source: FHWA.

Figure 77. Graph. E_{FWD}/E^*_{PRED} ratios along test lanes F1 and F3 using a frequency of 500 Hz for Alabama test section 01-0103.

Test Section 2: 01-0102—Thin AC Pavement Structure

Average E_{FWD}/E^*_{PRED} ratios were calculated for all AC layers using a load frequency of 15 Hz as was done for test section 01-0103. Ratios of 0.697 and 0.670 were determined for the WP and non-WP test lanes, respectively (see table 15). As was similar for test section 01-0103, no correspondence was found between cracking and the E_{FWD}/E^*_{PRED} ratio.

Figure 78 shows the backcalculated frequency (i.e., the frequency at which E_{FWD} equals E^*_{PRED}) compared to the middepth temperature of the AC layer. The backcalculated frequency increased

87

with an increase in middepth temperature. An equivalent frequency of 25 Hz was calculated at which the predicted $E*_{PRED}$ was approximately equal to E_{FWD} for the FWD test dates without cracking. As shown, the backcalculated frequency was dependent on middepth temperature for this section, which was thinner than for test section 01-0103.
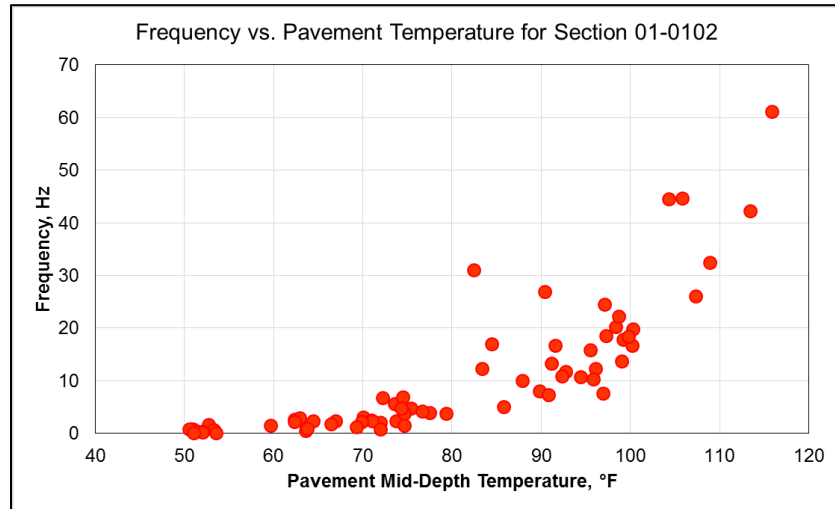
Source: FHWA.

Figure 78. Graph. Backcalculated FWD loading frequency for an $E_{FWD}/E*_{PRED}$ ratio of unity versus temperature for Alabama test section 01-0102.

Average adjusted modulus ratios for the next FWD test date shortly after construction were calculated as 1.180 and 1.146 for the WP and non-WP lanes, respectively. The time–series of modulus ratios is shown in figure 79 for the two test lanes. The plot of total pavement cracking versus time was shown in figure 60. No correspondence was found between the moduli ratios and total area of fatigue cracking. The modulus ratio was found to be statistically the same for the FWD test dates with and without cracking.
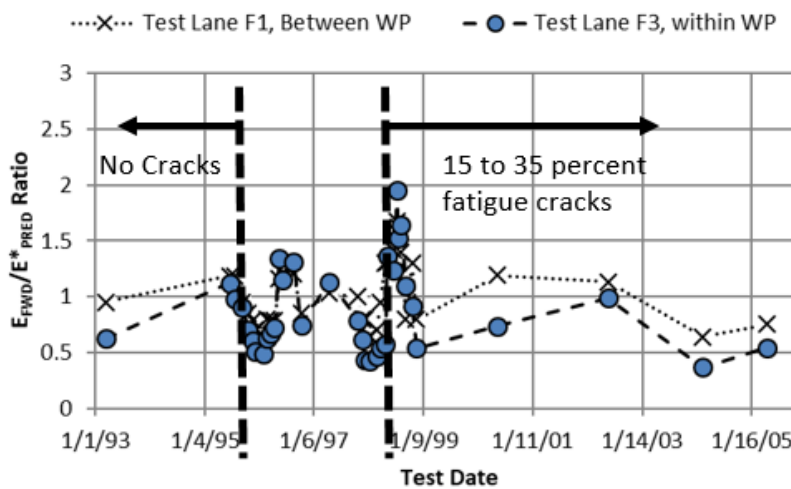
Source: FHWA.

Figure 79. Graph. $E_{FWD}/E*_{PRED}$ ratios along test lanes F1 and F3 using a frequency of 25 Hz (average of all AC layers) for Alabama test section 01-0102.

88

Test Section 3: 01-0110—Full-Depth AC Pavement Structure with Drainage Layer

Figure 80 and figure 81 illustrate the E_{FWD} data evaluation for the first FWD test data after construction for between and within the WP for test section 01-0110, respectively. Average E_{FWD}/E^*_{PRED} ratios were calculated for all AC layers for the first FWD test date. Ratios of 0.573 and 0.664 were determined for the WP and non-WP test lanes (see table 15). As for the other two Alabama test sections (i.e., 01-0103 and 01-0102), no correspondence was found between the E_{FWD}/E^*_{PRED} ratio and total amount of fatigue cracking.
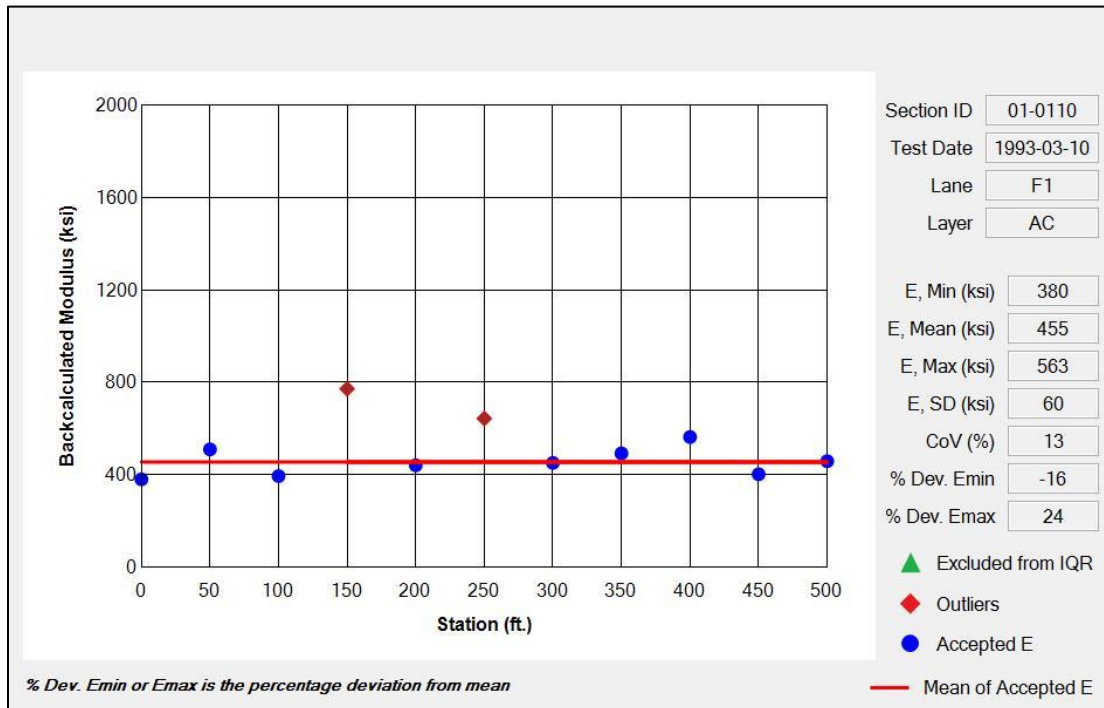
Source: FHWA.

Figure 80. Graph. Station backcalculated E for test lane F1 for Alabama test section 01-0110.
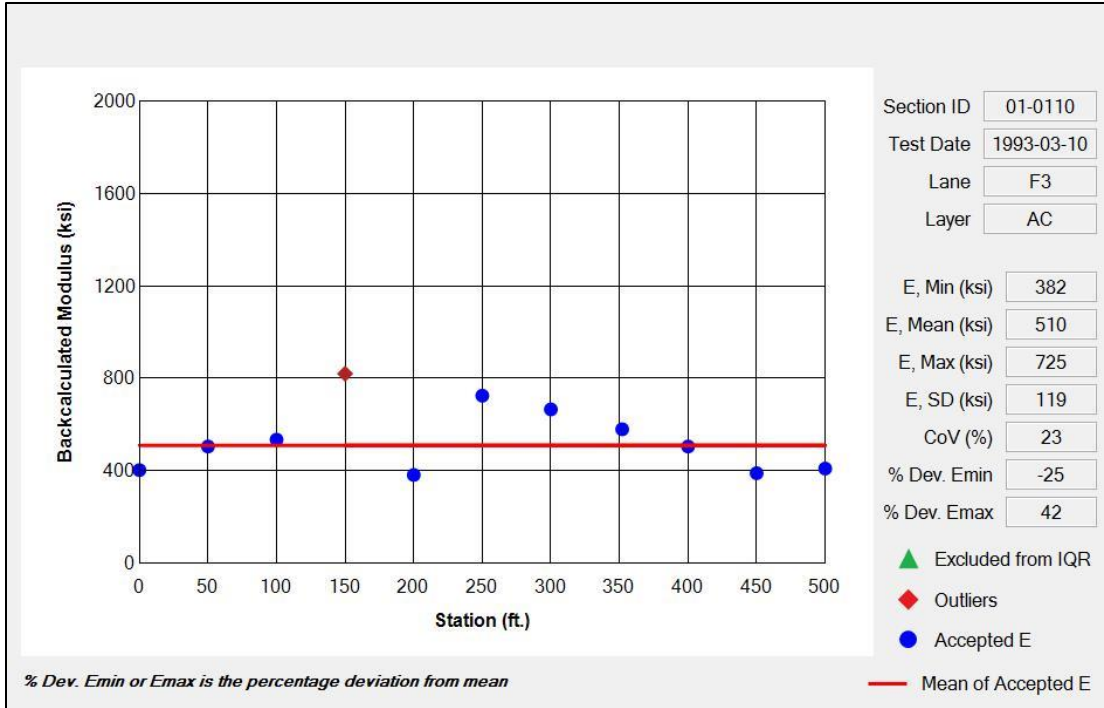
Source: FHWA.

Figure 81. Graph. Station backcalculated *E* for test lane F3 for Alabama test section 01-0110.

Figure 82 shows the backcalculated frequency compared to the middepth temperature of the AC layer. As shown, the backcalculated frequency was highly variable, but the values were significantly lower than for test section 01-0103 (see figure 76). An equivalent frequency of 8 Hz was calculated at which the predicted (undamaged) modulus was approximately equal to the backcalculated AC layer modulus for test section 01-0110.
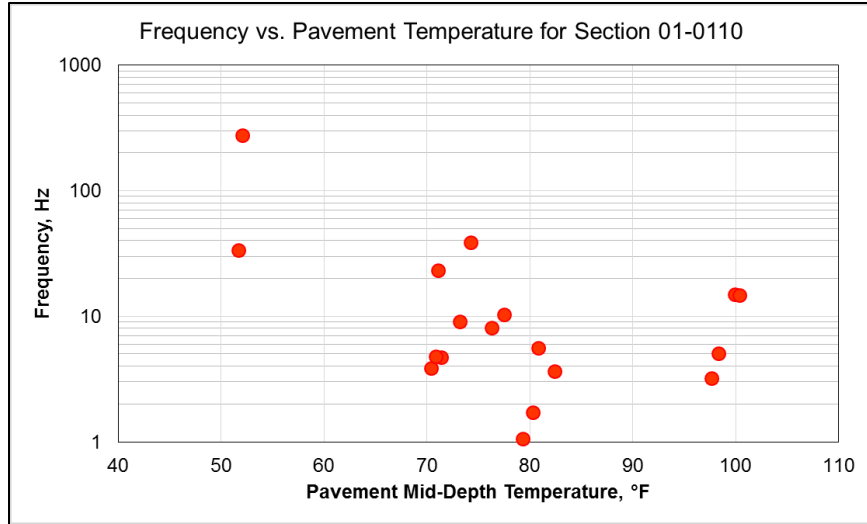
Source: FHWA.

Figure 82. Graph. Backcalculated FWD loading frequency for an $E_{FWD}/E*_{PRED}$ ratio of unity versus temperature for Alabama test section 01-0110.

Average frequency-adjusted $E_{FWD}/E*_{PRED}$ ratios for the FWD test date shortly after construction were 1.097 and 1.041 for the WP and non-WP lanes, respectively. The time–series of $E_{FWD}/E*_{PRED}$ ratios is shown in figure 83 for the two test lanes. The plot of total pavement cracking versus time is shown in figure 61. As for the other two Alabama SPS-1 sections (i.e., 01-0102 and 01-0103), no correspondence was found between the $E_{FWD}/E*_{PRED}$ ratios and total area of fatigue cracking. In fact, the $E_{FWD}/E*_{PRED}$ ratio generally increased (rather than decreased) with cracking.
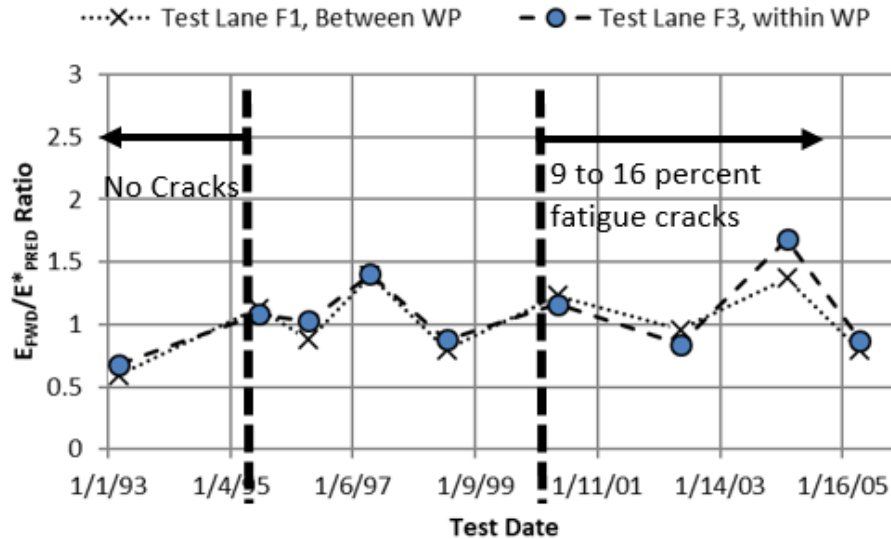
Source: FHWA.

Figure 83. Graph. $E_{FWD}/E*_{PRED}$ ratios along test lanes F1 and F3 using a frequency of 8 Hz (average of all AC layers) for Alabama test section 01-0110.

91

Test Section 4: 20-0903—Full-Depth Pavement Structure with Treated Base

Figure 84 and figure 85 illustrate the E_{FWD} data evaluation for the first FWD test data after construction for between and within the WP for Kansas test section 20-0903, respectively. E_{FWD}/E^*_{PRED} ratios were calculated for each test date between and within the WP test lanes as was done for the three Alabama test sections.
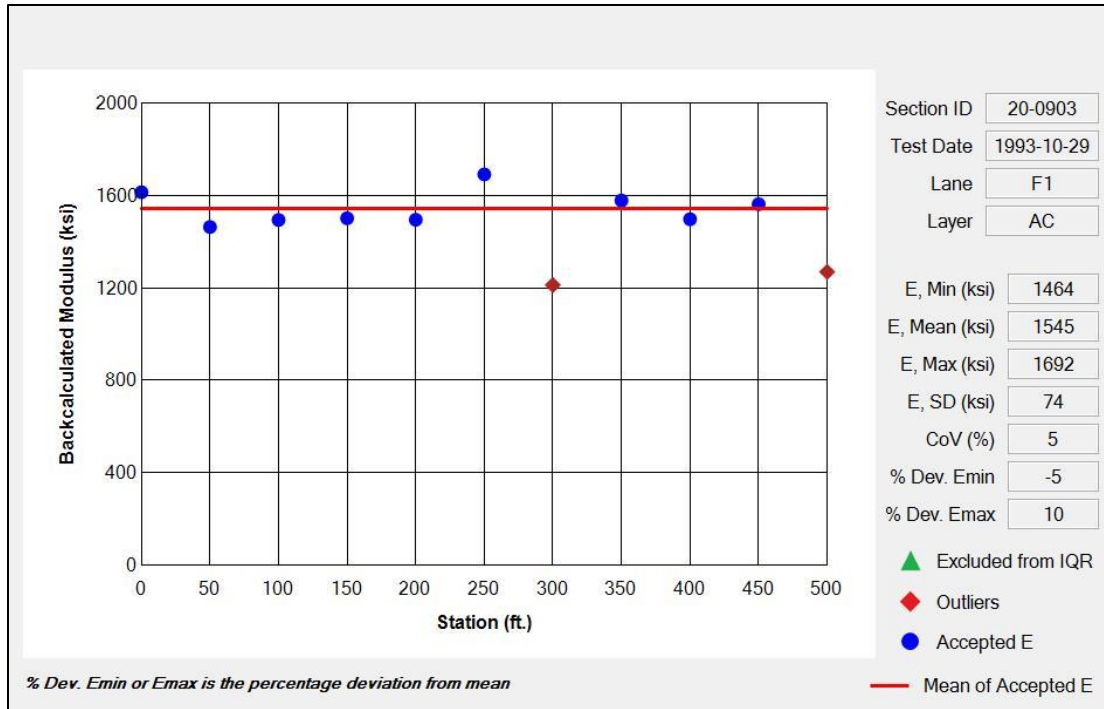
Source: FHWA.

Figure 84. Graph. Station backcalculated *E* for test lane F1 for Kansas test section 20-0903.
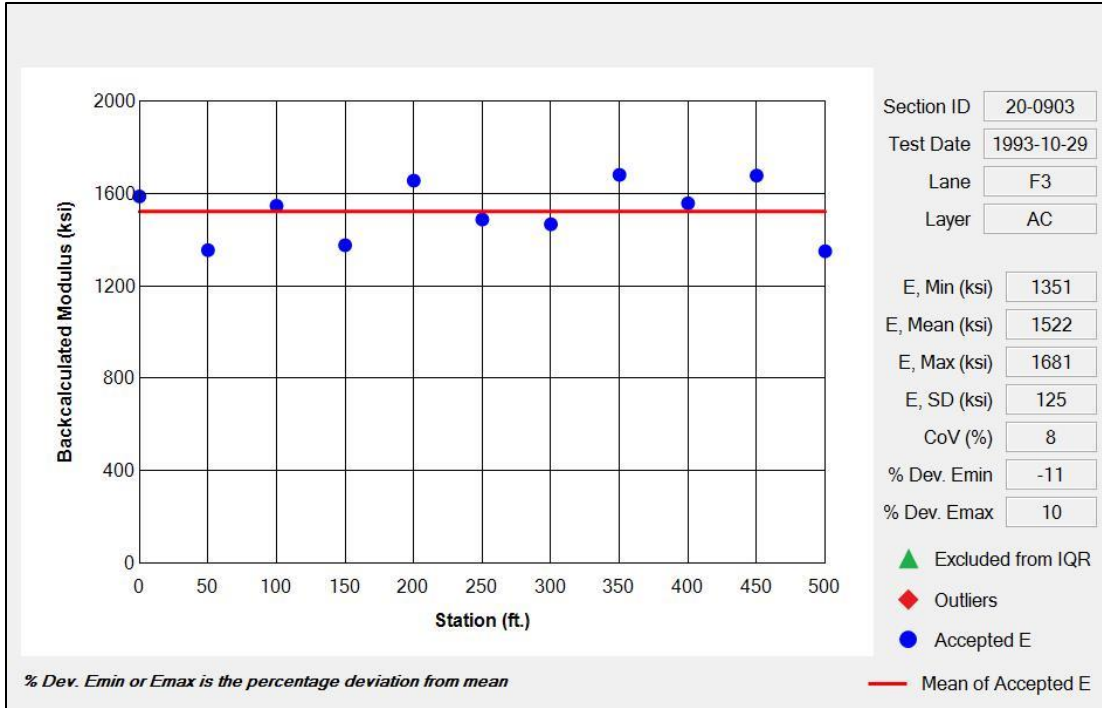
Source: FHWA.

**Figure 85. Graph. Station backcalculated *E* for test lane F3 for Kansas
test section 20-0903.**

Average E_{FWD}/E^*_{PRED} ratios were calculated for all AC layers for the first FWD test date. Ratios of 1.082 and 1.067 were determined for the WP and non-WP test lanes, respectively (see table 15). These ratios were found to be adequate in comparing E_{FWD} and E^*_{PRED}. Thus, a frequency of 15 Hz was used in the modulus ratio calculation for the other FWD test dates.

The time–series of E_{FWD}/E^*_{PRED} ratios is shown in figure 86 for the two test lanes at the equivalent FWD frequency of 15 Hz so that E_{FWD} equaled E^*_{PRED}. The plot of total pavement cracking versus time is shown in figure 62. No consistent trend existed between the E_{FWD}/E^*_{PRED} ratios and total area of fatigue cracking. Although the lower E_{FWD}/E^*_{PRED} ratio was computed for the higher amounts of cracking, the E_{FWD}/E^*_{PRED} ratio without cracking on two FWD test dates was only slightly higher than for the E_{FWD}/E^*_{PRED} ratio for over 40 percent total lane area of cracking.
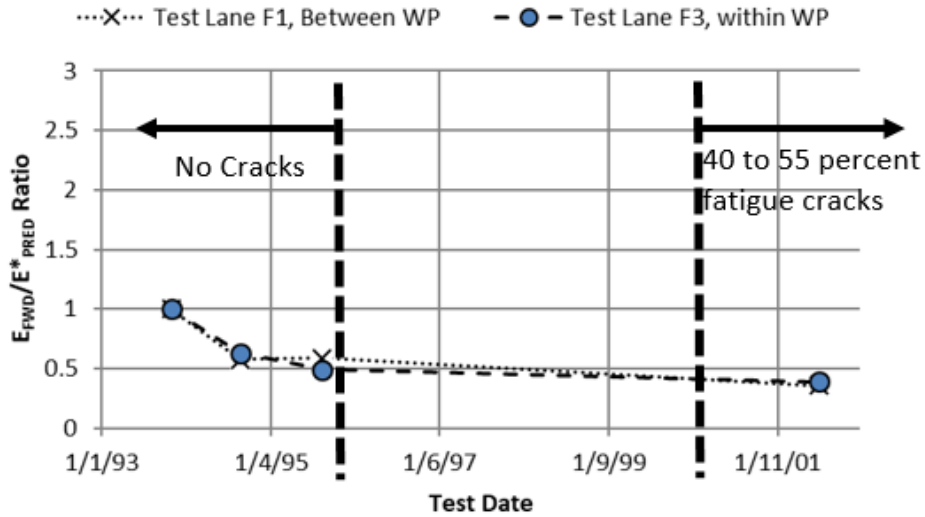
Source: FHWA.

Figure 86. Graph. E_{FWD}/E^*_{PRED} ratios normalized using first FWD test date along test lane F1 using frequency of 15 Hz (average of all AC layers) for Kansas test section 20-0903.

Test Section 5: 20-0901—Full-Depth AC Pavement with Treated Base Layer

Figure 87 and figure 88 illustrate the E_{FWD} data evaluation for the first FWD test data after construction for between and within the WP for Kansas test section 20-0901, respectively.
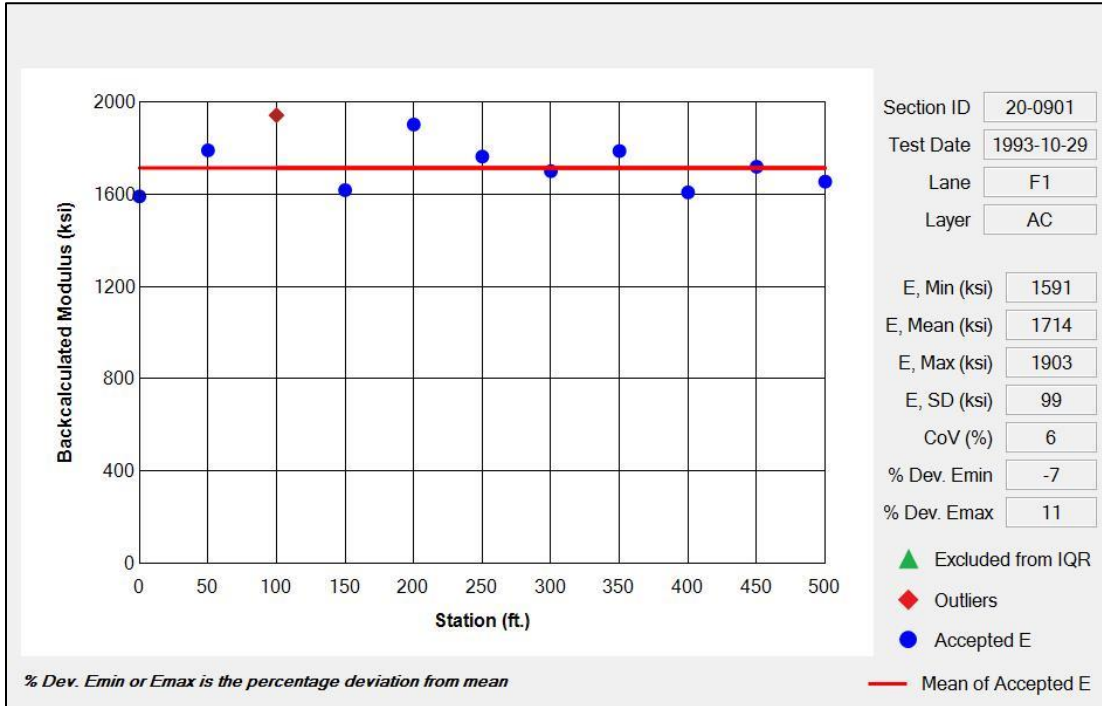
Source: FHWA.

Figure 87. Graph. Station backcalculated E for test lane F1 for Kansas test section 20-0901.
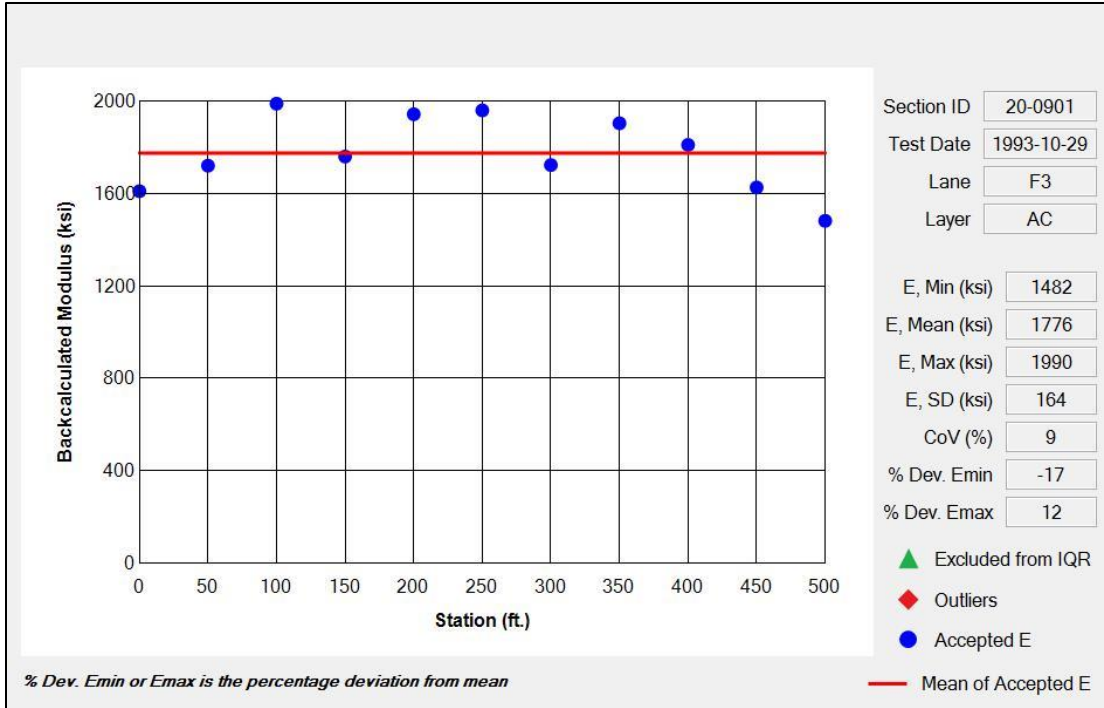
Source: FHWA.

**Figure 88. Graph. Station backcalculated *E* for test lane F3 for Kansas
test section 20-0901.**

Average E_{FWD}/E^*_{PRED} ratios were calculated for all AC layers for the first FWD test date.
Ratios of 1.07 and 1.11 were determined for the WP and non-WP test lanes, respectively
(see table 15). These ratios were similar to Kansas test section 20-0903 and were found to be
adequate in comparing the E_{FWD} and E^*_{PRED} values. Thus, a frequency of 15 Hz was used in the
ratio calculation for the other FWD test dates.

The time–series of modulus ratios is shown in figure 89 for the two test lanes. The plot of
total pavement cracking versus time is shown in figure 63. As for the other Kansas test section
(i.e., 20-0903), no correspondence was found between the E_{FWD}/E^*_{PRED} ratios and total area of
fatigue cracking. More importantly, the E_{FWD}/E^*_{PRED} ratio was greater than 1.0 over time for this
section—just the opposite of test section 20-0903.

95
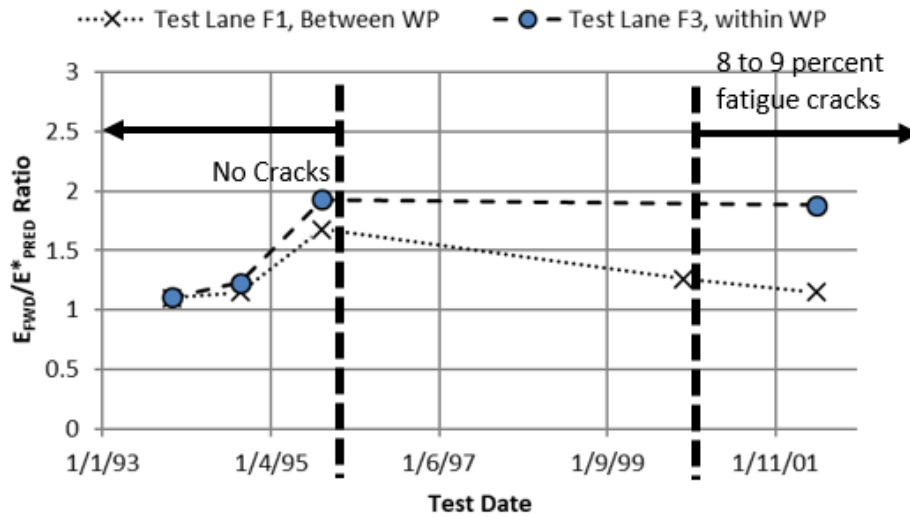
Figure 89. Graph. E_{FWD}/E^*_{PRED} ratios normalized using first FWD test date along test lanes F1 and F3 using frequency of 15 Hz (average of all AC layers) for Kansas test section 20-0901.

DISSIPATED WORK

Some previous studies have hypothesized the dissipated work or area within the hysteresis loop of the deflection–load–time series data from the FWD is an indicator of pavement performance (e.g., figure 27 in chapter 2).[33,47] The dissipated work at the center of the FWD load plate was calculated as the area enclosed by the load-deflection hysteresis loop. It was hypothesized that the dissipated work should slightly decrease after construction because of aging and then should significantly increase after cracking occurs.

In addition, the FWD deflection–time histories were simulated using a dynamic, viscoelastic program called ViscoWave for each test date and station. The input into the program includes the $E^*_{undamaged}$ HMA master curve calculated at the test temperature using the sigmoidal function coefficients and the base/subgrade moduli previously backcalculated using layered elastic programs (i.e., EVERCALC© or MODCOMP©). ViscoWave was used because the dissipated work could be determined at other temperatures and loading frequencies without aging and fatigue damage.

Test Section 1: 01-0103—Full-Depth AC Pavement Structure

Figure 90 shows an example of the measured deflection–time histories, while figure 91 shows the same example but for the simulated time histories created by ViscoWave. Hysteresis loops were also generated from the measured and simulated deflections (see figure 92 and figure 93), and, in turn, the theoretical undamaged dissipated work was calculated as the area enclosed by the simulated hysteresis loop. Table 17 summarizes the calculated dissipated work for each test lane and test date for section test 01-0103.
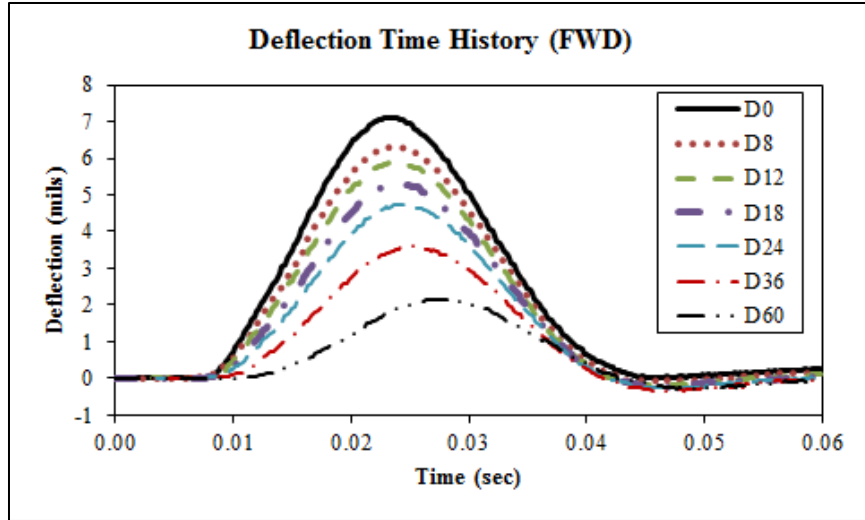
Figure 90. Graph. Measured deflection–time histories for test lane F1 on 03/11/1993 at station 200 for Alabama test section 01-0103.
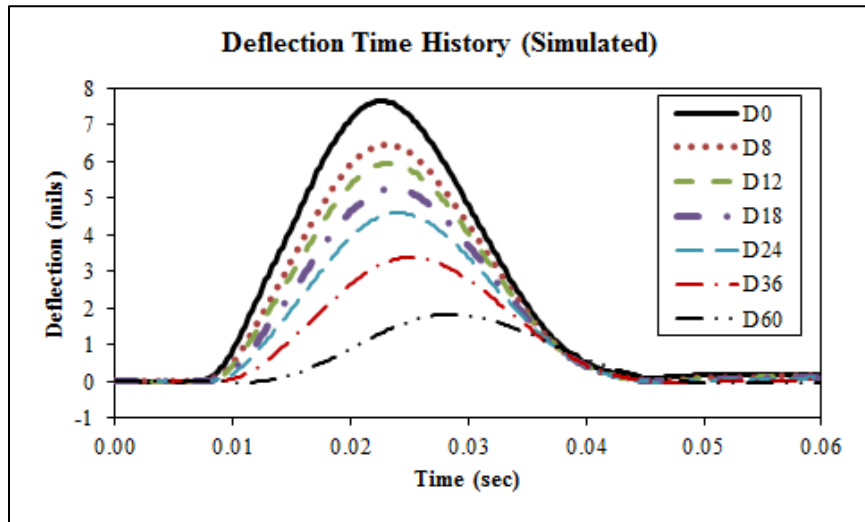
Figure 91. Graph. Simulated deflection–time histories for test lane F1 on 03/11/1993 at station 200 for Alabama test section 01-0103.

Source: FHWA.

Figure 92. Graph. Measured hysteresis loops for test lane F1 on 03/11/1993 at station 200 for Alabama test section 01-0103.
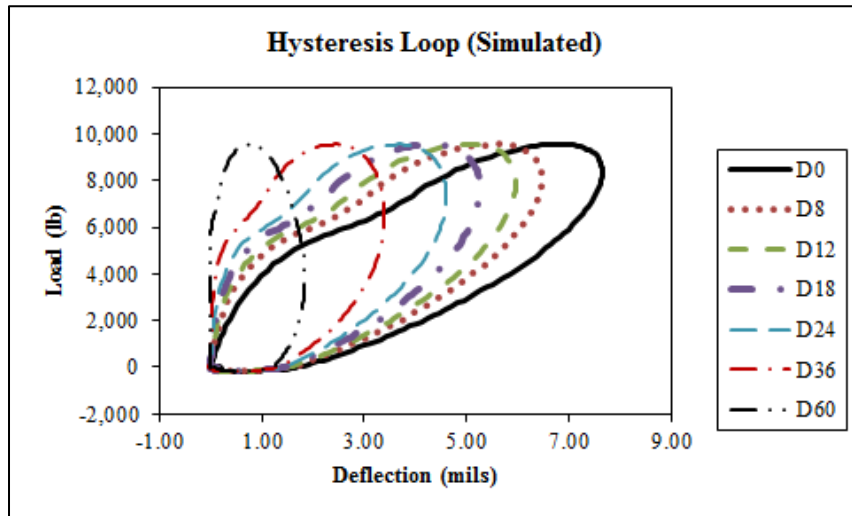
Source: FHWA.

Figure 93. Graph. Simulated hysteresis loops for test lane F1 on 03/11/1993 at station 200 for Alabama test section 01-0103.

Table 17. FWD and simulated dissipated work ratios for Alabama test section 01-0103.

	WP			Non-WP		
Test Date	FWD Dissipated Work (lb-Inch)	Simulated Dissipated Work (lb-Inch)	Ratio of Dissipated Work	FWD Dissipated Work (lb-Inch)	Simulated Dissipated Work (lb-Inch)	Ratio of Dissipated Work
3/11/1993	28.6	25.7	1.1	24.9	23.4	1.1
6/21/1995	34.9	22.6	1.6	32.1	21.9	1.5
4/19/1996	23.9	22.6	1.1	23.7	21.6	1.1
7/22/1998	53.8	26.8	2.0	51.4	24.7	2.1
5/18/2000	43.3	26.8	1.6	38.1	22.9	1.7
4/28/2005	28.1	21.4	1.3	24.7	20.9	1.2

Figure 94 shows the dissipated work calculated from FWD deflection–time histories over time, while figure 95 shows the plot of simulated dissipated work versus time. The simulated dissipated work represents or assumes no HMA damage and aging over time. As shown, the simulated dissipated work is more constant over time compared to the dissipated work calculated from the FWD time histories shown in figure 94.
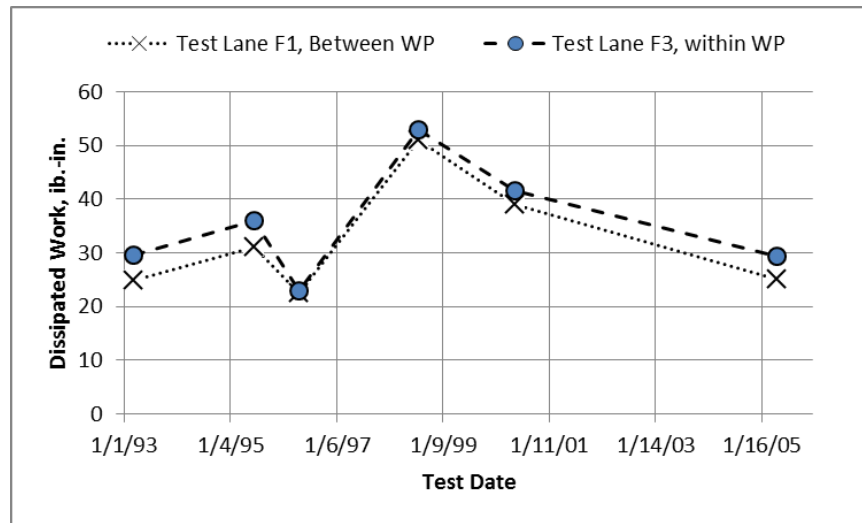
Source: FHWA.

Figure 94. Graph. FWD dissipated work along test lanes F1 and F3 for Alabama test section 01-0103.
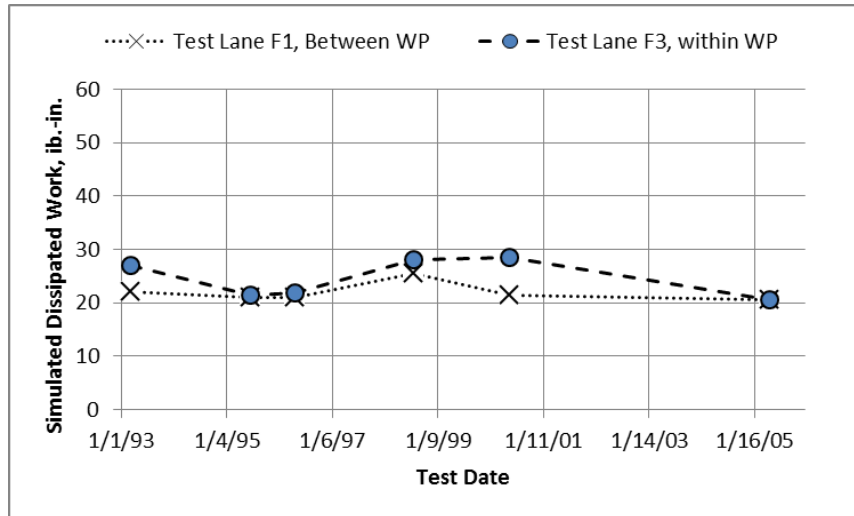
Source: FHWA.

Figure 95. Graph. Simulated dissipated work along test lanes F1 and F3 for Alabama test section 01-0103.

Figure 96 shows the plot of dissipated work ratio (i.e., the ratio of FWD to simulated dissipated work versus time), which shows that the ratio for the first FWD test date was calculated to be approximately 1.1 for both WP and non-WP locations. The ratio followed a similar trend as the FWD dissipated work due to the reduced variability in the simulated dissipated work. Overall, the dissipated work ratio increased over time but was variable and, more importantly, was lower for the greater amount of cracking.
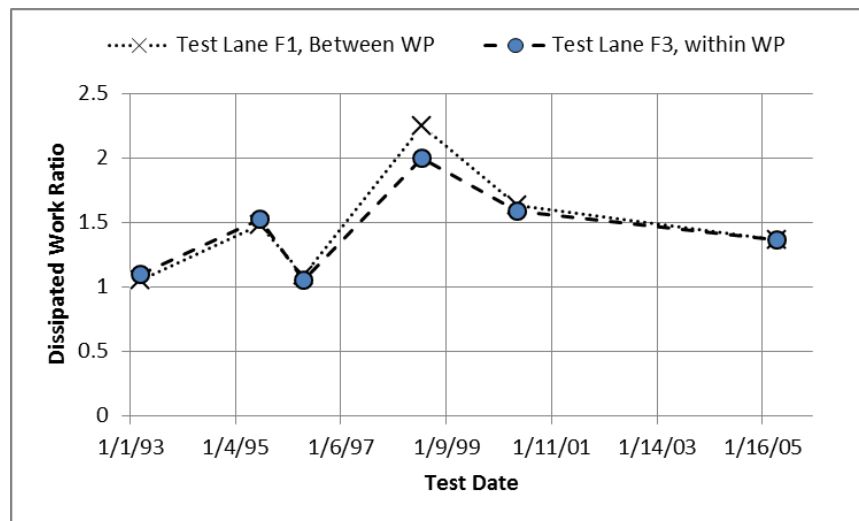
Source: FHWA.

Figure 96. Graph. Dissipated work ratio along test lanes F1 and F3 for Alabama test section 01-0103.

100

Test Section 2: 01-0102—Thin AC Pavement Structure

Figure 97 and figure 98 show the FWD measured and simulated deflection–time histories for Alabama test section 01-0102. The measured hysteresis loops for each sensor are provided in figure 99, while the hysteresis loops for the simulated deflections are shown in figure 100. The theoretical undamaged dissipated work was calculated as the area enclosed by the simulated hysteresis loop. Table 18 summarizes the calculated dissipated work and dissipated ratios for each test lane and test date for this section.
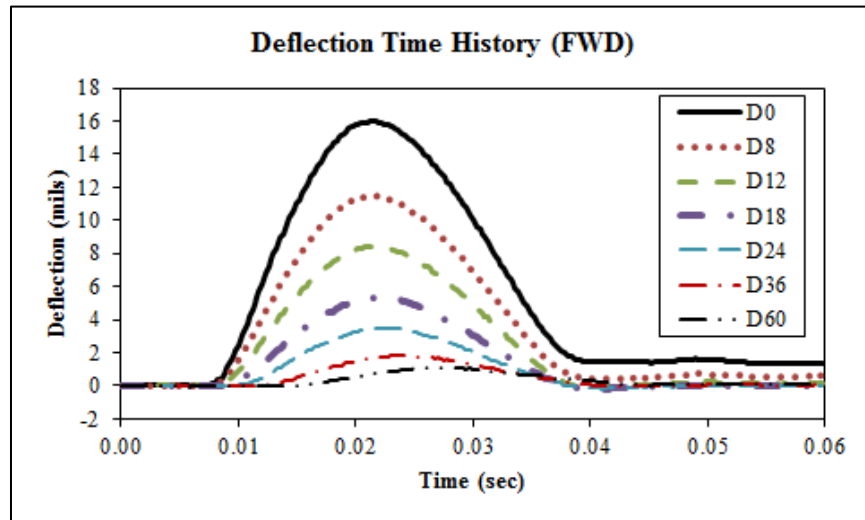
Source: FHWA.

Figure 97. Graph. Measured deflection–time histories for test lane F1 on 03/11/1993 at station 200 for Alabama test section 01-0102.
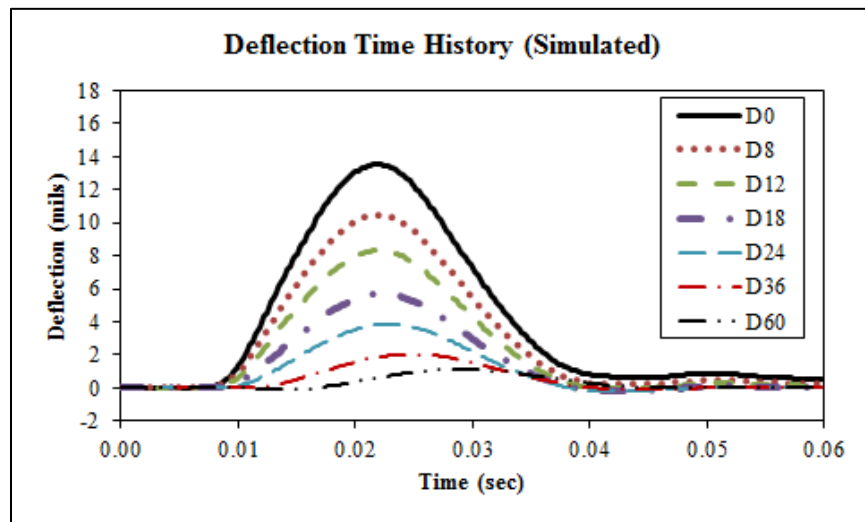
Source: FHWA.

Figure 98. Graph. Simulated deflection–time histories for test lane F1 on 03/11/1993 at station 200 for Alabama test section 01-0102.
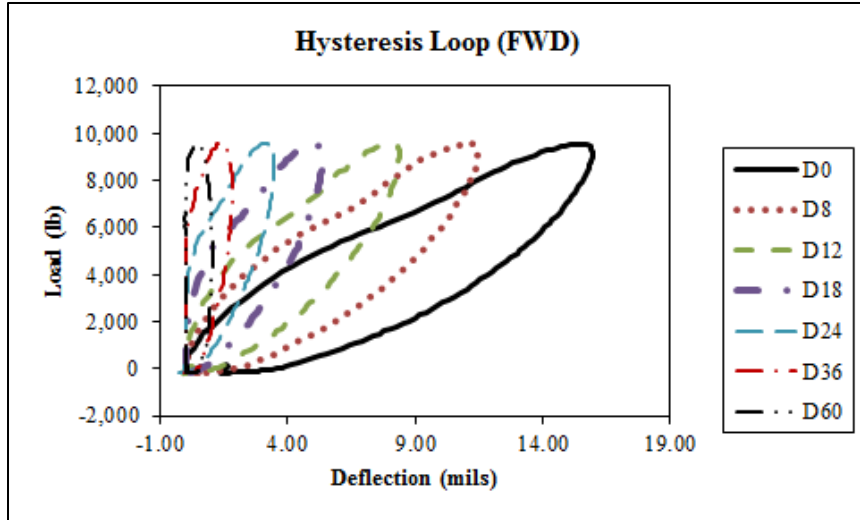
Source: FHWA.

Figure 99. Graph. Measured hysteresis loops for test lane F1 on 03/11/1993 at station 200 for Alabama test section 01-0102.

Source: FHWA.

Figure 100. Graph. Simulated hysteresis loops for test lane F1 on 03/11/1993 at station 200 for Alabama test section 01-0102.

Table 18. FWD and simulated dissipated work ratios for Alabama test section 01-0102.

Test Date	WP			Non-WP		
	FWD Dissipated Work (lb-Inch)	Simulated Dissipated Work (lb-Inch)	Ratio of Dissipated Work	FWD Dissipated Work (lb-Inch)	Simulated Dissipated Work (lb-Inch)	Ratio of Dissipated Work
3/11/1993	83.5	60.4	1.4	85.1	62.2	1.4
6/21/1995	72.2	45.4	1.6	71.8	46.1	1.6
4/17/1996	88.2	58.3	1.5	89.1	58.4	1.5
4/17/1997	77.7	51.1	1.5	78.7	50.2	1.6
7/23/1998	88.3	53.6	1.6	101.2	59.9	1.7
5/19/2000	87.0	63.1	1.4	90.0	59.7	1.5
4/29/2005	112.1	82.8	1.4	123.6	81.7	1.5

Figure 101 shows the dissipated work calculated from FWD deflection–time histories over time. Figure 102 shows the simulated dissipated work over time, which assumes no HMA damage and aging over time. Unlike test section 01-0103, the dissipated work from the simulated deflection–time series data followed a similar trend as the FWD measured dissipated work for test section 01-0102. Thus, the dissipated work ratio remained relatively constant over time, as shown in figure 103. The ratio for the first FWD test date was calculated to be approximately 1.4 for both WP and non-WP locations and did not increase with increasing amounts of cracking.

Source: FHWA.

Figure 101. Graph. FWD dissipated work measured over time for test lanes F1 and F3 for Alabama test section 01-0102.

103
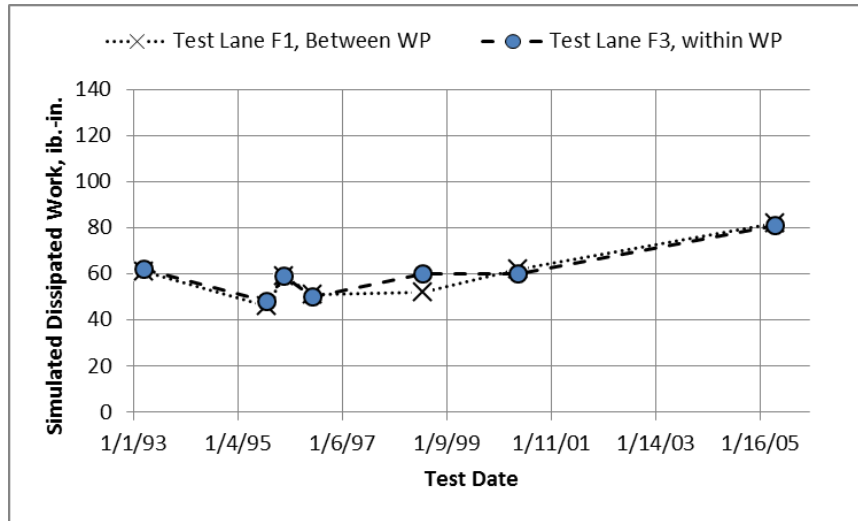
Source: FHWA.

Figure 102. Graph. Simulated dissipated work measured over time for test lanes F1 and F3 for Alabama test section 01-0102.

Source: FHWA.

Figure 103. Graph. Dissipated work ratio calculated over time for test lanes F1 and F3 for Alabama test section 01-0102.

Test Section 3: 01-0110—Full-Depth AC Pavement Structure with Drainage Layer

FWD deflection–time histories were also simulated using ViscoWave for test section 01-0110. Figure 104 and figure 105 show the measured and simulated deflection–time histories, respectively, for lane F1 at station 200 on 3/10/1993. The corresponding hysteresis loops from the measured deflection–time data are shown in figure 106. The hysteresis loops derived from the simulated FWD time history data are provided in figure 107. The simulated deflections were significantly smaller than the measured deflections (see figure 104), and, as a result, the simulated hysteresis loops were smaller than those from the FWD (see figure 105). As such, the

ratio of dissipated work at the first FWD test date was calculated to be 1.5 for the WP and 1.6 for the non-WP locations.
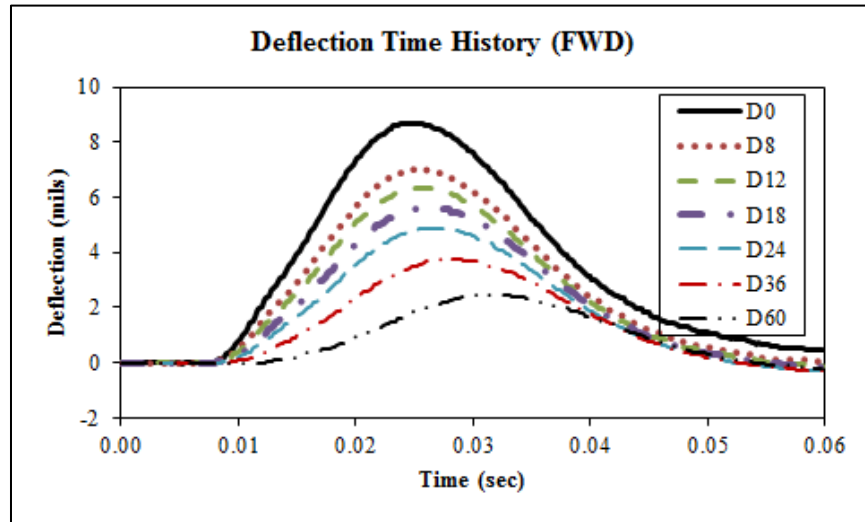
Source: FHWA.

Figure 104. Graph. Measured deflection–time histories for test lane F1 on 03/10/1993 at station 200 for Alabama test section 01-0110.
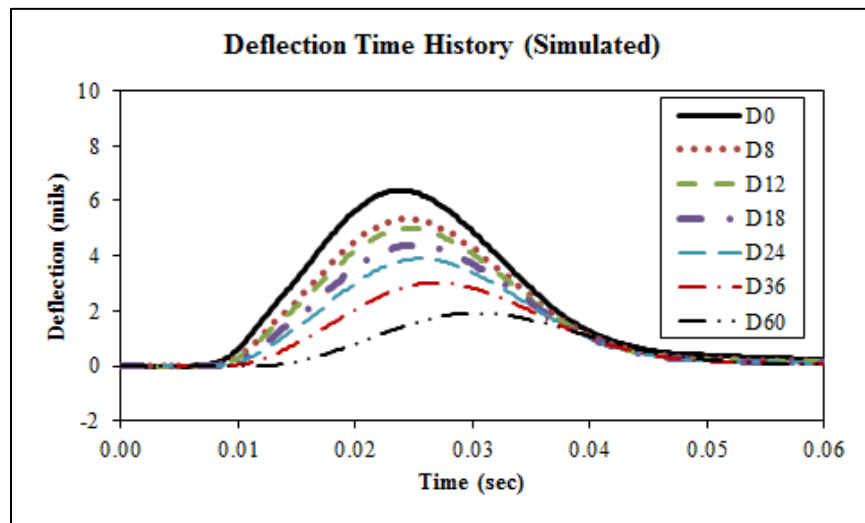
Source: FHWA.

Figure 105. Graph. Simulated deflection–time histories for test lane F1 on 03/10/1993 at station 200 for Alabama test section 01-0110.
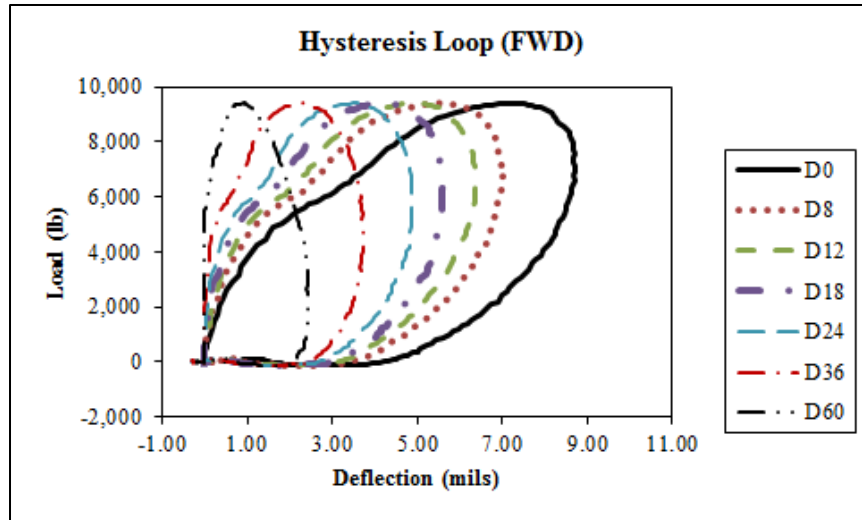
Source: FHWA.

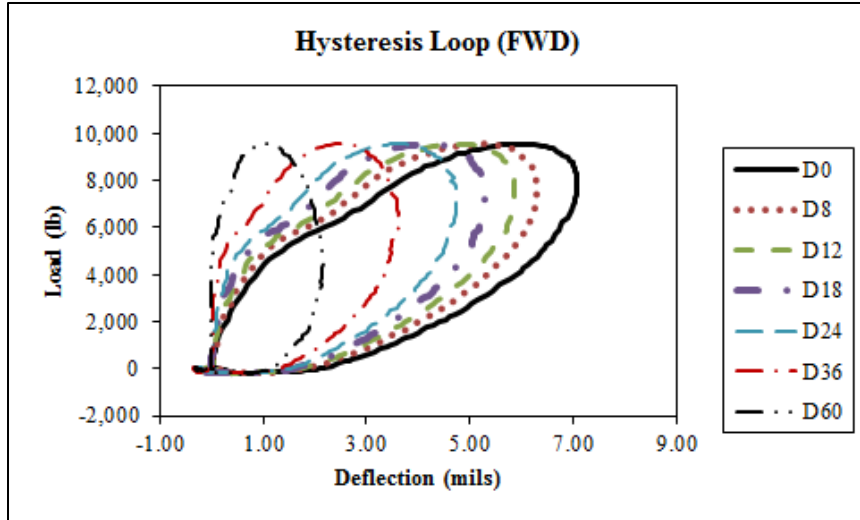**Figure 106. Graph. Measured hysteresis loops for test lane F1 on 03/10/1993 at station 200 for Alabama test section 01-0110.**
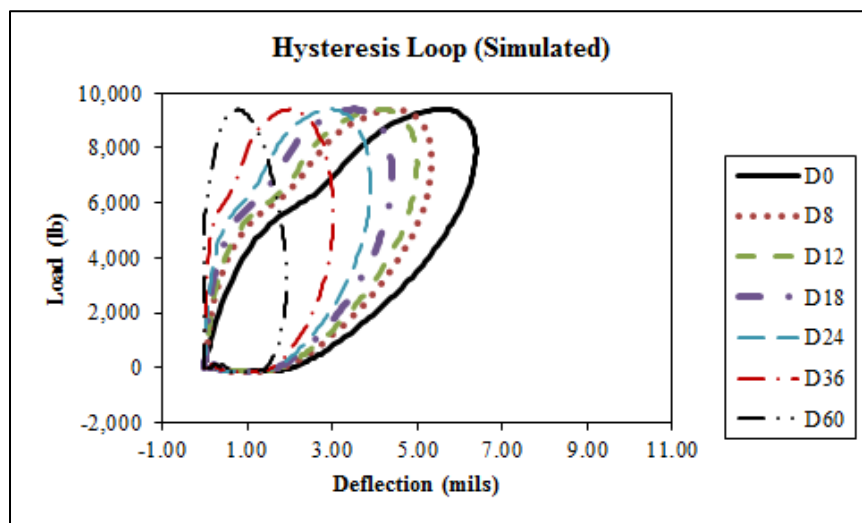
Source: FHWA.

Figure 107. Graph. Simulated hysteresis loops for test lane F1 on 03/10/1993 at station 200 for Alabama test section 01-0110.

Table 19 summarizes the FWD measured and simulated dissipated work and the dissipated work ratio. Figure 108 and figure 109 show the FWD measured and simulated dissipated work over time. Figure 110 shows the dissipated work ratio over time. Similar to test section 01-0103, the simulated dissipated work for test section 01-0110 showed less variability over time, and the ratio followed a similar trend as the FWD measured dissipated work. However, there was no significant difference in the dissipated work ratio between the FWD test dates with and without cracking.

Table 19. FWD and simulated dissipated work ratios for Alabama test section 01-0110.

	WP			Non-WP		
Test Date	FWD Dissipated Work (lb-Inch)	Simulated Dissipated Work (lb-Inch)	Ratio of Dissipated Work	FWD Dissipated Work (lb-Inch)	Simulated Dissipated Work (lb-Inch)	Ratio of Dissipated Work
3/10/1993	54.8	36.5	1.5	54.3	34.9	1.6
6/20/1995	37.1	27.4	1.4	36.7	27.7	1.3
4/18/1996	45.8	34.1	1.3	47.4	34.5	1.4
4/17/1997	33.6	25.4	1.3	33.1	25.5	1.3
7/21/1998	56.0	31.2	1.8	58.8	32.3	1.8
5/17/2000	50.4	30.4	1.7	50.0	31.0	1.6
4/27/2005	34.7	25.5	1.4	32.0	22.9	1.4
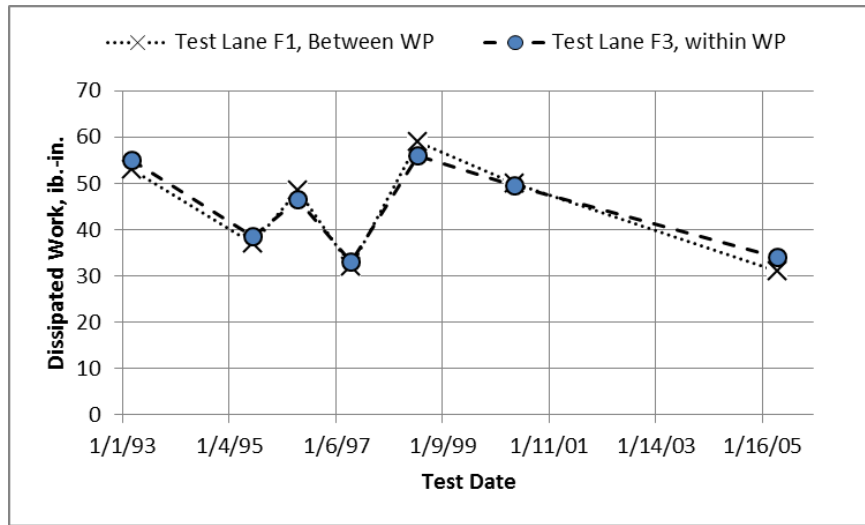
Source: FHWA.

Figure 108. Graph. FWD dissipated work measured over time for test lanes F1 and F3 for Alabama test section 01-0110.
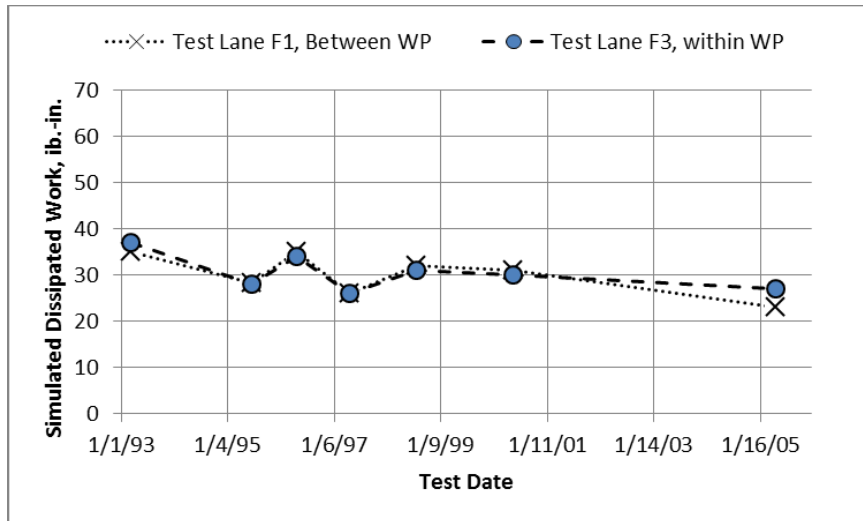
Source: FHWA.

Figure 109. Graph. Simulated dissipated work measured over time for test lanes F1 and F3 for Alabama test section 01-0110.
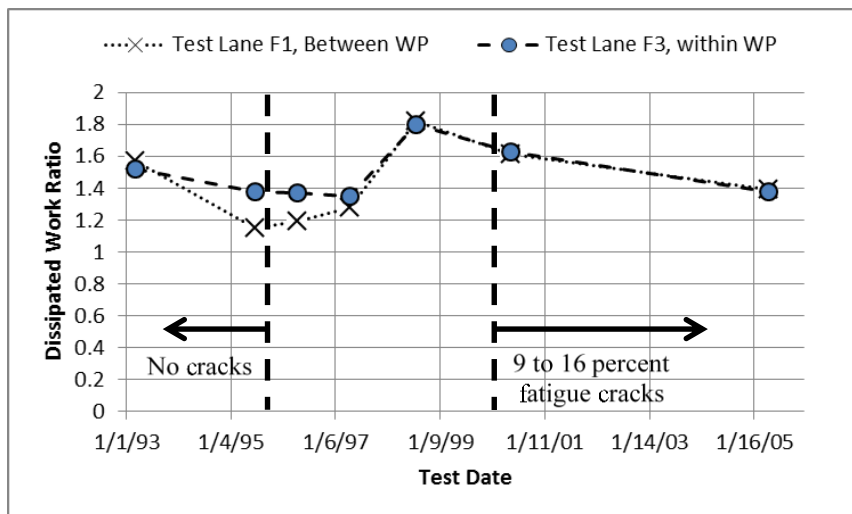
Source: FHWA.

Figure 110. Graph. Dissipated work ratio measured over time for test lanes F1 and F3 for Alabama test section 01-0110.

Test Section 4: 20-0903—Full-Depth Pavement Structure with Treated Base

Figure 111 shows the FWD measured deflection–time histories for test section 20-0903. The simulated deflection–time history generated with ViscoWave is shown in Figure 112. The corresponding FWD measured hysteresis loops are shown in figure 113, while the simulated hysteresis loops are shown in figure 114. The ratio of dissipated work at the first FWD test date was calculated to be 1.0 for both the WP and non-WP locations. Table 20 summarizes the FWD measured and simulated dissipated work and the dissipated work ratio.

108
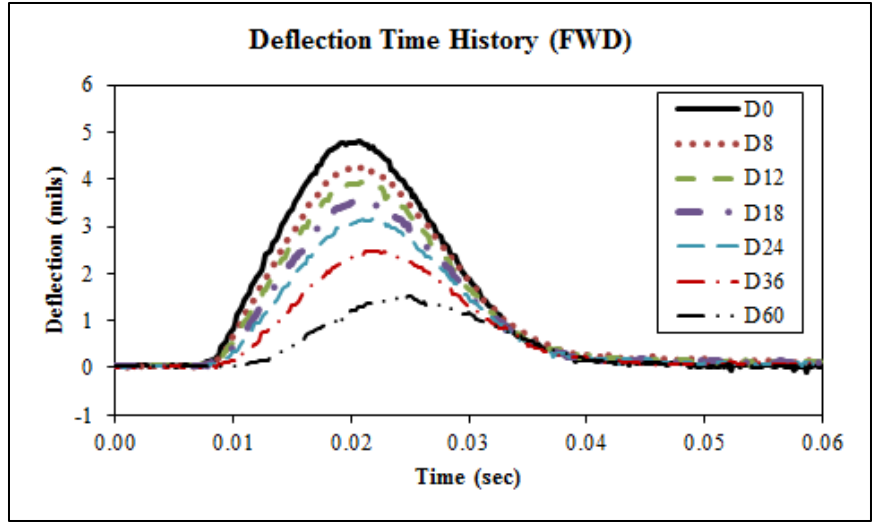
Source: FHWA.

Figure 111. Graph. Measured deflection–time histories for test lane F1 on 10/29/1993 at station 200 for Kansas test section 20-0903.
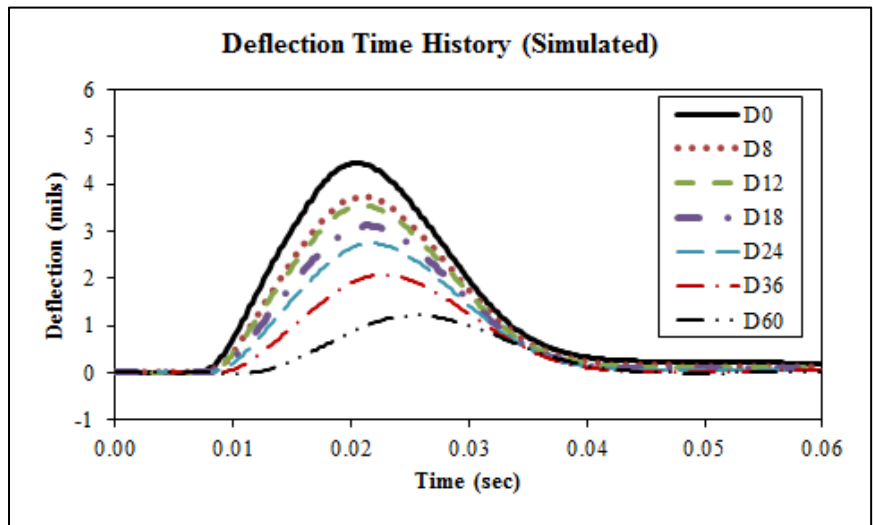
Source: FHWA.

Figure 112. Graph. Simulated deflection–time histories for test lane F1 on 10/29/1993 at station 200 for Kansas test section 20-0903.
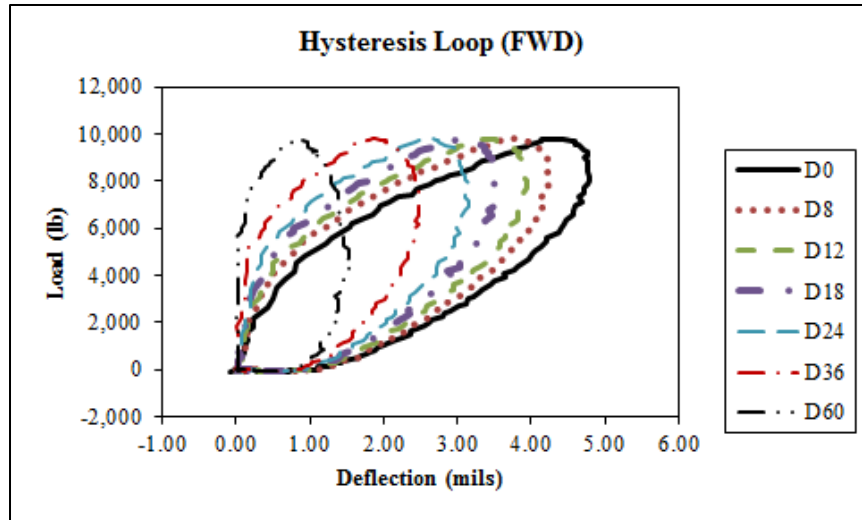
Source: FHWA.

Figure 113. Graph. Measured hysteresis loops for test lane F1 on 10/29/1993 at station 200 for Kansas test section 20-0903.
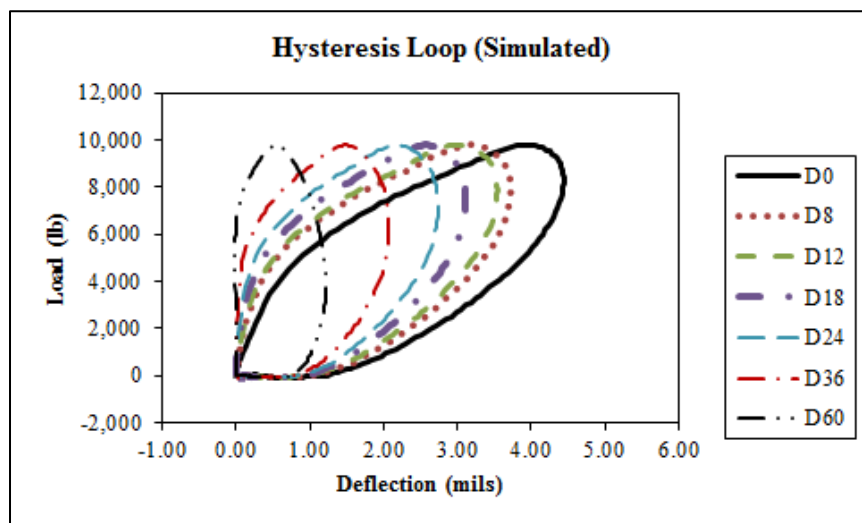
Source: FHWA.

Figure 114**. Graph. Simulated hysteresis loops for test lane F1 on 10/29/1993 at station 200 for Kansas test section 20-0903.**

Table 20. FWD and simulated dissipated work ratios for Kansas test section 20-0903.

Test Date	WP			Non-WP		
	FWD Dissipated Work (lb-Inch)	Simulated Dissipated Work (lb-Inch)	Ratio of Dissipated Work	FWD Dissipated Work (lb-Inch)	Simulated Dissipated Work (lb-Inch)	Ratio of Dissipated Work
10/29/1993	24.6	24.7	1.0	24.5	24.0	1.0
8/23/1994	59.8	25.6	2.3	51.2	21.9	2.3
8/15/1995	56.7	26.9	2.1	49.4	24.4	2.0
7/9/2001	68.9	26.1	2.6	65.2	24.6	2.6

Figure 115 and figure 116 show the FWD measured and simulated dissipated work over time, while figure 117 shows the dissipated work ratio over time. As shown, the dissipated work ratio significantly increased after the first FWD test date. However, the dissipated work ratio for the FWD test date with high amounts of cracking was only slightly higher than for the two FWD test dates without cracking.
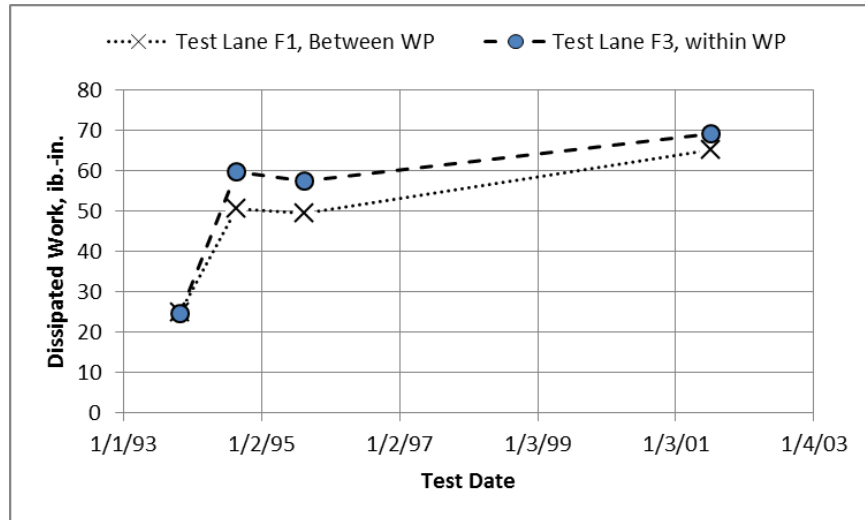
Source: FHWA.

Figure 115. Graph. FWD dissipated work measured over time for test lanes F1 and F3 for Kansas test section 20-0903.
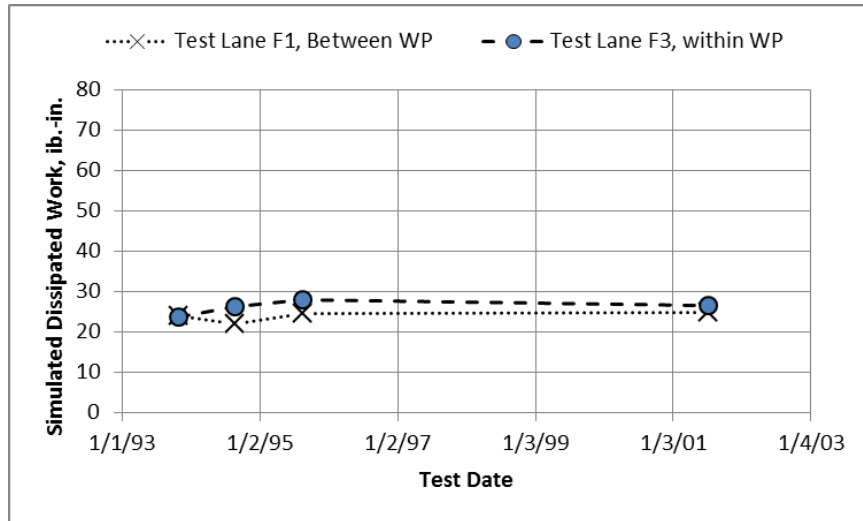
Source: FHWA.

Figure 116. Graph. Simulated dissipated work over time for test lanes F1 and F3 for Kansas test section 20-0903.
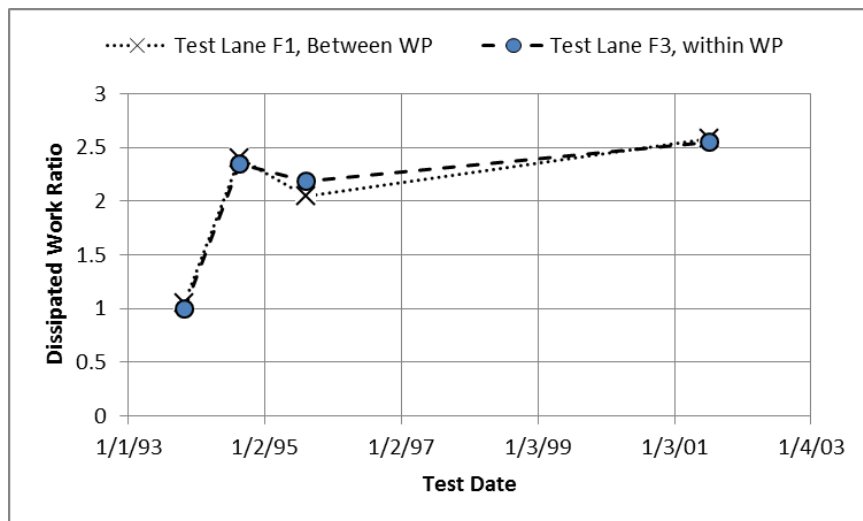
Source: FHWA.

Figure 117. Graph. Dissipated work ratio over time for test lanes F1 and F3 for Kansas test section 20-0903.

Test Section 5: 20-0901—Full-Depth AC Pavement with Treated Base Layer

Figure 118 shows the FWD measured deflection–time histories for Kansas test section 20-0901. The simulated deflection–time histories were generated by ViscoWave and are shown in figure 119. The corresponding FWD measured hysteresis loops are shown in figure 120, while the simulated hysteresis loops are provided in figure 121. The ratio of dissipated work at the first FWD test date was calculated to be 1.0 for both the WP and non-WP locations. Table 21 summarizes the FWD-measured and simulated dissipated work and the dissipated work ratio.

112
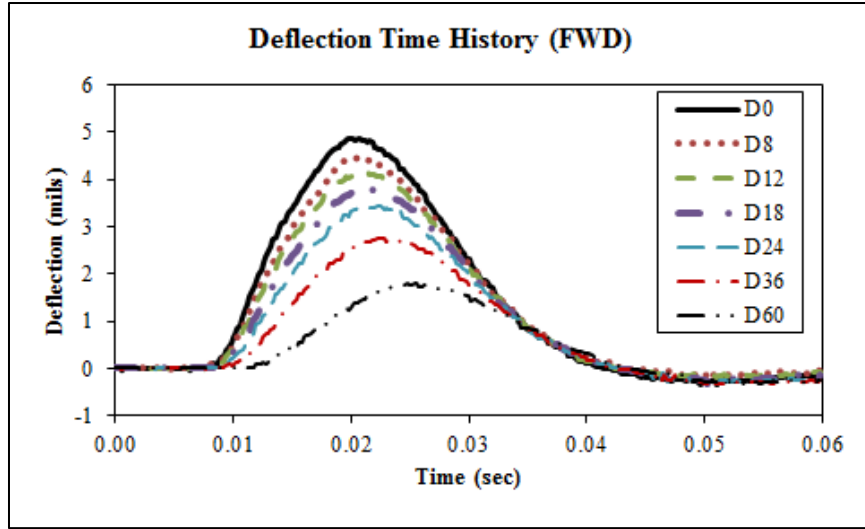
Source: FHWA.

Figure 118. Graph. Measured deflection–time histories for test lane F1 on 10/29/1993 at station 200 for Kansas test section 20-0901.
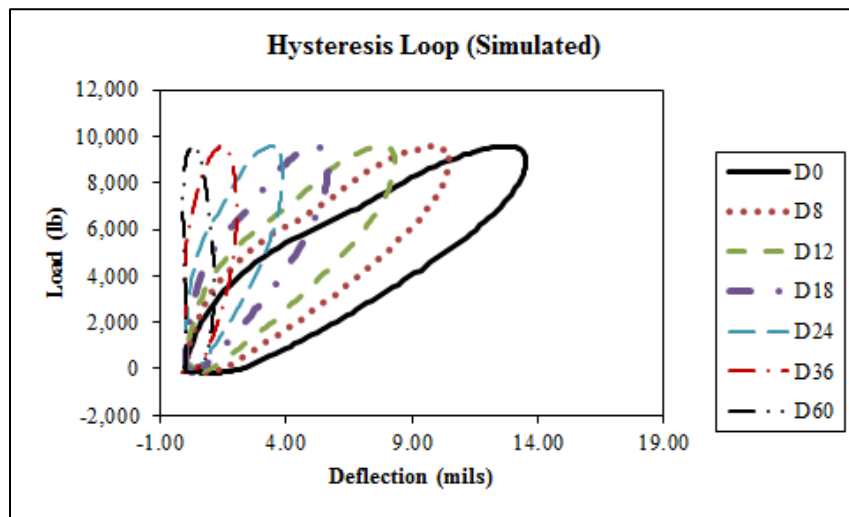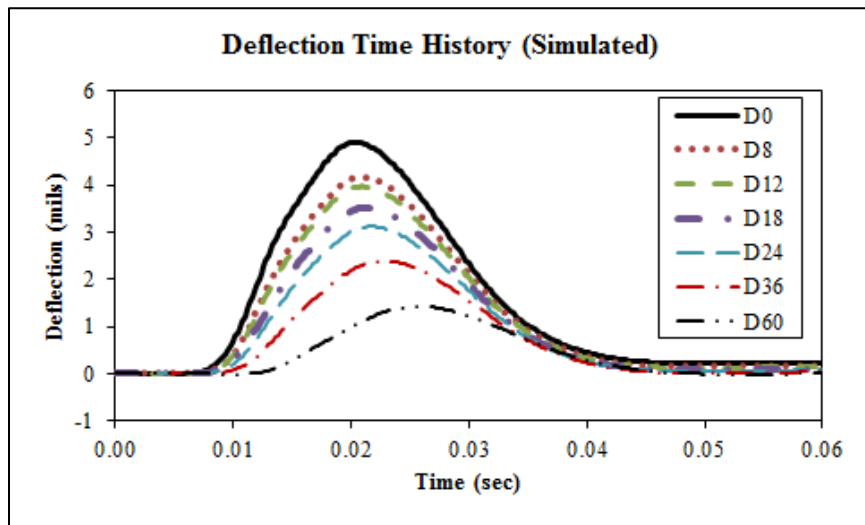

Source: FHWA.

Figure 119. Graph. Simulated deflection–time histories for test lane F1 on 10/29/1993 at station 200 for Kansas test section 20-0901.
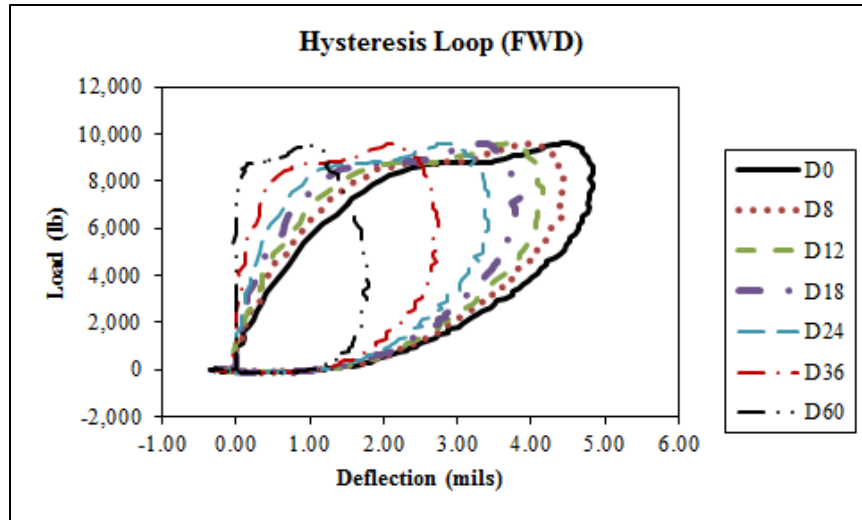
Source: FHWA.

Figure 120. Graph. Measured hysteresis loops for test lane F1 on 10/29/1993 at station 200 for Kansas test section 20-0901.
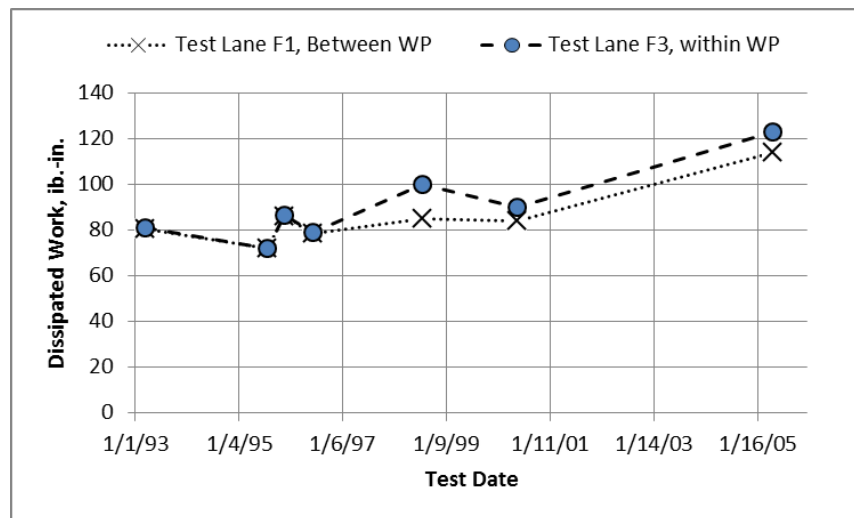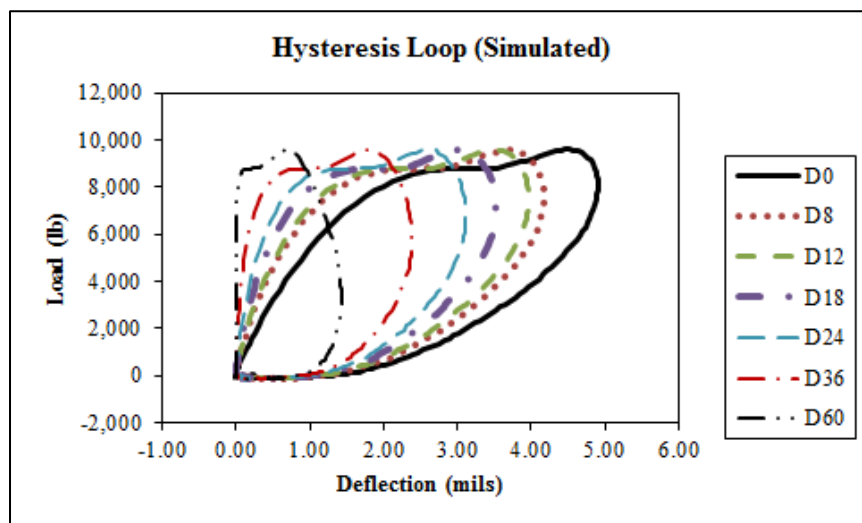

Source: FHWA.

Figure 121. Graph. Simulated hysteresis loops for test lane F1 on 10/29/1993 at station 200 for Kansas test section 20-0901.

Table 21. FWD and simulated dissipated work ratios for Kansas test section 20-0901.

Test Date	WP			Non-WP		
	FWD Dissipated Work (lb-Inch)	Simulated Dissipated Work (lb-Inch)	Ratio of Dissipated Work	FWD Dissipated Work (lb-Inch)	Simulated Dissipated Work (lb-Inch)	Ratio of Dissipated Work
10/29/1993	24.9	25.5	1.0	25.7	25.9	1.0
8/23/1994	33.1	21.7	1.5	34.3	22.0	1.6
8/15/1995	27.7	19.9	1.4	29.1	20.2	1.4
7/9/2001	36.7	24.2	1.5	38.2	23.9	1.6

Figure 122 and figure 123 show the FWD measured and simulated dissipated work over time, respectively, while figure 124 shows the dissipated work ratio over time. As shown, the dissipated work ratio over time showed a similar trend to test section 20-0901.
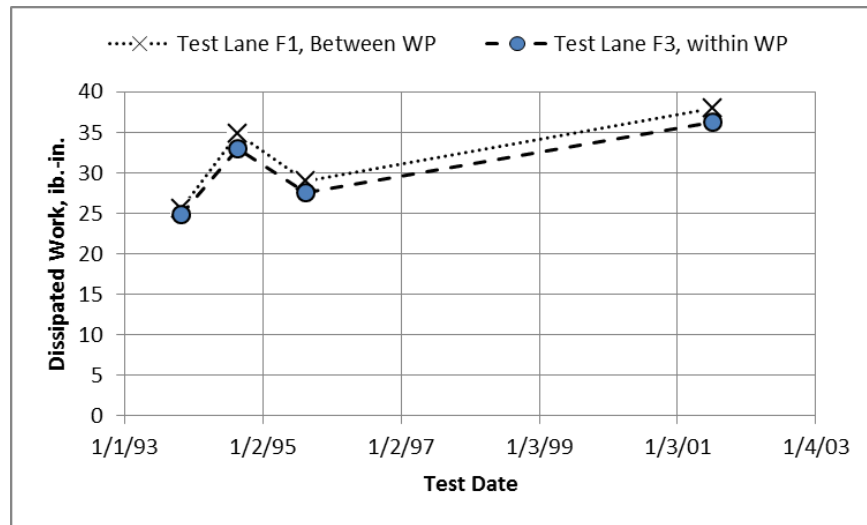
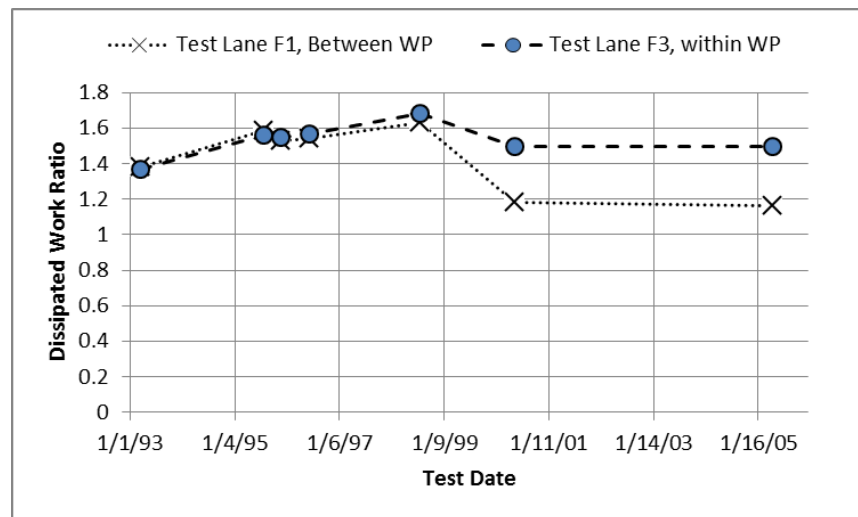Source: FHWA.

Figure 122. Graph. FWD dissipated work measured over time for test lanes F1 and F3 for Kansas test section 20-0901.
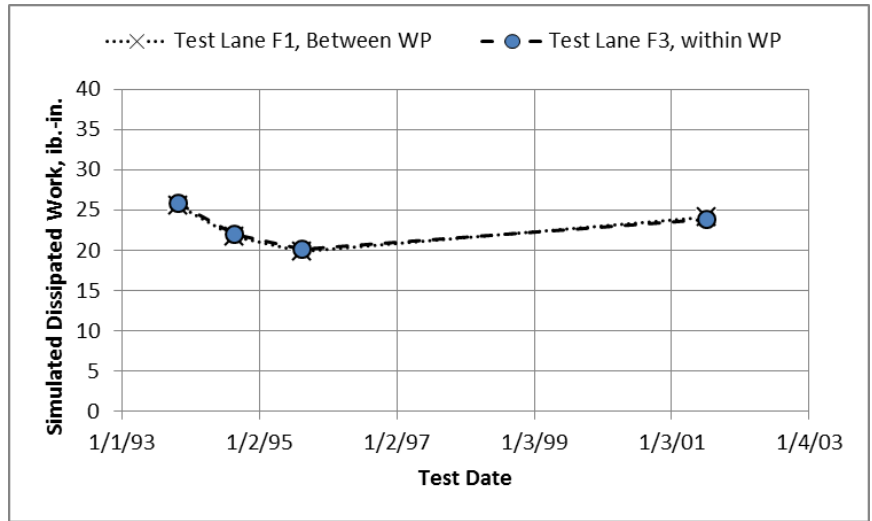
Source: FHWA.

**Figure 123. Graph. Simulated dissipated work measured over time for test lanes F1 and F3 for Kansas test section 20-0901.**
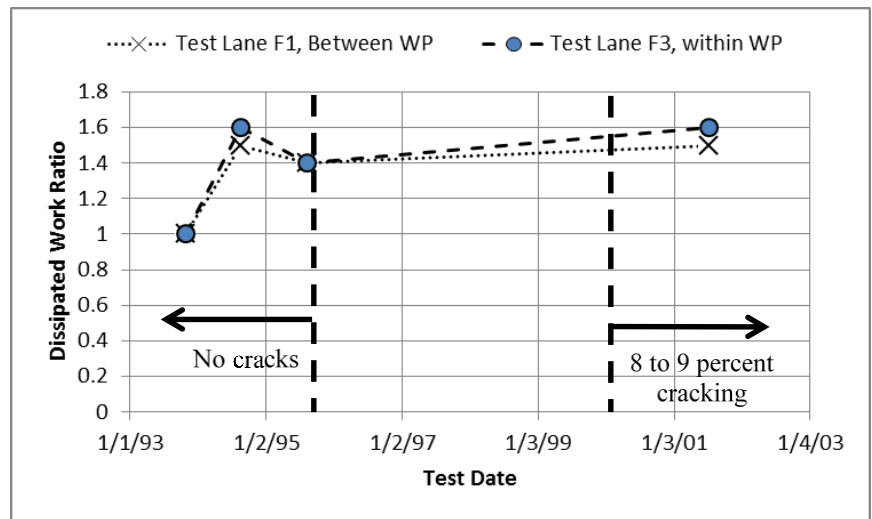
Source: FHWA.

Figure 124. Graph. Dissipated work ratio measured over time for test lanes F1 and F3 for Kansas test section 20-0901.

SUMMARY OF OUTCOMES FROM PRELIMINARY ANALYSIS

Table 22 summarizes the results from the preliminary analyses for the five LTPP test sections.

Table 22. Deflection-based parameters for the preliminary analyses.

Parameter	Test Section				
	Alabama			Kansas	
	01-0103	**01-0102**	**01-0110**	**20-0903**	**20-0901**
Total AC thickness (inches)	11.1	4.2	7.9	11.1	11.1
Other base layer	None	Aggregate base	PATB	ATB	ATB
Maximum amount of cracking (percent)	13.0	35.5	15.0	52.0	9.0
Backcalculated frequency (Hz)	25	500	8	15	15
Deflection–time duration (ms)	0.042	0.037	0.060	0.045	0.045
Dissipated work (kip-inch)	28.6	83.5	54.8	24.6	24.9
Damage ratio; no cracking	2.206	0.697	0.573	1.082	1.070
Dissipated work ratio; no cracking	1.1	1.4	1.5	1.0	1.0
Damage ratio	No consistent change over time	No consistent change over time	Increased over time	Decreased over time	Increased over time
Dissipated work ratio	Increased over time	No consistent change over time	No consistent change over time	Increased over time	Increased over time

The following list summarizes the outcomes from the preliminary analyses for the LTPP test sections as related to the hypotheses included in chapter 3:

- The modulus ratio (E_{FWD}/E^*_{PRED}) was not correlated to the amount of cracking, and there was no consistent trend in the change of the ratio over time.

- The dissipated work ratio was not correlated to the amount of cracking, and there was no consistent trend in the change of the ratio over time.

Thus, hypotheses 2, 3, and 5 from chapter 3 were rejected from the preliminary analyses. More test sections are needed to evaluate hypotheses 1 and 4, which are provided in chapter 7. The issue or reason why the hypotheses were rejected and E_{FWD}/E^*_{PRED} being highly variable could be that the assumptions referred to in chapter 3 are incorrect, which are noted and further discussed in this subsection.

The pavement middepth temperature and FWD load frequency were used as inputs in the $|E^*|$ sigmoidal function to calculate the undamaged modulus (E^*_{PRED}). Two sets of frequencies were calculated from the FWD data: E_{FWD} and load duration. The frequency determined from E_{FWD} generally decreased with increasing FWD drop load, while the frequency determined from the FWD load duration increased with increasing drop load. The frequency derived from the E_{FWD} exhibited much higher variability. The E_{FWD}/E^*_{PRED} ratios derived from both sets of frequencies (E_{FWD} and FWD load duration) shortly after construction (without cracking) was not equal. More importantly, when the E_{FWD}/E_{PRED} ratio was adjusted to unity for the test dates shortly after construction, the E_{FWD}/E^*_{PRED} ratio calculated over time did not improve on the relationship with the amount of cracking. In all probability, the frequency for calculating E_{PRED} is dependent on other factors or variables (i.e., thickness, stress sensitivity, temperature, etc.). As such, all further static analyses discussed were confined to the modulus ratio using a constant frequency of 30 Hz in terms of defining E^*_{PRED} when no fatigue damage should exist (i.e., shortly after construction).

For the thicker sections included in this limited analysis, much more variability was observed in the backcalculated elastic layer moduli. The test days further from construction with no load-related cracking typically resulted in higher elastic layer moduli. The higher moduli than expected were probably related to mixture aging near the surface that impacts the confinement in the lower AC layers or mixtures at the higher test temperatures. Confinement is another factor that can have an effect on the laboratory or undamaged modulus at the higher test temperatures.

Another potential issue is the assumption that E_{FWD} is equal to E^*_{PRED} with no damage. As noted previously in chapter 2, some researchers have reported differences between E_{FWD} and E^*_{PRED} at the same temperature and that difference is temperature dependent.[23,33] An outcome from the preliminary analysis is that E^*_{PRED} and E_{FWD} are not equal, even without any damage in the AC layer. As such, an analysis was conducted to compare the results between a dynamic and static analysis. ViscoWave was used to evaluate the magnitude of difference between the static and dynamic analysis, which is discussed in the next chapter.

CHAPTER 6. DYNAMIC BACKCALCULATION

The backcalculation results provided in chapters 4 and 5 were based on the modulus values derived from static backcalculation. The forward solutions embedded in the static backcalculation methodologies assumed that a pavement structure under applied load was in static equilibrium. In other words, these solutions did not allow for simulating the FWD load and deflection as functions of time. Consequently, the E_{FWD} values obtained from static backcalculation were independent of time and did not account for the dynamic and viscoelastic (i.e., time-dependent) nature of the FWD load and deflections.

Recent developments in dynamic backcalculation have shown potential for backcalculating the time-dependent modulus of asphalt from FWD time histories. Unlike static solutions, dynamic backcalculation methods utilize forward solutions that are capable of incorporating the viscoelasticity of the material (asphalt) and the wave propagation effects produced by the FWD (impact loading).

This chapter presents the results from a limited dynamic backcalculation conducted as part of this research to explain some of the observations in chapter 5. Specific objectives of the dynamic backcalculation study were as follows:

- Compare the asphalt E^* master curves constructed using the laboratory-obtained coefficients (LTPP E^* table) to those constructed from FWD data using dynamic analyses.

- Compare the FWD frequencies backcalculated using the E_{FWD} values from static backcalculation with master curves constructed using the LTPP E^* coefficients and master curves constructed from the FWD data (i.e., dynamic backcalculation).

- Determine if the field-derived, backcalculated E^* values using dynamic analyses are significantly different before and after cracking.

DYNAMIC BACKCALCULATION ALGORITHM

Backcalculation, in general, is carried out by matching the FWD load and deflection to those from a theoretical model. Therefore, the two crucial components of a backcalculation methodology are: (1) a forward solution or a theoretical model capable of simulating the FWD load and deflection and (2) an iterative or statistical routine capable of determining the optimum layer parameters that minimize the error between the measured and simulated results.

For this study, computational program ViscoWave was used as the forward solution for simulating the FWD deflection–time histories. ViscoWave is a finite layer solution capable of modeling the pavement dynamics and material viscoelasticity under a transient, nonperiodic loading.[58] On the other hand, a nonlinear optimization routine known as the generalized reduced gradient method was implemented in Microsoft® Excel™'s Solver application and used for calculating the optimum modulus with minimum error.[40]

SITES SELECTED FOR DYNAMIC BACKCALCULATION

For this dynamic backcalculation exercise, two sections from the preliminary study were selected: one from a cold climate zone (test section 36-0801 in New York) and the other from a warm climate zone (test section 01-0101 in Alabama). Both of these test sections are under LTPP's SMP and provide the FWD data collected over a wide range of temperatures. Additional information regarding the sites and the pavements is provided in the following subsections.

New York Test Section 36-0801

This SPS-8 section was constructed in June 1994. The pavement structure consisted of 5 inches of asphalt and 8.4 inches of granular base over an untreated coarse-grained subgrade. The cracking performance history of this section is shown in figure 125. The pavement was free of cracks for the first 2 yr of service and only exhibited a few minor longitudinal cracks until 1998. Fatigue cracks started to occur in 1999 and reached 42.5 percent in 2008 when the section became inactive. The total cracking for the last survey year was 50.9 percent.
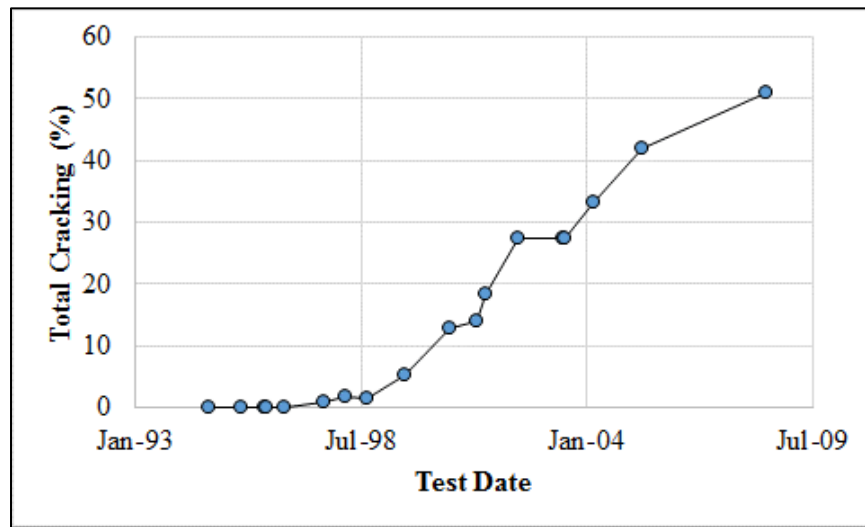
Source: FHWA.

Figure 125. Graph. Percent total cracking for New York test section 36-0801.

FWD testing was conducted numerous times throughout the year. The FWD deflection–time histories collected between August 1995 and July 1996 were used for backcalculating the $E^*_{undamaged}$ master curve values, whereas those collected in May and October 2008 were used for backcalculating the $E^*_{damaged}$ master curve values.

Alabama Test Section 01-0101

This SPS-1 section was constructed in 1993 and became inactive in 2005. The pavement structure consisted of 7.4 inches of asphalt and 7.9 inches of granular base on top of an untreated fine-grained subgrade. Figure 126 shows the total amount of cracking over time, which was similar to Alabama test sections 01-0103 (see figure 59) and 01-0110 (see figure 61). The pavement exhibited a steady increase in cracking and reached 14 percent cracking when it became inactive in 2005.
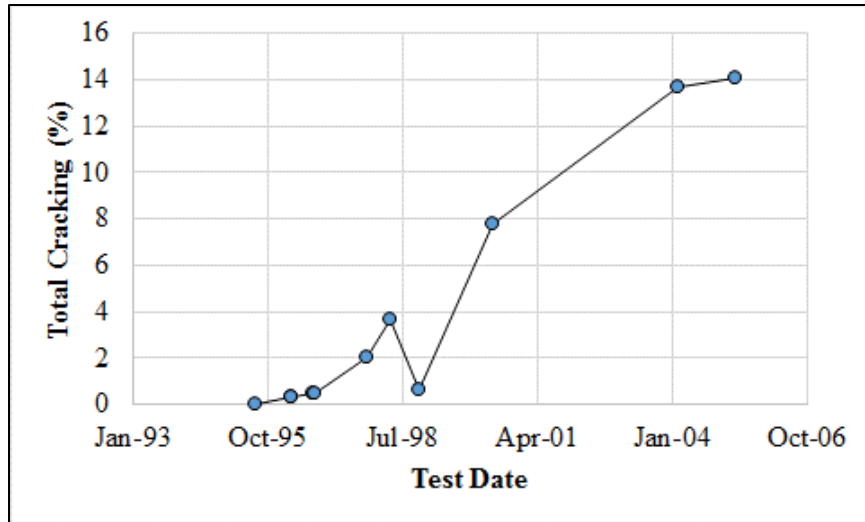
Source: FHWA.

Figure 126. Graph. Percent total cracking for Alabama test section 01-0101.

Similar to the New York section, the deflection data for this Alabama section were available for multiple test dates throughout the entire pavement life. FWD deflection–time histories, however, were unavailable for all of the FWD tests. More specifically, the deflection–time histories were available only for nine test dates, including five that were between 1993 and 1998. The last set of time histories were from 2005 just before the section became inactive. Therefore, the first five sets of deflection–time histories were used for backcalculating the $E^*_{undamaged}$ master curve values, while the last set of deflection–time histories were used for determining the $E^*_{damaged}$ master curve values.

PAVEMENT STRUCTURE AND SEED MODULI

Table 23 shows the pavement structure (i.e., layer thicknesses) used for dynamic backcalculation. Although the asphalt layers for both the New York and the Alabama test sections consisted of two lifts with different sigmoidal function parameters in the LTPP dynamic modulus table, the entire layer of asphalt was treated as a single combined layer for dynamic backcalculation. This is consistent with the static backcalculation process discussed in chapter 4. In addition, at each site, the top 24 inches of subgrade (designated as subgrade 1) was separated from the natural subgrade of infinite thickness (designated as subgrade 2), which was also consistent with the pavement structure used for static backcalculation analyses.

The initial estimates of the layer moduli (i.e., the seed moduli) had a significant effect on convergence and efficiency of dynamic backcalculation; hence, it is crucial to use a reasonable set of seed moduli.[59] For this study, the following two-step approach was used for dynamic backcalculation primarily to obtain a better set of seed moduli and to increase the overall efficiency of dynamic backcalculation:

121

1. Obtain a set of seed moduli for the first FWD test location (usually station 0) for each test date. The time-dependent seed modulus for the asphalt layer was assumed to be the dynamic modulus of the top lift of asphalt at a reference temperature of 72 °F regardless of the test temperature. The seed moduli for the unbound base and subgrade layers were arbitrarily chosen, as shown in table 23.

2. Conduct the dynamic backcalculation at the first test location using the seed values determined in step 1. The modulus values backcalculated from the first test location are used as seed values for backcalculating the modulus values at other locations.

Table 23. Layer thickness and seed moduli used for dynamic backcalculation.

	New York Test Section 36-0801		Alabama Test Section 01-0101	
Layer	Thickness (Inches)	Seed Modulus* (ksi)	Thickness (Inches)	Seed Modulus* (ksi)
Asphalt	5.0	Sigmoidal function (LTPP $|E^*|$ at 72 °F)	7.4	Sigmoidal function (LTPP $|E^*|$ at 72 °F)
Base	8.4	30.0	7.9	30.0
Subgrade 1	24.0	15.0	24.0	15.0
Subgrade 2	Infinite	25.0	Infinite	25.0

*These seed moduli values were used for only the first station tested.

The FWD deflection–time histories of drop height 2 (corresponding to a target peak load of 9,000 lb) and measured within the WPs were used for dynamic backcalculation because of stress sensitivity, as discussed in chapter 4.

DYNAMIC BACKCALCULATION RESULTS

The following subsections summarize the dynamic backcalculation results obtained from the New York (36-0801) and Alabama (01-0101) test sections. The results include examples of the measured and backcalculated FWD deflection–time histories, a comparison of the backcalculated $E^*_{undamaged}$ master curves to those obtained from the LTPP E^* table, a comparison of the backcalculated E^* master curve values before and after cracking, and any observations from the comparison to statically backcalculated modulus values.[10]

New York Test Section 36-0801

Typical time-dependent FWD load and the resulting deflection–time histories from test section 36-0801 are shown in figure 127 and figure 128, respectively. The time histories correspond to those collected on August 23, 1995, at the first test location (station 0). The middepth temperature of the asphalt layer at the time of FWD testing was 74.5 °F.
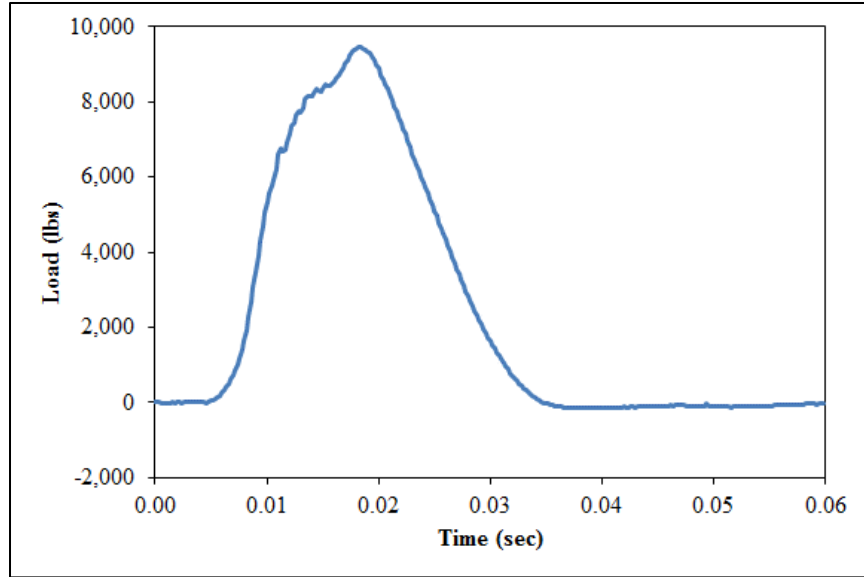
Figure 127. Graph. FWD load–time history for New York test section 36-0801 on 8/23/1995 at station 0.
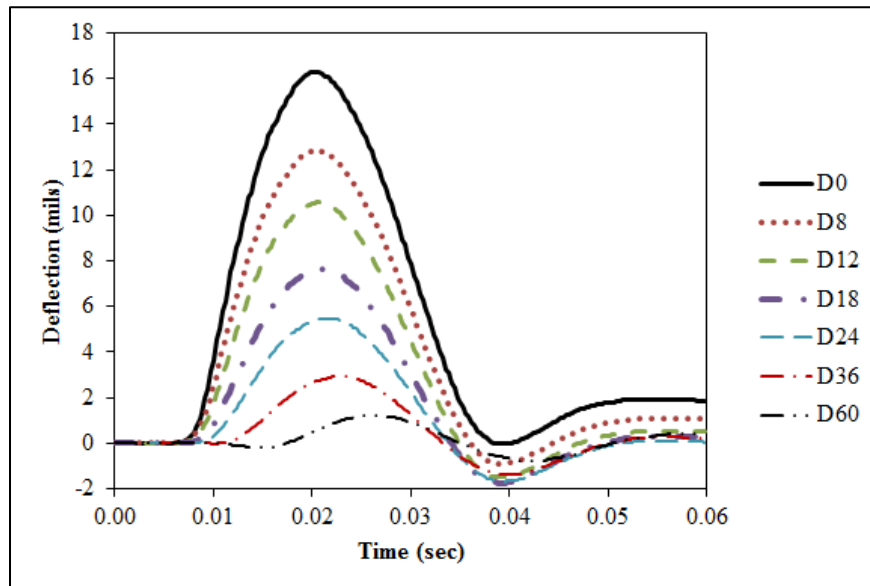
Figure 128. Graph. Measured deflection–time histories for New York test section 36-0801 on 8/23/1995 at station 0.

The deflections in figure 128 clearly show the effect of dynamics and material viscoelasticity. The evidence of dynamics is seen by the peak deflections measured at different offsets occurring at different time instances and the signs of free vibration toward the end of the load duration (i.e., negative deflection amplitudes that indicate the surface is being displaced upward). On the other hand, the effect of viscoelasticity is evidenced by the increased phase lag from deflections with higher peak magnitudes (i.e., the higher the deflections, the more time it needs to recover).[60]

Figure 129 shows the simulated deflection–time histories using the seed modulus values provided in table 23. It is immediately seen that the seed modulus values underestimated the deflection magnitudes and failed to capture the effect of free vibration. Conversely, figure 130 shows the simulated deflection–time histories after dynamic backcalculation. Both in terms of the deflection magnitudes and the effect of free vibration, the backcalculated time histories showed a significant improvement over the time histories simulated using the seed values.
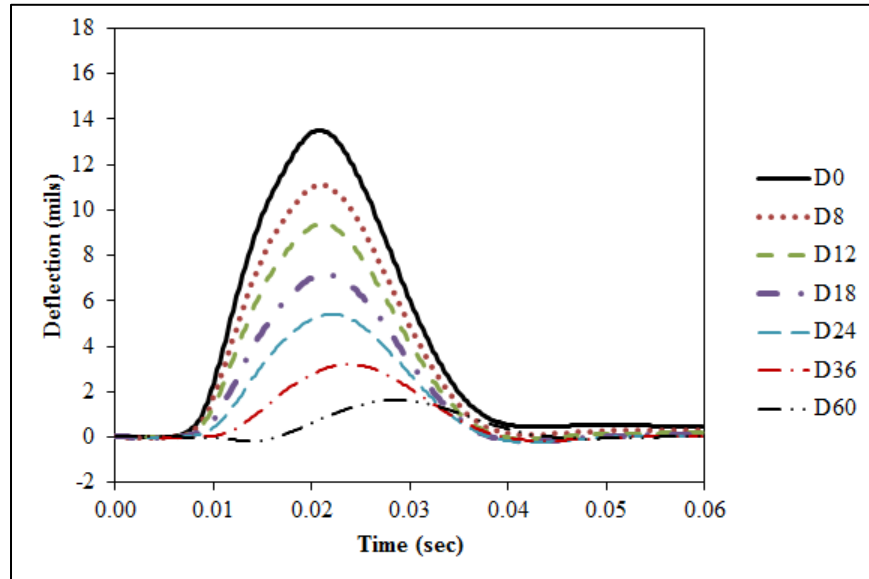
Source: FHWA.

Figure 129. Graph. Deflection–time histories simulated with seed modulus for New York test section 36-0801 on 8/23/1995 at station 0.
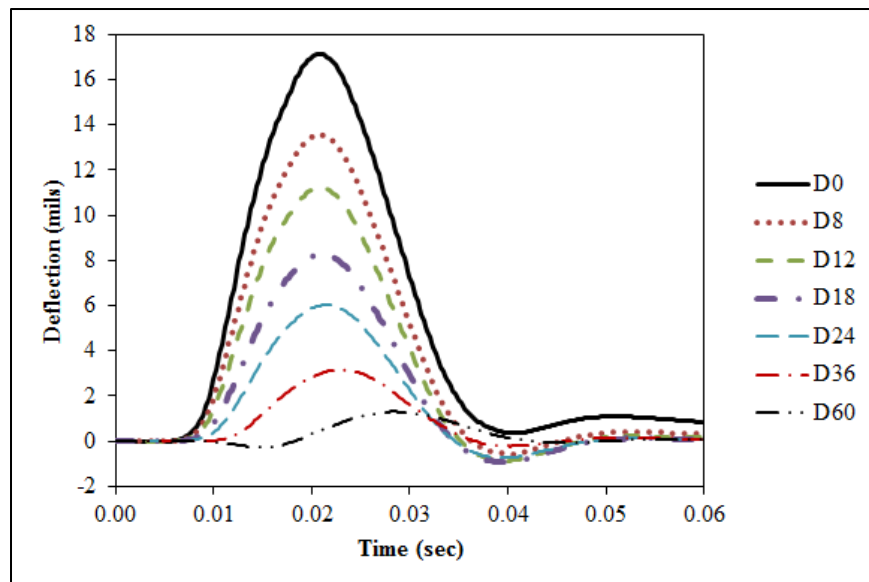
Source: FHWA.

Figure 130. Graph. Deflection–time histories simulated with backcalculated $E^*_{damaged}$ master curve for New York test section 36-0801 on 8/23/1995 at station 0.

124

Figure 131 shows the individual field-derived $E^*_{damaged}$ master curves backcalculated from the FWD deflection–time histories of New York test section 36-0801 collected on August 23, 1995, along with the average E^* master curve averaged across different stations.
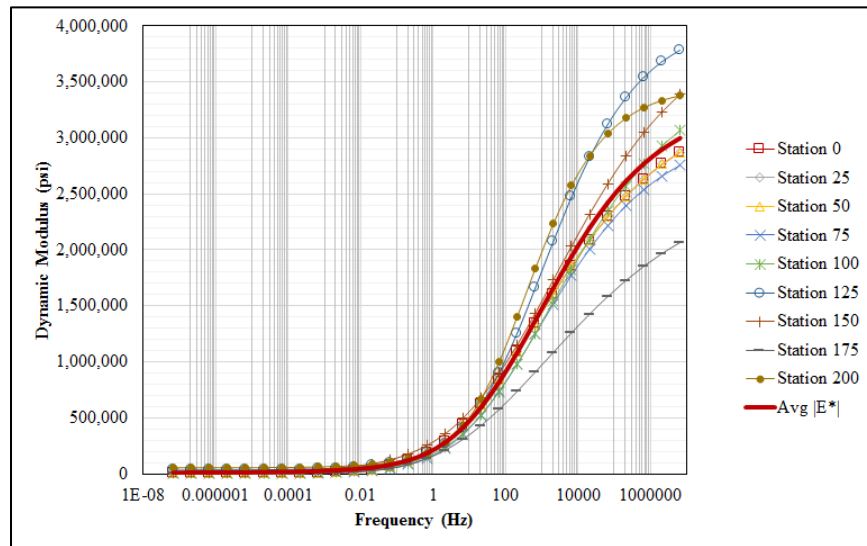
Source: FHWA.

Figure 131. Graph. Backcalculated $E^*_{damaged}$ master curves for New York test section 36-0801 on 8/23/1995.

Figure 132 shows that the averaged backcalculated $E^*_{damaged}$ master curve values were lower than those calculated using the LTPP laboratory-derived E^* master curve coefficients. As an example, the dynamic modulus at 10 Hz calculated using the LTPP dynamic modulus coefficients was 667.2 ksi, whereas the average backcalculated dynamic modulus at the same frequency was 411.6 ksi, which is a 38 percent reduction from the LTPP E^* values.
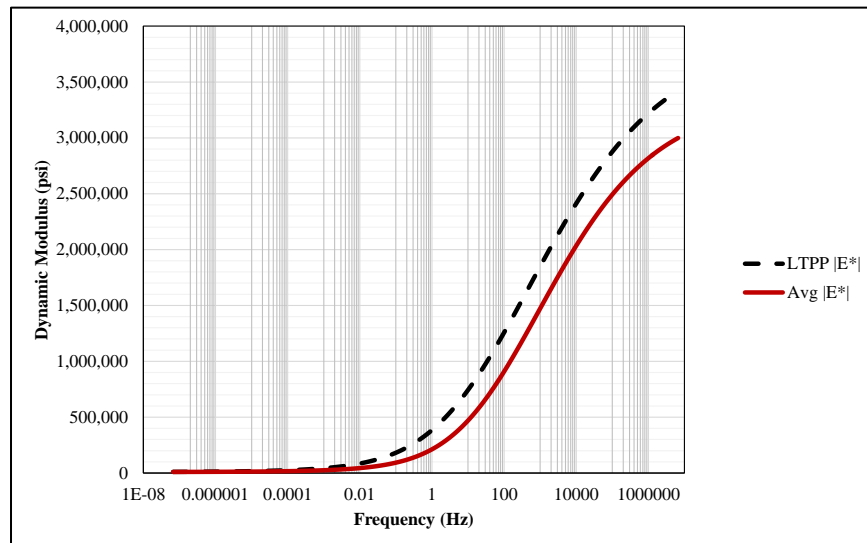
Source: FHWA.

Figure 132. Graph. Backcalculated $E^*_{damaged}$ versus LTPP laboratory-derived $E^*_{undamaged}$ master curves for New York test section 36-0801 for 8/23/1995 test date.

It was also observed from figure 131 that the backcalculated $E^*_{damaged}$ master curve showed significant dependence on test location (i.e., spatial variability), especially at higher frequencies. However, it should be noted that the frequencies contained in a typical FWD loading pulse were limited. To illustrate this, figure 133 shows the power spectral density (PSD) of the FWD load pulse shown previously in figure 127, which revealed that the frequency content of this particular FWD load pulse was mostly limited to frequencies less than 50 Hz.
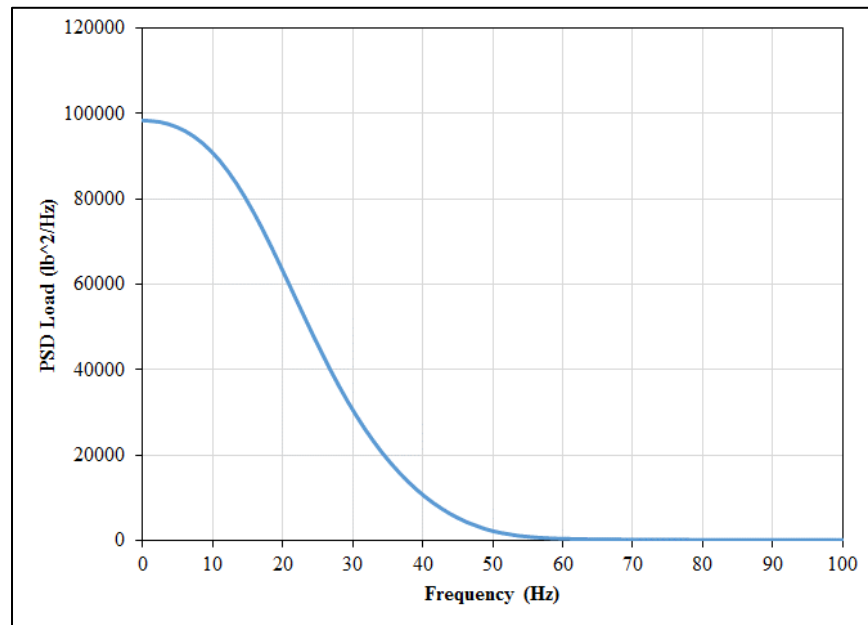
Source: FHWA.

Figure 133. Graph. PSD of FWD load for New York test section 36-0801 on 8/23/1995 at station 0.

This means that the pavement was not significantly loaded and, hence, would hardly respond to frequencies much higher than 50 Hz. In other words, the FWD deflection–time history did not include substantial information corresponding to frequencies beyond 50 Hz. It may cause challenges in backcalculating the E^* master curve especially at elevated frequencies, which, in turn, may reduce the reliability of the backcalculated E^* values corresponding to higher frequencies.

Figure 134 shows another example of field-derived backcalculated E^* from the individual FWD deflection–time histories. These time histories were collected on July 9, 1996, and the recorded middepth pavement temperature during FWD testing was 81.3 °F. Compared to the E^* master curves shown in figure 131, the curves in figure 134 showed less variability, especially at elevated frequencies. Figure 135 shows the average backcalculated master curve along with the curve constructed using the LTPP laboratory-derived E^* coefficients side by side and indicates that the two curves were in reasonable agreement. Nevertheless, for most of the test dates, the backcalculated E^* master curves were higher or lower than those obtained using the LTPP E^* master curve coefficients with the exception of the curve in figure 135.
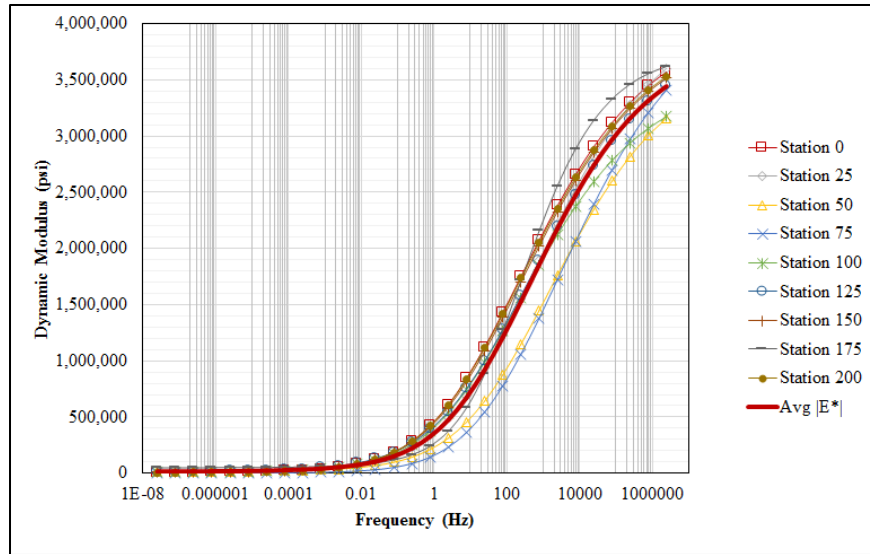
Source: FHWA.

Figure 134. Graph. Backcalculated $E^*_{damaged}$ master curves for New York test section 36-0801 on 7/9/1996.
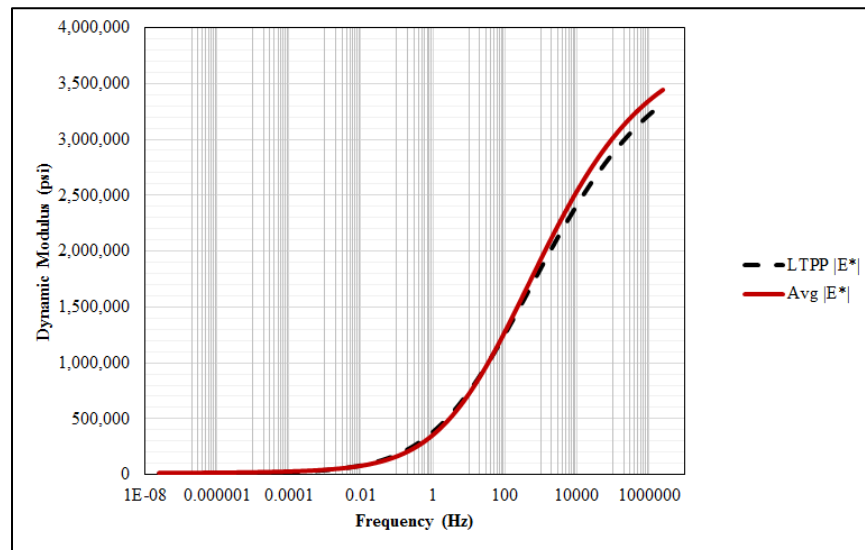
Source: FHWA.

Figure 135. Graph. Backcalculated $E^*_{damaged}$ master curve compared to LTPP laboratory-derived $E^*_{undamaged}$ master curve for New York test section 36-0801 on 7/9/1996.

Based on the LTPP laboratory-derived $E^*_{undamaged}$ master curve coefficients, the dynamic modulus at 10 Hz and at the corresponding temperature (81.3 °F) was determined to be 504.8 ksi. As expected, this was less than the value of 667.2 ksi obtained on August, 23, 1995, when the pavement was subjected to a slightly lower temperature (74.5 °F). However, the average backcalculated E^* from the July 9, 1996, data was determined to be 475.5 ksi, showing an increase from 411.6 ksi, which was backcalculated at a lower temperature (74.5 °F). Such a reversed trend in backcalculated E^* versus temperature caused challenges in backcalculating the time–temperature shift factors, as is discussed further in this chapter.

To construct the undamaged backcalculated *E** master curve, the *E** values at frequencies of 0.1, 0.5, 1, 5, 10, and 25 Hz were extracted from the average *E** master curves for each test date between August 1995 and July 1996 (see figure 136). The frequencies were selected by referring back to the PSD of the FWD load in figure 133 and assuming that the FWD load signal contained sufficient energy approximately up to 25 or 30 Hz.
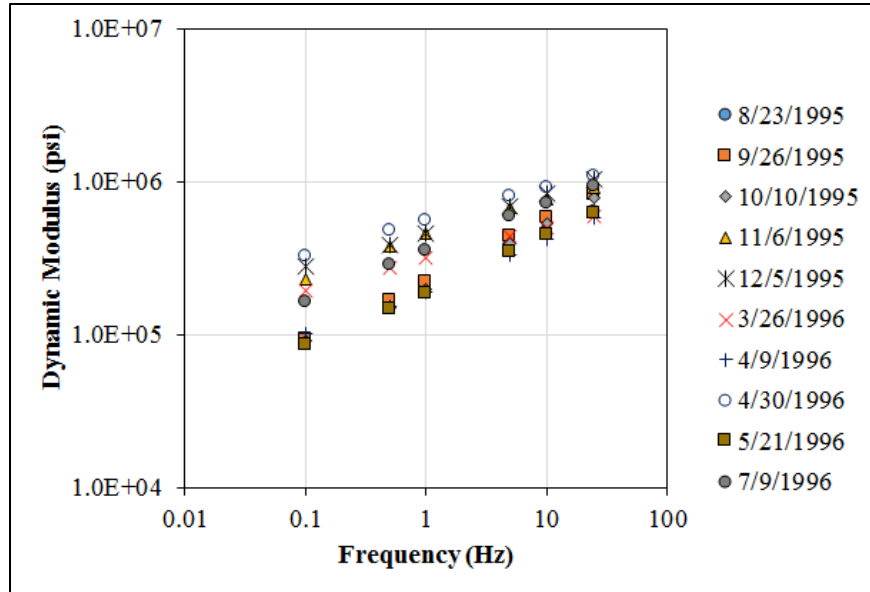
Source: FHWA.

Figure 136. Graph. Backcalculated *E** values from multiple test dates for New York test section 36-0801.

Using the time–temperature superposition principle, the *E** values in figure 136 were shifted to a reference temperature of 67.7 °F, which corresponded to the pavement middepth temperature on September, 26, 1995. Then, the *E** master curve in the form of a sigmoidal function was fitted through all of the backcalculated *E** values, as shown in figure 137.
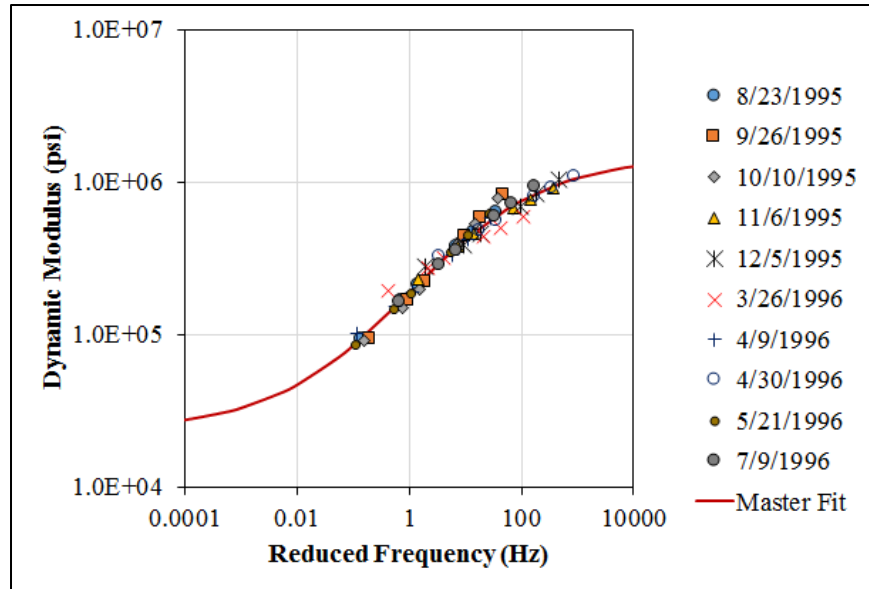
Source: FHWA.

Figure 137. Graph. Master curve fitting using backcalculated *E** values for New York test section 36-0801.

Figure 138 shows a comparison between the backcalculated E^* master curve and the LTPP laboratory-derived E^* master curve at 67.7 °F, which indicates that the backcalculated E^* master curve was significantly lower than the curve based on the LTPP E^* table. Obviously, the difference observed in the E^* values would have an effect on the backcalculated frequency using a statically backcalculated modulus, E_{FWD}. For example, if the modulus from static backcalculation, E_{FWD}, was 500 ksi, then the backcalculated frequency would be approximately 2.5 Hz based on the LTPP E^* master curve, whereas the frequency would be approximately 20 Hz based on the backcalculated E^* master curve. More results on the backcalculated frequency are presented in the Frequency Backcalculation from Static Modulus section of this report.
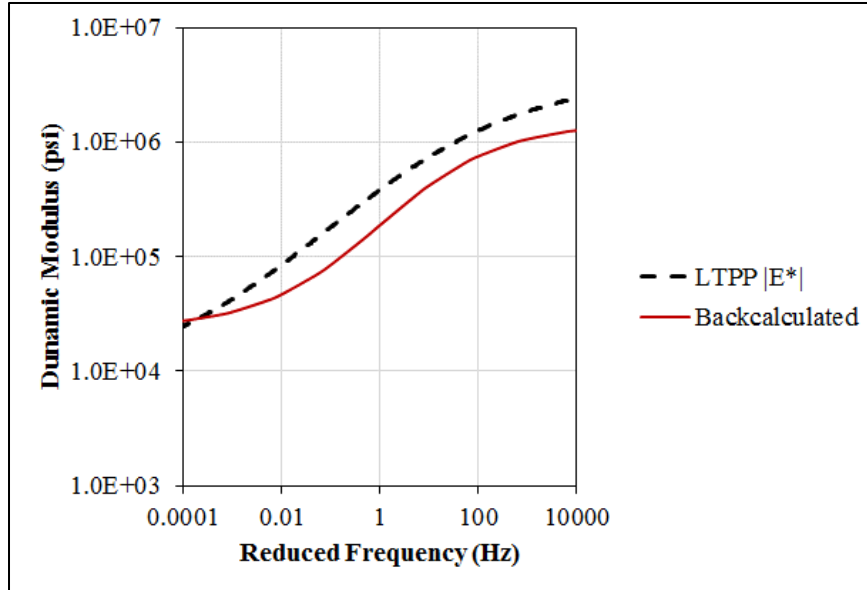
Source: FHWA.

Figure 138. Graph. Backcalculated $E^*_{damaged}$ master curve compared to LTPP laboratory-derived $E^*_{undamaged}$ master curve for New York test section 36-0801 at 67.7 °F.

The time–temperature shift factors obtained during the master curve fitting of the backcalculated E^* values are shown in figure 139. Unlike the shift factors obtained from the laboratory, the backcalculated shift factors showed a great amount of scatter, as indicated by the low coefficient of determination value of 0.21. While the cause of such a scatter is not clear, possible explanations are the noise in the FWD data that may have affected the backcalculated modulus and/or the lack of accuracy in the recorded temperature data.
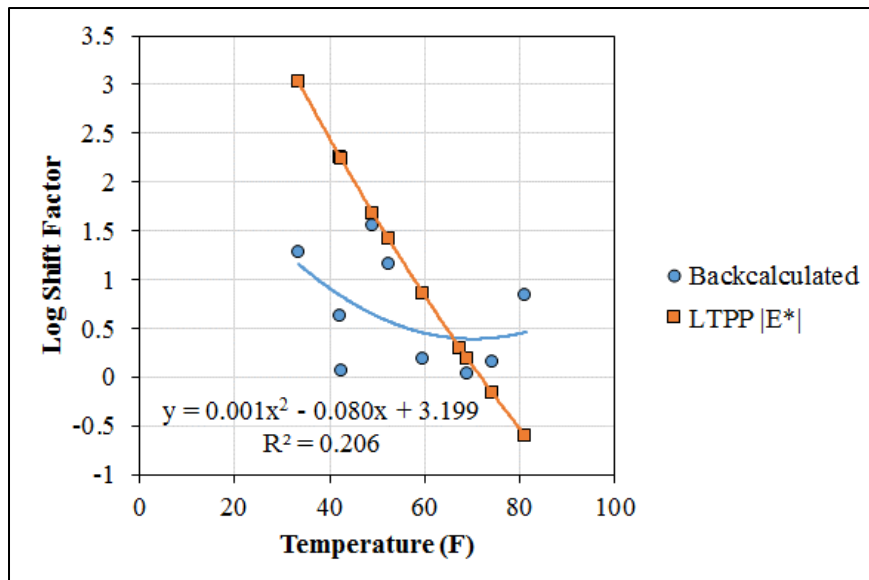
Source: FHWA.

Figure 139. Graph. Backcalculated $E^*_{damaged}$ values compared to LTPP laboratory-derived $E^*_{undamaged}$ temperature shift factors for New York test section 36-0801.

As mentioned previously, the $E^*_{damaged}$ master curve constructed in figure 138 was based on the FWD data from 1995 and 1996 where the pavement experienced no cracking.[10] Therefore, it was assumed that the master curve represented the undamaged modulus of the asphalt. To see if the presence of cracking had a significant effect in the backcalculated E^*, FWD data collected in May and October 2008 (when the pavement surface showed 50.9 percent cracking) were used independently for backcalculating the E^* values.[10]

The undamaged E^* master curve as well as the individual E^* values backcalculated from the 2008 FWD data are shown in figure 140. All of the E^* values were shifted to a reference temperature of 72 °F based on the backcalculated shift factors. Figure 140 shows there is only a negligible difference in the backcalculated E^* values before and after cracking. This observation supports the finding from the static backcalculation: modulus, E_{FWD} values, alone is insufficient to capture the in-place damage of an existing pavement.
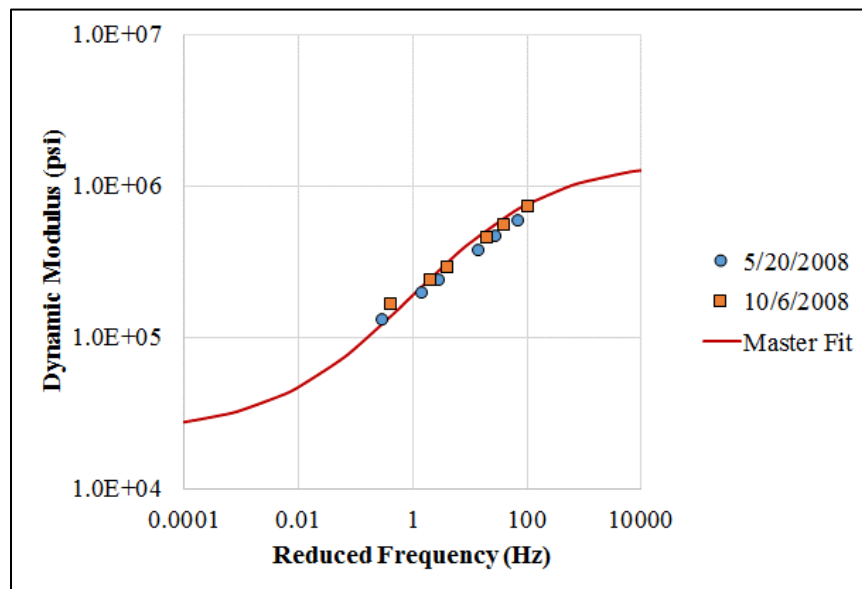
Source: FHWA.

Figure 140. Graph. Backcalculated E^* compared to LTPP laboratory-derived $E^*_{undamaged}$ master curve for New York test section 36-0801.

Alabama Test Section 01-0101

The dynamic backcalculation for Alabama test section 01-0101 followed the same procedure as the New York test section presented previously, and similar observations were made for many of the results. As such, presentation of the results from test section 01-0101 are kept to a minimum.

As an example of the typical FWD time histories from this test section, figure 141 and figure 142 show the measured and backcalculated FWD deflection–time histories, respectively, for a test date of June 21, 1995. The middepth pavement temperature recorded during the FWD testing was 93.7 °F. Due to the highly elevated temperature during testing, both figures show more pronounced viscoelastic behavior, whereas the dynamic effect (free vibration) was relatively small.
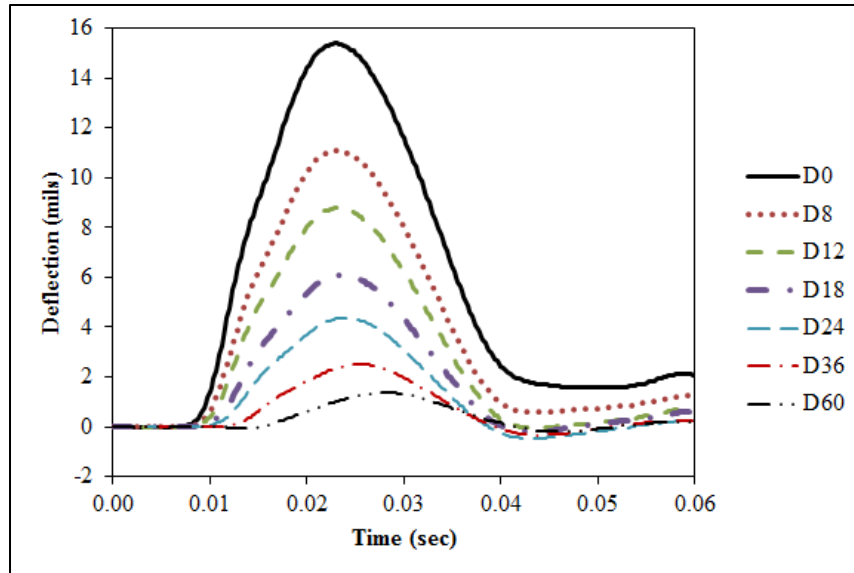
Source: FHWA.

Figure 141. Graph. Measured deflection–time histories for Alabama test section 01-0101 on 6/21/1995 at station 0.
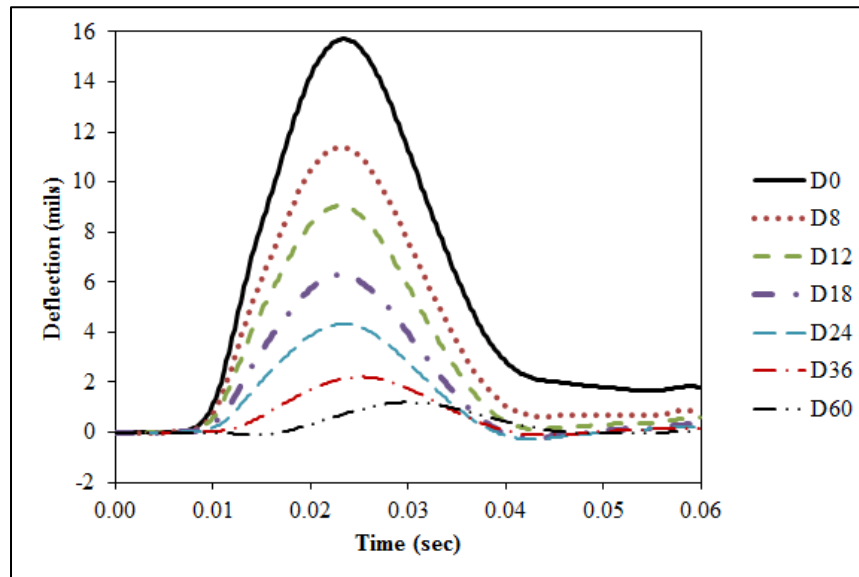
Source: FHWA.

Figure 142. Graph. Deflection–time histories simulated with backcalculated *E** values for Alabama test section 01-0101 on 6/21/1995 at station 0.

Figure 143 shows an example of the average backcalculated *E** master curve from test section 01-0101. Also shown in the figure is *E** calculated using the LTPP laboratory-derived *E** master curve coefficients. Unlike New York test section 36-0801, the backcalculated *E** for test section 01-0101 was consistently lower than the laboratory-derived *E** (i.e., similar to what is shown in figure 143).
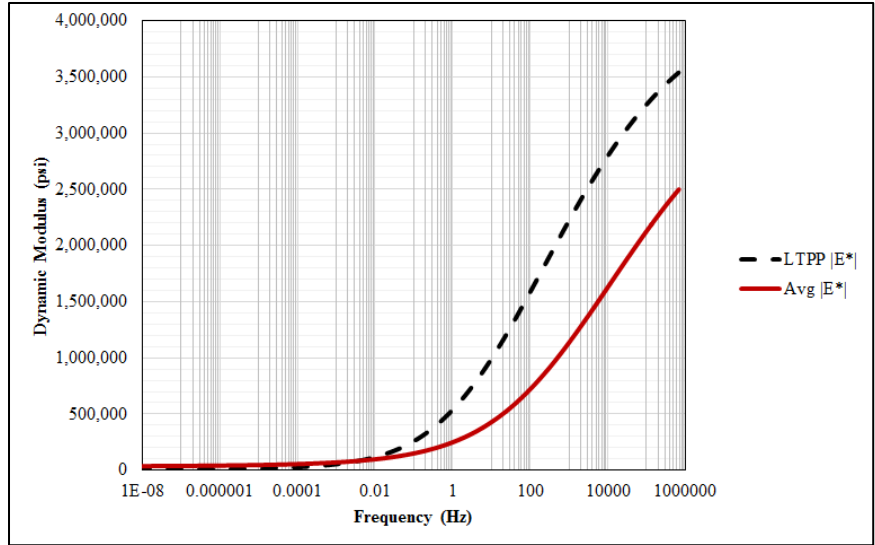
Source: FHWA.

Figure 143. Graph. Backcalculated AC $E^*_{damaged}$ master curve compared to the LTPP laboratory-derived $E^*_{undamaged}$ master curve for Alabama test section 01-0101 on 6/21/1995.

Figure 144 and figure 145 show E^* values calculated on the individual test dates and the E^* master curve constructed at a reference temperature of 71.3 °F, respectively. As mentioned previously, the master curve in figure 145 is assumed to represent the undamaged modulus of the asphalt for this section.
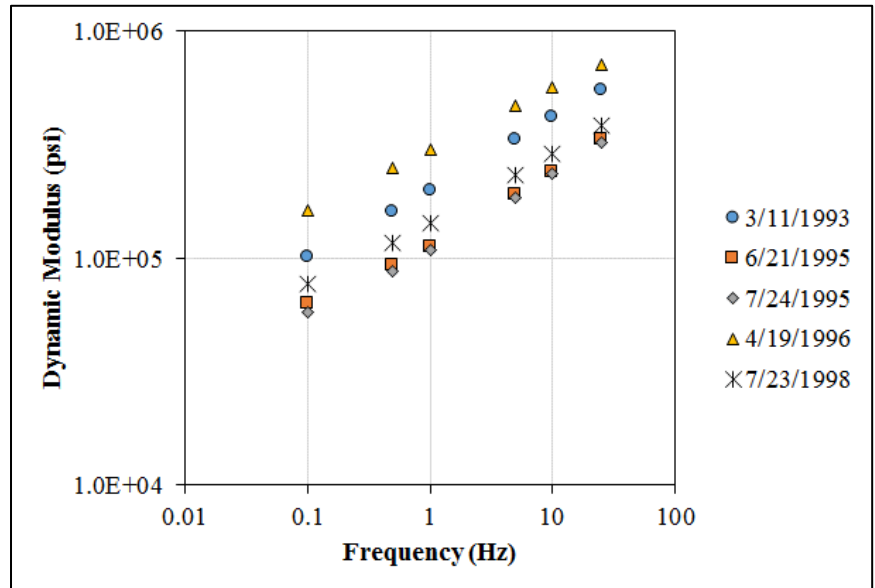
Source: FHWA.

Figure 144. Graph. Backcalculated E^* values from multiple dates for Alabama test section 01-0101.

133
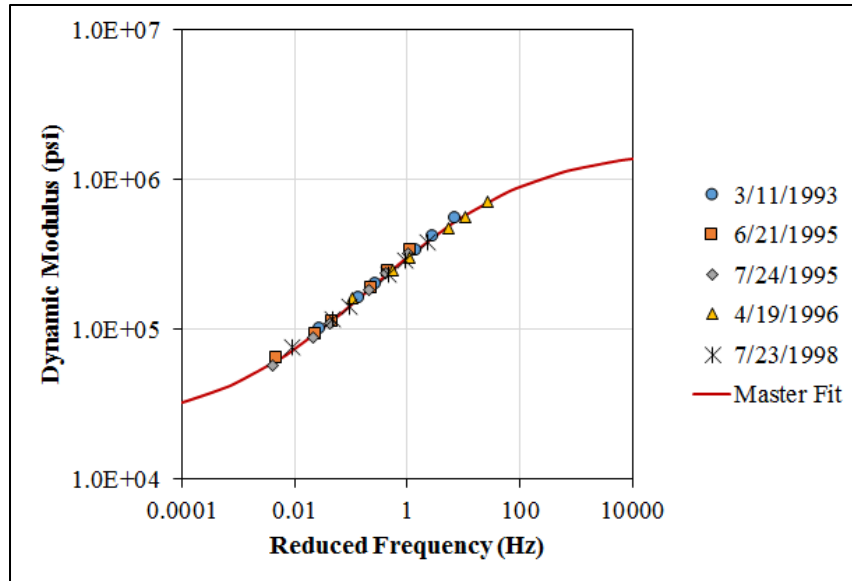
Source: FHWA.

Figure 145. Graph. Master curve fitting using backcalculated *E** values for Alabama test section 01-0101.

In addition, FWD deflection–time histories collected just before test section 01-0101 became inactive in 2005 were used to backcalculate the *E** values after cracking. Figure **146** shows the undamaged or laboratory-derived *E** master curve along with the damaged or backcalculated *E** values at a reference temperature of 72 °F. Counterintuitively, the figure shows that the backcalculated *E** modulus values were higher than the laboratory-derived *E** values. While there are other sources of error that may need to be studied to explain these results, it was generally concluded that the field cracking and hence the damage did not necessarily equate to a reduction in *E**.
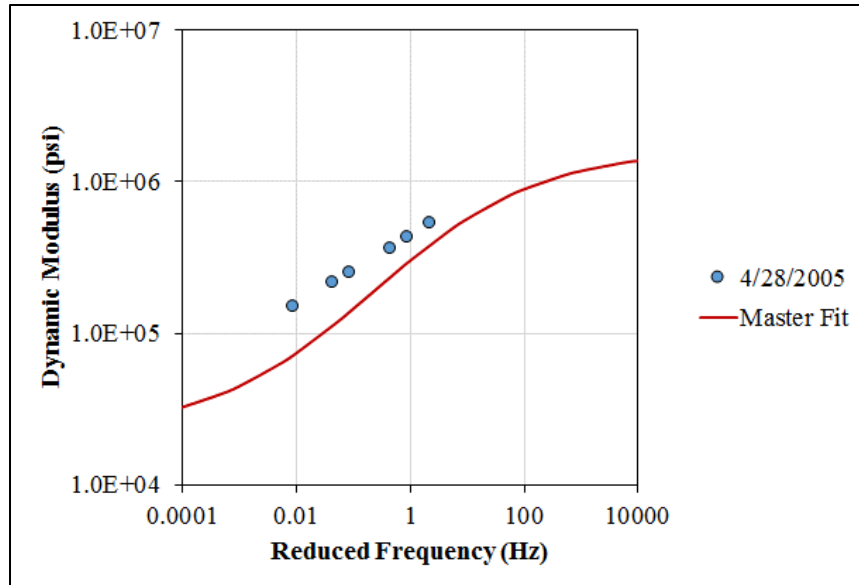
Source: FHWA.

Figure 146**. Graph. Backcalculated *E** values compared to the LTPP laboratory-derived *E**_{undamaged} master curve shift factors for Alabama test section 01-0101.**

FREQUENCY BACKCALCULATION FROM STATIC MODULUS

As mentioned in chapter 5, the frequency backcalculation involved calculation of the frequency that yielded an $E*$ value equal to the statically backcalculated modulus. For the frequency backcalculation, the $E*$ master curves were constructed using the LTPP laboratory-derived $E*$ master curve coefficients at the temperature corresponding to the pavement middepth.

However, the $E*$ values and the master curve obtained from dynamic backcalculation differed significantly from those calculated using the LTPP $E*$ table. Since the backcalculated frequency depends strongly on the $E*$ master curve, the frequency backcalculation was again carried out by using the backcalculated $E*$ in place of the laboratory $E*$ values. A summary of the backcalculated frequencies is provided in table 24. The table suggests the frequencies backcalculated from the LTPP $E*$ were mostly below 10 Hz and were lower than the values typically reported in the literature. On the other hand, the frequencies backcalculated from the dynamically backcalculated $E*$ were generally higher than those from the LTPP $E*$, which was expected as the backcalculated $E*$ values were lower than those from LTPP $E*$ values. While some of the frequencies seemed to show reasonable values between 15 and 30 Hz, some frequencies were much greater than the typical range, especially when the static modulus was higher than 1,000,000 psi.

135

Table 24. Summary of backcalculated frequencies.

| | | Backcalculated Frequency (Hz) | |
Test Date	Static Modulus (ksi)*	LTPP |E*|	Backcalculated |E*|
New York Test Section 36-0801			
8/23/1995	606.5	6.4	33.5
9/26/1995	740.0	3.6	20.8
10/10/1995	1,276.7	11.8	100.4
11/6/1995	1,730.4	19.3	94,631.2
12/5/1995	1,971.7	1.7	6,776.7
3/26/1996	1,888.3	6.4	4,121,958.6
4/9/1996	586.1	0.02	23.3
4/30/1996	1,694.7	9.7	3,809.6
5/21/1996	817.0	6.8	60.5
Alabama Test Section 01-0101			
3/11/1993	409.0	0.4	16.5
6/21/1995	287.5	1.7	22.1
4/19/1996	732.3	1.7	35.0
7/23/1998	314.3	3.7	18.3

*Average backcalculated modulus; this excludes outliers based on the MAD method.

SUMMARY

The dynamic backcalculation results suggest the following.

- The backcalculated E^* master curves were significantly different from those constructed using the laboratory obtained coefficients from the LTPP E^* table.[10] While the backcalculated E^* values were higher and lower than the laboratory E^* for New York test section 36-0801, the backcalculated E^* values were consistently lower for Alabama test section 01-0101.

- The backcalculated frequencies from statically and dynamically backcalculated modulus values showed some improvement. However, the backcalculated frequencies were outside the typical range when the static modulus was greater than 1 million psi (i.e., colder middepth pavement temperatures and/or thicker, stiffer asphalt layers).

- The backcalculated E^* values did not show any significant reduction after cracking. The E^* after cracking was higher than the undamaged or laboratory-derived E^*, especially for Alabama test section 01-0101. This indicates that additional parameters such as the fracture of the asphalt, aging, and healing must be incorporated in order to better correlate the material properties to field observed cracking.

CHAPTER 7. AC-LAYER DAMAGE AND FATIGUE CRACKING

Damage parameters, AC E_{FWD}, AC E^*_{PRED} (at different frequencies), and pavement cracking data were used to confirm the relationship between the E_{FWD}/E^*_{PRED} ratios or damage parameter $DI_{E-ratio}$ and the amount of cracking. This chapter summarizes the bottom–up fatigue cracking strength relationship and transfer function calibration coefficients for the individual sections included in the analysis. These project-specific calibration coefficients are used to enhance the accuracy for predicting bottom–up fatigue cracking in new and rehabilitated flexible pavements.

FATIGUE DAMAGE

Three different damage parameters were used to calibrate the fatigue cracking transfer function using the data synthesized in this study as follows:

- MEPDG default DI defined by the term d_{AC} (i.e., fatigue damage in the existing asphalt layer provided in figure 22).

- $DI_{E-ratio}$ (i.e., ratio of the E_{FWD} to the E^*_{PRED} or undamaged AC E^* provided in figure 58).

- Use of a horizontal shift (HS) rather than a vertical shift (VS), which is explained in further detail in the HS Factor section within this chapter).

d_{AC}

d_{AC} is used to calculate the amount of fatigue cracking for flexible pavements using the transfer function shown in figure 18 in chapter 2 (in this case, d_{AC} equals DI_{Bottom}) for both new and rehabilitated flexible pavements. d_{AC} is defined in terms of the laboratory-derived, undamaged AC modulus, E^*_{PRED}, and the field-derived, backcalculated modulus, E_{FWD} (see figure 22). The MEPDG relationship for $E^*_{damaged}$ is shown in figure 21. Rearranging the equation in figure 21 to obtain the expression for logarithm of d_{AC} is provided in figure 22. As shown in figure 22, the damage value converges to zero for an undamaged pavement (i.e., E_{FWD} equals E^*_{PRED}). In addition, the MEPDG assumes the damage is zero for all FWD tests where E_{FWD} is greater than E^*_{PRED}.[1]

$DI_{E-ratio}$

A simple damage parameter has been used to predict fatigue cracking and is defined as 1 minus the ratio of damaged to undamaged AC modulus, as shown in figure 58. This relationship has been used to estimate the coefficients of the fatigue cracking transfer function.

Theoretically, the upper limit of $DI_{E-ratio}$ is 1.0 when E_{FWD} equals 0. However, this boundary condition will never be achieved from a conventional backcalculation program. For an undamaged pavement, E_{FWD} from FWD deflection basins is theoretically equal to E^*_{PRED}; hence, the value of $DI_{E-ratio}$ is 0. In practice, however, it is possible to get negative DI values if E_{FWD} is greater than E^*_{PRED} as the AC ages or becomes stiffer. For the subsequent analysis, the individual FWD drops with negative DI values were removed from the dataset, and no damage was assumed.

By combining the mathematical relationships shown in the equations in figure 22 and figure 58, a mathematical relationship between $DI_{E\text{-}ratio}$ and d_{AC} can be derived, which is shown in figure 147. In the equation, d_{AC} is expressed as a function of DI as well as the ratio between 10^δ and E_{PRED}, where δ is the logarithm of the minimum E^*_{PRED} as defined in figure 21.

$$\text{Log}(d_{AC}) = 0.2\left[\ln\left(\frac{DI_{E\text{-}ratio}}{1 - \left(DI_{E\text{-}ratio} + \dfrac{10^\delta}{E^*_{PRED}}\right)}\right) + 0.3\right]$$

Figure 147. Equation. Relationship between d_{AC} and $DI_{E\text{-}ratio}$.

Figure 148 shows the relationship between d_{AC} and $DI_{E\text{-}ratio}$ included in the preliminary analysis. Mathematically, there was a relationship between d_{AC} and $DI_{E\text{-}ratio}$, and the effect of $10^\delta/E^*_{PRED}$ was insignificant. An important observation from figure 148 is that a d_{AC} of 1.0 (corresponding to 50 percent cracking based on the assumptions used during the global calibration) was equivalent to a $DI_{E\text{-}ratio}$ of 0.4 (a 40 percent loss in modulus).
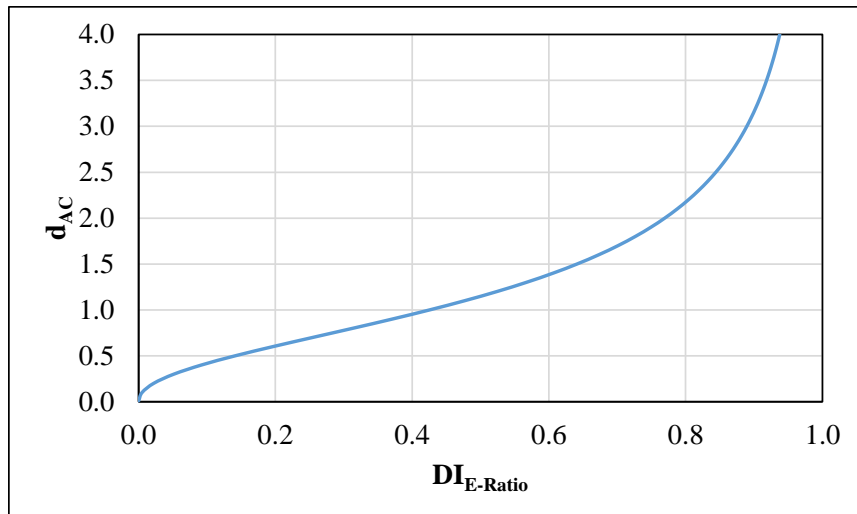
Source: FHWA.

Figure 148. Graph. Relationship between d_{AC} and $DI_{E\text{-}ratio}$.

HS Factor

The MEPDG calculates the E^* master curve of the damaged AC by shifting the undamaged master curve vertically downward, as illustrated in figure 149.[1]
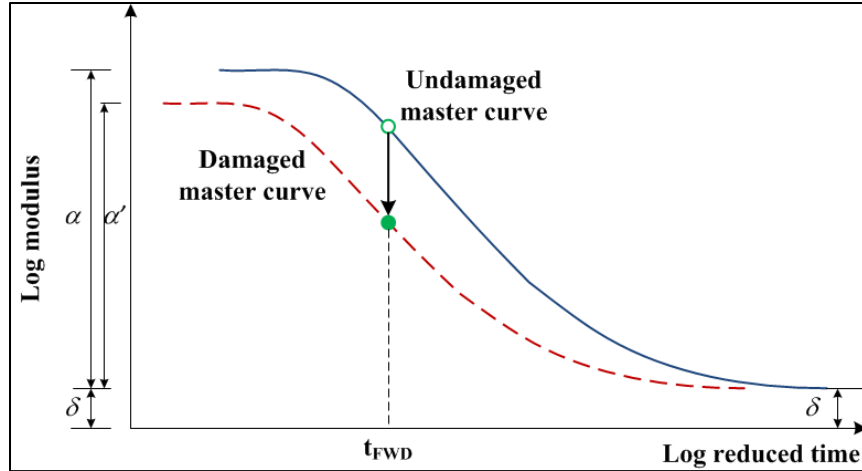
Source: FHWA.
Note: α and α are E* master curve coefficients.

Figure 149. Graph. Current MEPDG level 1 damaged AC $E^*_{damaged}$ master curve.

The minimum modulus represented by the δ parameter remained unchanged, whereas the maximum modulus was reduced from $(\delta + \alpha)$ to $(\delta + \alpha')$. The magnitude of VS was determined by E_{FWD} through which $E^*_{damaged}$ was made to pass. The α' term is a fitting parameter for the $E^*_{damaged}$ master curve that was used to create the $E^*_{damaged}$ master curve in comparison to $E^*_{undamaged}$.

The $E^*_{undamaged}$ AC master curve relationship in terms of t_r is shown in figure 150. t_r is a function of the loading time t and the temperature shift factor, a_T. t_r for the $E^*_{undamaged}$ master curve is mathematically shown in figure 151.

$$\log|E^*| = \delta + \frac{\alpha}{1 + e^{\beta + \gamma(\log t_r)}}$$

Figure 150. Equation. $E^*_{undamaged}$ master curve relationship.

Where β and γ are E* master curve coefficients.

$$\log t_r = \log t - \log a_T$$

Figure 151. Equation. Relationship to estimate t_r from the loading time and a_T.

Using the time–temperature superposition principle for AC, the effect of damage could also be achieved by shifting the AC $E^*_{undamaged}$ master curve horizontally. To introduce the additional shift due to damage, the curve was further translated along the x-axis by a factor of log t_{HS}, where t_{HS} is the damage-induced HS on the reduced time scale. The reduced time for the damaged master curve is mathematically shown in figure 152.

$$\log t_r = \log t - \log a_T - \log t_{HS}$$

Figure 152. Equation. Relationship to estimate t_r using the HS approach.

Figure 153 illustrates the HS master curve due to fatigue damage.
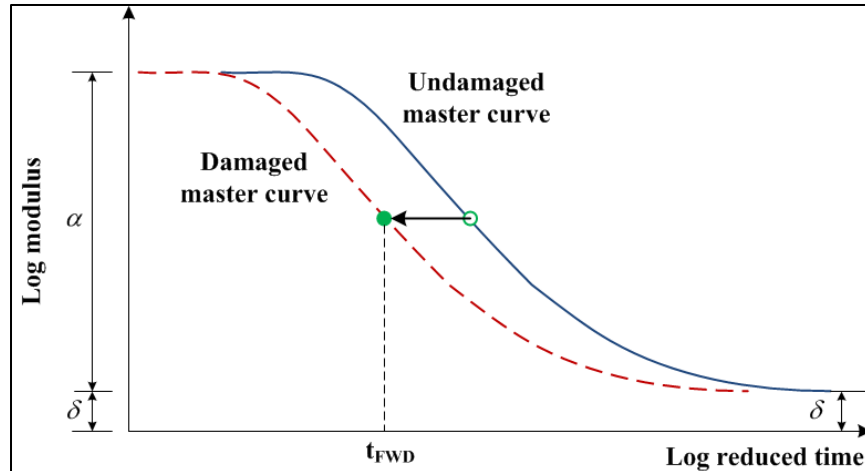
Source: FHWA.

Figure 153. Graph. HS to derive the AC $E*_{damaged}$ master curve.

Substituting the reduced time from the equation in figure 152 into the $E*_{undamaged}$ master curve equation shown in figure 150 results in the HS $E*_{damaged}$ master curve provided in figure 154. Simplifying the terminology used in the equation shown in figure 154 by replacing $\log_{10}|E*|$ by the log of E and inverting the equation yields an expression for the amount of HS shown in figure 155. The time, t, used to calculate the HS factor in figure 155 is calculated from the FWD load frequency, f.

$$\log_{10}|E*| = \delta + \frac{\alpha}{1+e^{\beta+\gamma(\log t_r)}} = \delta + \frac{\alpha}{1+e^{\beta+\gamma(\log t - \log a_T - \log t_{HS})}}$$

Figure 154. Equation. Mathematical relationship to determine the $E*_{damaged}$ master curve using the HS approach.

$$\log t_{HS} = \log t - \log a_T - \frac{1}{\gamma}\ln\left[\frac{\alpha+\delta-\log E}{\log E}\right] + \frac{\beta}{\gamma}$$

Figure 155. Equation. Mathematical relationship to determine the magnitude of the HS.

COMPARISON OF TOTAL CRACKING TO DAMAGE COEFFICIENTS

The fatigue cracking transfer function in the MEPDG is based on the relationship between fatigue cracking and DI, which is expressed in the form of a sigmoidal function, as shown in figure 18 in chapter 2.[1] The coefficients of the bottom–up fatigue cracking transfer function (C_1 and C_2) were used to evaluate and compare the predicted and measured cracking for verifying the rehabilitation input level 1 concept and approach for flexible pavements.

For the LTPP test sections listed in table 5 in chapter 3, C_1 and C_2 were derived using the assumptions previously listed in chapter 3. The global fatigue cracking transfer function had a constraint of C_1 equivalent to C_2; however, it was more appropriate to calibrate the transfer function without using this constraint. In fact, most agencies that have completed a local

140

calibration excluded this constraint (see table 9). Thus, the following two conditions were evaluated to illustrate the difference between the two conditions:

- C_1 is equal to C_2.
- C_1 is independent of C_2.

Constraint (C_1 Equals C_2)

Figure 156 shows a comparison of the measured and calculated fatigue cracking as a function of d_{AC} for test lane F3 (WP). Initially, the fatigue cracking transfer function was forced to pass through 50 percent cracking and a d_{AC} of 1.0 (i.e., the equation in figure 18 for which C_1 equals C_2) for the global calibration (NCHRP project 1-37A).[1]
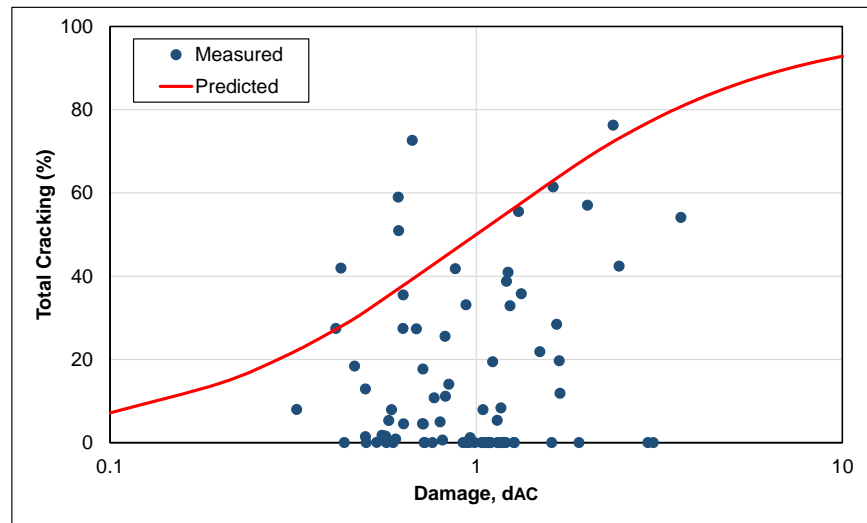
Source: FHWA.

Figure 156. Graph. Percentage cracking compared to d_{AC} for pavements with granular base for test lane F3 where frequency equals 15 Hz, C_1 equals C_2, and 50 percent cracking at d_{AC} equals 1.0.

The residual standard error of the estimate (SEE) for the relationship between fatigue cracking and d_{AC} was 39.13 percent based on 78 DOF. Using that restriction or constraint resulted in a poor correlation with a significant bias. The SEE from the bottom–up fatigue cracking global calibration of the transfer function was 5.2 percent. However, the number of data points and the amount of cracking between the datasets used for the global calibration (NCHRP 1-37A report) and in this study were significantly different.[1] Details of the global calibration, however, are not fully explained in NCHRP 1-37A. It is important to recognize the amount of cracking exhibited on the LTPP test sections has increased since the global calibration was completed. This increase in cracking allows a more accurate assessment of the fatigue cracking coefficients to simulate crack propagation growth rates with higher amounts of cracking.

The fatigue cracking transfer function was constrained to pass through different damage values at 50 percent cracking, and the regression was done to determine whether C_1 equals C_2 at each constraint to eliminate the bias shown in figure 156. Figure 157 shows the plot of fatigue cracking versus d_{AC} when the cracking is equal to 50 percent at d_{AC} equals 2.0. As shown, the

correspondence between the amount of fatigue cracking and d_{AC} did not significantly improve in comparison to figure 156, but the bias was removed.
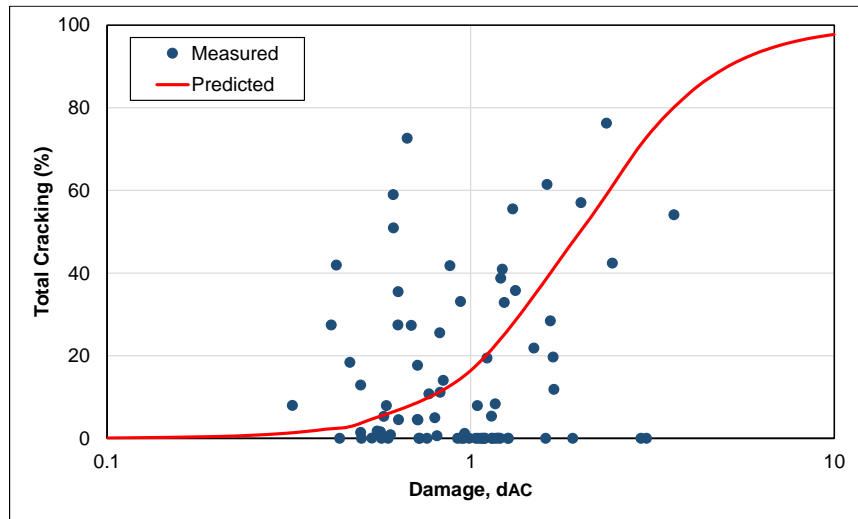
Source: FHWA.

Figure 157. Graph. Percentage cracking compared to d_{AC} for pavements with granular base for test lane F3 where frequency equals 15 Hz, C_1 equals C_2, and 50 percent cracking at d_{AC} equals 2.0.

The significance of the transfer function passing through 50 percent cracking at d_{AC} value of 1.0 versus 2.0 can be realized further from figure 148, which shows the relationship between d_{AC} and $DI_{E\text{-}ratio}$. It was mentioned previously that a d_{AC} value of 1.0 was equivalent to a 40 percent loss in modulus. This means that the transfer function shown in figure 148 and figure 156 was constrained to pass through 50 percent cracking at 40 percent reduction in modulus. However, figure 148 also suggests that a d_{AC} value of 2.0 was approximately equivalent to a modulus reduction of 75 percent. In other words, the transfer function shown in figure 148 passes through 50 percent cracking when an approximate modulus reduction of 75 percent is reached. As such, this constraint was evaluated and the d_{AC} value corresponding to 50 percent cracking determined while considering the modulus reduction shown in figure 147.

No Constraint (C_1 Independent of C_2)

Figure 158 shows the total amount of fatigue cracking versus d_{AC} for test lane F3 when C_1 and C_2 were determined separately or assumed to be independent. The plot shows that in order to minimize the standard error, C_1 equals 1.0 and C_2 equals 0.67, which results in a SEE of 19.76 with 78 DOF. The model resulted in a slightly lower SEE compared to when C_1 equaled C_2 but required a very large value of d_{AC} for 50 percent cracking. More importantly, a SEE of nearly 20 percent was unacceptable for research analyses using these data as well as for pavement design.
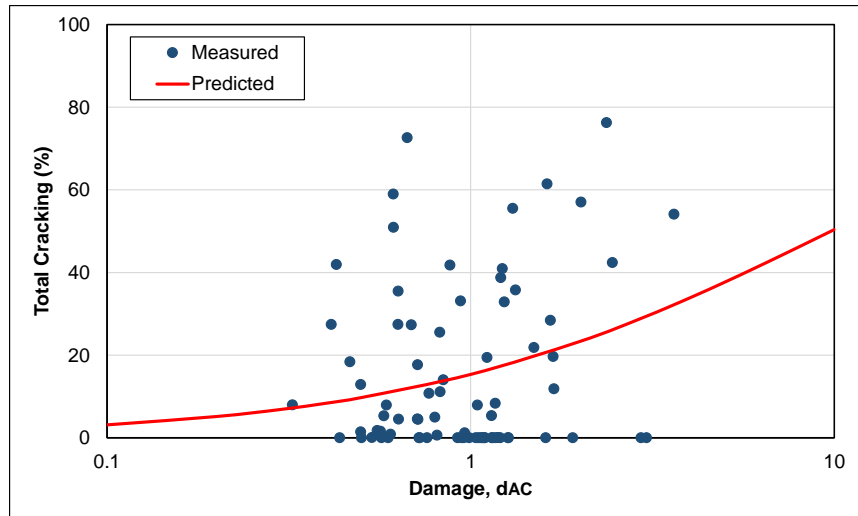
Source: FHWA.

Figure 158. Graph. Percentage cracking compared to d_{AC} for pavements with granular base for test lane F3 where frequency equals 15 Hz and C_1 is unequal to C_2.

Regression Analyses to Identify Significant Factors

Regression analyses were performed to identify site features, frequency calculation method, and/or other mixture characteristics that can explain a lot of the error and improve on the relationship between DI and cracking. In addition, the analyses were performed to derive the regression coefficients C_1 and C_2, which resulted in a best fit between d_{AC} and cracking using the HS approach in comparison to the VS approach. Table 25 summarizes C_1 and C_2 and residual standard error for the regression models fitted using the FWD moduli measured in the outer WP (lane number F3) for the two conditions: (1) C_1 equals C_2 for which the cracking-damage constraint was valid and (2) C_1 is independent of C_2 (no constraint on the fit).

143

Table 25. Statistical analysis results for fatigue cracking transfer function calibration.

Base Type	Frequency (Hz)	d_{AC}	Condition 1		Condition 2			DOF
			$C_1 = C_2$	SEE (Percent)	C_1	C_2	SEE (Percent)	
Granular	15	VS	0.6932	39.134	0.8125	0.6730	19.763	78
Granular	15	HS	0.3133	39.468	0.3673	0.2224	20.110	78
Granular	30	VS	0.1220	40.214	0.7593	0.7803	19.562	79
Granular	30	HS	0.0330	40.278	0.4328	0.3025	19.941	79
Granular	1/t	VS	0.0750	39.774	0.4455	0.3447	21.126	63
Granular	1/t	HS	0.0087	39.808	0.2225	0.0196	21.236	63
Granular	1/2t	VS	0.3970	39.604	0.4805	0.3984	20.933	61
Granular	1/2t	HS	0.1465	39.461	0.2088	0.0000	21.406	62
Treated bases (all types)	15	VS	0.9593	38.175	0.6888	0.4164	26.103	70
Treated bases (all types)	15	HS	0.6592	37.562	0.6130	0.6426	25.623	72
Treated bases (all types)	30	VS	0.7723	39.916	0.7778	0.4845	25.433	75
Treated bases (all types)	30	HS	0.5277	39.385	0.7537	0.4552	24.592	79
Treated bases (all types)	1/t	VS	0.6755	40.186	0.8783	0.6015	26.786	64
Treated bases (all types)	1/t	HS	0.5016	39.926	0.9591	0.6664	25.686	67
Treated bases (all types)	1/2t	VS	0.9028	38.162	0.7854	0.5328	27.183	61
Treated bases (all types)	1/2t	HS	0.7115	37.217	0.7821	0.5305	26.343	63
PATB	15	VS	1.3683	34.330	0.7300	0.4892	25.670	41
PATB	15	HS	0.9453	33.951	0.6198	0.3802	25.276	42
PATB	30	VS	1.4230	35.887	0.9306	0.6668	24.776	45
PATB	30	HS	0.9176	35.673	0.8046	0.5350	23.831	48
PATB	1/t	VS	1.2826	36.442	4.0556	0.8091	25.894	38
PATB	1/t	HS	0.8870	36.864	1.0828	0.8171	24.675	40
PATB	1/2t	VS	1.2470	34.668	0.8342	0.6156	26.729	35
PATB	1/2t	HS	1.0000	33.432	0.8392	0.6223	25.532	37
Non-PATB	15	VS	0.4020	41.927	0.8260	0.5131	26.404	29
Non-PATB	15	HS	0.3530	41.113	0.7341	0.4234	25.809	30
Non-PATB	30	VS	0.0000	42.148	0.7508	0.4261	26.104	30
Non-PATB	30	HS	0.1360	42.109	0.8435	0.5035	25.428	31
Non-PATB	1/t	VS	0.0000	41.887	0.7968	0.4874	27.633	26
Non-PATB	1/t	HS	0.1149	42.105	0.9472	0.6181	26.672	27
Non-PATB	1/2t	VS	0.3878	41.575	0.8908	0.5961	27.412	26
Non-PATB	1/2t	HS	0.3718	41.008	0.8478	0.5530	27.024	26

Overall, d_{AC} defined by the VS method had a slightly lower SEE compared to the SEE from the HS. The more important observation from this regression analysis, however, was that segregating the dataset by base type and calculated frequency method did not improve on the correlation between d_{AC} and total amount of fatigue cracking. Another important observation was that the regression coefficients for the transfer function in table 25 were different than most from the local calibration studies listed in table 9. In summary, the relationship was not improved by considering mixture type, soil classification, and structure. As such, other parameters are believed to be more important that were not considered in the regression analysis or represent significant confounding factors.

Multiple factors could be causing the poor correlations in comparison to the global and local calibration studies that have been completed (i.e., comparing figure 56 and figure 57 to figure 158).[27,32,53] These factors relate to the assumptions used in the pavement structure simulation and the mechanism causing surface cracks. Most of the local calibration studies have recognized the importance of making correct assumptions and including a forensic investigation as part of their local calibration process. A few of the factors identified during forensic investigations include the following:

- **Top–down versus bottom–up cracking**: This includes segregating test sections between surface-initiated and bottom-initiated fatigue cracks. Top–down cracks can begin much earlier in a pavement's service life and have a significant impact on the C_1 and C_2 if not identified. Different distress mechanisms within the same dataset can significantly increase variability, making it difficult to identify other factors having a smaller impact on cracking. The Georgia local calibration study included a coring program to exclude sections with top–down cracking.[27]

- **Full versus no bond between AC layers**: Full bond is assumed for all test sections. For some of the local calibration studies, a coring program was included to identify sections where the surface fatigue cracking was a result of a loss of bond between adjacent AC layers.[55]

- **No moisture damage in AC mixtures versus test sections with moisture damage**: All AC mixtures were assumed to be moisture damage resistant, which is not always a good assumption. The Georgia local calibration study found some of their high recycled asphalt pavement (RAP) mixtures exhibited stripping from their field investigation.[27] Their AC dense graded specification was revised based on premature cracking, so those high RAP mixtures were excluded from the local calibration that reduced the SEE for fatigue cracking and rutting.

- **Polymer modified versus neat AC mixtures**: The AI, CDOT, and GDOT have all derived fatigue cracking transfer functions that are mixture type dependent. E^* by itself does not accurately account for the difference in mixture or binder type. Segregating the test sections by mixture type reduced the SEE for the fatigue cracking and rutting transfer functions by most agencies.

- **The AC modulus backcalculated from FWD deflection-basin data shortly after construction when no fatigue damage should be present is equal to $E*_{PRED}$ determined at the same temperature and load frequency**: This hypothesis was assumed during the global calibration as well as for most local calibration studies. However, some researchers have challenged that assumption.

Another important factor or assumption relates to crack propagation. Crack propagation was assumed to be constant for all mixtures and/or was correctly accounted for through the field shift factor that was indirectly included in the MEPDG approach through global calibration.[1] However, cracks propagate differently between brittle (i.e., ATB layers with lower asphalt contents) and viscoelastic or crack-resistant mixtures (i.e., stone matrix asphalt). The diversity in crack propagation had an impact on the coefficient of the fatigue strength relationship (see figure 14) as well as the coefficients for the fatigue cracking transfer function (see figure 18).

Few forensic investigations have been completed on the LTPP test sections that have been taken out of service to verify the pavement structure and material assumptions. Thus, the remainder of this chapter provides a more detailed evaluation of selected LTPP test sections included within this study to explain the high error between d_{AC} and total cracking.

E_{FWD} AND $E*_{PRED}$

An analysis was conducted to compare the field-derived (i.e., E_{FWD} backcalculated from deflection basins) to the laboratory-derived (i.e., $E*_{PRED}$ dynamic) moduli for FWD test dates shortly after construction. $E*_{PRED}$ was calculated using the master curve coefficients stored in the LTPP database with middepth pavement temperatures and a fixed load frequency of 30 Hz.[10] A fixed load frequency was used because of the findings (i.e., extremely high variability in backcalculated loading frequency) reported in chapter 5 and chapter 6 as well as the regression analyses summarized in figure 25. The middepth AC layer temperatures were extracted from the LTPP backcalculated CPTs, which were determined in accordance with the procedure explained by Von Quintus et al.[47]

Figure 159 and figure 160 show examples from two LTPP experiments, SPS-1 and -8, respectively. The E_{FWD} values were more temperature-sensitive for the thicker AC layer in comparison to the thinner layer for the Alabama SPS-1 project (see figure 159). The middepth temperature used for the thin and thick AC layer was different and taken into account in figure 159. The $E*$ master curve for the HMA mixture for Alabama test sections 01-0102 and 01-0101 was the same because the mixtures were the same. Thus, $E*_{PRED}$ was inconsistent with E_{FWD}. Figure 160 shows the field-derived E_{FWD} values for two dense-graded HMA mixtures from different SPS-8 projects for FWD test dates without any cracking. The different mixtures exhibited a similar temperature-E_{FWD} relationship for similar AC-layer thicknesses.
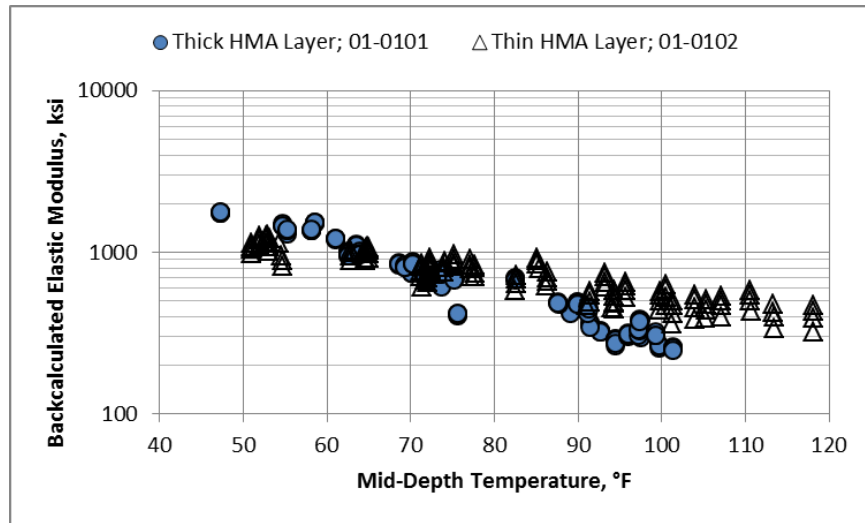
Source: FHWA.

Figure 159. Graph. E_{FWD} compared to the middepth pavement temperature for thin and thick HMA layers within the Alabama SPS-1 project.
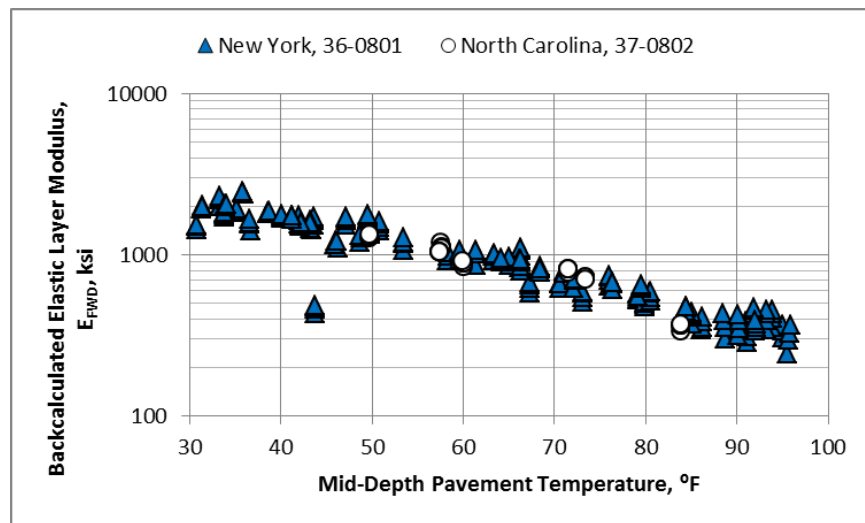
Source: FHWA.

Figure 160. Graph. E_{FWD} compared to the middepth pavement temperature for an HMA wearing surface from two SPS-8 projects.

Figure 161 and figure 162 provide similar examples but for different AC mixtures: dense-graded AC and a more brittle (i.e., lower asphalt content) ATB for the same SPS-1 project. As shown, the E_{FWD} values for the ATB were lower in comparison to the dense-graded AC at the colder temperatures but were within the same range at the higher test temperatures. Another important observation from the E_{FWD} values was the variability measured for different pavement structures. The importance of the pavement structure simulation for E_{FWD} values is well known throughout the industry.[33,47] Small errors or deviations in layer thickness will increase the variability and bias between the E_{FWD} and E^*_{PRED} values.

147
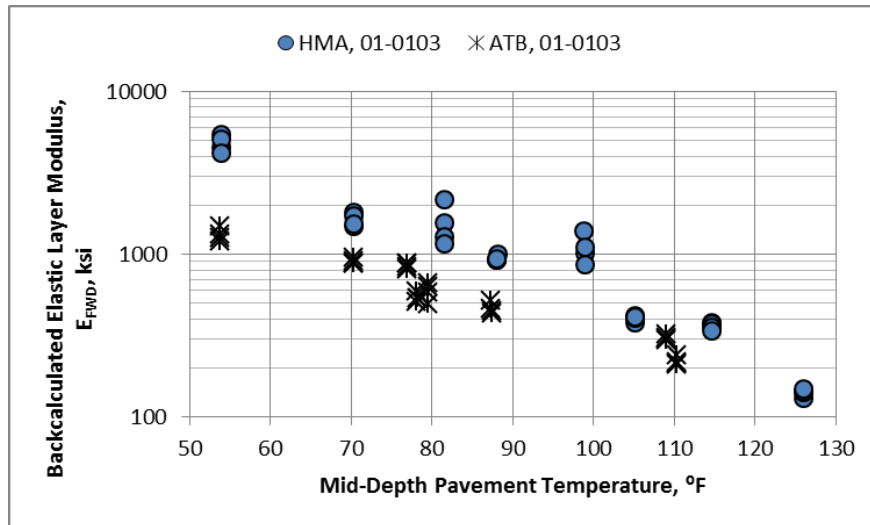
Source: FHWA.

Figure 161. Graph. E_{FWD} compared to the middepth pavement temperature for the HMA and ATB layers for Alabama test section 01-0103 in the SPS-1 project.
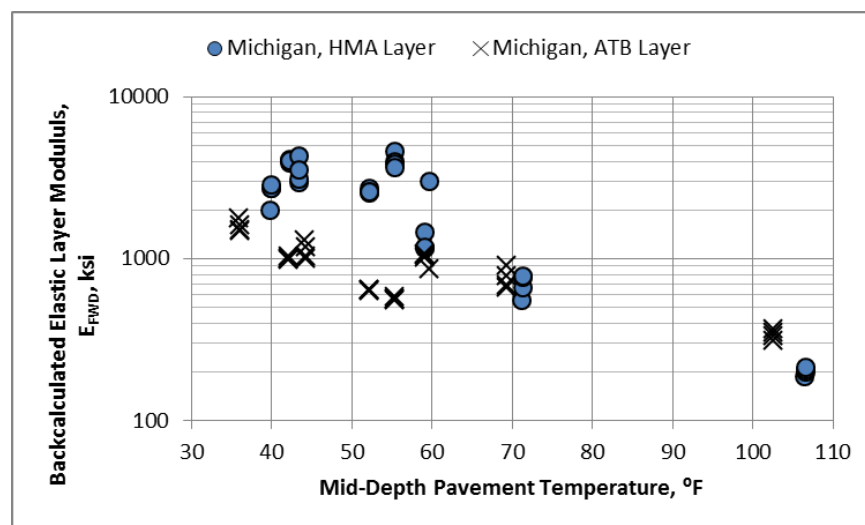
Source: FHWA.

Figure 162. Graph. E_{FWD} compared to the middepth pavement temperature for the HMA and ATB layers for Michigan test section 26-0124 in the SPS-1 project.

Figure 163 provides a graphical comparison between the E_{FWD} (field-derived) and E^*_{PRED} (laboratory-derived) ratios and temperature for test dates shortly after construction (i.e., no fatigue damage was assumed). The E_{FWD}/E^*_{PRED} ratios were variable but were generally greater than 1.0 and consistent with the findings from some other researchers.[19,27] The field adjustment factors for equating E_{FWD} to E^*_{PRED} were dependent on temperature and possibly other variables (i.e., layer thickness). Both thickness and temperature related to the confinement of the AC layer of a viscoelastic material.

148
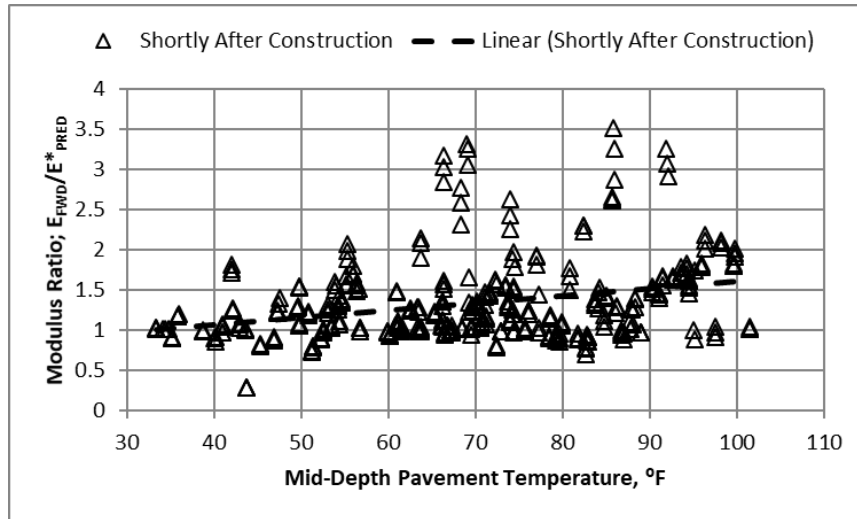
Source: FHWA.

Figure 163. Graph. $E_{FWD}/E*_{PRED}$ ratio compared to pavement temperature for FWD test dates shortly after construction.

Conversely, figure 164 provides a graphical comparison between the $E_{FWD}/E*_{PRED}$ ratio except for the FWD test dates when fatigue cracking was observed. Although there was a lot of variability, the ratios were generally lower than those in Figure 163. Specifically, more ratios in figure 164 were less than 1.0 because of the cracking or in-place damage. However, it should be pointed out there was no statistical difference between the two datasets because of the wide range of ratios (i.e., figure 163 compared to figure 164). Figure 165 includes a comparison between the E_{FWD} and $E*_{PRED}$ moduli for the sites without cracking over a range of AC-layer thicknesses (thin (less than 6 inches) to moderate (6 to 14 inches)). Note that the AC-layer thicknesses are not identified or separated out in the figure. E_{FWD} and $E*_{PRED}$ were approximately equal for the colder temperatures or stiffer mixtures and then diverged with increasing temperatures or softer mixtures with $E*_{PRED}$ becoming larger than E_{FWD}.
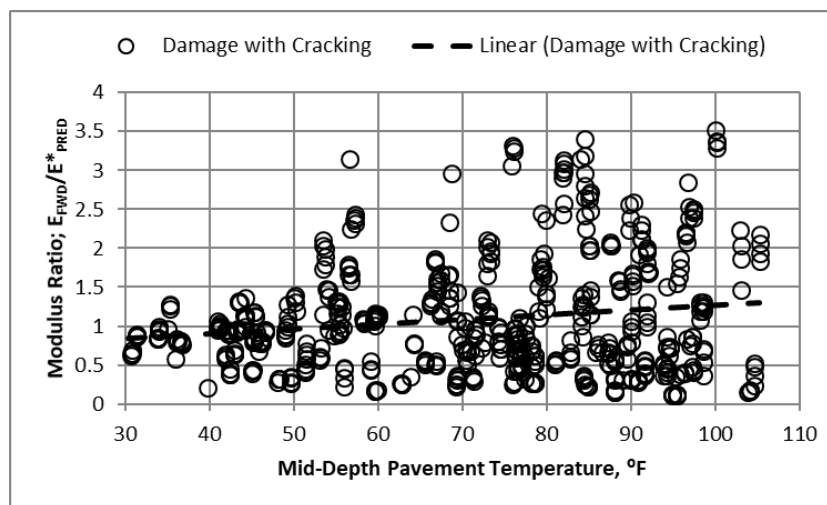
Source: FHWA.

Figure 164. Graph. $E_{FWD}/E*_{PRED}$ ratio compared to pavement temperature for FWD test dates with various amounts of cracking.

149
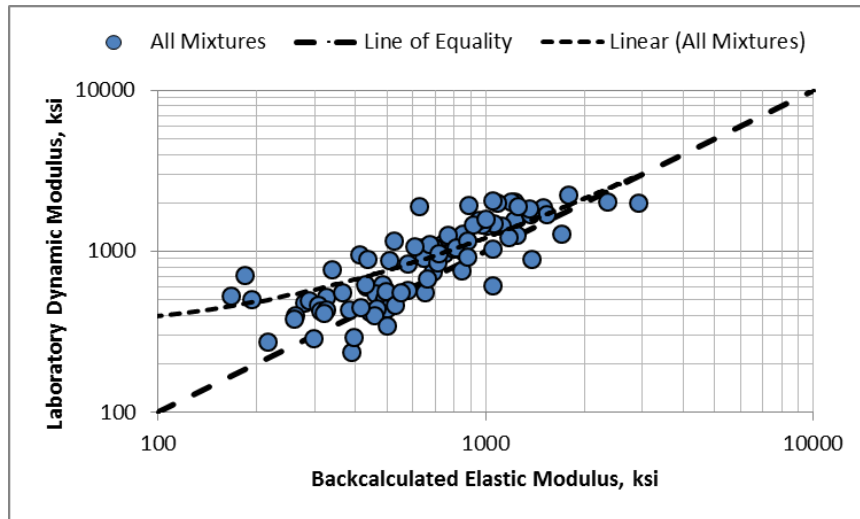
Source: FHWA.

Figure 165. Graph. E_{FWD} compared to E^*_{PRED}.

It should be noted that the three points with the lowest E_{FWD} (less than 200 ksi) could be biasing the trend between E_{FWD} (field-derived) and E^*_{PRED} (laboratory-derived). These data points were not considered outliers, so they were included in the analysis.

The other factor considered in causing a difference between the E_{FWD} and E^*_{PRED} AC moduli was stress sensitivity. Stress sensitivity was considered through the drop height, but its impact was much smaller than for thickness and temperature. Thus, stress sensitivity was ignored or considered a confounding factor (noise) to determine the adjustment factors. In summary, the average adjustment factors between E_{FWD} and E^*_{PRED} without fatigue damage (see figure 163) were stiffness and/or temperature dependent as described as follows:

- **Middepth temperature less than 40 °F and/or E^*_{PRED} greater than 1,000 ksi**: On the average, the E_{FWD}/E^*_{PRED} ratio was 1.0.

- **Middepth temperature 60 to 70 °F and/or E^*_{PRED} of 600–800 ksi**: On the average, the E_{FWD}/E^*_{PRED} ratio was 1.3.

- **Middepth temperature greater than 90 °F and/or E^*_{PRED} less than 500 ksi**: On the average, the E_{FWD}/E^*_{PRED} ratio was 1.6.

As shown, differences between E^*_{PRED} and E_{FWD} were not explained solely by fatigue damage or the amount of cracking. The effect of temperature for the thicker section appeared to be much greater for the thinner AC layers. More importantly, the type of AC mixture had an impact on the damage, which is not explained solely by differences in E^*_{PRED} and volumetric properties. The next section provides a detailed evaluation regarding differences caused by mixture type and layer thickness.

TEST SECTION/MIXTURE-SPECIFIC CRACKING COEFFICIENTS

The following steps were used to derive test section specific fatigue cracking coefficients for the fatigue cracking strength equation in figure 14 and the transfer function in figure 18:

1. Determine the combination of C_1 and C_2 to simulate the growth in fatigue cracking observed on an individual test section basis (see figure 18). The site-specific C_1 and C_2 coefficients were used to evaluate the impact of thickness on d_{AC} and $E_{FWD}/E*_{PRED}$ moduli ratios. The original fatigue equation included in the NCHRP 1-37A procedure included AC-layer thickness to account for strain- versus stress-controlled conditions (see figure 16 in chapter 2).[1]

2. Determine the intercept coefficient of the fatigue strength equation (k_{f1} in figure 14) to minimize SEE and eliminate any bias between the measured and predicted fatigue cracking because all AC mixtures did not have the same fracture strength and/or crack propagation properties. k_{f1} includes the field shift factor equating results from laboratory flexural fatigue tests to crack initiation and propagation in the AC mixtures placed on the roadway.

3. Identify different groups or combinations of C_1 and C_2 values for which crack growth is considerably different to separate other significant contributions to fatigue cracking growth that are not related to the application of repeated truck loadings. Crack propagation and crack growth should be different between brittle and viscoelastic mixtures (e.g., dense-graded AC wearing surfaces or binder layers versus ATB layers that have a larger aggregate and/or lower asphalt content).

4. Determine the d_{AC} damage coefficient using the test section-specific intercept of the fatigue strength equation and coefficients of the transfer function. This coefficient is included in the AASHTOWare Pavement ME Design® software output.[3,4] This step assumes that the climate, traffic, and other pavement layer properties are correct for an individual test section.

5. Determine the loss of modulus from the d_{AC} value or the $DI_{E-ratio}$ that corresponds to that damage value using figure 148.

6. Calculate the $DI_{E-ratio}$ from E_{FWD} and $E*_{PRED}$ or undamaged dynamic modulus. Based on the analyses explained in chapters 5 and 6, an FWD load frequency of 30 Hz was initially used to calculate the $E*_{PRED}$.

7. Compare the $DI_{E-ratio}$ to other site- and mixture-specific parameters to identify confounding factors that need to be considered during the use of MEPDG rehabilitation input level 1.[1]

Figure 166 through figure 168 show examples comparing the predicted and measured cracking over time for three LTPP test sections with different crack growth rates. The resulting fatigue cracking intercept (k_{f1} in figure 14) and the coefficients of the transfer function (C_1 and C_2 in figure 18) are included in the figures for each test section and are a good simulation of the measured fatigue cracking observed at each site. Another important observation is that k_{f1}, C_1,

and C_2 values significantly varied between the three LTPP sites. As such, $E*$ by itself does not accurately explain differences in fatigue cracking.
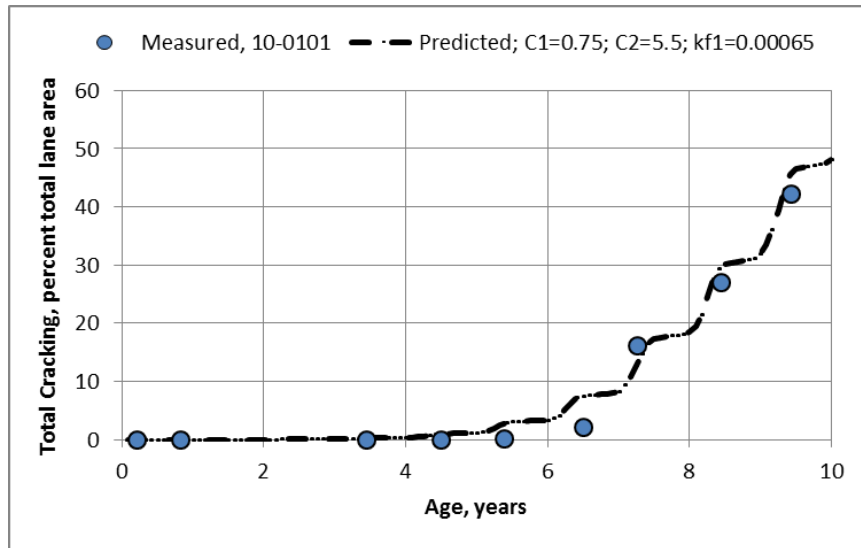
Source: FHWA.

Figure 166. Graph. Measured and predicted total fatigue cracking for Delaware SPS-1 project test sections with high rates of crack growth.
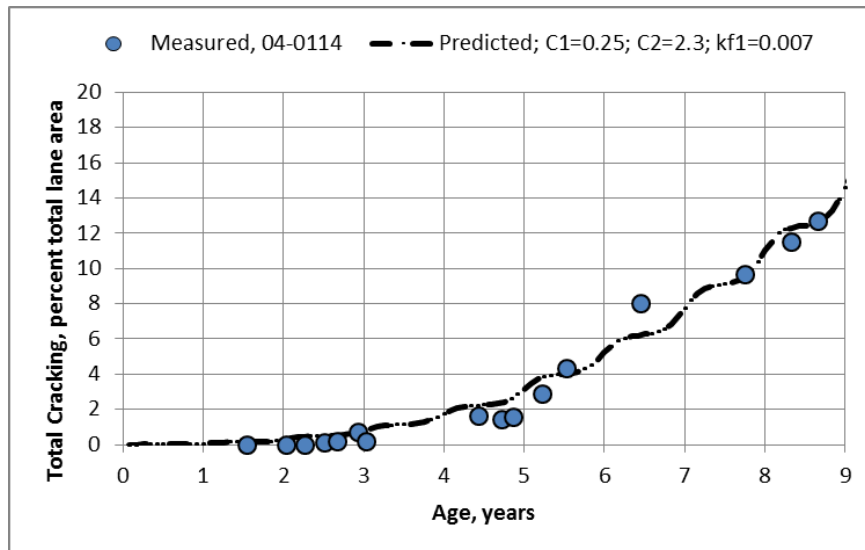
Source: FHWA.

Figure 167. Graph. Measured and predicted total fatigue cracking for Arizona SPS-1 project test sections with low rates of crack growth.
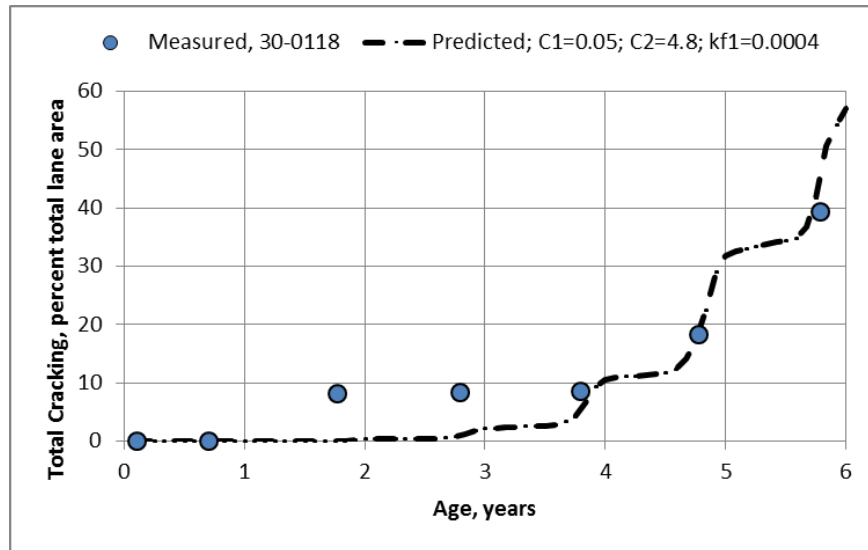
Source: FHWA.

Figure 168. Graph. Measured and predicted total fatigue cracking for Montana SPS-1 project test sections with nontypical rates of crack growth.

Table 26 summarizes the resulting fatigue cracking coefficients for some of the preliminary test sections listed in chapter 3. C_1 is also summarized in table 26 but does not appear to be related to mixture type or AC thickness. The C_1 coefficient is discussed further in the Layer/Mixture Type section in this report.

Table 26. Summary of fatigue cracking coefficients derived for individual projects.

State	Test Section	Type of Section or Mixture	Fatigue-Cracking Coefficient		
			k_{f1}	C_1	C_2
Alabama	01-0102	Thin AC with aggregate base and 4.2-inch AC	0.020000	1.00	2.25
Alabama	01-0105	AC with ATB/aggregate base and 8.2-inch AC	0.005000	1.00	2.25
Alabama	01-0103	AC with ATB (full-depth) and 11.6-inch AC	0.001570	1.00	2.85
Alabama	01-0101	Thick, full-depth AC and 15.3-inch AC	0.000750	1.00	3.75
Alabama	01-0104	Thick AC with ATB (full-depth) and 18.5-inch AC	0.000500	1.00	4.50
Arizona	04-0113	Thin AC with aggregate base and 4.4-inch AC	0.009000	0.25	2.00
Arizona	04-0114	AC with aggregate base and 6.8-inch AC	0.007000	0.25	2.30
Arizona	04-0117	AC with ATB/aggregate base and 11.8-inch AC	0.001900	0.05	3.50
Arizona	04-A901	AC with aggregate base and 6.9-inch AC	0.025000	0.25	2.40
Arizona	04-A902	AC with aggregate base and 6.5-inch AC	0.008000	0.05	2.40
Arizona	04-A903	AC with aggregate base and 6.7-inch AC	0.008000	0.05	2.40
Arizona	04-0902	AC with aggregate base and 7.0-inch AC	0.008000	0.05	2.40
Delaware	10-0102	Thin AC with aggregate base and 4.1-inch AC	0.009000	1.00	1.50
Delaware	10-0101	Thick AC with aggregate base and 15.0-inch AC	0.000650	0.75	5.50
Delaware	10-0106	Thick AC with ATB/aggregate base and 15.2-inch AC	0.000350	0.75	4.00
Delaware	10-0104	Thick AC (full-depth) and 18.7-inch AC	0.000250	0.75	4.50
Florida	12-0102	Thin AC with aggregate base and 4.7-inch AC	0.025000	1.00	2.10
Florida	12-0101	AC with aggregate base and 7.4-inch AC	0.005500	1.00	2.80
Florida	12-0106	Thick AC with ATB/aggregate base and 16.0-inch AC	0.000275	1.10	5.00
Florida	12-0104	Thick AC with ATB (full-depth) and 19.4-inch AC	0.000230	0.75	5.90
Kansas	20-0103	AC with ATB/aggregate base and 8.0-inch AC	0.008500	0.50	2.45
Kansas	20-0901	Thick AC with ATB (full-depth) and 17.4-inch AC	0.000650	0.50	5.60
Kansas	20-0902	Thick AC with ATB (full-depth) and 17.0-inch AC	0.000650	0.50	5.60
Kansas	20-0903	Thick AC with ATB (full-depth) and 17.0-inch AC	0.000650	0.50	5.60
Michigan	26-0117	AC with ATB/aggregate base and 11.6-inch AC	0.001550	1.00	3.95
Michigan	26-0115	Thick AC with ATB (full-depth) and 15.6-inch AC	0.000250	1.00	4.80
Montana	30-0113	Thin AC with aggregate base and 5.8-inch AC	0.003500	0.05	2.80
Montana	30-0114	AC with aggregate base and 7.5-inch AC	0.007000	0.50	2.60
Montana	30-0117	AC with ATB/aggregate base and 11.8-inch AC	0.000700	0.05	3.30

State	Test Section	Type of Section or Mixture	Fatigue-Cracking Coefficient		
			k_{f1}	C_1	C_2
Montana	30-0118	AC with ATB/aggregate base and 13.1-inch AC	0.000480	0.05	4.80
Montana	30-0115	Thick AC with ATB (full-depth) and 16.6-inch AC	0.000350	0.10	5.50
Nevada	32-0102	Thin AC with aggregate base and 4.3-inch AC	0.033000	0.85	1.80
Nevada	32-0106	Thick AC with ATB/aggregate base and 16.0-inch AC	0.000310	0.80	5.40
New Mexico	35-0101	AC with aggregate base and 7.4-inch AC	0.006900	1.00	2.40
New Mexico	35-0102	AC with aggregate base and 6.0-inch AC	0.010000	1.00	2.10
New Mexico	35-0104	Thick AC with ATB (full-depth) and 19.4-inch AC	0.000360	1.00	5.50
New Mexico	35-0105	AC with ATB/aggregate base and 9.9-inch AC	0.003000	1.00	3.40
Ohio	39-0901	Thick AC with ATB (full-depth) and 15.8-inch AC	0.000550	1.00	5.40
Ohio	39-0106	AC with ATB/aggregate base and 14.6-inch AC	0.000500	1.00	5.60
Ohio	39-0104	Thick AC with ATB (full-depth) and 18.9-inch AC	0.000500	1.00	5.60
Oklahoma	40-0113	Thin AC with aggregate base and 4.5-inch AC	0.012000	1.00	1.90
Oklahoma	40-0114	AC with aggregate base and 8.1-inch AC	0.004100	1.00	2.50
Oklahoma	40-0115	Thick AC with ATB (full-depth) and 16.6-inch AC	0.000460	1.00	4.90
Oklahoma	40-0116	Thick AC with ATB (full-depth) and 15.8-inch AC	0.000500	1.00	4.50
Oklahoma	40-0117	AC with ATB/aggregate base and 11.9-inch AC	0.001000	1.00	3.60
Oklahoma	40-0118	AC with ATB/aggregate base and 12.9-inch AC	0.000800	1.00	4.00
Virginia	51-0113	Thin AC with aggregate base and 4.0-inch AC	0.150000	1.00	1.80
Virginia	51-0114	AC with aggregate base and 7.3-inch AC	0.006100	1.00	2.60
Virginia	51-0115	Thick AC with ATB (full-depth) and 15.0-inch AC	0.000490	1.00	4.50
Virginia	51-0116	Thick AC with ATB (full-depth) and 16.6-inch AC	0.000300	1.00	5.30
Virginia	51-0117	AC with ATB/aggregate base and 10.6-inch AC	0.002500	1.00	3.20

Note: All test sections with a PATB layer were not included in the analyses because bottom–up fatigue cracking is heavily dependent on the air voids and asphalt content of the lower AC layer or the PATB.

Figure 169 and figure 170 compare the derived coefficients (k_{f1} and C_2) to AC-layer thickness for a diverse range of mixtures placed in different climates. As shown, k_{f1} and C_2 were related to total AC thickness. (None of the test sections with PATB layers were included in the comparison because these layers have high air voids.)
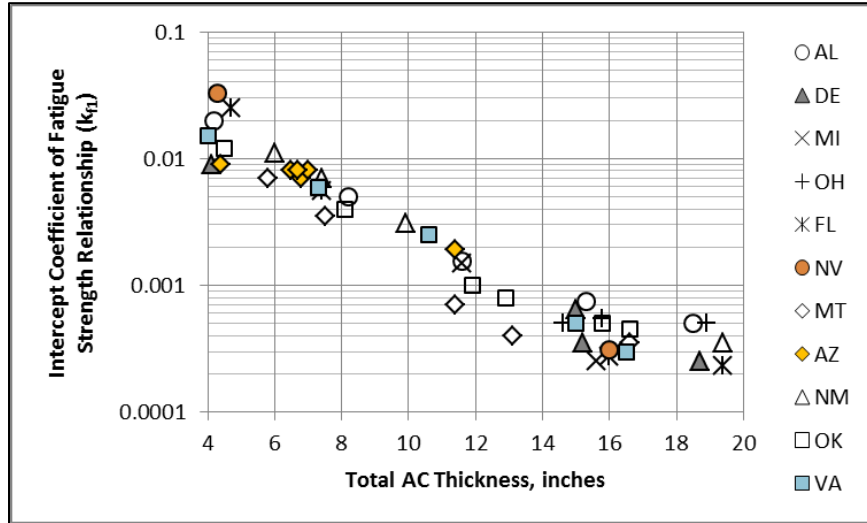
Source: FHWA.

Figure 169. Graph. Fatigue strength relationship between k_{f1} and AC-layer thickness.
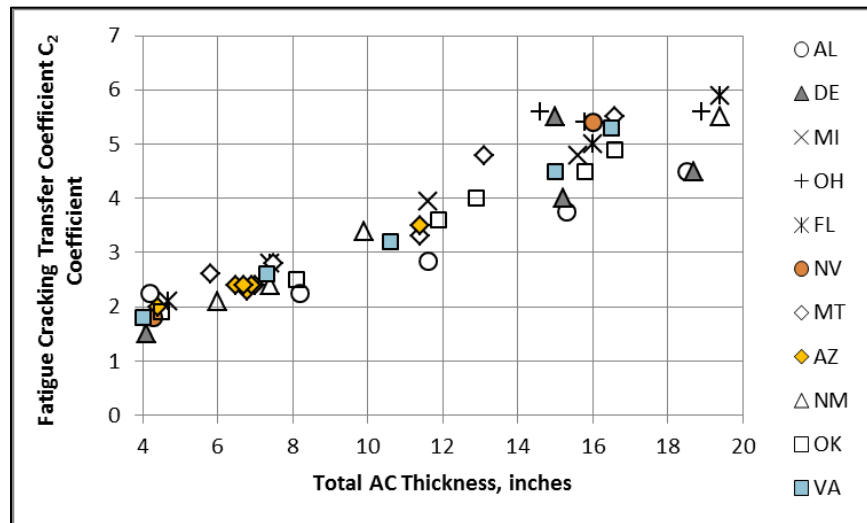
Source: FHWA.

Figure 170. Graph. Relationship between C_2 and total AC-layer thickness.

FACTORS CONTROLLING CRACK PROPAGATION AND GROWTH

The following subsections describe factors controlling crack propagation and growth.

AC-Layer Thickness

The MEPDG fatigue strength relationship (see figure 14 and figure 16) includes a term dependent on AC-layer thickness to account for differences between strain- and stress-controlled flexural fatigue tests (thin and thick layers). However, the thickness correction term (i.e., C_H defined in figure 16 for bottom–up cracking) did not adequately explain the impact of AC thickness related to crack propagation. Thus, AC total thickness related to crack propagation needs to be considered in estimating the fatigue strength or allowable number of load applications.

The test section derived coefficients for the fatigue strength equation and transfer function suggest that k_{f1} and C_2 become independent of AC thickness at 15 inches. The following observations are from the data and analysis using the MEPDG fatigue cracking prediction methodology and approach.

k_{f1} can be grouped into the following three thickness ranges:

- **Less than 5 inches**: The tensile strains at the bottom of the AC layer start decreasing because the neutral axis starts to decrease or approach the bottom of the AC layer.

- **5–15 inches**: k_{f1} is proportional to total AC-layer thickness (linear on a semi-log plot).

- **Greater than 15 inches:** k_{f1} is independent of AC-layer thickness and suggests the thickness for long-lasting AC pavements or the endurance limit.

C_2 can be grouped into the following two thickness ranges:

- **Less than 15 inches**: Crack propagation and growth are thickness dependent.

- **Greater than 15 inches**: Crack propagation and growth are thickness independent or the result of another mechanism.

Layer/Mixture Type

d_{AC} was extracted from the MEPDG output files for the LTPP test sections included in the analyses to compare the differences between mixtures and layer thickness. Figure 171 and figure 172 show the resulting MEPDG d_{AC} for two LTPP projects with different AC mixtures (dense-graded HMA binder versus dense-graded ATB). As shown, the intercept coefficient was highly variable and depended on mixture type and layer thickness—an indicator of differences in crack propagation. For the Alabama SPS-1 project (see figure 171), mixture type and layer thickness had less of an impact on the damage versus cracking relationship, while AC-layer thickness (HMA and ATB layers) for the Delaware SPS-1 project (see figure 172) had a larger impact on the damage versus cracking relationship.

157
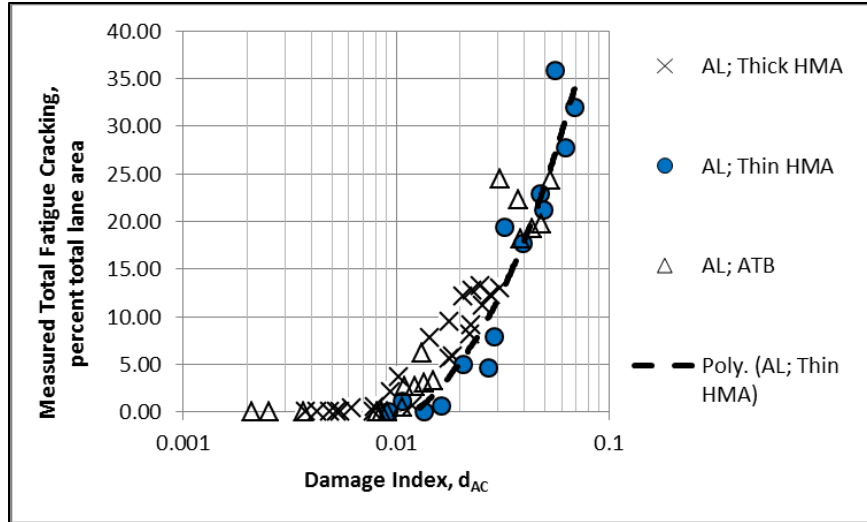
Source: FHWA.

Figure 171. Graph. Amount of fatigue cracking compared to d_{AC} for Alabama SPS-1 test sections.
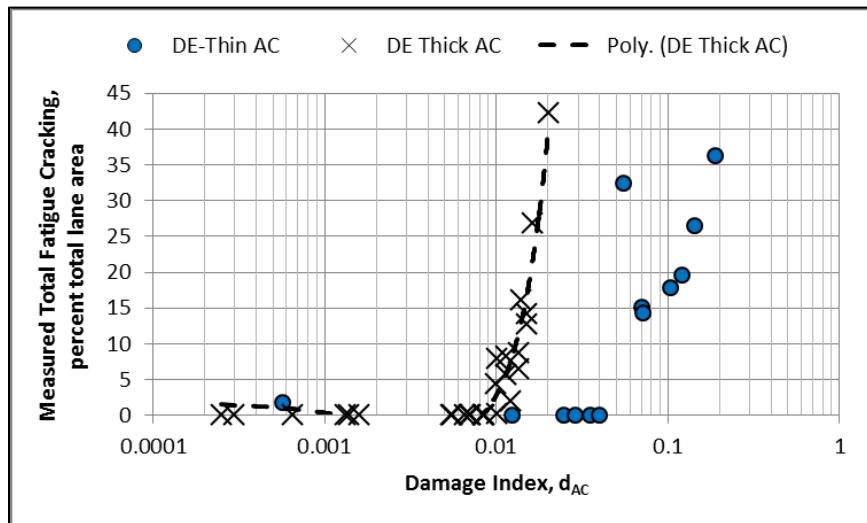
Source: FHWA.

Figure 172. Graph. Amount of fatigue cracking compared to d_{AC} for the Delaware SPS-1 test sections.

The test sections used in the preliminary analysis were initially segregated into two groups: sections with and without an ATB layer. The ATB mixtures generally had lower asphalt content and were designated as brittle mixtures. The sections with an ATB layer were further segregated into two sections: with a thin ATB layer (less than or equal to 5 inches) and with a thick ATB layer (more than 5 inches). The sections with a thin or thick AC layer were designated as elastic and viscoelastic mixtures, respectively, so the initial two groups were expanded into four groups. d_{AC} was extracted from the MEPDG output file for each site and compared to the amount of cracking for these groups of LTPP test sections.

Based on the authors' experience from previous forensic investigations, the cracking–time history data and the C_1 coefficient are two parameters that can be used to identify material/construction anomalies relative to bottom–up fatigue cracks. In some of the previous local calibration studies, the indirect tensile strength and tensile strain at failure were available to segregate the mixtures and explain the difference in crack propagation.[27,33,55] No fracture or bending beam fatigue test was available for the mixtures included in the LTPP database. The following list describes the process used to segregate the LTPP test sections that exhibit different crack growth rates:

- It was hypothesized that the fatigue cracking in or adjacent to the WP exhibiting a nontypical growth rate initiated at or near the pavement surface. Top–down cracks can start within 2 to 4 yr after construction regardless of the total AC thickness, increase to some amount and remain relatively constant, or increase at a slow rate for a period of time and then start to increase at an increasing rate. As such, the LTPP test sections exhibiting nontypical crack growth rates were excluded from sites used to evaluate the damage versus cracking relationship.

- C_1 in table 26 was significantly lower than 1.0 for some of the LTPP test sections. C_1 significantly less than 1.0 suggests some type of construction or mixture anomaly. Thus, it was hypothesized that test sections with C_1 less than 0.5 are representative of significant increases in cracking in a short time period, which could be caused by moisture damage, loss of bond between two adjacent AC lifts, accelerated aging, and other factors. As such, the LTPP test sections where C_1 was less than 0.5 were excluded from the sites used to evaluate the damage versus cracking relationship.

Figure 173 provides a comparison of d_{AC} and total cracking for each group. As shown, there is a significant difference between the segregated test sections. The difference between different agencies and climates was significantly lower when the test sections were segregated into the groups noted previously. Table 27 and Table 28 summarize observations made from the analysis related to the fatigue DI, d_{AC}, and level of cracking. In summary, it is the authors' opinion that the MEPDG approach and LTPP data explain the differences between traffic, climate, and other site-specific features but not the difference between thin and thick pavements or different types of mixtures. The question becomes: Why was there so much difference in crack propagation between thin and thick pavements that was not identified in some of the local calibration studies?
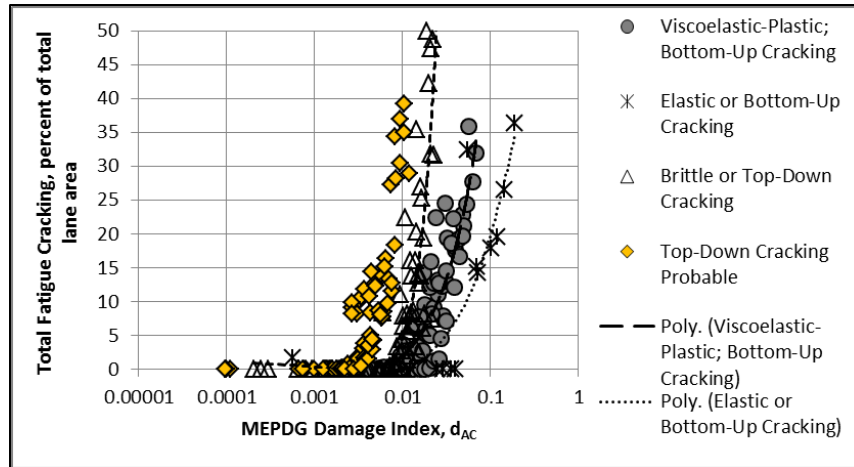
Source: FHWA

Figure 173. Graph. Amount of fatigue cracking compared to d_{AC} for the preliminary test sections that were grouped by type of mixture and cracking mechanism.

Table 27. MEPDG fatigue DI at which different levels of fatigue cracking occurred and/or were recorded in the LTPP database.

Cracking Amount	Mixture and/or Test Section Group			
	Top–down Cracking Probable	Brittle or Top–down Cracking	Viscoelastic-Plastic; Bottom–up Cracking	Elastic; Bottom–up Cracking
DI at which cracks were recorded in LTPP database	0.0040	0.0085	0.0085	0.0250

Table 28. MEPDG d_{AC} at which different levels of fatigue cracking occurred and/or were recorded in the LTPP database.

Percent of Total Lane Area	Mixture and/or Test Section Group			
	Top–down Cracking Probable	Brittle or Top–down Cracking	Viscoelastic-Plastic; Bottom–up Cracking	Elastic; Bottom–up Cracking
10	0.0060	0.012	0.025	0.050
20	0.0085	0.015	0.035	0.105
40	0.0095	0.025	0.075	0.200
50	0.0100	0.035	0.085	0.250

Other Factors

The difference in damage levels (both DI and d_{AC}) is believed to be related to the type of cracking mechanisms: top–down versus bottom–up cracking and mixtures that are and are not susceptible to moisture damage. The local calibration studies including field forensic investigations segregated or excluded top–down cracking and mixtures exhibiting stripping for calibrating the bottom–up fatigue cracking transfer function.[27,55] In addition, many of the

160

mixtures used in local calibration studies had similar characteristics and/or fatigue strength. The issue or question is how to systematically identify top–down cracking and moisture damage (stripping) susceptible mixtures as well as how to differentiate between different mixtures in cold and hot climates. To evaluate this question, the modulus ratio damage was used.

It is hypothesized that no significant reduction in E_{FWD}/E^*_{PRED} modulus ratios will be measured for test sections with top–down cracking because the AC is still intact at the bottom. In other words, the load transfer across the crack is near 100 percent. A significant reduction in modulus will only occur after the cracks propagate through the entire AC layer. However, many factors and/or construction-mixture defects have an impact on the AC E_{FWD}, two of which are as follows:

- Debonding between the AC layers will cause the deflections to increase or a reduction in the AC elastic modulus.

- Stripping and/or moisture damage in the lower AC layers (like an ATB layer) will result in higher deflections or a reduction in the AC elastic modulus; whether the backcalculation process can identify this condition as a separate layer depends on the layer thickness and depth below the surface.

Summary Analysis

An analysis was completed to evaluate and compare the MEPDG fatigue DI, d_{AC}, and amount of fatigue cracking to the modulus damage ratio, $DI_{E\text{-}ratio}$. Figure 174 shows a comparison between $DI_{E\text{-}Ratio}$ and d_{AC} for the four groups of LTPP sites shown in figure 173: viscoelastic-plastic bottom–up cracking, elastic or bottom–up cracking, brittle and/or top–down cracking, and top–down cracking probable. The data were highly variable, but the LTPP sites categorized as brittle and/or top–down cracking generally had a lower d_{AC} for similar modulus damage ratios in comparison to the two bottom–up cracking groups. Figure 175 shows the $DI_{E\text{-}ratio}$ values with the amount of cracking for the sections that fall within the same four categories. The categories identified as top–down cracking exhibited the higher amounts of cracking at the lower $DI_{E\text{-}ratio}$.
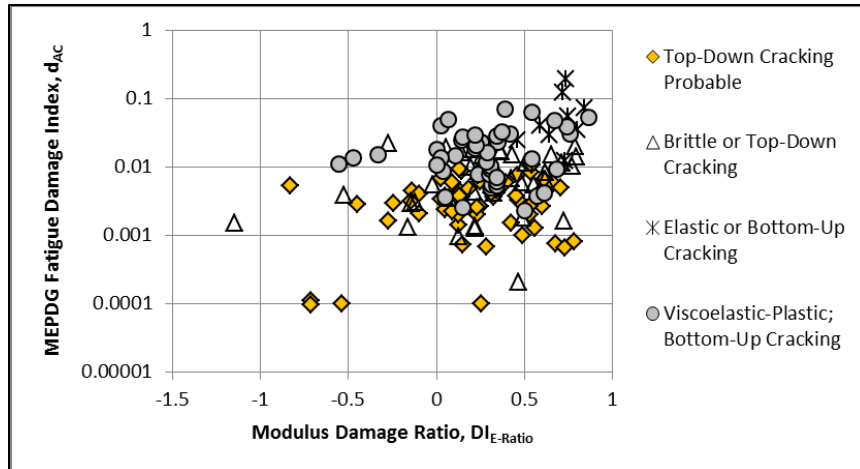
Source: FHWA.

Figure 174. Graph. Comparison of $DI_{E-ratio}$ to d_{AC} for the four types of LTPP sites.
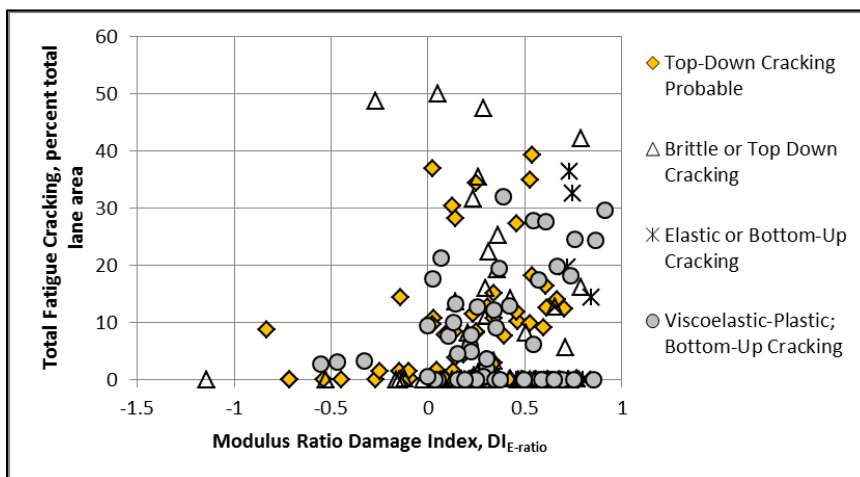
Source: FHWA.

Figure 175. Graph. Comparison of $DI_{E-ratio}$ and total of fatigue cracking for the four types of LTPP sites.

Overall, there was a poor correlation between the $DI_{E-ratio}$ values and area of fatigue cracking, as well as d_{AC}. This observation suggests the hypothesis that the AC E_{FWD} is directly proportional to the in-place damage of AC layers is invalid or would be rejected (see figure 174 and figure 175). In summary, figure 173 through figure 175 were used to evaluate the damage indices between different levels of cracking. Table 29 summarizes the combination of the $DI_{E-Ratio}$ values and total fatigue cracking in terms of expected cracking mechanism related to selecting a rehabilitation strategy. The combinations are defined as possible:

- **Neutral not classified**: Cells or combination of fatigue cracking and $DI_{E\text{-}ratio}$ values where it was difficult to determine (without the use of cores) whether the cracks were propagating bottom–up or top–down.

- **Top–down**: Cells or combination of fatigue cracking and $DI_{E\text{-}ratio}$ values with a higher probability of top–down cracking, debonding near the surface, or some other near surface defect. The recommendation is to use rehabilitation input level 1.

- **Bottom–up**: Cells or combination of fatigue cracking and $DI_{E\text{-}ratio}$ values with a higher probability of: bottom–up cracking (all cracks may not have reached the surface), moisture damage, debonding, or other lower AC layer defects. The lower the amount of cracking for the same $DI_{E\text{-}ratio}$, the greater the difference between rehabilitation designs using input levels 1 and 2.

Table 29. Areas with greater probability of top–down versus bottom–up cracking combining results from the distress surveys and FWD deflection testing.

$DI_{E\text{-}Ratio}$	Fatigue Cracking (Percent Total Lane Area)						
	0	0–2	2–10	10–20	20–35	35–50	>50
Negative	NN	Top–down	Top–down	Top–down	Top–down	Top–down	Top–down
0–0.25	Bottom–up	NN	NN	Top–down	Top–down	Top–down	Top–down
0.25–0.50	Bottom–up	Bottom–up	Bottom–up	NN	NN	Top–down	Top–down
0.50–0.75	Bottom–up	Bottom–up	Bottom–up	Bottom–up	Bottom–up	NN	Top–down
>0.75	Bottom–up	Bottom–up	Bottom–up	Bottom–up	Bottom–up	Bottom–up	NN

NN = neutral not classified.
Note: All cells with NN are shaded gray.

To confirm or provide support for the above hypothesis, E_{FWD} (field-derived) and E^*_{PRED} (laboratory-derived) were used to group FWD test dates for the LTPP sections using the temperature and thickness adjustment factors identified in figure 163. Five groups of the $DI_{E\text{-}ratio}$ values were considered as listed in table 29. A forensic investigation would be needed to confirm the above hypotheses, which was beyond the scope of this project. Table 27 through table 29 can be used in selecting a rehabilitation strategy as well as in a forensic investigation of the project site for preparing a site-specific sampling-coring plan.

CHAPTER 8. SUMMARY OF FINDINGS AND CONCLUSIONS

This chapter summarizes the findings from this study and provides conclusions relative to the use of the MEPDG in designing rehabilitation strategies for flexible pavements.[1] The findings are presented in terms of the assumptions and hypotheses that have been used for designing rehabilitation strategies using ME-based methodologies for flexible pavements as presented in chapter 3. In addition, various questions were asked and addressed for evaluating the hypotheses. The conclusions are presented in terms of the hypotheses included within this study and in using the MEPDG for designing rehabilitation strategies for flexible pavements.

SUMMARY OF FINDINGS AND RESULTS

The findings and results from this study as related to the assumptions listed in chapter 3 are summarized in this section. In addition, other findings and results are included as related to each item listed as follows:

1. **Cracks within or adjacent to the WP (alligator or longitudinal) will impact the deflection basin and result in a loss of stiffness of the AC layer if the cracks propagate through the AC layer**: The number of sections included in the preliminary analyses was insufficient to determine whether this assumption was true (see table 22). However, the $DI_{E\text{-}ratio}$ (see figure 58) did increase over time, or there was a decrease in E_{FWD} of the AC layer for many of the LTPP sections with higher amounts of fatigue cracking (see figure 50, figure 51, figure 57, and figure 175). The $DI_{E\text{-}ratio}$ did not increase over time for other sections with fatigue cracking (see figure 75, figure 79, figure 83, and figure 89 in chapter 5). The important question to answer is: do the cracks propagate through the entire AC layer? Cores are needed to determine the depth of cracks and conclusively state the assumption is correct or incorrect. Figure 148 is the mathematical tie between d_{AC} and $DI_{E\text{-}ratio}$ from E_{FWD} (i.e., as $DI_{E\text{-}ratio}$ increases, there is a corresponding increase in d_{AC}). Figure 171 through figure 175 provide data supporting the assumption— increases in d_{AC} result in higher amounts of fatigue cracking. Thus, increases in fatigue cracking will result in a decrease in E_{FWD} or increase in $DI_{E\text{-}ratio}$, so the assumption is believed to be correct in the authors' opinion.

2. **All alligator cracks within or adjacent to the WP were bottom–up cracks, all LTPP test sections included in this study had full bond between the lifts, and no moisture damage or stripping was present in the AC mixtures**: Without the use of cores, the assumptions of full bond between lifts and no moisture damage cannot be accurately evaluated. Cores were beyond the scope of this study, and forensic investigations have been completed on only a few of the LTPP test sections, so these assumptions become potential confounding factors in evaluating the hypotheses.

   Two types of load-related cracking occur in flexible pavements: (1) bottom–up area fatigue cracks that are identified as alligator cracks and (2) top–down linear cracks that are identified as longitudinal cracks within or adjacent to the WPs. The MEPDG assumes that the mechanism causing both types of cracks is the same (i.e., repeated tensile strains from truck axle loadings).[1] The mechanism of repeated tensile strains at or near the top of the wearing surface for top–down longitudinal cracks, however, is debatable. The *Mechanistic-Empirical Pavement Design Guide—A Manual of Practice* recommends that

top–down cracking be excluded as a design criterion for both new pavement and rehabilitation designs.[2]

The results from this study question the validity of this assumption that all of the alligator cracks on the LTPP test sections initiated at the bottom of the AC layer because the damage computations and coefficients of the transfer function are significantly different between thin and thick pavements. AC thickness was found to be a significant parameter in the C_2 regression coefficient of the fatigue cracking transfer function as well as the k_{f1} intercept coefficient of the fatigue strength relationship (see figure 169 and figure 170). The thickness parameter in the fatigue strength relationship (to consider the difference between strain- and stress-controlled fatigue tests or thin and thick pavements) did not adequately explain the differences in fatigue cracking between thin and thick AC pavements. Although a coring program is the only way to accurately determine which sites exhibit top–down and bottom–up cracks, the authors believe some of the thicker sites exhibit top–down alligator cracking.

In summary, the assumption that all alligator or area cracks located within the WP are bottom–up fatigue cracks was rejected or is incorrect. The thickness-dependent coefficients (i.e., C_1, C_2, and k_{f1}) can be used to initially segregate the LTPP sites with a high probability of top–down cracking (see table 26, figure 169, and figure 170). Obviously, a fracture test is critically needed to define the fatigue and/or crack propagation properties of the AC mixture to properly account for different layer thicknesses and mixture types.

3. **E_{FWD} is equal to E^*_{PRED} for the AC layer without any fatigue damage**: The MEPDG assumes that E_{FWD} and E^*_{PRED} are equal when no fatigue damage exists in the pavement.[1] In other words, E_{FWD} is equal to E^*_{PRED} at the same temperature and load frequency without any fatigue damage. No adjustment or correction is needed for translating E_{FWD} to E^*_{PRED}.

   Hao found the AC moduli from laboratory tests for AC layers were about 70 percent of the backcalculated moduli.[23] In addition, Von Quintus and Killingsworth reported the differences or ratios between the laboratory-measured moduli using the indirect tensile test and backcalculated elastic moduli for AC layers are temperature dependent.[33] At cold temperatures (e.g., 40 °F), E_{FWD}/E^*_{PRED} was 1.0, while the ratio decreased to 0.36 in the intermediate temperature range (e.g., 77 °F) and to 0.25 in the high temperature range (e.g., 104 °F).

Although the data were highly variable, the comparisons made within this study suggest E_{FWD} and E^*_{PRED} were different and that the difference was temperature dependent (see figure 163 through figure 165). Unless this difference is properly accounted for, MEPDG rehabilitation input level 1 will result in fatigue damage for thick AC pavements (greater than 15 inches) as well as AC pavements tested right after construction. At colder temperatures (i.e., stiffer or more elastic mixtures), the E_{FWD}/E^*_{PRED} ratio is close to unity, but with increasing temperatures (i.e., softer or more viscoelastic mixtures), the ratio starts to diverge from unity (see figure 163 through figure 165). E_{FWD} becomes significantly higher in comparison to E^*_{PRED}. Although not defined through this study, some of the difference is believed to be related to aging because

166

E*PRED from the master curve coefficients included in the LTPP database represent the original condition of the AC mixtures.

In summary, this assumption is questionable because there is insufficient data within the LTPP program to statistically define the relationship between *E_{FWD}* and *E*PRED* over a range of test temperatures. However, the temperature dependent difference between *E_{FWD}* and *E*PRED* (see figure 163) should be taken into account in planning deflection testing programs for rehabilitation designs and/or completing forensic investigations of flexible pavements.

Results and findings for issues related to other topics are as follows:

1. **Damage and the amount of cracking predicted over time**: The relationship between surface cracking and structural capacity of pavement structures was investigated using field data from FHWA testing facilities.[18] Results suggest the *E_{FWD}* values of the AC layers can be reduced by 20 to 50 percent before any cracking appears on the surface. This demonstrated the loss of structural capacity of AC pavements before surface cracking and the fact that using surface cracking by itself (rehabilitation input level 2) to assess damage might underestimate cumulative damage. Another important point is that the difference between new and existing AC layers can be used to create an *E*_{damaged}* master curve used for the existing AC layers based on their in-place condition. The *E*_{damaged}* master curve becomes the basis for calculating future AC responses and fatigue damage in the existing AC layers after the placement of a new overlay. The MEPDG methodology does not continue to reduce the AC modulus with continued increases in the cumulative fatigue DI.[1] In other words, the *E*_{damaged}* master curve remains constant with continued truck loadings and additional fatigue damage after rehabilitation. This concept or issue is debatable and is inconsistent with the other materials (like PCC and cement-treated bases) in evaluating and predicting fatigue damage but was not investigated or evaluated as part of this study.

2. **FWD load frequency**: One of the questions identified in chapter 2 was: What frequency should be used to estimate the undamaged *E**? Most of the previous studies including the global calibration have used a constant frequency but recognized that frequency is probably temperature and/or structure dependent. (See references 1, 27, 53–55, and 57.) Drop height 4 (target load of 16 kips) yielded a reasonable loading frequency of 35 Hz, but the loading frequency from drop height 1 (target load of 6 kips) was an order of magnitude greater. This suggests that the backcalculated frequency is highly variable and/or outside the typical range reported in the literature. It is also important to note that many of the backcalculated frequencies for drop height 1 were significantly greater than for drop heights 2, 3, and 4, which was consistent with the observation from figure 49 in chapter 4. One reason for this wide range of values is a result of the stress-sensitivity from the *E_{FWD}* values, while no stress-sensitivity is considered or included in the laboratory generated master curve. Another important observation is the load duration decreased (corresponding increase in load frequency) with drop height or load. This observation was just the opposite for many sites where the backcalculated frequency from *E_{FWD}* for drop height 1 was greater than *E_{FWD}* for drop height 4. The inverse of load duration, and simply assuming a frequency of 30 Hz, exhibited about the same percentage of points (10 percent) above the line of equality. These two methods resulted

in the fewer backcalculated elastic moduli from the FWD deflection basis, but that does not mean that the resulting damaged elastic moduli were more representative of the in-place damage. In summary, a frequency of 30 Hz is recommended for use in adjusting the $E^*_{undamaged}$ master curve based on the AC E_{FWD} values.

3. **Thickness effect**: The AC deflection-derived elastic moduli were different between thin and thick AC, which was not explained by middepth temperature differences. The thinner AC layer consistently exhibited higher backcalculated elastic layer moduli in comparison to the thicker AC layer. Both temperature and load frequency during FWD testing, however, can vary between thin and thick AC layers. k_{f1} and C_2 were found to be highly dependent on thickness (see figure 169 and figure 170). As such, crack propagation is an important factor that needs to be considered through some type of fracture test.

4. **Stress sensitivity effect**: The ATB or deeper layers were less affected by drop height, while the upper HMA layers consistently exhibited high elastic moduli for drop height 1 in comparison to the values for drop height 4. Similar results were observed for other SPS-1 projects. Although the stress-sensitivity was considered low, this issue was investigated in an effort to reduce the variability and explain as much of the variance as possible. It is not considered a significant factor, but drop heights 2, 3, or 4 should be used in backcalculating the AC elastic modulus for rehabilitation purposes in defining the in-place damage.

Findings and results from the previously provided hypotheses are as follows:

1. **The mechanism causing top–down and bottom–up cracks is the same (i.e., repeated tensile strains from truck axle loadings)**: As noted under assumption 2, two types of load-related cracking occur in flexible pavements: (1) bottom–up area fatigue cracks that are identified as alligator cracks and (2) top–down linear cracks that are identified as longitudinal cracks within or adjacent to the WPs. The MEPDG assumes the mechanism causing both types of cracks is the same—repeated tensile strains from truck axle loadings.[1] The mechanism of repeated tensile strains at or near the top of the wearing surface for top–down longitudinal cracks, however, is debatable. The *Mechanistic-Empirical Pavement Design Guide—A Manual of Practice* recommends that top–down cracking be excluded as a design criterion for both new pavement and rehabilitation designs.[2] In addition, NCHRP project 01-52 was authorized to confirm the mechanism for top–down cracking or develop a new methodology.[8] As such, top–down cracking was excluded from this study in terms of damage accumulation, but longitudinal cracks in the WP were included and added to the total amount of cracking observed at the pavement surface. It was assumed that cracks within or adjacent to the WP (alligator or longitudinal) will impact the deflection basin and result in a loss of stiffness of the AC layer if the cracks propagate through the AC layer (i.e., see assumption 1).

2. **The amount of fatigue cracking is directly related to or caused by damage accumulation in the form of the DI**: With accumulated damage, there is a threshold DI value for which cracks will propagate through the AC layers and will be observed at the pavement surface. Assumption 3 was found to be questionable, so it was difficult to evaluate the appropriateness of this hypothesis confined to the LTPP database.[10] It is the

opinion of the authors, based on other findings, that the softening approach to simulate different amount of cracking is appropriate if the other factors of AC total thickness (crack propagation), mixture type (brittle versus viscoelastic), and temperature (elastic versus viscoelastic) are properly taken into account. In other words, there were insufficient data to conclusively reject this hypothesis. Table 28 presents the d_{AC} for which cracks start to appear on the pavement surface. The MEPDG assumes the adjustment of the undamaged AC master curve is only dependent on the amount of cracking.[1] In other words, the tensile strains calculated the bottom of the AC layers for the undamaged and damaged master curves derived for different levels of cracking will result in the same amount of predicted cracking over time. This hypothesis was accepted, but the DI was found to be mixture or layer type dependent (see table 27 and figure 173).

3. **Damage in the AC layer can be solely simulated as a softening effect or loss of modulus from its original condition at the time of placement**: No in-place fatigue damage should exist in the AC layers shortly after placement. As such, the ratio of E_{FWD} and the laboratory-measured dynamic modulus (E^*_{PRED}) should be unity (i.e., equal to 1). As cracking increases, $DI_{E\text{-}ratio}$ should increase. The hypothesis that d_{AC} increases with time and is correlated to the area of fatigue cracking was accepted. However, the DI values for different levels of cracking are mixture and thickness dependent (see table 27 and figure 173). The hypothesis that the MEPDG modulus ratio (E_{FWD}/E^*_{PRED}) is highly correlated to cracking was rejected (see figure 175). Different construction/material anomalies affect the E_{FWD} value. More importantly, $DI_{E\text{-}ratio}$ will not necessarily increase with increasing area of fatigue cracking if those fatigue cracks initiated at or near the surface. Although the hypothesis was not proven or accepted, the AC E_{FWD} values in comparison to the total amount of fatigue cracks provide important information and can be used to determine the rehabilitation strategy for a specific project (see table 29).

4. **The AC E^* master curve, air voids, and effective asphalt content by volume can be used to accurately predict the occurrence of bottom–up fatigue cracks**: This indicates that one set of fatigue strength coefficients is applicable to and can explain differences in fatigue cracking between projects for all AC mixtures placed within the LTPP Program. The MEPDG uses the AC E^* master curve, air voids, and effective asphalt content by volume to predict the occurrence of bottom–up fatigue cracks.[1] In addition, the hypothesis implies there is a common shift factor for all mixtures and layer thicknesses for translating laboratory flexural beam fatigue tests to measured fatigue cracking, as identified under assumption 3. The shift factor was indirectly included in the MEPDG through the global and local calibration processes.

The comparison of the predicted and observed total cracking made within this study, however, was found to be thickness and mixture type dependent, which suggests this assumption is rejected. In addition, the fatigue cracking transfer function coefficients (C_1 and C_2) for bottom–up cracking derived by different agencies from the local calibration process varied significantly between different agencies. Some agencies have also revised the intercept of k_{f1}. Thus, AC layer and/or mixture specific intercepts of the fatigue strength relationship and coefficients of the fatigue cracking transfer function were derived within this study and found to be dependent on layer thickness and mixture type (viscoelastic versus brittle mixtures). k_{f1} was found to be highly dependent on AC-layer

thickness. The data suggest that the traditional flexural fatigue tests did not adequately explain or account for crack propagation through thin and thick AC layers. Fatigue cracks will propagate through the AC layers differently for different AC mixtures (brittle versus viscoelastic mixtures). No fracture tests or flexural beam fatigue tests are available within the LTPP database, so evaluating the shift factor dependence on AC-layer thickness was not completed.

In the opinion of the authors, k_{f1} and C_1 varied with mixture type (i.e., ATB mixtures versus dense-graded wearing surfaces), while the shift factor and C_2 varied with AC-layer thickness. This AC thickness and mixture type dependency should be taken into account when determining the damage indices for different levels of fatigue cracking for MEPDG rehabilitation input levels 2 and 3.

The hypothesis that d_{AC} increases with time and is correlated to the area of fatigue cracking was accepted on a project-by-project basis. However, the DI values for different levels of cracking were mixture and thickness dependent (see table 27, table 28, and figure 173). Stated differently, k_{f1} and C_2 were found to be highly dependent on total AC thickness. One field shift factor was not applicable for all mixtures and AC-layer thicknesses. Thus, this hypothesis was rejected. As for assumption 2, a fracture test is needed to properly define the shift factor for different mixture and layer thickness combinations.

5. **Crack propagation is independent of AC mixture type, asphalt grade, and AC-layer thickness**: Finn et al. applied this hypothesis to the AASHO road test cracking data and derived the intercept of the fatigue relationship (k_{f1} in figure 14) for different amounts of fatigue cracking.[43] This hypothesis was rejected because cracking was found to be dependent on the type of mixture, and k_{f1} and C_2 were found to be highly dependent on AC total layer thickness (see figure 169 and figure 170).

CONCLUSIONS

The following list summarizes the conclusions from this study relative to designing rehabilitation strategies in accordance with the MEPDG:[1]

- As noted for assumption 1, MEPDG rehabilitation input level 1 assumes that E_{FWD} and E^*_{PRED} moduli are equal when no fatigue damage exists. Results from this study suggest that E_{FWD} includes a bias relative to the laboratory E^* and that bias is temperature dependent. In the interim, it is recommended that an adjustment factor be applied to E_{FWD} values entered into the MEPDG AASHTOWare Pavement ME Design® software, similar to the c-factors for unbound layers.[3,4] The following list contains the recommended adjustment factors to be multiplied by the backcalculated elastic moduli so the bias is removed, on the average, in comparison to E^*_{PRED} (see figure 163 through figure 165):

  o **Middepth temperature less than 40 °F and/or E^*_{PRED} greater than 1,000 ksi**: The E_{FWD}/E^*_{PRED} ratio is 1.0.

- o **Middepth temperature of 60 to 70 ºF and/or E^*_{PRED} of 600–800 ksi**: The E_{FWD}/E^*_{PRED} ratio is 1.3.

  - o **Middepth temperature greater than 90 ºF and/or E^*_{PRED} less than 500 ksi**: The E_{FWD}/E^*_{PRED} ratio is 1.6.

- The E_{FWD}/E^*_{PRED} ratio was not highly correlated to the amount of fatigue cracking, and there was no consistent trend in the change of the ratio over time. As noted previously, hypotheses 2 and 3 were rejected. The other important conclusion from these comparisons and analyses is that large differences in the design or predicted amount of fatigue cracking can be expected between MEPDG rehabilitation input levels 1 and 2, all other inputs being equal. It is recommended that the backcalculated AC elastic moduli and $DI_{E\text{-}ratio}$ be compared to the amount of cracking exhibited on the pavement surface for selecting a rehabilitation input level to be used for design in accordance with table 29table 29.

- A loading frequency of 30 Hz is recommended for the FWD in the interim when using rehabilitation input level 1.

- The dissipated work ratio was not correlated to the amount of cracking, and there was no consistent trend in the change of the ratio over time.

- k_{f1} and C_2 were highly dependent on total AC thickness. As such, one field shift factor is not applicable for all mixtures and AC-layer thicknesses. In the interim, it is recommended that figure 169 be used to estimate k_{f1} and figure 170 be used to estimate C_2 for a specific problem. More importantly, a fracture test is needed to adequately explain the crack propagation for different mixtures. Based on the analysis, a total AC thickness of 15 inches is where k_{f1} becomes less dependent on AC thickness. It is the authors' opinion that this thickness value is near what is considered the thickness needed for long life pavements. The cracking exhibited on those test sections with more than 15 inches are believed to be a result of other mechanisms (top–down cracking) or construction defects/anomalies.

- The fatigue DI values that relate to the amount of cracking or the subjective condition ratings for MEPDG rehabilitation input level 3 included as default values in the MEPDG AASHTOWare Pavement ME Design® software are higher than the values derived from this study but obviously depend on the type of cracking (e.g., top–down versus bottom–up cracking (see figure 173)).[3,4] Local calibration will account for this difference when using MEPDG rehabilitation input levels 1 and 2. As such, MEPDG rehabilitation input level 3 is not recommended for use.

The time of year for measuring the amount of in-place damage is probably important. More importantly, the mathematical relationship used in the MEPDG for calculating damage may need to be revised to be temperature dependent.[1]

Simply testing along two lanes can reduce the number of cores that are now required to determine the in-place damage for rehabilitation design and to manage an agency's roadway

network for planning future rehabilitation projects. Simply measuring the deflection basins in the WP versus outside the WP provides a comparison of elastic moduli and whether damage is starting to occur. As extensive surface cracking starts to occur and spread beyond the WPs, however, any difference between measurements made within and outside the WPs is expected to decrease.

ACKNOWLEDGEMENTS

REFERENCES

1. ARA, Inc. (2004). *Guide for Mechanistic-Empirical Design of New and Rehabilitated Pavement Structures*, NCHRP Project 1-37A, National Cooperative Highway Research Program, Washington, DC.

2. American Association of State and Highway Transportation Officials. (2008). *Mechanistic-Empirical Pavement Design Guide—A Manual of Practice*, American Association of State and Highway Transportation Officials, Washington, DC.

3. American Association of State and Highway Transportation Officials. (2017). "AASHTOWare Pavement," (website) American Association of State Highway and Transportation Officials, Washington, DC. Available online: http://www.aashtoware.org /Pages/default.aspx, last accessed July 1, 2017.

4. American Association of State Highway and Transportation Officials. (2017). "AASHTOWare Pavement ME Design," (website) American Association of State Highway and Transportation Officials, Washington, DC. Available online: http://me-design.com, last accessed, July 1, 2017.

5. Lytton, R.L., Tsai, F.L., Lee, S-I., Luo, R., Hu, S., and Zhou, F. (2010). *Models for Predicting Reflection Cracking of Hot-Mix Asphalt Overlays*, NCHRP Report 669, National Cooperative Highway Research Program, Washington, DC.

6. Von Quintus, H.L. et al. (2012). *Calibration of Rutting Models for HMA Structural and Mixture Design*, NCHRP Report 719, National Cooperative Highway Research Program, Washington, DC.

7. Khazanovich, L. and Tompkins, D. (2017). *Incorporating Slab/Underlying Layer Interaction into the Concrete Pavement Analysis Procedures*, NCHRP Web-Only Document 236, National Cooperative Highway Research Program, Washington, DC. Available online: http://apps.trb.org/cmsfeed/TRBNetProjectDisplay.asp?ProjectID=3151, last accessed July 1, 2017.

8. Lytton, R.L. (2017). *A Mechanistic-Empirical Model for Top-Down Cracking of Asphalt Pavement Layers*, NCHRP 01-52, National Cooperative Highway Research Program, Washington, DC. Available online: http://apps.trb.org/cmsfeed/TRBNetProjectDisplay.asp? ProjectID=3152, last accessed July 1, 2017.

9. American Association of State and Highway Transportation Officials. (1993). *AASHTO Guide for Design of Pavement Structure*s, American Association of State Highway and Transportation Officials, Washington, DC.

10. Federal Highway Administration. (2017). "LTPP Infopave^{TM}," (website) U.S. Department of Transportation, Washington, DC. Available online: https://infopave.fhwa.dot.gov/Data/ StandardDataRelease, last accessed July 1, 2017.

11. Smith, K.D., Bruinsma, J.E., Wade, M.J., Chatti, K., Vandenbossche, J.M., and Yu, H.T. (2017). *Using Falling Weight Deflectometer Data with Mechanistic-Empirical Design and Analysis, Volume 1: Final Report*, Report No. FHWA-HRT-16-009, Federal Highway Administration, Washington, DC.

12. Carvalho, R., Stubstad, R., Briggs, R., Selezneva, O., Mustafa, E., and Ramachandran, A. (2012). *Simplified Techniques for Evaluation and Interpretation of Pavement Deflections for Network-Level Analysis*, Report No. FHWA-HRT-12-023, Federal Highway Administration, Washington, DC.

13. Stubstad, R.N., Jiang, Y.J., and Lukanen, E.O. (2006). *Guidelines for Review and Evaluation of Backcalculation Results*, Report No. FHWA-HRT-05-152, Federal Highway Administration, Washington, DC.

14. Xu, B., Ranjithan, S.R., and Kim, Y.R. (2002). "New Condition Assessment Procedure for Asphalt Pavement Layers Using Falling Weight Deflectometer Deflections," *Transportation Research Record No. 1806*, pp. 57–69, Transportation Research Board, Washington, DC.

15. Xu, B., Ranjithan, S.R., and Kim, Y.R. (2002). "New Relationships Between Falling Weight Deflectometer Deflections and Asphalt Pavement Layer Condition Indicators," *Transportation Research Record No. 1806*, pp. 48–56, Transportation Research Board, Washington, DC.

16. Kim, Y.R. and Park, H. (2002). *Use of Falling Weight Deflectometer Multi-Load Data for Pavement Strength Estimation*, Report No. FHWA/NC/2003-06, North Carolina Department of Transportation, Raleigh, NC.

17. Garg, N. and Thomson, M.R. (1998). *Mechanistic-Empirical Evaluation of the Mn/Road Low Volume Road Test Sections*, Report No. FHWA-IL-UI-262, Illinois Department of Transportation, Springfield, IL.

18. Thompson, M.R. (1989). "ILLI-PAVE Based NDT Analysis Procedures," *Nondestructive Testing of Pavements and Backcalculation of Moduli*, pp. 229–244, Bush III, A.J. and Baladi, G.Y. (eds.), ASTM International, West Conshohocken, PA.

19. Thyagarajan, S., Sivaneswaran, N., Petros, K., and Muhunthan, B. (2011). *Development of a Simplified Method for Interpreting Surface Deflections for In-Service Flexible Pavement Evaluation*, Eighth International Conference on Managing Pavement Assets, Santiago, Chile.

20. Diefenderfer, B.K. (2010). *Investigation of the Rolling Wheel Deflectometer as a Network-Level Pavement Structural Evaluation Tool*, Report No. VTRC 10-R5, Virginia Department of Transportation, Richmond, VA.

21. Mostafa, A.E., Abdel-Khalek, A.M., Gaspard, K., Zhang, Z., and Ismail, S. (2012). "Evaluation of Continuous Deflection Testing Using the Rolling Wheel Deflectometer in Louisiana," *Journal of Transportation Engineering*, *138*(4), American Society of Civil Engineers, Reston, VA.

22. Sebaaly, P., Tabatabaee, N., Bonaquist, R., and Anderson, D. (1989). "Evaluating Structural Damage of Flexible Pavements Using Cracking and Falling Weight Deflectometer Data," *Transportation Research Record No. 1227*, pp. 44–52, Transportation Research Board, Washington, DC.

23. Yin, H. (2012). "Simulation of Flexible Pavement Response to FWD Loads: A Mechanistic Approach," *International Journal of Pavement Research and Technology*, *5*(4), pp. 257–266, Chinese Society of Pavement Engineering, Elsevier, New York City, NY.

24. Kutay, M.E., Chatti, K., and Lei, L. (2011). "Backcalculation of Dynamic Modulus Mastercurve from Falling Weight Deflectometer Surface Deflections," *Transportation Research Record No. 2227*, pp. 87–96, Transportation Research Board, Washington, DC.

25. Brown, E.R., Cooley Jr., L.A., Hanson, D., Lynn, C., Powell, B., Prowell, B., and Watson, D. (2002). *NCAT Test Track Design, Construction and Performance*, NCAT Report 02-12, National Center for Asphalt Technology, Auburn, AL.

26. Attoh-Okine, N. and Offei, A. (2013). *Pavement Condition Surveys—Overview of Current Practices*, Delaware Department of Transportation, Newark, DE.

27. Von Quintus, H.L, Darter, M.I., Bhattacharya, B., and Titus-Glover, L. (2015). *Calibration of the MEPDG Transfer Functions in Georgia: Task Order 2 Report*, Report No. FHWA/GA-014-11-17, Georgia Department of Transportation, Atlanta, GA.

28. Papagiannakis, A., Gharaibeh, N., Weissmann, J., and Wimsatt, A. (2009). *Pavement Scores Synthesis*, Report No. FHWA/TX-09/0-6386-1, Texas Department of Transportation, Austin, TX.

29. Garcia, M. and Cheng, D. (2014). *Performance Modeling of Rubberized Hot Mix Asphalt—A Literature Review*, California Department of Resources Recycling and Recovery, California Department of Resources, Recycling and Recovery Report CP2-2014-101, Sacramento, CA.

30. Asphalt Institute. (2009). *Asphalt Overlays for Highway and Street Rehabilitation, MS-17*, Asphalt Institute, Lexington, KY.

31. Abaza, K.A. (2005). "Performance-Based Models for Flexible Pavement Structural Overlay Design," *Journal of Transportation Engineering*, *131*(2), pp. 149–159, American Society of Civil Engineers, Reston, VA.

32. Applied Research Associates, University of Minnesota, and Arizona State University. (2006). *Changes to the Mechanistic-Empirical Pavement Design Guide Software through Version 0.900*, NCHRP Research Results Digest 308, National Cooperative Highway Research Center, Washington, DC.

33. Von Quintus, H.L. and Killingsworth, B. (1998). *Analyses Relating to Pavement Material Characterizations and Their Effects on Pavement Performance*, Report No. FHWA-RD-97-085, Federal Highway Administration, Washington, DC.

34. Deblois, K., Bilodeau, J., and Dore, G. (2010). "Use of Falling Weight Deflectometer Time History Data for the Analysis of Seasonal Variation in Pavement Response," *Canadian Journal of Civil Engineering*, *37*(9), pp. 1,224–1,231, NRC Research Press, Canadian Science Publishing, Ottawa, Canada.

35. Salour, F. and Erlingsson, S. (2012). *Pavement Structural Behavior During Spring Thaw: Interpretation of FWD Measurements by Monitoring Environmental Data from County Road 126 at Torpsbruk*, VTI Report No. 738A, Swedish Transport Administration, Borlänge, Sweden.

36. Maruyama, K. and Kumagai, M. (2014). "Evaluation of Fatigue Damage in Asphalt Pavement Using FWD Dissipated Work in Asphalt Pavements," *Proceedings of the International Conference on Asphalt Pavements*, pp. 461–470, Kim, Y.R. (ed.), CRC Press, Raleigh, NC.

37. Dongre, R., Myers, L., and D'Angelo, J. (2006). *Conversion of Testing Frequency to Loading Time: Impact on Performance Predictions Available Online the M-E Pavement Design Guide*, Paper No. 06-2394, Presented at the 85th Annual Meeting of Transportation Research Board, Washington, DC.

38. Leiva-Villacorta, F. and Timm, D.H. (2013). *Falling Weight Deflectometer Loading Pulse Duration and its Effect on Predicted Pavement Responses*, Paper No. 13-2171, Annual Meeting of the Transportation Research Board Compendium of Papers, Washington, DC.

39. Hall, J. (1995). *Prediction of Deflection Response of Flexible Pavements Under Dynamic Loads*, Ph.D. Dissertation, Auburn University, Auburn, AL.

40. Lasdon, L.S., Waren, A.D., Jain, A., and Ratner, M. (1976). *Design and Testing of a Generalized Reduced Gradient Code for Nonlinear Programming*, Technical Report SOL 76-3, Systems Optimization Laboratory, Stanford University, Stanford, CA.

41. Chatti, K. and Lee, D. (2002). "Development of New Profile-Based Truck Dynamic Load Index," *Transportation Research Record No. 1806*, pp. 149–159, Transportation Research Board, Washington, DC.

42. Al-Qadi, I.L., Xie, W., and Elseifi, M.A. (2008). "Frequency Determination from Vehicular Loading Time Pulse to Predict Appropriate Complex Modulus in MEPDG," *Journal of the Asphalt Paving Technologists Association*, *77*, pp. 739–772, Association of Asphalt Paving Technologists, Lino Lakes, MN.

43. Finn, F.N., Nair, K., and Monismith, C. (1973). *Minimizing Premature Cracking of Asphalt Concrete Pavements*, NCHRP Report 195, National Cooperative Highway Research Program, Washington, DC.

44. Rauhut, J., Brent, H.L., Von Quintus, H.L., and Eltahan, A. (2000). *Performance of Rehabilitated Asphalt Concrete Pavements in the LTPP Experiments—Data Collected Through February 1997*, Report No. FHWA-RD-99-00-029, Federal Highway Administration, Washington, DC.

45. Google Maps™. (2016). *General locations of SPS sites*. Generated via Google Maps™ online by Dinesh Ayyala. Available online: https://www.google.com/maps/d/edit?hl=en&mid= 1SjC7savJVsNPJF92i0bCa5Qpaoc&ll=35.17018929007419%2C-94.34161241027823&z=4. Generated May 1, 2016.

46. Titus-Glover, L., Darter, M.I., and Von Quintus, H.L. (2016). *Impact of Environmental Factors on Pavement Performance in the Absence of Heavy Loads*, Report No. FHWA-HRT-16-078, Federal Highway Administration, Washington, DC.

47. Von Quintus, H.L., Rao, C., and Irwin, L. (2015). *Candidate Methods and Evaluation Criteria, Backcalculation of the Long-Term Pavement Performance Program Deflection Data*, Report No. FHWA-HRT-15-036, Federal Highway Administration, Washington, DC.

48. Von Quintus, H. and Killingworth, B. (1997). *Backcalculation of Layer Moduli of LTPP General Pavement Study (GPS) Sites*, FHWA-RD-97-086, Federal Highway Administration, Washington, DC.

49. Von Quintus, H.L. and Simpson, A.L. (2001). *Back-Calculation of Layer Parameters for LTPP Test Sections Volume II: Layered Elastic Analysis for Flexible and Rigid Pavements, LTPP DATS*, Report No. FHWA-RD-01-0113, Federal Highway Administration, Washington, DC.

50. Strategic Highway Research Program. (1993). *Distress Identification Manual for the Long-Term Pavement Performance Program*, Report No. SHRP-P-338, National Research Council, Washington, DC.

51. WSDOT. (2005). *EVERSERIES© Users Guide: Pavement Analysis Computer Software and Case Studies*, Washington State Department of Transportation, Seattle, WA.

52. Irwin, L.H. (1994). *Instructional Guide for Back-Calculation and the Use of MODCOMP*, CLRP Publication No. 94-10, Local Roads Program, Cornell University, Ithaca, NY.

53. Von Quintus, H.L., Rao, C., and Bhattacharya, B. (2014). *Implementation and Preliminary Local Calibration of Pavement ME Design in Mississippi: Volume I*, Report No. FHWA/MS-DOT-RD-013-170, Mississippi Department of Transportation, Jackson, MS.

54. Darter, M.I., Titus-Glover, L., Von Quintus, H.L., Bhattacharya, B., and Mallela, J. (2014). *Calibration and Implementation of the AASHTO Mechanistic-Empirical Pavement Design Guide in Arizona*, Report No. FHWA-AZ-14-606, Arizona Department of Transportation, Phoenix, AZ.

55. Mallela, J., Titus-Glover, L., Sadasivam, S., Bhattacharya, B., Darter, M.I., and Von Quintus, H.L. (2013). *Implementation of the AASHTO Mechanistic-Empirical Pavement Design Guide for Colorado*, Report No. CDOT-2013-4, Colorado Department of Transportation, Denver, CO.

56. Kim, Y.R., Jodoun, F.M., Hou, T., and Muthadi, N. (2011). *Local Calibration of the MEPDG for Flexible Pavement Design*, Report Number FHWA/NC/2007-07, North Carolina Department of Transportation, Raleigh, NC.

57. Bhattacharya, B., Von Quintus, H.L., and Darter, M.I. (2015). *Implementation and Local Calibration of the MEPDG Transfer Functions in Wyoming*, Technical Report No. FHWA-16/02F, Wyoming Department of Transportation, Cheyenne, WY.

58. Lee, H.S. (2014). "ViscoWave—A New Solution for Viscoelastic Wave Propagation of Layered Structures Subjected to an Impact Load," *International Journal of Pavement Engineering*, *15*(6), pp. 542–557, Taylor and Francis Group, London, England.

59. Lee, H.S. (2013). Development of a New Solution for Viscoelastic Wave Propagation of Pavement Structures and Its Use in Dynamic Backcalculation, Ph.D. Dissertation, Michigan State University, East Lansing, MI.

60. Ferry, J.D. (1980). *Viscoelastic Properties of Polymers*, Third Edition, John Wiley & Sons, Hoboken, NJ.